Institute for Problems in Mechanical Engineering
of the Russian Academy of Sciences

Smirnov Alexey Sergeevich

Dynamics, Motion Control and Optimization of Oscillation Damping Modes of Spatial Double Pendulum

Scientific speciality
1.1.7. Theoretical mechanics, dynamics of machines

Dissertation is submitted for the degree
of Candidate of Physical and Mathematical Sciences

Translation from Russian

Scientific Supervisor:
Candidate of Physical and Mathematical Sciences
Smolnikov Boris Alexandrovich

Saint Petersburg
2024

Table of Contents

Introduction

Relevance of the Research Topic

The mathematical pendulum and its varieties have been the key models of analytical mechanics for more than four centuries, starting from the youthful experimental discoveries and subsequent fundamental works of the outstanding scientist G. Galilei, as well as many of his followers. They are not only of theoretical interest, but also of great practical importance for applications. Among the many pendulum systems, much attention is drawn to the double pendulum, which is two pivotally connected mathematical or physical pendulums, as well as its numerous modifications. They are extremely popular objects of study not only in the field of the theory of oscillations of systems with several degrees of freedom, but also in a number of related disciplines.

An extensive layer of both domestic and foreign publications is devoted to the study of the dynamic behavior of such systems under a wide variety of conditions, which number is continuously increasing every year. Such serious attention to the double pendulum is connected, first of all, with its practical applications. The rise of interest in biomechanics, which began in the middle of the last century, accompanied by the active design of manipulators and other anthropomorphic devices, received significant development and aroused interest in the creation of multi-link pendulum structures equipped with power drives and control circuits, as well as in the development of various kinds of androids intended to replace humans working in hazardous conditions. Of course, the main interest here is precisely the double pendulum as the simplest multi-link pendulum, on the example of which it is possible to qualitatively and quantitatively describe the dynamics of various robotic structures, and, in addition, to identify a number of new provisions in theoretical terms and evaluate the possibility of their application in engineering.

Particular attention along this path is attracted by spatial two-link pendulums with cylindrical joints, whose axes are not collinear to each other. In this case, the configurations of the system will have a more complex form than for a flat double pendulum, and this circumstance also finds some application in practice. However, such systems are far from being studied sufficiently in comparison with flat versions of two-link structures. First of all, in their analysis questions arise about the study of their small and large oscillations, which are of a periodic character and suitable for practical use, as well as about the accelerating and braking modes of their movement, which have effective properties and are again dictated by the needs of practice. This leads to the need for a thorough study of such important problems as the construction of nonlinear oscillation modes, the formation of rational control actions, the search for optimal parameters for passive and active oscillations damping, as well as a whole range of related tasks.

Summarizing all the above, it can be argued that the study of the movements of spatial double pendulum under various conditions of its functioning is a **actual** task that **deserves the most serious attention**, which was the reason for writing this dissertation.

Research Methodology

The work uses the methods of analytical mechanics, the theory of mechanical oscillations, the theory of control of mechanical systems, optimization of mechanical systems, as well as approximate asymptotic methods of nonlinear mechanics. In addition, the numerical integration of the motion equations in the software environment **MATLAB** is carried out in the work, and for this purpose the universal solver **ode45** is used, which designed for systems of ordinary differential equations and based on the implementation of the numerical Runge-Kutta method 4-5 order of accuracy.

Aim and Tasks of the Work

The aim of this dissertation is to study the dynamic behavior of spatial double pendulum with identical parameters of its loads and links, whose joint axes are not collinear to each other. It consists in studying conservative, dissipative and

controllable models of this system in a linear and nonlinear formulations, as well as in solving the problem of finding the optimal parameters of passive and active damping of its oscillations.

In the course of this work, the following **tasks** were set and considered in detail:

1) To build a mathematical model of oscillations of spatial double pendulum and to consider its particular variants of a flat and orthogonal double pendulum. To investigate the frequencies and modes of its small vibrations depending on the angle between the joint axes. To establish qualitatively and quantitatively the influence of dissipative forces of viscous friction in articulated joints on its dynamic behavior.

2) To investigate the question of nonlinear oscillation modes of spatial double pendulum and its particular variants using asymptotic methods of nonlinear mechanics. To give their visual graphical interpretation. To compare the analytical expressions with the results obtained by numerical integration of the motion equations.

3) To form various options for control actions that will allow overclocking spatial double pendulum on each of its oscillation modes separately from small to sufficiently large deviations. To identify the gradual drift of the oscillation mode and demonstrate it graphically based on numerical results. To take into account the influence of dissipative effects and determine the possible motion modes of the system.

4) To determine the best parameters of passive and active damping of spatial double pendulum separately according to various criteria characterizing the efficiency of the damping processes of the system motions. To consider the joint accounting of two variants of oscillation suppression and determine the optimal parameters of active damping for given parameters of passive damping. To compare all the results.

Scientific Novelty

The dissertation contains a number of new results that clarify the behavior of spatial double pendulum in various modes of its motion. In the presented study, for the first time, the most detailed analytical solution was constructed

for the problem of small oscillations of spatial double pendulum in the absence and presence of viscous friction in the joints, an analytical and numerical study of its nonlinear oscillation modes of was carried out, its autoresonant overclocking modes were studied under the action of collinear control with a constant and variable gain coefficient, as well as a joint accounting of dissipative and control actions was carried out and the optimal parameters of passive and active damping were determined based on criteria characterizing the efficiency of the attenuation processes of system motions.

Theoretical and Practical Significance of the Work

The study of the movements of spatial double pendulum is of considerable theoretical interest and makes a certain contribution to one of the most important for applications and rapidly developing branches of mechanics – the dynamics of pendulum structures. The considered mathematical models and the given analytical and numerical solutions provide the basis for studying the movement character of more complex pendulums with several degrees of freedom, as well as many related issues. The obtained results can find some practical application in the field of robotics and biomechanics, namely, in the development, design and analysis of the dynamic behavior of various devices: two-link manipulators, elements of complex multi-link systems, numerous androids and other mobile robots. Moreover, the problems presented in the work and their detailed solutions are also interesting as illustrative examples of applied mechanics of pendulum systems in pedagogical and engineering practice.

Reliability of Results

The reliability of the results obtained in the work is ensured by using existing exact and approximate mathematical methods for studying linear and nonlinear oscillations of mechanical systems in the absence and presence of dissipative effects and control actions, as well as by comparing analytical expressions with the results found by numerically integrating the motion equations. Besides, for particular variants of a flat and orthogonal double pendulum, the obtained expressions are compared with previously known formulas from the literature.

Structure and Scope of the Work

The dissertation consists of an introduction, 5 chapters and a conclusion. The volume of the dissertation is 168 pages with 67 figures. The list of references contains 156 titles. The **Introduction** presents the relevance of the research topic and formulates the aim and tasks of the work. **Chapter 1** is devoted to the research history of the double pendulum, as well as a discussion of current directions in its analysis. In **Chapter 2**, the motion equations of spatial double pendulum are derived, its particular variants of a flat and orthogonal double pendulum are considered, and its small oscillations are studied, including in the presence of viscous friction in the articulated joints. In **Chapter 3**, nonlinear oscillation modes of spatial double pendulum and its particular variants are constructed and studied in detail with the help of asymptotic methods, and they are compared with the results of numerical integration. **Chapter 4** is devoted to the analytical and numerical study of the controlled motions of spatial double pendulum and its particular variants under the action of a collinear control, which allows to overclock the system on each of its oscillation modes separately with a smooth transition from a linear zone to a nonlinear one and can have both constant and and a variable gain factor, and also the possibility of viscous friction is taken into account and the motion modes of the system under the influence of dissipative and control actions are studied. In **Chapter 5**, the issues of optimal selection of parameters for passive and active damping of oscillations of spatial double pendulum are solving separately and with their cooperative action according to various optimization criteria that characterize the efficiency of damping processes of its movements, and a comparison of the results is carried out. The **Conclusion** summarizes the results of the study and draws the main findings on the work.

Author's Publications on the Dissertation Topic

On the topic of the dissertation, the author published 17 scientific papers in journals included in the list of peer-reviewed scientific journals recommended by the Higher Attestation Commission; and in publications indexed in the RSCI database and international citation databases Web of Science and Scopus:

1) **Smirnov A. S.**, Smolnikov B. A. Controlling the sway process of the swing. Week of Science SPbPU. Materials of the scientific forum with international participation. Institute of Applied Mathematics and Mechanics. 2016. Pp. 106–109. (In Russian)

2) **Smirnov A. S.**, Smolnikov B. A. Optimal damping of free oscillations in linear mechanical systems. Mashinostroenie i inzhenernoe obrazovanie. 2017. No. 3 (52). Pp. 8–15. (In Russian)

3) **Smirnov A. S.**, Smolnikov B. A. Resonance oscillations control of the nonlinear mechanical systems based on the principles of biodynamics. Mashinostroenie i inzhenernoe obrazovanie. 2017. No. 4 (53). Pp. 11–19. (In Russian)

4) **Smirnov A. S.**, Smolnikov B. A. Resonance oscillations control in the nonlinear mechanical systems. Transactions of seminar "Computer methods in continuum mechanics" 2016-2017. St. Petersburg University publishing house. 2018. Pp. 23–39. (In Russian).

5) Leontev V. A., **Smirnov A. S.**, Smolnikov B. A. Optimal damping of two-link manipulator oscillations. Robotics and Technical Cybernetics. 2018. No. 2 (19). Pp. 52–59. (In Russian)

6) Leontev V. A., **Smirnov A. S.**, Smolnikov B. A. Collinear control of dissipative double pendulum. Robotics and Technical Cybernetics. 2019. Vol. 7. No. 1. Pp. 65–70. (In Russian)

7) **Smirnov A. S.**, Smolnikov B. A. Double pendulum research history. History of Science and Engineering. 2020. No. 12. Pp. 3–12. (In Russian)

8) **Smirnov A. S.**, Smolnikov B. A. Oscillations of Double Mathematical Pendulum with Noncollinear Joints. Advances in Mechanical Engineering. Selected Contributions from the Conference "Modern Engineering: Science and Education", St. Petersburg, Russia, June 2020. 2021. Pp. 185–193.

9) **Smirnov A. S.**, Smolnikov B. A. Nonlinear oscillation modes of double pendulum. IOP Conference Series: Materials Science and Engineering. International Conference of Young Scientists and Students "Topical Problems of Mechanical Engineering" (ToPME 2020) 2nd–4th December 2020, Moscow, Russia. 2021. Vol. 1129, 012042.

10) **Smirnov A. S.**, Smolnikov B. A. Collinear control of single-link manipulator motion with variable gain. Youth and Science: actual problems of fundamental and applied research. Materials of the IV All-Russian scientific conference of

students, postgraduates and young scientists. Komsomolsk-on-Amur. April 2021, 12-16. Vol. 2. Pp. 70–73. (In Russian)

11) **Smirnov A. S.**, Smolnikov B. A. Nonlinear oscillation modes of spatial double pendulum. Journal of Physics: Conference Series. The International Scientific Conference on Mechanics "The Ninth Polyakhov's Reading" (ISCM) 9-12 March 2021, St. Petersburg, Russian Federation. 2021. Vol. 1959, 012046.

12) **Smirnov A. S.**, Smolnikov B. A. Collinear control of oscillation modes of spatial double pendulum with variable gain. Cybernetics and physics. 2021. Vol. 10. Is.2. Pp. 90–96.

13) **Smirnov A. S.**, Smolnikov B. A. Dissipative Model of Double Mathematical Pendulum with Noncollinear Joints. Advances in Mechanical Engineering. Selected Contributions from the Conference "Modern Engineering: Science and Education", St. Petersburg, Russia, June 2021. 2022. Pp. 38–47.

14) **Smirnov A. S.**, Smolnikov B. A. The history of mechanical resonance – from initial studies to autoresonance. Chebyshevskii sbornik. 2022. Vol. 23. No. 1. Pp. 269–292. (In Russian)

15) **Smirnov A. S.**, Smolnikov B. A. Optimization of oscillation damping modes of spatial double pendulum. I. Formulation of the problem. Vestnik of St. Petersburg University. Mathematics. Mechanics. Astronomy. 2022. Vol. 9 (67). Iss. 2. Pp. 357–365. (In Russian)

Engl. transl.: **Smirnov A. S.**, Smolnikov B. A. Optimization of Oscillation Damping Modes of a Spatial Double Pendulum: 1. Formulation of the Problem. Vestnik St. Petersburg University, Mathematics. 2022. Vol. 55. No. 2. Pp. 243–248.

16) **Smirnov A. S.**, Smolnikov B. A. Optimization of oscillation damping modes of spatial double pendulum. II. Solving the problem and analyzing the results. Vestnik of St. Petersburg University. Mathematics. Mechanics. Astronomy. 2023. Vol. 10 (68). Iss. 1. Pp. 121–138. (In Russian)

Engl. transl.: **Smirnov A. S.**, Smolnikov B. A. Optimization of Oscillation Damping Modes of a Spatial Double Pendulum: 2. Solution of the Problem and Analysis of the Results. Vestnik St. Petersburg University, Mathematics. 2023. Vol. 56. No. 1. Pp. 93–106.

17) **Smirnov A. S.**, Smolnikov B. A. Nonlinear autoresonance in problems of controlling oscillations of multidimensional mechanical systems. XIII All-Russian Congress on Theoretical and Applied Mechanics: collection of works in 4 volumes.

August 21-25, 2023, St. Petersburg, Russia. Vol. 1. General and applied mechanics. 2023. Pp. 214–216. (In Russian)

Approbation of the Work

Separate parts of the work were presented at the following scientific seminars and conferences:

1) At the seminars of the Department (Higher School) "Mechanics and Control Processes" of Peter the Great St. Petersburg Polytechnic University (St. Petersburg, 2016, 2020);

2) At the conference "Week of Science SPbPU" with international participation (St. Petersburg, 2016, 2024);

3) At the city seminar "Computer Methods in Continuum Mechanics" (St. Petersburg, 2016);

4) At the laboratory seminar "Control of the Complex Systems" of Institute for Problems in Mechanical Engineering of the Russian Academy of Sciences (St. Petersburg, 2017);

5) At the International Scientific and Practical Conference "Modern Engineering: Science and Education MMESE" (St. Petersburg, 2020, 2021);

6) At the Seminar on the History of Mathematics at St. Petersburg Department of Steklov Mathematical Institute of the Russian Academy of Sciences (St. Petersburg, 2020, 2021);

7) At the meetings of the Section of Theoretical Mechanics named after Prof. N. N. Polyakhov in the M. Gorky House of Scientists of the Russian Academy of Sciences (St. Petersburg, 2020, 2021);

8) At the XXXII International Conference of Young Scientists and Students "Topical Problems of Mechanical Engineering" ToPME (Moscow, 2020);

9) At the International scientific conference on mechanics "The Ninth Polyakhov's Reading" (St. Petersburg, 2021);

10) At the IV All-Russian scientific conference of students, postgraduates and young scientists "Youth and Science: actual problems of fundamental and applied research" (Komsomolsk-on-Amur, 2021);

11) At the XIII All-Russian Congress on Theoretical and Applied Mechanics (St. Petersburg, 2023).

Gratitude

The author expresses his sincere gratitude to his teacher and supervisor of this dissertation, Candidate of Physical and Mathematical Sciences, Senior Researcher at the Institute for Problems in Mechanical Engineering of the Russian Academy of Sciences (IPME RAS) **Boris A. Smolnikov** for the constant attention to the work, support and parting words at all stages of its writing. In addition, the author would like to express his gratitude to his colleague, mentor and co-author of scientific papers, Candidate of Physical and Mathematical Sciences, Senior Researcher at the Russian State Scientific Center for Robotics and Technical Cybernetics (RSSC RTC) **Viktor A. Leontev** for valuable comments and help in improving the text of the work.

Main Scientific Results

1) The dependencies of the frequencies and modes of small oscillations of a spatial double pendulum with identical parameters of the loads and links on the angle between the joint axes were found, and it was also demonstrated that with identical dissipative coefficients, the viscous friction forces in the joints do not distort the oscillation modes of the conservative model, only reducing their amplitudes, and all the characteristics of the dissipative process are determined. The results were published in the papers: [144] (pp. 188–191), [141] (pp. 40–43).

2) It has been established that the nonlinear oscillation modes of a spatial double pendulum and its particular version of a flat double pendulum become noticeably more complex compared to the traditional linear oscillation modes with increasing energy level of the system, and the key quantities reflecting the dynamic behavior of the system when moving on a nonlinear mode are determined, depending on the amplitude and the angle between the joint axes. The results were published in the papers: [142] (pp. 3–9), [143] (pp. 2–8).

3) It is shown that collinear control at a constant gain does not distort the modes of small oscillations of the original conservative model of a spatial double pendulum and its flat version and allows the system to be accelerated for each of them separately with a gradual transition from a linear zone to a nonlinear one up to sufficiently large deviations, and collinear control with a variable gain

makes it possible to achieve a smooth transition of the system to a steady state mode of nonlinear periodic oscillations with a given energy level. The results were published in the papers: [73] (pp. 14–18), [140] (pp. 92–95).

4) The problem of finding the best values of oscillation damping parameters of a spatial double pendulum in accordance with two optimization criteria characterizing the efficiency of the processes of damping the movements of the system is posed and solved, and the dependencies of the optimal values of the active damping parameter on the given passive damping parameter and the angle between the joint axes according to these criteria are determined. The results were published in the papers: [68] (pp. 11–14), [69] (pp. 358–362), [70] (pp. 128–134).

The author's personal participation in obtaining all the results presented: specific formulations of problems, their detailed solution and a thorough review of all the analytical and numerical results found. The applicant discussed the research methods and results obtained with the co-authors of scientific papers published on the topic of the dissertation.

Provisions to be Defended

1) The design scheme of a spatial double mathematical pendulum with identical parameters of loads and links, whose joint axes are not collinear to each other, is considered. Nonlinear equations of motion of the system are derived and a linear model of its small oscillations is studied. The forces of viscous friction in the joints were taken into account and their influence on the character of the damping of the system's movements was established.

2) Based on asymptotic methods of nonlinear mechanics, nonlinear oscillation modes of a spatial double pendulum in the first approximation and its particular variants of a flat and orthogonal double pendulum in the first and second approximations were constructed and analyzed. The obtained analytical solutions are compared with the results of numerical integration of the motion equations.

3) The controlled motion of a spatial double pendulum and its particular variants under the action of moments in joints formed according to the principle of collinear control with a constant gain is considered. A modification of the collinear law is proposed, which contains a variable gain associated with the current energy of the system. Within the framework of a linear controlled model with a constant

gain, consideration of viscous friction is considered and a classification of possible modes of motion of such a system is given.

4) The issues of optimal damping of oscillations of a spatial double pendulum under the influence of dissipative and control influences were studied, and two optimization criteria were adopted: maximizing the degree of stability of the system and minimizing the integral energy-time indicator. A comparison of the optimal damping parameters found using the specified criteria is given.

1. Overview of Double Pendulum Research

1.1. Historical Studies of Double Pendulum

The double pendulum problem has a long and rich history. Therefore, it is of interest to turn first to the historical studies of the double pendulum [64]. The history of the double pendulum dates back to the first half of the 18th century, and it is associated with the names of prominent scientists of that time – A. Clairaut, D. Bernoulli and L. Euler.

A double pendulum was first described in 1735 by A. Clairaut [25]. He gave a lecture at the Paris Academy of Sciences, after which he published an article *"Solution of some dynamics problems"* [99], published in 1736. Clairaut's creation was prompted by discussions with A. Fontaine, who published an article [106] in 1734, which dealt with the definition of a curve described by the vertex of an angle whose sides slide along some given curve. In Clairaut's preface to his work [99] there is the phrase "The discussion about the tractrix between Mr. Fontaine and myself, which lasted for several assemblies, prompted me to the research that I propose" [87]. Clairaut's work was devoted to solving seven problems on the motion of a bunch of two points in a horizontal or vertical plane. It is assumed that the trajectory of one of the points or the center of gravity of the system is considered to be given (a straight line, a circle, or an arbitrary plane curve), and the problem is to determine the trajectory of another point or both points when the magnitudes and directions of their initial velocities are given. At the same time, Clairaut used both traditional geometric techniques and methods of differential calculus to solve these problems. Referring to D. Bernoulli, Clairaut based the solution of his problems on the principle of conservation of living forces,

which at that time was still questioned and subsequently canonized by Lagrange under the name "theorem of the change in kinetic energy". It should be emphasized that Clairaut's work was historically the first work of its kind. An important difference between Clairaut's work and the works of his predecessors is that he studied the movement of not just two interconnected points, but the behavior of one point, on which given geometric connections [87] are superimposed. This approach was important for creating the foundations of the non-free motion mechanics of a point, a system of points and a rigid body, which were subsequently laid down in the works of J. d'Alembert.

The next contribution to the analysis of the double pendulum was made by D. Bernoulli, who published in 1738 an article *"Theorem on oscillations of bodies suspended vertically on an elastic thread and on a chain"* [92]. A complete theory of small swings of a double gravitational pendulum is given in it for the first time [25]: its oscillation modes are determined for identical mathematical pendulums, and the general case of different masses of loads and different lengths of links is considered. Subsequently, Bernoulli published a number of other articles on this topic, the most significant of which was the article of 1774 *"Special physical-mechanical reasoning on mutual compound motions. Easily observable studies of the double pendulum in support of the principle of coexistence of simple oscillations"* [91]. The discussion of the possibility of the appearance of internal resonances in the system, when the oscillation frequencies are related as integers, is of interest in this article, and as a result the conditions on the system parameters under which they are realized are determined. It is shown that if the lengths of both pendulums are equal and the masses of the first and second loads are related as $16 : 9$, then the resonance $1 : 2$ will take place, and if these masses are related as $9 : 16$, then the resonance $1 : 3$ will be implemented.

Finally, L. Euler, who published in 1741 an article *"On oscillations of a flexible wire, on which an arbitrary number of small loads is suspended"* [105], closes the top three historical studies. The author analyzes in it not only the problem of a double pendulum (a drawing from this work is shown in Fig. 1.1), for which expressions for the oscillation modes are given, but also generalizes this problem to the case of any number of loads, thereby coming to calculation scheme of a multilink mathematical pendulum.

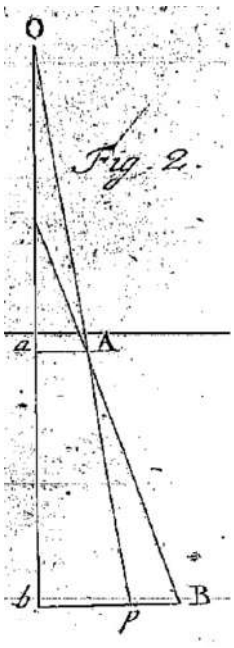

Fig. 1.1. Drawing from Euler's paper

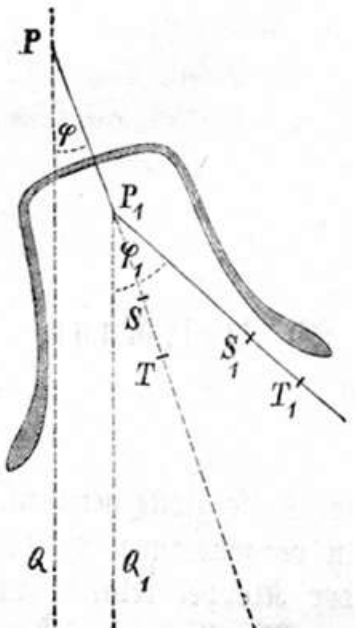

Fig. 1.2. Cologne bell and its tongue: real construction and its design scheme from Veltmann's article

The problem of the double pendulum first received serious practical application, which was associated with the solution of the problem of the "silent" Cologne bell, only in the second half of the 19th century. In 1875, an interesting case was observed on the bell tower of the Cologne Cathedral (German Empire): a bell hollow inside (*Kaiserglocke* – an imperial bell) and a tongue jointed to it oscillated as one whole (Fig. 1.2). This amazing phenomenon was strictly explained by W. Veltmann in the article *"On the movement of the bell"* [151], where he interpreted the system as a double pendulum: the bell played the role of the first pendulum, and its tongue – the second one. The design scheme of the system in the deflected position from the mentioned work is also presented in Fig. 1.2. To solve this problem, the Lagrange equations of the second kind were used and the question of when two differential motion equations admit a particular solution, in which both the bell and its tongue deviate by the same angle all the time, was considered. As a result, a condition for the system parameters was obtained, when the tongue does not move relative to the bell. With accuracy sufficient for practice, this condition can be given a simple physical interpretation: the bell moves as a single body and therefore cannot sound if the bell's swing center at rest coincides with the swing center of its tongue. So, the reduced length of the Cologne Cathedral bell is 328.2 cm, the reduced length of its tongue is 262.9 cm, and the distance

between the suspension points of the tongue and the bell is 66.7 cm. Therefore, the tongue swing center was 262.9+66.7=329.6 cm away from the bell suspension axis, i.e. it almost coincided with the bell swing center [25]. This explains the almost complete absence of relative movements of the tongue, which made such small oscillations in relation to the bell that it could not strike, although the tongue was long enough to reach the walls of the bell [121]. The bell began to ring only after the length of its tongue was increased. It should be emphasized that in deriving the mentioned condition, the global nonlinear model of the system was used, and not the linearized one. Finally, the article [151] has a table that presents data on all the bells of the Cologne Cathedral and demonstrates that all bells, except *Kaiserglocke*, did not experience sounding problems, since their parameters deviated too much from the obtained ratio. This problem is very instructive not only for bell designers, but also for a wide range of engineers, and therefore it was included in a number of canonical books on mechanics – both foreign [115, 117] and domestic [26].

The next important application of the double pendulum was discovered in the first half of the 20th century, when in 1923 it was proposed by V. P. Vetchinkin and N. G. Chentsov for the experimental determination of the moments of inertia of solids using the swing method in the work *"A flat pendulum with two degrees of freedom and the determination of the center of gravity height and the moment of inertia of a rigid body using it"* [15]. As a result, a corresponding theory was developed, which was also considered by L. G. Loitsyansky and A. I. Lurie [43]. This method has received wide practical application for determining the moments of inertia of aircraft, and a special suspension PE1 was designed and built in TsAGI, which makes it possible to swing an aircraft on a bifilar suspension like a double pendulum [25]. Subsequently, this design was improved and a PE2 suspension was built. These experiments were described in detail by Yu. A. Pobedonostsev in the articles [57, 58]. It should be noted that this method was also used abroad [112]. The work [25] details the way to derive the formula for the moment of inertia. To determine the moment of inertia of the body about the main central axis, it is suspended on two rods (or two bands) of equal length, located symmetrically about the center of gravity (or its intended location). It is also necessary to keep in mind that when the system is in equilibrium, the horizontal segments connecting the upper and lower ends of the rods must be parallel to the

given axis (Fig. 1.3). To find the moment of inertia, we need to determine the periods of both main oscillations by selecting the initial conditions, achieving the oscillations of the aircraft only on one of the modes of its oscillations.

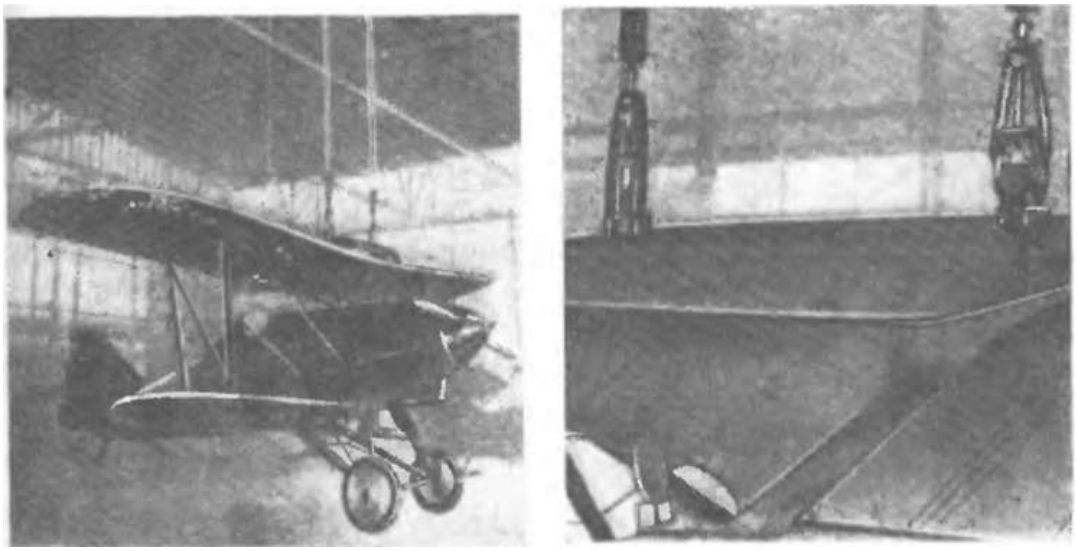

Fig. 1.3. Suspension of the aircraft (suspension PE1 TsAGI)

As a result, the scheme of a double pendulum and the calculation of its oscillations in various formulations entered both foreign [95, 119, 147], as well as numerous domestic [7, 28, 34, 48, 86] engineering, scientific and educational literature. The results presented in these works relate to the analysis of small oscillations of a double mathematical or double physical pendulum within the framework of a linear model and the determination of the frequencies and modes of its small oscillations and the consideration of various particular or limiting cases.

1.2. Main Directions of Modern Research of Double Pendulum

In the last few decades, there has been a sharp increase in interest in the double pendulum mechanics and its varieties. As mentioned earlier in the introduction, this is primarily due to its use in robotics as the simplest model of a two-link manipulator, which must perform working movements with both small and very large amplitudes, and as an element of complex multi-link structures, as well as in problems of biodynamics, since a double pendulum can imitate the limbs of

living organisms [74,75,77]. In this case, the movements of a double pendulum are investigated not only analytically or numerically, but as a result of experiments. Fig. 1.4 shows various designs of a double mathematical and double physical pendulum, created as demonstration setups and borrowed from the works of [90, 133], as well as from video recordings of experiments that are in open access.

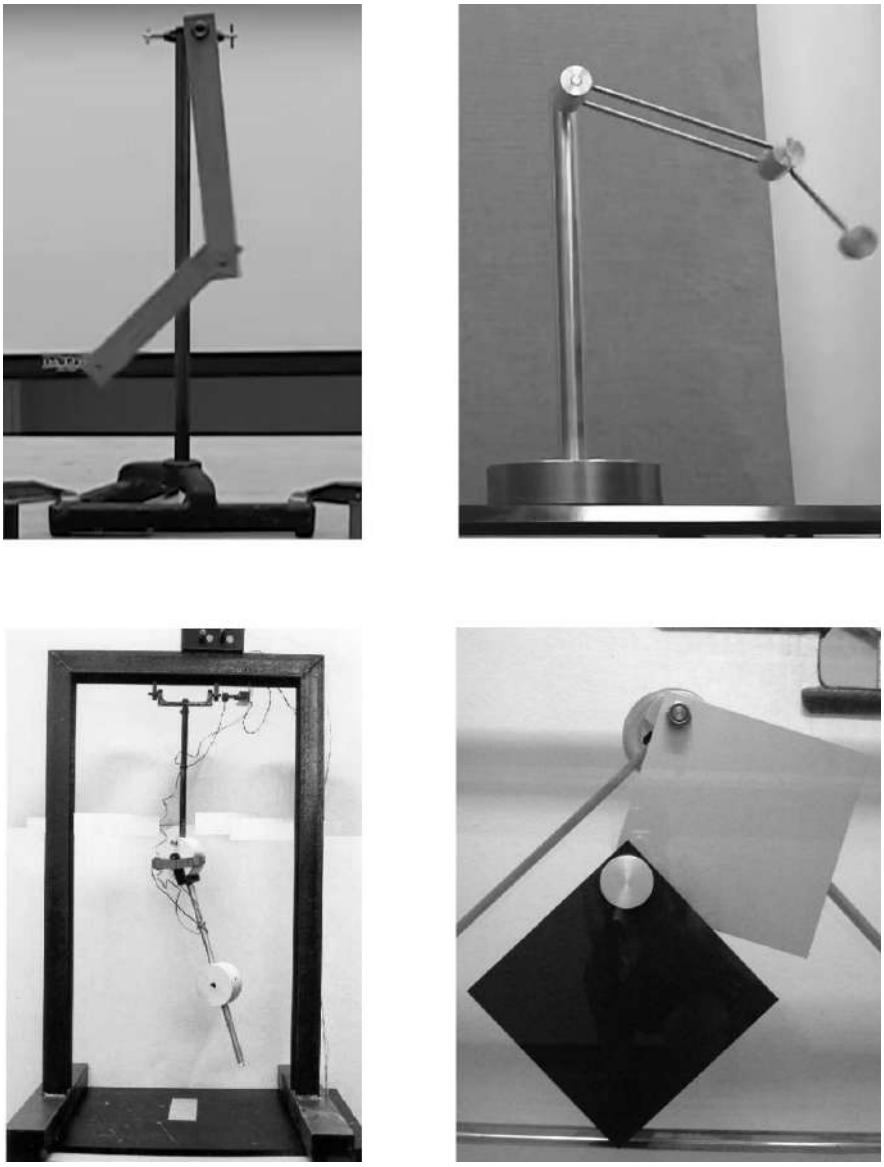

Fig. 1.4. Various double pendulum designs

Let us single out the main directions of modern research on the gravitational double pendulum, related to the last three decades, and accompany them with references to relevant articles and books in which new problems of this kind are encountered. Of course, the division presented below is generally conditional, since some publications can be attributed to several areas.

1. Analysis of forced oscillations and controlled movements of a double pendu-

lum under various operation conditions, including the issues of optimal control of its movement and optimal suppression of its oscillations [3, 8, 36, 83, 88, 120, 123, 155].

2. Dynamics, stabilization and control of an inverted double pendulum and its modifications [2, 44, 55, 59, 60, 94, 107, 114, 134, 154].

3. Dynamics of a double pendulum with a vibrating suspension point [13, 19, 56, 84, 97, 116, 139].

4. Stability of equilibrium positions, dynamics and motion control of spatial modifications of a double pendulum [1, 50, 85, 90, 124].

5. Numerical and experimental study of various problems of a double pendulum, computer simulation of a double pendulum in application software packages with visual visualization of its dynamic behavior [30, 33, 89, 93, 98, 100, 103, 104, 111, 129, 152, 156].

6. Analytical study of the movements of a double pendulum with large deviations [38, 39, 113, 118, 128, 133, 146].

7. Analysis of the chaotic behavior of a double pendulum [49, 52, 101, 122, 125, 132, 138, 145].

Summarizing the above, we can conclude that the double pendulum is a fairly well-studied object in many respects. As can be seen, a significant number of publications are devoted to the numerical integration of the motion equations of a double pendulum, which are preliminarily written in a form convenient for this purpose (Lagrangian or Hamiltonian), and the subsequent establishment of various features of its behavior. In this case, the flat variant of the double pendulum is most often considered, which greatly simplifies all constructions and reasoning.

1.3. Conclusions on First Chapter

The presented detailed literature review of publications devoted to the mechanics of a double pendulum allows us to identify some areas in which research on this object can be continued. First of all, of great interest is just the mechanics of spatial variants of a double pendulum, which movements can have a more diverse character and will cover a wider variety of configurations than a flat double pendulum. Nevertheless, it must be emphasized that even for the flat two-link

pendulum there are still a number of issues that require serious discussion and thorough research. As for the spatial variants of the double pendulum, one of them is a double pendulum whose joint axes are not collinear to each other. Naturally, the range of applicability of these pendulums turns out to be much larger, and they are widely used in practice, since such non-collinearity is characteristic of many real manipulator designs. As a result, questions arise in the study of conservative, dissipative and controllable models of the mentioned systems in a linear or nonlinear formulation, as well as questions of optimal damping of their oscillatory motions, which are of serious theoretical and applied importance and should be solved using a reasonable combination of analytical and numerical methods. This dissertation is in this direction.

2. Equations of Motion of Spatial Double Pendulum and Analysis of its Small Oscillations

2.1. Design Scheme of Spatial Double Pendulum

We turn to a study of the design scheme of double pendulum consisting of two pivotally connected identical mathematical pendulums of length l and with end loads of mass m [144]. In the future, such an identity will make it possible to construct analytical solutions to all the posed tasks and conduct their exhaustive study. We assume that axes of both cylindrical joints are horizontal and form an angle α between themselves in their main equilibrium position, when both links lie on the same vertical, and joint angles of their rotation are equal to zero, so that these axes are not collinear to each other (Fig. 2.1). Without loss of generality, we can consider this angle to be acute if it is counted appropriately. As result, the geometry and kinematics of this system are much more complicated than in the case of a simple flat double pendulum.

The Fig. 2.2 shows the deflected position of the considered double pendulum. We consider the articulated rotation angles θ_1 and θ_2 as the generalized coordinates. For the convenience of further actions, we introduce a rectangular Cartesian coordinate system xyz with the fixed orthogonal basis $\underline{i}\underline{j}\underline{k}$ connected, so that in the state of main equilibrium the first link is directed along the unit vector $\underline{i}$. In addition, we introduce a movable orthogonal basis $\underline{i}'\underline{j}'\underline{k}'$ connected with the

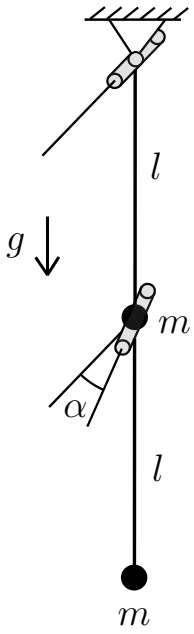

Fig. 2.1. Equilibrium position

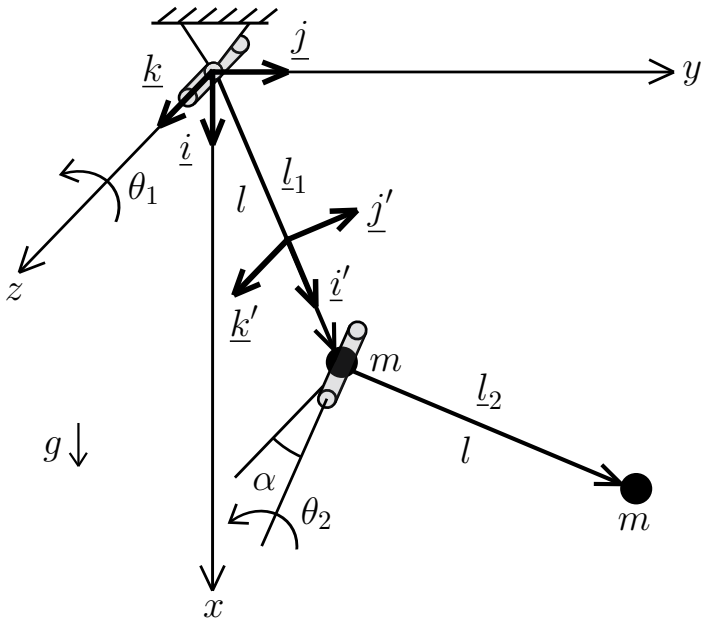

Fig. 2.2. Deflected position

first link, where unit vector $\underline{i}'$ is directed along the axis of this link from the input (first) joint to the output (second) joint rotated by an angle α relatively to the input joint.

2.2. Motion Equations of Spatial Double Pendulum

In order to derive the motion equations of spatial double pendulum we proceed to the calculation of its kinetic and potential energies. It is clear that energies of the first load are easily determined and cause no problems, since its speed is $v_1 = l\dot{\theta}_1$ and the vertical coordinate is given by expression $x_1 = l\cos\theta_1$. Main difficulty here is to find the speed and vertical coordinate of the second end load which makes a complex spatial motion determined by the angles θ_1, θ_2 and α. The simplest way to find the velocity of this load is a coordinate method in which it is necessary to determine the Cartesian coordinates of this load in a fixed basis and then find the projections of velocity on the corresponding coordinate axes.

With this purpose, we obtain the expression for radius vector $\underline{r}_2$ of the second load. For this we first find the vectors $\underline{l}_1$ and $\underline{l}_2$ which have the following length and direction of links in the basis $\underline{i}'\underline{j}'\underline{k}'$ with simple representations. The expression

for $\underline{l}_1$ is obvious, while to determine $\underline{l}_2$ it is necessary to refer to Fig. 2.3, where the coordinate system $x'y'z'$ is represented, to which the basis $\underline{i}'\underline{j}'\underline{k}'$ corresponds. As a result, it is easy to obtain that

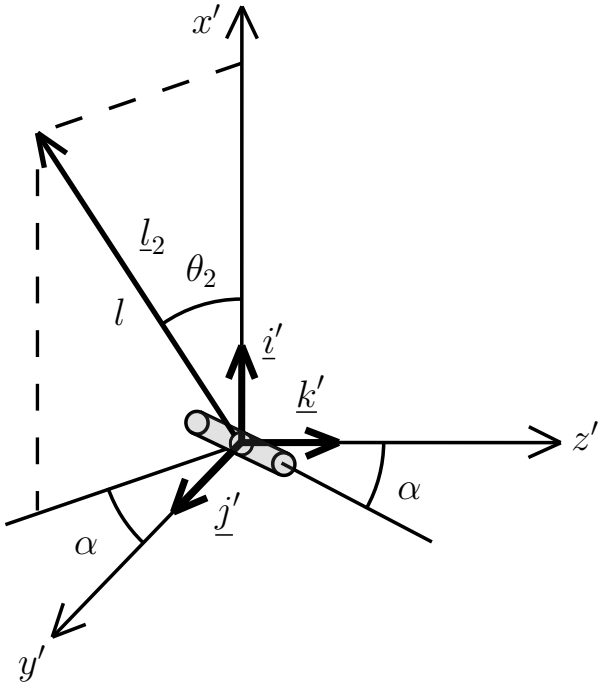

Fig. 2.3. To the calculation of the vector $\underline{l}_2$

$$\underline{l}_1 = l\underline{i}', \quad \underline{l}_2 = l(\cos\theta_2\underline{i}' + \cos\alpha\sin\theta_2\underline{j}' - \sin\alpha\sin\theta_2\underline{k}'). \tag{2.2.1}$$

Summarizing these vectors, we obtain the desired vector $\underline{r}_2$:

$$\underline{r}_2 = \underline{l}_1 + \underline{l}_2 = l\left[(1+\cos\theta_2)\underline{i}' + \cos\alpha\sin\theta_2\underline{j}' - \sin\alpha\sin\theta_2\underline{k}'\right]. \tag{2.2.2}$$

Considering the obvious relations between the unit vectors of the bases $\underline{i}'\underline{j}'\underline{k}'$ and $\underline{i}\underline{j}\underline{k}$

$$\underline{i}' = \cos\theta_1\underline{i} + \sin\theta_1\underline{j}, \quad \underline{j}' = -\sin\theta_1\underline{i} + \cos\theta_1\underline{j}, \quad \underline{k}' = \underline{k}, \tag{2.2.3}$$

we get the expression for $\underline{r}_2$ in motionless basis $\underline{i}\underline{j}\underline{k}$:

$$\begin{aligned}\underline{r}_2 = l\,[&((1+\cos\theta_2)\cos\theta_1 - \cos\alpha\sin\theta_2\sin\theta_1)\,\underline{i} + \\ &+ ((1+\cos\theta_2)\sin\theta_1 + \cos\alpha\sin\theta_2\cos\theta_1)\,\underline{j} - \sin\alpha\sin\theta_2\underline{k}\big].\end{aligned} \tag{2.2.4}$$

From this expression, Cartesian coordinates of the second load in the xyz coordinate system can be found:

$$\begin{cases} x_2 = l\,[(1+\cos\theta_2)\cos\theta_1 - \cos\alpha\sin\theta_2\sin\theta_1] \\ y_2 = l\,[(1+\cos\theta_2)\sin\theta_1 + \cos\alpha\sin\theta_2\cos\theta_1] \\ z_2 = -l\sin\alpha\sin\theta_2 \end{cases}. \tag{2.2.5}$$

Differentiating these expressions by time, one can find the projection of the velocity of second load on coordinate axes:

$$\begin{cases} \dot{x}_2 = l\left[(-(1+\cos\theta_2)\sin\theta_1 - \cos\alpha\sin\theta_2\cos\theta_1)\,\dot{\theta}_1 - \right. \\ \qquad\qquad \left. - (\sin\theta_2\cos\theta_1 + \cos\alpha\cos\theta_2\sin\theta_1)\,\dot{\theta}_2\right] \\ \dot{y}_2 = l\left[((1+\cos\theta_2)\cos\theta_1 - \cos\alpha\sin\theta_2\sin\theta_1)\,\dot{\theta}_1 + \right. \\ \qquad\qquad \left. + (-\sin\theta_2\sin\theta_1 + \cos\alpha\cos\theta_2\cos\theta_1)\,\dot{\theta}_2\right] \\ \dot{z}_2 = -l\sin\alpha\cos\theta_2\dot{\theta}_2 \end{cases}. \tag{2.2.6}$$

As a result, it is possible to determine the desired velocity of the second load:

$$v_2^2 = \dot{x}_2^2 + \dot{y}_2^2 + \dot{z}_2^2 = l^2\left[\left(1+\cos^2\alpha + 2\cos\theta_2 + \sin^2\alpha\cos^2\theta_2\right)\dot{\theta}_1^2 + \right. \\ \left. + 2\cos\alpha(1+\cos\theta_2)\dot{\theta}_1\dot{\theta}_2 + \dot{\theta}_2^2\right]. \tag{2.2.7}$$

Therefore, kinetic energy of the system is determined by expression:

$$T = \frac{1}{2}m(v_1^2 + v_2^2) = \frac{1}{2}ml^2\left[\left(2+\cos^2\alpha + 2\cos\theta_2 + \sin^2\alpha\cos^2\theta_2\right)\dot{\theta}_1^2 + \right. \\ \left. + 2\cos\alpha(1+\cos\theta_2)\dot{\theta}_1\dot{\theta}_2 + \dot{\theta}_2^2\right] = \frac{1}{2}\dot{\boldsymbol{\theta}}^{\mathrm{T}}\mathbf{A}(\boldsymbol{\theta})\dot{\boldsymbol{\theta}}. \tag{2.2.8}$$

Here $\boldsymbol{\theta} = [\theta_1, \theta_2]^{\mathrm{T}}$ is the column of generalized coordinates, and kinetic energy matrix $\mathbf{A}(\boldsymbol{\theta})$ is determined by expression:

$$\mathbf{A}(\boldsymbol{\theta}) = ml^2\begin{bmatrix} 2+\cos^2\alpha + 2\cos\theta_2 + \sin^2\alpha\cos^2\theta_2 & \cos\alpha(1+\cos\theta_2) \\ \cos\alpha(1+\cos\theta_2) & 1 \end{bmatrix}, \tag{2.2.9}$$

and it is symmetric: $\mathbf{A}^{\mathrm{T}} = \mathbf{A}$. Potential energy of this system has the form:

$$\Pi = mg(3l - x_1 - x_2) = \\ = mgl\left[3 - (2+\cos\theta_2)\cos\theta_1 + \cos\alpha\sin\theta_2\sin\theta_1\right] = \Pi(\boldsymbol{\theta}), \tag{2.2.10}$$

where an additive constant is added, so that $\Pi = 0$ at equilibrium position $\theta_1 = 0$, $\theta_2 = 0$. This was done for the convenience of expanding Π into a Taylor series in the further study of small oscillations.

Substituting expressions (2.2.8) and (2.2.10) into Lagrange equations of the second kind in matrix form [45]

$$\frac{d}{dt}\frac{\partial T}{\partial\dot{\boldsymbol{\theta}}} - \frac{\partial T}{\partial\boldsymbol{\theta}} = -\frac{\partial\Pi}{\partial\boldsymbol{\theta}}, \tag{2.2.11}$$

we obtain, after series of transformations, the equations of motion of spatial double pendulum in the well-known matrix form

$$\mathbf{A}(\boldsymbol{\theta})\ddot{\boldsymbol{\theta}} + \mathbf{B}(\boldsymbol{\theta}, \dot{\boldsymbol{\theta}}) + \mathbf{C}(\boldsymbol{\theta}) = 0, \tag{2.2.12}$$

where the matrix $\mathbf{A}(\boldsymbol{\theta})$ has the representation (2.2.9), and the columns $\mathbf{B}(\boldsymbol{\theta}, \dot{\boldsymbol{\theta}})$ and $\mathbf{C}(\boldsymbol{\theta})$ are determined by expressions:

$$\begin{gathered}\mathbf{B}(\boldsymbol{\theta}, \dot{\boldsymbol{\theta}}) = ml^2 \sin\theta_2 \begin{bmatrix} -\left(2\left(1+\sin^2\alpha\cos\theta_2\right)\dot{\theta}_1 + \cos\alpha\dot{\theta}_2\right)\dot{\theta}_2 \\ (1+\sin^2\alpha\cos\theta_2)\dot{\theta}_1^2 \end{bmatrix}, \\ \mathbf{C}(\boldsymbol{\theta}) = mgl \begin{bmatrix} (2+\cos\theta_2)\sin\theta_1 + \cos\alpha\sin\theta_2\cos\theta_1 \\ \sin\theta_2\cos\theta_1 + \cos\alpha\cos\theta_2\sin\theta_1 \end{bmatrix}.\end{gathered} \tag{2.2.13}$$

Due to the conservatism of the system under consideration, the energy integral $T + \Pi = E = \text{const}$ takes place, or explicitly:

$$\begin{aligned}E = \frac{1}{2}ml^2 \Big[\left(2+\cos^2\alpha+2\cos\theta_2+\sin^2\alpha\cos^2\theta_2\right)\dot{\theta}_1^2 + 2\cos\alpha(1+\cos\theta_2)\dot{\theta}_1\dot{\theta}_2 + \\ +\dot{\theta}_2^2\Big] + mgl\left[3-(2+\cos\theta_2)\cos\theta_1+\cos\alpha\sin\theta_2\sin\theta_1\right] = \text{const}\,.\end{aligned} \tag{2.2.14}$$

This integral will be needed later to control the correctness of the expressions that will be obtained in the analysis of nonlinear oscillation modes of spatial double pendulum.

The nonlinear mathematical model (2.2.12) is the basis for all subsequent studies in this work. As is known, the Lagrange equations can be solved with respect to the generalized accelerations, since the matrix $\mathbf{A}$ is nonsingular [48]. Therefore, for numerical integration of the nonlinear matrix equation (2.2.12), it is convenient to represent it in the following form:

$$\ddot{\boldsymbol{\theta}} = -\mathbf{A}^{-1}(\boldsymbol{\theta})\left[\mathbf{B}(\boldsymbol{\theta}, \dot{\boldsymbol{\theta}}) + \mathbf{C}(\boldsymbol{\theta})\right]. \tag{2.2.15}$$

2.3. Particular Variants of Flat and Orthogonal Double Pendulum

Let us consider two interesting particular cases to which special attention should be paid. The results obtained for these cases will later help to control the

correctness of general formulas where the dependence on angle α will take place.

1. Flat double pendulum. In the case when $\alpha = 0$, i.e. the double pendulum is flat (Fig. 2.4), the expressions for the energies (2.2.8) and (2.2.10) take the simpler form [126]:

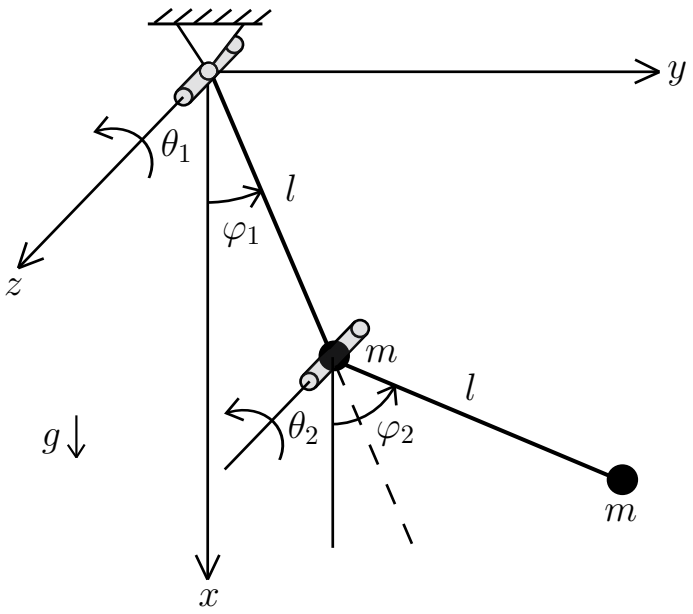

Fig. 2.4. Flat double pendulum

$$T = \frac{1}{2} ml^2 \left[(3 + 2\cos\theta_2)\,\dot\theta_1^2 + 2(1 + \cos\theta_2)\dot\theta_1\dot\theta_2 + \dot\theta_2^2 \right], \tag{2.3.1}$$

$$\Pi = mgl\,[3 - (2 + \cos\theta_2)\cos\theta_1 + \sin\theta_2 \sin\theta_1]\,. \tag{2.3.2}$$

Then the motion equations have the form (2.2.12), where according to (2.2.9) and (2.2.13)

$$\mathbf{A}(\boldsymbol{\theta}) = ml^2 \begin{bmatrix} 3 + 2\cos\theta_2 & 1 + \cos\theta_2 \\ 1 + \cos\theta_2 & 1 \end{bmatrix},$$

$$\mathbf{B}(\boldsymbol{\theta}, \dot{\boldsymbol{\theta}}) = ml^2 \sin\theta_2 \begin{bmatrix} -(2\dot\theta_1 + \dot\theta_2)\dot\theta_2 \\ \dot\theta_1^2 \end{bmatrix}, \quad \mathbf{C}(\boldsymbol{\theta}) = mgl \begin{bmatrix} 2\sin\theta_1 + \sin(\theta_1 + \theta_2) \\ \sin(\theta_1 + \theta_2) \end{bmatrix}. \tag{2.3.3}$$

We emphasize that the motion equations of a flat double pendulum will take an even simpler form if we introduce another pair of generalized coordinates φ_1 and φ_2, assuming $\varphi_1 = \theta_1$ and $\varphi_2 = \theta_1 + \theta_2$. These new coordinates represent the absolute deviation angles of the pendulum links from the vertical (Fig. 2.4). As a

result, we get from (2.3.1) the expression for the kinetic energy [22]:

$$T = \frac{1}{2}ml^2\left[2\dot{\varphi}_1^2 + 2\cos(\varphi_2 - \varphi_1)\dot{\varphi}_1\dot{\varphi}_2 + \dot{\varphi}_2^2\right] = \frac{1}{2}\dot{\boldsymbol{\varphi}}^{\mathrm{T}}\mathbf{A}(\boldsymbol{\varphi})\dot{\boldsymbol{\varphi}}, \tag{2.3.4}$$

where $\boldsymbol{\varphi} = [\varphi_1, \varphi_2]^{\mathrm{T}}$, and the symmetric matrix $\mathbf{A}(\boldsymbol{\varphi})$ now has the form:

$$\mathbf{A}(\boldsymbol{\varphi}) = ml^2\begin{bmatrix} 2 & \cos(\varphi_2 - \varphi_1) \\ \cos(\varphi_2 - \varphi_1) & 1 \end{bmatrix}. \tag{2.3.5}$$

Potential energy according to (2.3.2) will then be determined by the formula:

$$\Pi = mgl\,(3 - 2\cos\varphi_1 - \cos\varphi_2)\,. \tag{2.3.6}$$

Using again the Lagrange equations of the second kind in matrix form

$$\frac{d}{dt}\frac{\partial T}{\partial\dot{\boldsymbol{\varphi}}} - \frac{\partial T}{\partial\boldsymbol{\varphi}} = -\frac{\partial\Pi}{\partial\boldsymbol{\varphi}}, \tag{2.3.7}$$

we arrive after transformations at a notation similar to (2.2.12), namely:

$$\mathbf{A}(\boldsymbol{\varphi})\ddot{\boldsymbol{\varphi}} + \mathbf{B}(\boldsymbol{\varphi}, \dot{\boldsymbol{\varphi}}) + \mathbf{C}(\boldsymbol{\varphi}) = 0, \tag{2.3.8}$$

where the columns $\mathbf{B}(\boldsymbol{\varphi}, \dot{\boldsymbol{\varphi}})$ and $\mathbf{C}(\boldsymbol{\varphi})$ are now defined by expressions:

$$\mathbf{B}(\boldsymbol{\varphi}, \dot{\boldsymbol{\varphi}}) = ml^2\sin(\varphi_2 - \varphi_1)\begin{bmatrix} -\dot{\varphi}_2^2 \\ \dot{\varphi}_1^2 \end{bmatrix}, \quad \mathbf{C}(\boldsymbol{\varphi}) = mgl\begin{bmatrix} 2\sin\varphi_1 \\ \sin\varphi_2 \end{bmatrix}. \tag{2.3.9}$$

It can be seen that this notation is more preferable in the study of free motions of a flat double pendulum. This ensures the advantage of the angles φ_1 and φ_2 over the interlink angles θ_1 and θ_2, in which the motion equations have a more complex form. We also write the energy integral for this case based on the expressions (2.3.4) and (2.3.6):

$$E = \frac{1}{2}ml^2[2\dot{\varphi}_1^2 + 2\dot{\varphi}_1\dot{\varphi}_2\cos(\varphi_2 - \varphi_1) + \dot{\varphi}_2^2] + mgl\,(3 - 2\cos\varphi_1 - \cos\varphi_2) = \text{const}\,. \tag{2.3.10}$$

For numerical integration of the matrix equation (2.3.8), it should be solved with respect to the column of generalized accelerations by analogy with (2.2.15):

$$\ddot{\boldsymbol{\varphi}} = -\mathbf{A}^{-1}(\boldsymbol{\varphi})\left[\mathbf{B}(\boldsymbol{\varphi}, \dot{\boldsymbol{\varphi}}) + \mathbf{C}(\boldsymbol{\varphi})\right]. \tag{2.3.11}$$

2. Orthogonal double pendulum. Let us now consider another particular case, when $\alpha = \pi/2$. Such a double pendulum will be further called orthogonal,

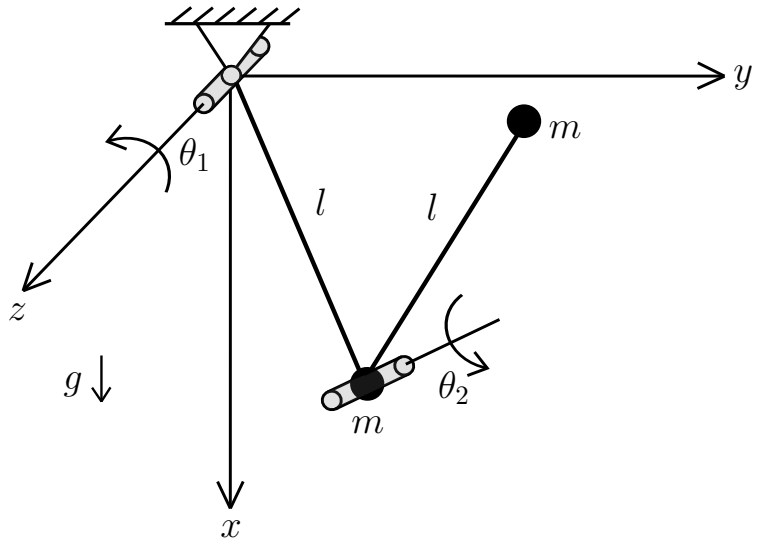

Fig. 2.5. Orthogonal double pendulum

and thus emphasizes that in this version the joint axes of both pendulums are perpendicular (Fig. 2.5) [50]. In this case, the expressions (2.2.9) and (2.2.13) are also significantly simplified, becoming:

$$\mathbf{A}(\boldsymbol{\theta}) = ml^2 \begin{bmatrix} 2 + 2\cos\theta_2 + \cos^2\theta_2 & 0 \\ 0 & 1 \end{bmatrix}, \quad \mathbf{A}^{\mathrm{T}} = \mathbf{A}, \tag{2.3.12}$$

$$\mathbf{B}(\boldsymbol{\theta}, \dot{\boldsymbol{\theta}}) = ml^2 \sin\theta_2 \begin{bmatrix} -2\,(1 + \cos\theta_2)\,\dot{\theta}_1\dot{\theta}_2 \\ (1 + \cos\theta_2)\dot{\theta}_1^2 \end{bmatrix}, \quad \mathbf{C}(\boldsymbol{\theta}) = mgl \begin{bmatrix} (2 + \cos\theta_2)\sin\theta_1 \\ \sin\theta_2 \cos\theta_1 \end{bmatrix}. \tag{2.3.13}$$

2.4. Determination of Frequencies and Modes of Small Oscillations of Spatial Double Pendulum

We turn now to the analysis of the linear model of spatial double pendulum. For this purpose, we linearize the nonlinear motion equation (2.2.12) near the stable equilibrium $\theta_1 = 0$, $\theta_2 = 0$ and obtain the traditional linear matrix equation:

$$\mathbf{A}_0\ddot{\boldsymbol{\theta}} + \mathbf{C}_0\boldsymbol{\theta} = 0, \tag{2.4.1}$$

where the constant symmetric matrices of inertial $\mathbf{A}_0$ and quasi-elastic $\mathbf{C}_0$ coefficients have the forms:

$$\mathbf{A}_0 = ml^2 \begin{bmatrix} 5 & 2\cos\alpha \\ 2\cos\alpha & 1 \end{bmatrix}, \quad \mathbf{C}_0 = mgl \begin{bmatrix} 3 & \cos\alpha \\ \cos\alpha & 1 \end{bmatrix}. \tag{2.4.2}$$

The equation (2.4.1) corresponds to the following quadratic approximations of the kinetic and potential energies:

$$\begin{aligned} T &= \frac{1}{2}ml^2\left(5\dot{\theta}_1^2 + 4\cos\alpha\dot{\theta}_1\dot{\theta}_2 + \dot{\theta}_2^2\right) = \frac{1}{2}\dot{\boldsymbol{\theta}}^{\mathrm{T}}\mathbf{A}_0\dot{\boldsymbol{\theta}}, \\ \Pi &= \frac{1}{2}mgl\left(3\theta_1^2 + 2\cos\alpha\theta_1\theta_2 + \theta_2^2\right) = \frac{1}{2}\boldsymbol{\theta}^{\mathrm{T}}\mathbf{C}_0\boldsymbol{\theta}. \end{aligned} \tag{2.4.3}$$

1. Determination of oscillation frequencies. We will seek the solution of the matrix equation (2.4.1) in the form of single-frequency harmonic oscillations:

$$\boldsymbol{\theta} = \boldsymbol{\Theta}\cos(k_0 t + \psi_0), \tag{2.4.4}$$

where $\boldsymbol{\Theta}$ is the unknown column of oscillation amplitudes of generalized coordinates, k_0 is the oscillation frequency, ψ_0 is the initial oscillation phase. Substituting the solution (2.4.4) into the equation (2.4.1), we obtain a matrix algebraic equation with respect to the column $\boldsymbol{\Theta}$:

$$(\mathbf{C}_0 - k_0^2\mathbf{A}_0)\boldsymbol{\Theta} = 0. \tag{2.4.5}$$

This equation has a nontrivial solution only when determinant of matrix $\mathbf{C}_0 - k_0^2\mathbf{A}_0$ turns to zero:

$$\det(\mathbf{C}_0 - k_0^2\mathbf{A}_0) = 0. \tag{2.4.6}$$

Revealing this determinant taking into account representations (2.4.2), we arrive at the frequency equation, which is biquadratic with respect to the required frequency k_0:

$$(1 + 4\sin^2\alpha)k_0^4 - 4(1 + \sin^2\alpha)\frac{g}{l}k_0^2 + (2 + \sin^2\alpha)\frac{g^2}{l^2} = 0. \tag{2.4.7}$$

For the convenience of further actions, we introduce the notation: $k = \sqrt{g/l}$ is the frequency of small oscillations of an ordinary mathematical pendulum of length l, $p_0 = k_0/k$ is the dimensionless oscillation frequency of spatial double pendulum. Then the equation (2.4.7) becomes:

$$(1 + 4\sin^2\alpha)p_0^4 - 4(1 + \sin^2\alpha)p_0^2 + 2 + \sin^2\alpha = 0. \tag{2.4.8}$$

Solving this equation with respect to p_0, we find the dimensionless frequencies:

$$p_{s0} = \sqrt{\frac{2(1+\sin^2\alpha) \pm \sqrt{2-\sin^2\alpha}}{1+4\sin^2\alpha}}, \quad s = 1, 2. \tag{2.4.9}$$

Natural frequencies k_{s0} are obtained by multiplying the dimensionless frequencies by factor k. We emphasize that here and below the lower sign corresponds to the first frequency (for $s = 1$), and the upper sign corresponds to the second frequency (for $s = 2$). We also note that here, for convenience, the frequencies are provided with the index "0", in order not to confuse them with the frequencies of the dissipative and controlled systems, as well as with the frequencies of the nonlinear system.

Let us analyze the dependencies of the dimensionless frequencies on the angle α (2.4.9). It is easy to see that for a flat double pendulum to which the value $\alpha = 0$ corresponds, we obtain widely known results [14]:

$$p_{10} = \sqrt{2-\sqrt{2}} \approx 0.7654, \quad p_{20} = \sqrt{2+\sqrt{2}} \approx 1.8478. \tag{2.4.10}$$

For an orthogonal double pendulum with $\alpha = \pi/2$ we have:

$$p_{10} = \sqrt{\frac{3}{5}} \approx 0.7746, \quad p_{20} = 1. \tag{2.4.11}$$

It is easy to understand that the first of these frequencies corresponds to the movement of a two-link pendulum as a single link with two weights of mass m fixed on it at distances l and $2l$ from the fixed joint, and the other frequency corresponds to the second link movement as an ordinary pendulum with the fixed first link.

It is also possible to obtain approximate dependencies for oscillation frequencies near the boundary values $\alpha = 0$ and $\alpha = \pi/2$. Expanding (2.4.9) into a Taylor series in α in the locality of point $\alpha = 0$ and holding only one correction, we find:

$$p_{10} = \sqrt{2-\sqrt{2}}\left(1 + \frac{5\sqrt{2}-7}{8}\alpha^2\right), \quad p_{20} = \sqrt{2+\sqrt{2}}\left(1 - \frac{5\sqrt{2}+7}{8}\alpha^2\right). \tag{2.4.12}$$

It can be seen that coefficient at α^2 in the bracket for the frequency p_{10} is 0.0089, while for the frequency p_{20} it is (-1.7589). Therefore, as α increases from 0, the first frequency increases very slightly, while the second frequency begins to

decrease significantly. Similarly, approximate formulas can also be obtained near $\alpha = \pi/2$ by expanding expressions (2.4.9) in the power series of a small parameter $\varepsilon = \pi/2 - \alpha$, keeping as before only one correction:

$$p_{10} = \sqrt{\frac{3}{5}}\left(1 - \frac{1}{60}\varepsilon^2\right), \quad p_{20} = 1 + \frac{1}{4}\varepsilon^2. \tag{2.4.13}$$

It can be seen from this, that with decreasing α from $\pi/2$, the first frequency decreases only slightly, while the second frequency increases to a greater extent.

Curves of the dependence of dimensionless frequencies p_{s0} on the angle α are presented in Fig. 2.6. It is seen clearly from them that the first frequency is almost independent of α. Indeed, its highest value (at $\alpha = \pi/2$) differs from the lowest one (at $\alpha = 0$) by only 1.2%. The second frequency depends on α much more significantly.

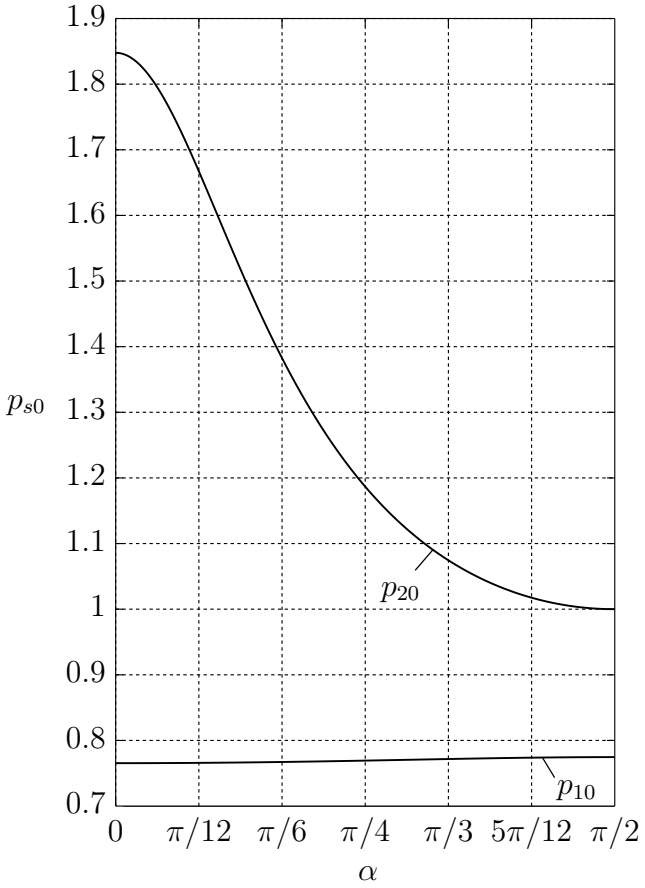

Fig. 2.6. Graph dependencies of frequencies p_{10} and p_{20} on angle α

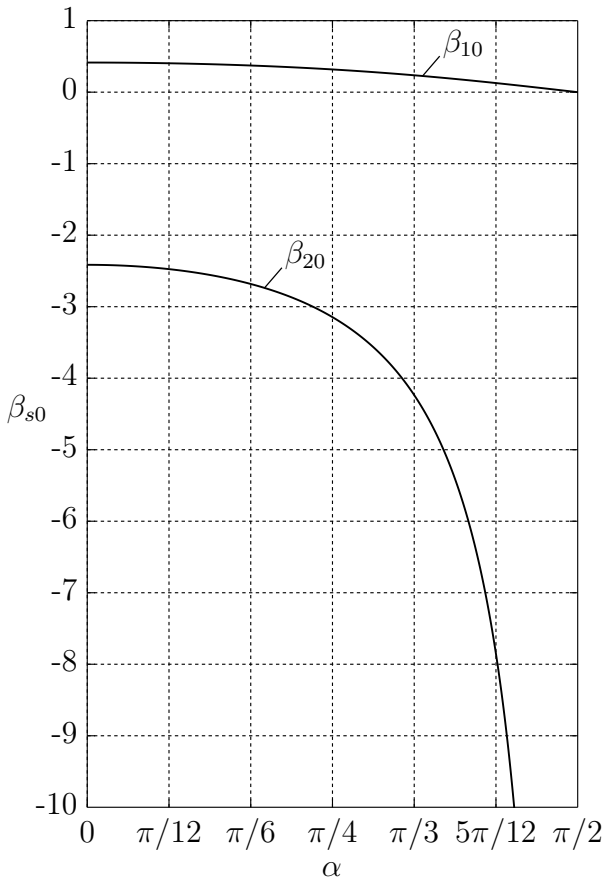

Fig. 2.7. Graph dependencies of values β_{10} and β_{20} on angle α

2. Determination of oscillations modes. Let us now find the eigenmodes corresponding to the found frequencies p_{s0}. They are determined by the ratio between the components of the column $\mathbf{\Theta} = [\Theta_1, \Theta_2]^{\mathrm{T}}$, i.e., by the ratio between

the oscillation amplitudes Θ_2 and Θ_1 of the rotation angles θ_2 and θ_1 in the pendulum joints. We characterize the oscillation mode by the relation $\beta_{s0} = \Theta_{2s}/\Theta_{1s}$. This value can be found from any of the two scalar equations corresponding to the matrix equation (2.4.5), for example, the second as simpler, because these equations become linearly dependent after substituting frequencies in them due to the condition (2.4.6). As a result, after transformations we obtain:

$$\beta_{s0} = -\frac{\cos\alpha(1-2p_{s0}^2)}{1-p_{s0}^2} = -\frac{3 \pm 2\sqrt{2-\sin^2\alpha}}{\cos 2\alpha \pm \sqrt{2-\sin^2\alpha}}\cos\alpha, \quad s = 1, 2. \quad (2.4.14)$$

Of course, the oscillation modes $\mathbf{\Theta}_{(s)}$ are determined up to a constant factor. Therefore, for further actions, it will be necessary to set some value Θ_{1s}, for example, $\Theta_{1s} = 1$. Then the value Θ_{2s} will be equal to β_{s0}, and the oscillation modes can be written as: $\mathbf{\Theta}_{(s)} = [1, \beta_{s0}]^{\mathrm{T}}$.

Let's look again at particular cases. For a flat double pendulum, when $\alpha = 0$, we find according to (2.4.14):

$$\beta_{10} = \sqrt{2} - 1 \approx 0.4142, \quad \beta_{20} = -1 - \sqrt{2} \approx -2.4142. \quad (2.4.15)$$

If we consider the oscillation modes, taking the absolute angles φ_1 and φ_2 as generalized coordinates, then another relation should be introduced: $\mu_{s0} = \Phi_{2s}/\Phi_{1s}$ $= \Theta_{2s}/\Theta_{1s} + 1 = \beta_{s0} + 1$ because $\varphi_1 = \theta_1$, $\varphi_2 = \theta_1 + \theta_2$. Then we get the following values μ_{s0}:

$$\mu_{10} = \sqrt{2} \approx 1.4142, \quad \mu_{20} = -\sqrt{2} \approx -1.4142. \quad (2.4.16)$$

Assuming for simplicity that for each of the oscillation modes $\Phi_{1s} = 1$, we obtain $\Phi_{2s} = \mp\sqrt{2}$, so that the oscillation modes in the case under consideration can be represented as the following columns:

$$\mathbf{\Phi}_{(1)} = \begin{bmatrix} 1 \\ \sqrt{2} \end{bmatrix}, \quad \mathbf{\Phi}_{(2)} = \begin{bmatrix} 1 \\ -\sqrt{2} \end{bmatrix}. \quad (2.4.17)$$

For the case $\alpha = \pi/2$ corresponding to an orthogonal double pendulum we find the following relations $\beta_{s0} = \Theta_{2s}/\Theta_{1s}$ according to (2.4.14):

$$\beta_{10} = 0, \quad \beta_{20} = -\infty, \quad (2.4.18)$$

and in the second case we have indeterminacy $0/0$, which is easily revealed, for example, according to L'Hopital's rule. Formulas (2.4.18) mean that in this case,

we can take the oscillation modes in the form: $\mathbf{\Theta}_{(1)} = [1, 0]^{\mathrm{T}}$ and $\mathbf{\Theta}_{(2)} = [0, 1]^{\mathrm{T}}$, so the oscillations in both degrees of freedom in this case are independent. This fact also is followed from expressions for matrices (2.4.2), when each of them becomes diagonal at $\alpha = \pi/2$

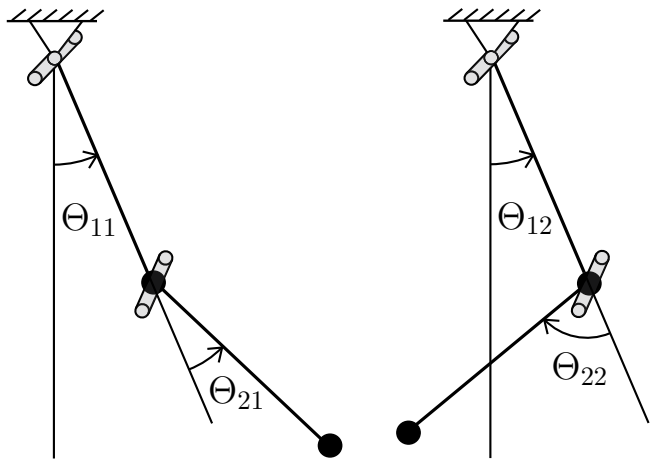

Fig. 2.8. Oscillation modes of spatial double pendulum

We also obtain approximate formulas for the values β_{s0} near the points $\alpha = 0$ and $\alpha = \pi/2$. Expanding (2.4.14) into a Taylor series in α in the locality of point $\alpha = 0$ and keeping only one correction, we find:

$$\beta_{s0} = \left(-1 \mp \sqrt{2}\right)\left(1 \pm \frac{\sqrt{2}}{4}\alpha^2\right). \tag{2.4.19}$$

To find approximating formulas near the point $\alpha = \pi/2$ we set again $\varepsilon = \pi/2 - \alpha$ and obtain the following approximate expressions:

$$\beta_{10} = \frac{\varepsilon}{2}, \quad \beta_{20} = -\frac{2}{\varepsilon}. \tag{2.4.20}$$

Curves of the dependence of values β_{s0} on the angle α are presented in Fig. 2.7. Considering that we have $\beta_{10} > 0$ and $\beta_{20} < 0$ for any value α in the range from 0 to $\pi/2$, we can schematically represent the oscillation modes of spatial double pendulum in Fig. 2.8.

3. Orthogonality conditions and normalization coefficients. We note that the found oscillation modes satisfy the orthogonality conditions [147]:

$$\mathbf{\Theta}_{(1)}^{\mathrm{T}}\mathbf{A}_0\mathbf{\Theta}_{(2)} = 0, \quad \mathbf{\Theta}_{(1)}^{\mathrm{T}}\mathbf{C}_0\mathbf{\Theta}_{(2)} = 0. \tag{2.4.21}$$

In addition, we will also need the normalization coefficients N_s, which are determined by the formulas:

$$\boldsymbol{\Theta}_{(s)}^{\mathrm{T}}\mathbf{A}_0\boldsymbol{\Theta}_{(s)} = N_s, \quad \boldsymbol{\Theta}_{(s)}^{\mathrm{T}}\mathbf{C}_0\boldsymbol{\Theta}_{(s)} = N_s k_{s0}^2. \tag{2.4.22}$$

In the case under consideration, we have:

$$N_s = ml^2\left(5 + 4\cos\alpha\beta_{s0} + \beta_{s0}^2\right). \tag{2.4.23}$$

For further calculations, it is also convenient to introduce dimensionless normalization coefficients $H_s = N_s/ml^2$:

$$H_s = 5 + 4\cos\alpha\beta_{s0} + \beta_{s0}^2. \tag{2.4.24}$$

We note that when studying a flat double pendulum, it is more convenient to introduce normalization coefficients for modes written in absolute angles. In this case, according to (2.3.5) and (2.3.9), the constant matrices of inertial and quasi-elastic coefficients are determined by the expressions:

$$\mathbf{A}_0 = ml^2\begin{bmatrix} 2 & 1 \\ 1 & 1 \end{bmatrix}, \quad \mathbf{C}_0 = mgl\begin{bmatrix} 2 & 0 \\ 0 & 1 \end{bmatrix}. \tag{2.4.25}$$

Given these expressions, it is easy to check directly that the previously recorded oscillation modes (2.4.17) also satisfy the orthogonality conditions:

$$\boldsymbol{\Phi}_{(1)}^{\mathrm{T}}\mathbf{A}_0\boldsymbol{\Phi}_{(2)} = 0, \quad \boldsymbol{\Phi}_{(1)}^{\mathrm{T}}\mathbf{C}_0\boldsymbol{\Phi}_{(2)} = 0, \tag{2.4.26}$$

and the normalization coefficients for these modes in the original and dimensionless versions will be equal to

$$N_s = \boldsymbol{\Phi}_{(s)}^{\mathrm{T}}\mathbf{A}_0\boldsymbol{\Phi}_{(s)} = 2(2 \mp \sqrt{2})ml^2, \quad H_s = 2(2 \mp \sqrt{2}). \tag{2.4.27}$$

4. Construction of a general solution. The general solution of the problem of small free oscillations of spatial double pendulum can be written as a superposition of two oscillation modes:

$$\boldsymbol{\theta} = \boldsymbol{\Theta}_{(1)}a_1\cos\psi_1 + \boldsymbol{\Theta}_{(2)}a_2\cos\psi_2, \tag{2.4.28}$$

where the full phases ψ_1 and ψ_2 are defined by the formulas:

$$\psi_1 = k_{10}t + \psi_{10}, \quad \psi_2 = k_{20}t + \psi_{20}, \tag{2.4.29}$$

where ψ_{10}, ψ_{20} are the initial values of these phases, and a_1 and a_2 are values characterizing the amplitudes of each of the oscillation modes in the solution (2.4.28), and they are determined by given columns of initial conditions $\boldsymbol{\theta}_0$, $\dot{\boldsymbol{\theta}}_0$ for $t = 0$. It can be seen from (2.4.28) that, in the general case, the oscillations of a double pendulum have a two-frequency character, i.e., they are not strictly periodic. However, if the initial conditions are chosen in a special way, then it is possible to achieve oscillations of the system in only one of the modes. To discuss this issue in more detail, we write a system for determining unknown integration constants:

$$\begin{cases} \boldsymbol{\theta}_0 = \boldsymbol{\Theta}_{(1)} a_1 \cos\psi_{10} + \boldsymbol{\Theta}_{(2)} a_2 \cos\psi_{20} \\ \dot{\boldsymbol{\theta}}_0 = -\boldsymbol{\Theta}_{(1)} a_1 k_{10} \sin\psi_{10} - \boldsymbol{\Theta}_{(2)} a_2 k_{20} \sin\psi_{20} \end{cases}. \tag{2.4.30}$$

Multiplying each of these equations by $\boldsymbol{\Theta}_{(1)}^{\mathrm{T}}\mathbf{A}_0$ on the left and taking into account the first orthogonality condition (2.4.21), we find:

$$C_1 = a_1 \cos\psi_{10} = \frac{\boldsymbol{\Theta}_{(1)}^{\mathrm{T}}\mathbf{A}_0\boldsymbol{\theta}_0}{N_1}, \quad D_1 = -a_1 \sin\psi_{10} = \frac{\boldsymbol{\Theta}_{(1)}^{\mathrm{T}}\mathbf{A}_0\dot{\boldsymbol{\theta}}_0}{N_1 k_{10}}. \tag{2.4.31}$$

Similarly, if we multiply each of the equations (2.4.30) by $\boldsymbol{\Theta}_{(2)}^{\mathrm{T}}\mathbf{A}_0$ on the left, we get two more relations:

$$C_2 = a_2 \cos\psi_{20} = \frac{\boldsymbol{\Theta}_{(2)}^{\mathrm{T}}\mathbf{A}_0\boldsymbol{\theta}_0}{N_2}, \quad D_2 = -a_2 \sin\psi_{20} = \frac{\boldsymbol{\Theta}_{(2)}^{\mathrm{T}}\mathbf{A}_0\dot{\boldsymbol{\theta}}_0}{N_2 k_{20}}. \tag{2.4.32}$$

It should be emphasized that it does not make sense to find the constants ψ_{10}, ψ_{20}, a_1 and a_2, since the expression (2.4.28) taking into account (2.4.29), (2.4.31) and (2.4.32) can be rewritten as:

$$\boldsymbol{\theta} = \boldsymbol{\Theta}_{(1)} \left(C_1 \cos k_{10}t + D_1 \sin k_{10}t\right) + \boldsymbol{\Theta}_{(2)} \left(C_2 \cos k_{20}t + D_2 \sin k_{20}t\right), \tag{2.4.33}$$

therefore it is sufficient to know only C_1, D_1, C_2 and D_2 according to (2.4.31) and (2.4.32). Now it is easy to understand that in order for the motion of a double pendulum to be single-frequency, i.e., to represent only one mode, for example, the first one, we should set the initial conditions in the form:

$$\boldsymbol{\theta}_0 = \mu\boldsymbol{\Theta}_{(1)}, \quad \dot{\boldsymbol{\theta}}_0 = \eta\boldsymbol{\Theta}_{(1)}, \tag{2.4.34}$$

i.e. proportional to this modes, where μ and η are arbitrary constants. Indeed, in this case, according to (2.4.32), we will have $C_2 = 0$, $D_2 = 0$. Similarly, to excite only the second mode, the initial motion conditions should be set in the form:

$$\boldsymbol{\theta}_0 = \mu\boldsymbol{\Theta}_{(2)}, \quad \dot{\boldsymbol{\theta}}_0 = \eta\boldsymbol{\Theta}_{(2)}. \tag{2.4.35}$$

2.5. Dissipative Model of Spatial Double Pendulum

The conservative model of spatial double pendulum was considered above and its small oscillations were analyzed. At the same time, it is clear that in any real system there are inevitably resistance forces that arise naturally (friction in the articulation joints, resistance from the environment, etc.), which must be taken into account in order to build a more adequate model of this system. In addition, dissipative forces can be specially introduced into the system using friction elements (oscillation dampers). Various dissipative models of a flat double pendulum in the presence of viscous, dry and quadratic friction are presented in [18, 45, 115, 136].

Let us turn to the study of the simplest dissipative model of spatial double pendulum, assuming that it has viscous friction in both of its joints with the same coefficient b [141]. As is known, a dissipative Rayleigh function is constructed to take into account friction forces, and it has the following form in the case under consideration [32]:

$$R = \frac{1}{2}b(\dot{\theta}_1^2 + \dot{\theta}_2^2) = \frac{1}{2}\dot{\boldsymbol{\theta}}^{\mathrm{T}}\mathbf{B_0}\dot{\boldsymbol{\theta}}, \quad \mathbf{B}_0 = b\begin{bmatrix} 1 & 0 \\ 0 & 1 \end{bmatrix}, \tag{2.5.1}$$

where the matrix of dissipative coefficients $\mathbf{B}_0$ is diagonal. Using the Lagrange equations of the second kind for a dissipative system in matrix form

$$\frac{d}{dt}\frac{\partial T}{\partial \dot{\boldsymbol{\theta}}} - \frac{\partial T}{\partial \boldsymbol{\theta}} = -\frac{\partial \Pi}{\partial \boldsymbol{\theta}} - \frac{\partial R}{\partial \dot{\boldsymbol{\theta}}} \tag{2.5.2}$$

and bearing in mind the further study of the linear model of the dissipative process, let us substitute into (2.5.2) immediately the quadratic approximations of the kinetic and potential energies (2.4.3), as well as the dissipative function (2.5.1). As a result, we can arrive at a matrix equation in the classical form [10]:

$$\mathbf{A}_0\ddot{\boldsymbol{\theta}} + \mathbf{B}_0\dot{\boldsymbol{\theta}} + \mathbf{C}_0\boldsymbol{\theta} = 0, \tag{2.5.3}$$

where constant matrices of inertial $\mathbf{A}_0$ and quasi-elastic $\mathbf{C}_0$ coefficients have representations (2.4.2). We will look for a solution of the equation (2.5.3) in the form

$$\boldsymbol{\theta} = \boldsymbol{\Theta}e^{\lambda t}. \tag{2.5.4}$$

Substituting (2.5.4) into (2.5.3), we arrive at an algebraic matrix equation for the unknown column $\mathbf{\Theta}$:

$$(\mathbf{A}_0\lambda^2 + \mathbf{B}_0\lambda + \mathbf{C}_0)\mathbf{\Theta} = 0, \tag{2.5.5}$$

for which the condition for the existence of a nontrivial solution has the form:

$$\det\left(\mathbf{A}_0\lambda^2 + \mathbf{B}_0\lambda + \mathbf{C}_0\right) = 0. \tag{2.5.6}$$

To solve this characteristic equation, we analyze the structure of the matrices $\mathbf{A}_0$, $\mathbf{B}_0$, and $\mathbf{C}_0$. It is easy to establish that for any value of the angle α there is a simple linear relationship between them:

$$\mathbf{A}_0 + \frac{1}{2n}\mathbf{B}_0 = \frac{2}{k^2}\mathbf{C}_0, \quad 2n = \frac{b}{ml^2}, \tag{2.5.7}$$

where, for convenience, the value n is introduced, which has the meaning of the damping factor of small oscillations of an ordinary mathematical pendulum of length l with an end load of mass m, and viscous friction with coefficient b acts in its joint. Eliminating (2.5.7) matrix $\mathbf{B}_0$ from (2.5.6), we get the following equation:

$$\det\left[\mathbf{A}_0(\lambda^2 - 2n\lambda) + \mathbf{C}_0\left(1 + \frac{4n}{k^2}\lambda\right)\right] = 0. \tag{2.5.8}$$

By comparing it with the frequency equation of the conservative system (2.4.6), which is satisfied by the natural frequencies k_{s0} without dissipative forces, we establish that values λ are determined from the following two equations:

$$\lambda^2 - 2n\lambda = -k_{s0}^2\left(1 + \frac{4n}{k^2}\lambda\right), \quad s = 1, 2. \tag{2.5.9}$$

It also follows from this that oscillation modes of the dissipative system, determined from (2.5.5) taking into account (2.5.7) and (2.5.9), will remain the same as in the conservative system, i.e., they will match the previously found columns $\mathbf{\Theta}_{(s)}$ [10].

It is well known that dissipative forces in a multidimensional mechanical system in the general case distort free oscillation modes, which took place in the absence of friction [147]. In addition, if the dissipative forces are quite large, which occurs when friction elements (oscillation dampers) are specially introduced into the system, then they can significantly distort the oscillation modes [78]. However, in some cases of damping, which are of particular interest, it turns out that the introduction of both small and large dissipative forces into the system does not

violate its conservative oscillation modes [16, 61]. This circumstance will make it possible to damp the oscillations of the systems according to its own, i.e., natural movements, without distorting their general character, but only by decreasing the amplitudes of each mode. In particular, if the movement of the system represents only one oscillation mode, then only this mode should be smoothly extinguished without complicating its structure. It is known that a similar effect occurs only for the so-called "proportional damping", which takes place in our case, since the matrix $\mathbf{B}_0$ is a linear combination of matrices $\mathbf{A}_0$ and $\mathbf{C}_0$ according to (2.5.7). This remarkable property of spatial double pendulum with identical geometrical, inertial and dissipative parameters at any angle α makes it possible to obtain the simplest analytical expressions and qualitatively analyze the movements of spatial double pendulum in the presence of viscous friction, as well as investigate in detail many additional issues. We note that if the friction is too high, the fading of some part of the solution may already be aperiodic, and as a result, it is more correct to call the column $\mathbf{\Theta}_{(s)}$ corresponding to it not the oscillation mode, but the motion mode.

We emphasize that for an arbitrary spatial double pendulum with different masses of end loads and different lengths of links, proper selection of two dissipative coefficients of articulated viscous friction can ensure the independence of the oscillation modes from damping. Indeed, the "proportional damping" condition $\mathbf{B}_0 = \gamma_A \mathbf{A}_0 + \gamma_C \mathbf{C}_0$ in scalar form gives a system of three equations for finding four values – two dissipative coefficients and two uncertain parameters γ_A, γ_C, so that it is underdetermined. As a result, there is not one solution, but a family of them, which allows to choose dissipative coefficients to provide the desired condition, as shown in [141]. However, for more complex multi-link structures, the situation is completely different. For example, for a three-link pendulum, we can control the values of the dissipative coefficients in each of the three joints and we have two more undefined parameters γ_A and γ_C, while the "proportional damping" condition will already give six scalar equations. Therefore, in this situation we get an overdetermined system, which is incompatible in the general case. A similar conclusion can be drawn for systems with a large number of degrees of freedom, so that of all multi-links, only a two-link with arbitrary parameters of its links and loads can have the property of independence of the oscillation modes from damping.

Returning now to the equations (2.5.9) for the original scheme of spatial double pendulum with identical geometric, inertial and dissipative parameters, we transform them to the form:

$$\lambda^2 + 2n_s\lambda + k_{s0}^2 = 0, \quad s = 1, 2, \tag{2.5.10}$$

where the following notation is introduced:

$$n_s = (2p_{s0}^2 - 1)n = \frac{3 \pm 2\sqrt{2 - \sin^2\alpha}}{1 + 4\sin^2\alpha}n. \tag{2.5.11}$$

The solutions of the equations (2.5.10) obviously have the form:

$$\lambda_{1,2} = -n_1 \pm ik_1, \quad \lambda_{3,4} = -n_2 \pm ik_2, \tag{2.5.12}$$

where the notation is also adopted:

$$k_s = \sqrt{k_{s0}^2 - n_s^2}. \tag{2.5.13}$$

It is clear that the values k_s can be both real and imaginary. If they are real, they will represent the frequencies of free oscillations of spatial double pendulum with viscous friction, and the values n_s represent then the damping factors of each mode. Otherwise, already aperiodic damping will take place according to the form $\mathbf{\Theta}_{(s)}$. To assess the character of the oscillating fading of the modes, we introduce dimensionless coefficients $\eta_s = n_s/n$ and write down their expressions:

$$\eta_s = 2p_{s0}^2 - 1 = \frac{3 \pm 2\sqrt{2 - \sin^2\alpha}}{1 + 4\sin^2\alpha}, \quad s = 1, 2. \tag{2.5.14}$$

This shows that $\eta_2 < \eta_1$, so the oscillation modes are not damped in the same way, and the second mode always fades out faster than the first one. The graph dependencies of the values η_1 and η_2 on the angle α are shown in Fig. 2.9. It can be seen that η_1 increases slightly with increasing angle α, while η_2 decreases, changing much more significantly.

Let us write down the expressions for the dimensionless oscillation frequencies $p_s = k_s/k$:

$$\begin{aligned} p_s &= \sqrt{p_{s0}^2 - (2p_{s0}^2 - 1)^2\nu^2} = \\ &= \sqrt{\frac{2(1 + \sin^2\alpha) \pm \sqrt{2 - \sin^2\alpha}}{1 + 4\sin^2\alpha} - \left(\frac{3 \pm 2\sqrt{2 - \sin^2\alpha}}{1 + 4\sin^2\alpha}\right)^2 \nu^2}, \end{aligned} \tag{2.5.15}$$

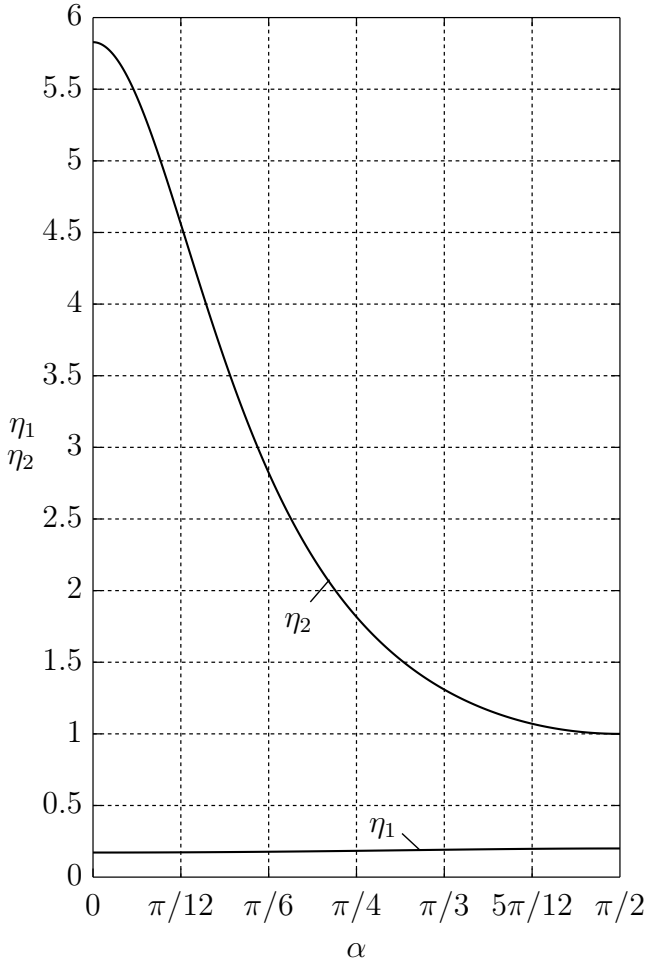

Fig. 2.9. Graph dependencies of values η_1 and η_2 on angle α

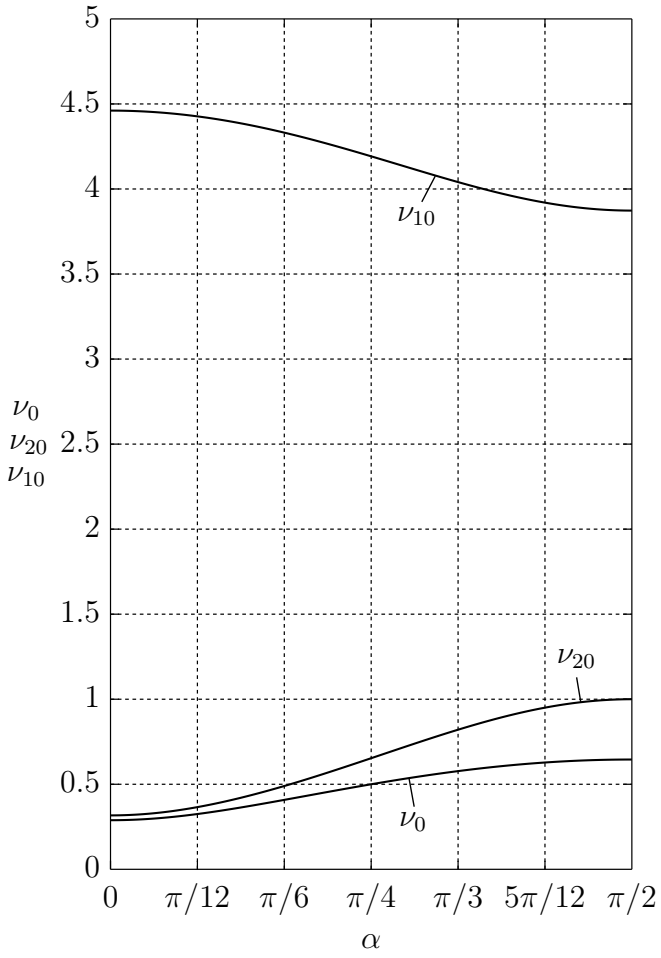

Fig. 2.10. Graph dependencies of values ν_{10}, ν_{20} and ν_0 on angle α

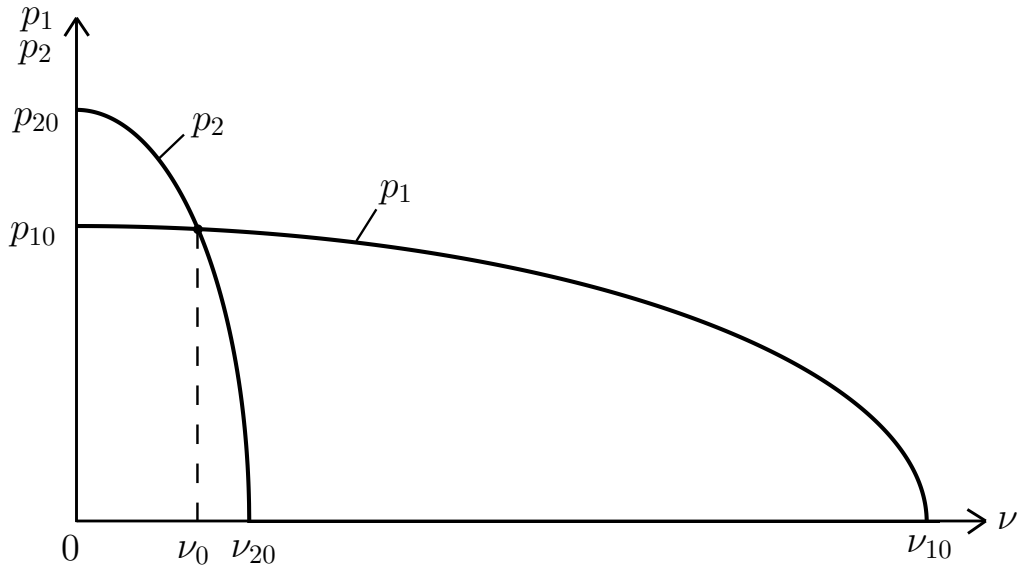

Fig. 2.11. Graph dependencies of oscillation frequencies p_1 and p_2 with viscous friction on the parameter ν

where $\nu = n/k$ is dimensionless damping factor of an ordinary pendulum which can also be called the dimensionless dissipative coefficient. It can be seen from (2.5.15) that the values p_s are real if the following conditions are respectively fulfilled:

$$p_s \in R \Rightarrow \nu < \nu_{s0} = \frac{p_{s0}}{2p_{s0}^2 - 1} = \sqrt{\frac{(1 + 4\sin^2\alpha)\left[2(1 + \sin^2\alpha) \pm \sqrt{2 - \sin^2\alpha}\right]}{\left(3 \pm 2\sqrt{2 - \sin^2\alpha}\right)^2}}. \tag{2.5.16}$$

It is not hard to show that $\nu_{20} < \nu_{10}$. Indeed, since $p_{20} > p_{10}$, then the following chain of relations takes place:

$$\nu_{20} = \frac{p_{20}}{2p_{20}^2 - 1} = \frac{1}{p_{20}} \frac{1}{2 - 1/p_{20}^2} < \frac{1}{p_{10}} \frac{1}{2 - 1/p_{10}^2} = \frac{p_{10}}{2p_{10}^2 - 1} = \nu_{10}. \tag{2.5.17}$$

Consequently, the second frequency becomes zero with increasing ν earlier than the first one. This means that the second frequency will become less than the first, starting from a certain value ν, which we will designate as ν_0. To determine this value, let us equate the frequencies p_1 and p_2 according to (2.5.15) to each other. As a result, we get the following equation:

$$\sqrt{p_{10}^2 - (2p_{10}^2 - 1)^2\nu_0^2} = \sqrt{p_{20}^2 - (2p_{20}^2 - 1)^2\nu_0^2}. \tag{2.5.18}$$

Solving it relatively ν_0, we find:

$$\nu_0 = \frac{1}{2\sqrt{p_{10}^2 + p_{20}^2 - 1}} = \frac{\sqrt{1 + 4\sin^2\alpha}}{2\sqrt{3}}. \tag{2.5.19}$$

The graph dependencies of values ν_{10}, ν_{20} and ν_0 on the angle α art presented in Fig. 2.10. These graphs, together with the dependencies shown in Fig. 2.9, clearly illustrate the change in the basic values that characterize the dissipative model of spatial double pendulum with increasing the angle between the joint axes. The graph dependencies of values p_1 and p_2 on ν are qualitatively presented in Fig. 2.11, where the case of coincidence of frequencies $p_1 = p_2$ is clearly visible, which can be called dissipative internal resonance, and it can be of certain theoretical and practical interest. These considerations emphasize the fact that instead of the terms “first frequency” (i.e., the lowest) and “second frequency” (i.e., the highest), it is sometimes preferable to use the terms “first mode” and “second mode”.

Now we consider the particular cases and write out the specific values of all key parameters for them. So, for a flat double pendulum ($\alpha = 0$) we have from (2.5.14):

$$\eta_1 = 3 - 2\sqrt{2} \approx 0.1716, \quad \eta_2 = 3 + 2\sqrt{2} \approx 5.828, \tag{2.5.20}$$

whence it can be seen that $\eta_2/\eta_1 = 17 + 12\sqrt{2} \approx 33.97$, i.e., the damping factor for the second mode is much greater than for the first one. Therefore, the second mode disappears very quickly, and then there is a slow attenuation on the first mode. We find from formulas (2.5.15) at $\alpha = 0$ the expressions for dimensionless frequencies [42]:

$$p_1 = \sqrt{2 - \sqrt{2} - (17 - 12\sqrt{2})\nu^2}, \quad p_2 = \sqrt{2 + \sqrt{2} - (17 + 12\sqrt{2})\nu^2}, \tag{2.5.21}$$

and we also determine from formulas (2.5.16) and (2.5.19) values:

$$\nu_{10} = \sqrt{10 + 7\sqrt{2}} \approx 4.4609, \quad \nu_{20} = \sqrt{10 - 7\sqrt{2}} \approx 0.3170, \quad \nu_0 = \frac{1}{2\sqrt{3}} \approx 0.2887. \tag{2.5.22}$$

In another particular case of an orthogonal double pendulum ($\alpha = \pi/2$) we find from (2.5.14):

$$\eta_1 = \frac{1}{5} = 0.2, \quad \eta_2 = 1, \tag{2.5.23}$$

whence it follows that $\eta_2/\eta_1 = 5$, i.e., this ratio is an order of magnitude less than it was for $\alpha = 0$. We find from (2.5.15) at $\alpha = \pi/2$ the expressions:

$$p_1 = \sqrt{\frac{3}{5} - \frac{1}{25}\nu^2}, \quad p_2 = \sqrt{1 - \nu^2}, \tag{2.5.24}$$

and we also determine the values from formulas (2.5.16) and (2.5.19):

$$\nu_{10} = \sqrt{15} \approx 3.873, \quad \nu_{20} = 1, \quad \nu_0 = \frac{\sqrt{5}}{2\sqrt{3}} \approx 0.6455. \tag{2.5.25}$$

Returning now to the matrix motion equation (2.5.3), we compose its general solution in complex form:

$$\boldsymbol{\theta} = \boldsymbol{\Theta}_{(1)} e^{-n_1 t} \left(A_1 e^{ik_1 t} + B_1 e^{-ik_1 t} \right) + \boldsymbol{\Theta}_{(2)} e^{-n_2 t} \left(A_2 e^{ik_2 t} + B_2 e^{-ik_2 t} \right). \tag{2.5.26}$$

Therefore, the column of generalized velocities will have the form:

$$\begin{aligned} \dot{\boldsymbol{\theta}} = \boldsymbol{\Theta}_{(1)} e^{-n_1 t} \left[A_1 (ik_1 - n_1) e^{ik_1 t} - B_1 (ik_1 + n_1) e^{-ik_1 t} \right] + \\ + \boldsymbol{\Theta}_{(2)} e^{-n_2 t} \left[A_2 (ik_2 - n_2) e^{ik_2 t} - B_1 (ik_2 + n_2) e^{-ik_2 t} \right]. \end{aligned} \tag{2.5.27}$$

The complex integration constants A_s and B_s, $s = 1, 2$ from the reality condition for $\boldsymbol{\theta}$ must satisfy the relation $B_s = \overline{A_s}$, and they are determined from the initial conditions and $\boldsymbol{\theta}_0$, $\dot{\boldsymbol{\theta}}_0$ by analogy with how it was done earlier for a conservative system. As a result, we can get:

$$A_s = \frac{(n_s + ik_s)\boldsymbol{\Theta}_{(s)}^{\mathrm{T}}\mathbf{A}_0\boldsymbol{\theta}_0 + \boldsymbol{\Theta}_{(s)}^{\mathrm{T}}\mathbf{A}_0\dot{\boldsymbol{\theta}}_0}{2ik_sN_s}, \quad B_s = \frac{-(n_s - ik_s)\boldsymbol{\Theta}_{(s)}^{\mathrm{T}}\mathbf{A}_0\boldsymbol{\theta}_0 - \boldsymbol{\Theta}_{(s)}^{\mathrm{T}}\mathbf{A}_0\dot{\boldsymbol{\theta}}_0}{2ik_sN_s}. \tag{2.5.28}$$

It is easy to understand that if the initial conditions are accepted in the form (2.4.34), then taking into account (2.4.21) from (2.5.28) we have $A_2 = 0$, $B_2 = 0$, i.e., the damping of movements will be carried out only according to the first mode. By analogy, under the conditions (2.4.35) the damping will take place only on the second mode.

Note that the resulting solution (2.5.26), taking into account (2.5.28), is valid for any value of the coefficient ν – both in the case of real values of k_s, and in the case when some of them is a purely imaginary value, as well as when these values individually become equal to zero. We emphasize that in the latter case, when the s-th frequency turns out to be equal to zero, the characteristic equation will have multiple roots. Therefore, we will have a limit-aperiodic motion according to the s-th mode, and the above solution should be understood in the limit sense, i.e., at $k_s \to 0$. Indeed, the expression $A_se^{ik_st} + B_se^{-ik_st}$, taking into account (2.5.28), will be at $k_s \to 0$ (i.e. $n_s \to k_{s0}$) an uncertainty $0/0$, which is easily revealed:

$$A_se^{ik_st} + B_se^{-ik_st} \to \frac{1}{N_s}\left[\boldsymbol{\Theta}_{(s)}^{\mathrm{T}}\mathbf{A}_0\boldsymbol{\theta}_0 + \left(k_{s0}\boldsymbol{\Theta}_{(s)}^{\mathrm{T}}\mathbf{A}_0\boldsymbol{\theta}_0 + \boldsymbol{\Theta}_{(s)}^{\mathrm{T}}\mathbf{A}_0\dot{\boldsymbol{\theta}}_0\right)t\right]. \tag{2.5.29}$$

Therefore, in this case, there will be components containing the functions $e^{-k_{s0}t}$ and $te^{-k_{s0}t}$ in the part of the solution that corresponds to the mode $\boldsymbol{\Theta}_{(s)}$, as it is well known from mathematical analysis.

2.6. Conclusions on Second Chapter

In this chapter, a mathematical model of oscillations of spatial double pendulum was constructed, in which the axes of cylindrical joints are not collinear to each other. This construction is the simplest scheme of spatial two-link manipulator. Small oscillations of such a pendulum in conservative formulation were investigated

and the frequencies and modes of its oscillations were determined depending on the angle between the joint axes. In addition, the problem of system small oscillations in the presence of viscous friction in articulated joints is considered. It is shown that in the case of identical parameters of loads, links and friction in the joints, dissipative forces do not distort the oscillation modes of the conservative model, but only reduce their amplitudes. Therefore, this example clearly demonstrates the property of preserving the eigenmodes of conservative oscillations when dissipation is introduced. This circumstance makes it possible to damp oscillations of this system according to its natural movements – its eigenmodes, without distorting or complicating their qualitative character. The revealed property of the dissipative double pendulum allowed to get the most representative and rather simple analytical expressions for all key values of the damping process. The obtained results were clearly illustrated by graphical dependencies.

3. Construction and Analysis of Nonlinear Oscillation Modes of Spatial Double Pendulum

3.1. Problem Statement of Finding Nonlinear Oscillation Modes

An extensive bibliography is devoted to the study of nonlinear oscillations of various pendulum structures – in particular, in relation to a double pendulum, one can single out the works [38, 103, 104, 128, 129, 156]. As mentioned earlier, the overwhelming majority of publications are devoted to the numerical study of the behavior of a double pendulum based on the Lagrangian or Hamiltonian form of writing the equations of its motion. Of course, this way leads to a quantitative assessment of the motion characteristics, but does not allow to reveal in detail their main qualitative features, which are most clearly demonstrated on the basis of analytical dependencies. Moreover, the question naturally arises of how such a pendulum smoothly passes from the zone of small (i.e., linear) oscillations to the nonlinear zone. It is clear that of all the possible motion modes of nonlinear systems, regular modes that have periodicity are the most valuable, because it is advisable to use them in practice to achieve specific goals [142]. Finding such modes is closely related to the well-known problem of definition nonlinear oscillation modes of multidimensional mechanical systems, which has recently

attracted a large number of specialists both in theoretical and practical terms [46, 82, 130, 135, 137, 148–150]. At the same time, pendulum systems are often taken as objects of study [37, 47, 111, 118]. A nonlinear oscillation mode means a single-frequency motion in all degrees of freedom in a nonlinear system, and it is a natural development of the concept of a linear oscillation mode. We note that the main characteristics of the linear mode are the frequency and the ratio of the oscillation amplitudes, however, when studying a nonlinear mode, due to its nonharmonic nature, it is not enough to know, in addition to the frequency, only the ratio of the amplitudes, although it is an important characteristic of the nonlinear mode. For its complete description, it is necessary to indicate the specific dependencies of all generalized coordinates on time [143].

There are many different ways of constructing solutions of nonlinear systems corresponding to nonlinear oscillation modes [153]. The most frequently used variant is based on the application of asymptotic methods of nonlinear mechanics specially developed for this purpose [11]. It should be emphasized that a double pendulum is a system with two degrees of freedom, for which the construction of approximate analytical solutions in a nonlinear zone turns out to be much more difficult than for systems with one degree of freedom, where there is no question of constructing oscillation modes. Therefore, in most works on the dynamics of a double pendulum, its nonlinear oscillations are studied only with the help of numerical methods. Thus, the main interest is analytical study of periodic system motions, which will clearly demonstrate the drift of oscillation frequencies and modes with a gradual increase in the amplitudes of oscillations of the links. This chapter is devoted to the construction of nonlinear oscillation modes of spatial double pendulum in the first approximation, and for its particular variants of the double flat and orthogonal pendulums, it is possible to construct an approximate solution not only in the first, but also in the second approximation [72].

3.2. Nonlinear Oscillation Modes of Orthogonal Double Pendulum

Let us first turn to the study of nonlinear oscillation modes of an orthogonal double pendulum, when $\alpha = \pi/2$, since in this case they are most easily found.

To do this, we go back to the nonlinear matrix motion equation (2.2.12) and expressions (2.3.12) and (2.3.13). It is easy to see that this equation admits two partial modes of motion:

$$\ddot{\theta}_1 + k_{10}^2 \sin\theta_1 = 0, \quad \theta_2 \equiv 0, \quad k_{10} = \sqrt{\frac{3}{5}}k, \tag{3.2.1}$$

$$\ddot{\theta}_2 + k_{20}^2 \sin\theta_2 = 0, \quad \theta_1 \equiv 0, \quad k_{20} = k. \tag{3.2.2}$$

These equations show that in the case of orthogonal double pendulum and within the framework of a nonlinear model, one generalized coordinate can oscillate while the other coordinate is zero. Wherein, each of the equations (3.2.1) and (3.2.2) is equation of oscillations of ordinary mathematical pendulum. Therefore, the question of nonlinear oscillation modes in this situation is solved by examining these second-order differential equations separately. We consider, for example, the first of them. The technique for constructing approximate asymptotic solutions for ordinary pendulum is well known, and it is described in [11]. To do this, the equation (3.2.1) should be rewritten so that the left side contains linear terms corresponding to small oscillations, and everything else must be transferred to the right side. Then we come to the study of the equation:

$$\ddot{\theta}_1 + k_{10}^2\theta_1 = Q(\theta_1), \quad Q(\theta_1) = k_{10}^2\left(\theta_1 - \sin\theta_1\right). \tag{3.2.3}$$

The function $Q(\theta_1)$ can be interpreted as a perturbing force that excites oscillations in a linear system. To construct the first two approximations to the solution, it suffices to expand the function $Q(\theta_1)$ in Taylor series and keep two nonlinear terms in this expansion, one of which has the third order of smallness, and the other term has the fifth order of smallness:

$$Q = Q^{(\mathrm{I})} + Q^{(\mathrm{II})}, \quad Q^{(\mathrm{I})} = k_{10}^2\frac{\theta_1^3}{6}, \quad Q^{(\mathrm{II})} = -k_{10}^2\frac{\theta_1^5}{120}. \tag{3.2.4}$$

1. Construction of the first approximation. We will look for the solution of the equation (3.2.3) in the initial approximation in the same form as in the linear model, namely:

$$\theta_1 = a\cos\psi, \tag{3.2.5}$$

where still $a = \mathrm{const}$, but the total phase ψ (or frequency) already depends in some way on a. It is easy to understand that the correction to the oscillation

frequency will have the second order of smallness in a:

$$\dot{\psi} = k_{10}\left(1 + \rho^{(\mathrm{I})}a^2\right) = k_1^{(\mathrm{I})}(a). \tag{3.2.6}$$

The value a can be treated here as a small parameter. To determine the value $\rho^{(\mathrm{I})}$, we use the harmonic balance equation [11]:

$$\int_0^{2\pi} (\ddot{\theta}_1 + k_{10}^2\theta_1 - Q)\cos\psi d\psi = 0. \tag{3.2.7}$$

This equation must be performed with required accuracy. In the first approximation, it is necessary that it be fulfilled up to terms of the third order of smallness in a. Referring to the formula (3.2.5), we calculate $\dot{\theta}_1$ and $\ddot{\theta}_1$ up to the third order of smallness, taking into account (3.2.6):

$$\dot{\theta}_1 = -ak_{10}\sin\psi\left(1 + \rho^{(\mathrm{I})}a^2\right), \quad \ddot{\theta}_1 = -ak_{10}^2\cos\psi\left(1 + 2\rho^{(\mathrm{I})}a^2\right). \tag{3.2.8}$$

To determine the perturbing force with the same accuracy, it suffices to substitute the expression (3.2.5) into $Q^{(\mathrm{I})}$, and as a result we get:

$$Q = \left(U^{(\mathrm{I})}\cos\psi + V^{(\mathrm{I})}\cos 3\psi\right)k_{10}^2a^3, \quad U^{(\mathrm{I})} = \frac{1}{8}, \quad V^{(\mathrm{I})} = \frac{1}{24}. \tag{3.2.9}$$

Substituting now (3.2.5), (3.2.8), and (3.2.9) into the equation (3.2.7), we get a simple expression for $\rho^{(\mathrm{I})}$:

$$\rho^{(\mathrm{I})} = -\frac{U^{(\mathrm{I})}}{2} = -\frac{1}{16}. \tag{3.2.10}$$

Then the expression for the oscillation frequency in the first approximation will take the following form:

$$k_1^{(\mathrm{I})}(a) = k_{10}\left(1 - \frac{a^2}{16}\right) = k_{10}(1 - 0.0625a^2). \tag{3.2.11}$$

Now we have the opportunity to clarify the solution, namely, to construct it up to the third order of smallness. It is clear that the harmonic $\cos\psi$ is already balanced, but the harmonic $\cos 3\psi$ is still unbalanced. Let us consider the oscillations that it excites in the unperturbed system, i.e., we will find a particular solution $\widetilde{\theta}_1^{(\mathrm{I})}$ of the following equation:

$$\ddot{\theta}_1 + k_{10}^2\theta_1 = V^{(\mathrm{I})}k_{10}^2a^3\cos 3\psi, \tag{3.2.12}$$

which obviously looks like:

$$\widetilde{\theta}_1^{(\mathrm{I})}(a,\psi) = \frac{V^{(\mathrm{I})}k_{10}^2 a^3}{k_{10}^2 - 9k_1^2(a)}\cos 3\psi. \tag{3.2.13}$$

To keep only the terms of the third order of smallness in this expression, it is sufficient to substitute the constant value k_{10} instead of $k_1(a)$. Adding (3.2.13) with the expression (3.2.5), we find a solution with the specified accuracy [96]:

$$\theta_1^{(\mathrm{I})} = a\cos\psi + \widetilde{\theta}_1^{(\mathrm{I})} = a\cos\psi - \frac{a^3}{192}\cos 3\psi. \tag{3.2.14}$$

Assuming $\psi = 0$, we can find from here the oscillation amplitude A depending on the parameter a, which plays the role of the amplitude of the first harmonic in the representation (3.2.14):

$$A = a - \frac{a^3}{192}. \tag{3.2.15}$$

To control the correctness of the obtained expressions, it is advisable to calculate the total mechanical energy E and make sure that when it is calculated with the required accuracy, it remains unchanged in time. The expression for the total energy has the form (2.2.14), and in the case $\alpha = \pi/2$ and under the condition $\theta_2 \equiv 0$ it will take a simple form:

$$E = \frac{5}{2}ml^2\dot{\theta}_1^2 + 3mgl(1-\cos\theta_1) = \frac{5}{2}ml^2\left[\dot{\theta}_1^2 + 2k_{10}^2(1-\cos\theta_1)\right]. \tag{3.2.16}$$

Therefore, up to terms of the fourth order of smallness, we obtain the following expression:

$$E = \frac{5}{2}ml^2\left[\dot{\theta}_1^2 + k_{10}^2\left(\theta_1^2 - \frac{\theta_1^4}{12}\right)\right]. \tag{3.2.17}$$

We also calculate $\dot{\theta}_1$ by differentiating the expression (3.2.14) according to (3.2.11) and keeping the terms no higher than the third order of smallness in a:

$$\dot{\theta}_1^{(\mathrm{I})} = k_{10}\left[-\left(a - \frac{a^3}{16}\right)\sin\psi + \frac{a^3}{64}\sin 3\psi\right]. \tag{3.2.18}$$

Substituting the expressions (3.2.14) and (3.2.18) into the formula (3.2.17), we obtain, up to the fourth order in a, the following expression:

$$E^{(\mathrm{I})} = E_0\left(1 - \frac{3}{32}a^2\right), \quad E_0 = \frac{3}{2}mgla^2, \tag{3.2.19}$$

where E_0 is the total energy of the system within the linear model. It can be seen that the energy $E^{(\mathrm{I})}$ depends according to (3.2.19) only on a and does not depend on ψ, which once again confirms the correctness of the obtained expressions.

2. Construction of the second approximation. The obtained expressions can now be used to construct the second approximation. In this case, the harmonic balance equation must be performed up to the fifth order of smallness in a. Let us introduce one more correction $\rho^{(\mathrm{II})}$ to the frequency, which should have the fourth order of smallness:

$$\dot{\psi} = k_{10}\left(1 + \rho^{(\mathrm{I})}a^2 + \rho^{(\mathrm{II})}a^4\right) = k_1^{(\mathrm{II})}(a). \tag{3.2.20}$$

Taking into account the orthogonality conditions of trigonometric functions, we can rewrite the harmonic balance equation (3.2.7) in the following form:

$$\int_0^{2\pi}\left(\frac{d^2x}{dt^2} + k_{10}^2 x - Q\right)\cos\psi d\psi = 0, \tag{3.2.21}$$

where $x = a\cos\psi$. Let us now calculate the expression up to the fifth order of smallness:

$$\frac{d^2x}{dt^2} + k_{10}^2 x = \left[-2\rho^{(\mathrm{I})}a^3 - \left(\rho^{(\mathrm{I})^2} + 2\rho^{(\mathrm{II})}\right)a^5\right]k_{10}^2\cos\psi. \tag{3.2.22}$$

We also calculate Q up to the fifth order of smallness:

$$Q = \left[\left(U^{(\mathrm{I})}a^3 + U^{(\mathrm{II})}a^5\right)\cos\psi + \left(V^{(\mathrm{I})}a^3 + V^{(\mathrm{II})}a^5\right)\cos 3\psi + W^{(\mathrm{II})}a^5\cos 5\psi\right]k_{10}^2, \tag{3.2.23}$$

where the old notation for $U^{(\mathrm{I})}$ and $V^{(\mathrm{I})}$ is retained according to (3.2.9), and new notation is made:

$$U^{(\mathrm{II})} = -\frac{3}{512}, \quad V^{(\mathrm{II})} = -\frac{1}{256}, \quad W^{(\mathrm{II})} = -\frac{3}{2560}. \tag{3.2.24}$$

As a result, we again arrive at the relation (3.2.10) for $\rho^{(\mathrm{I})}$, as expected, and also find:

$$\rho^{(\mathrm{II})} = -\frac{\rho_1^{(\mathrm{I})^2}}{2} - \frac{U^{(\mathrm{II})}}{2} = \frac{1}{1024}. \tag{3.2.25}$$

Therefore, the oscillation frequency in the second approximation is determined by the formula:

$$k_1^{(\mathrm{II})}(a) = k_{10}\left(1 - \frac{a^2}{16} + \frac{a^4}{1024}\right) \approx k_{10}(1 - 0.0625a^2 + 0.00098a^4). \tag{3.2.26}$$

By analogy, we can now obtain a solution up to the fifth order of smallness. To do this, we obtain a particular solution $\widetilde{\theta}_1^{(\mathrm{II})}$ of the equation

$$\ddot{\theta}_1 + k_{10}^2\theta_1 = \left[\left(V^{(\mathrm{I})}a^3 + V^{(\mathrm{II})}a^5\right)\cos 3\psi + W^{(\mathrm{II})}a^5\cos 5\psi\right]k_{10}^2, \tag{3.2.27}$$

which has the following form:

$$\widetilde{\theta}_1^{(\mathrm{II})}(a,\psi) = \frac{\left(V^{(\mathrm{I})}a^3 + V^{(\mathrm{II})}a^5\right)k_{10}^2}{k_{10}^2 - 9k_1^2(a)}\cos 3\psi + \frac{W^{(\mathrm{II})}k_{10}^2a^5}{k_{10}^2 - 25k_1^2(a)}\cos 5\psi. \tag{3.2.28}$$

To keep in this expression the terms not higher than the fifth order of smallness in a, it is enough to substitute the formula (3.2.11) instead of $k_1(a)$ in the first of the fractions, and the constant value k_{10} in the second. Adding the resulting expression with the expression (3.2.5), we find a solution with the required accuracy:

$$\theta_1^{(\mathrm{II})}(a,\psi) = a\cos\psi + \widetilde{\theta}_1^{(\mathrm{II})} = a\cos\psi - \left(\frac{a^3}{192} + \frac{a^5}{4096}\right)\cos 3\psi + \frac{a^5}{20480}\cos 5\psi. \tag{3.2.29}$$

We can find from here the oscillation amplitude A depending on the parameter a in the considered approximation:

$$A = a - \frac{a^3}{192} - \frac{a^5}{5120}. \tag{3.2.30}$$

It remains to calculate the total energy with the required accuracy. To do this, we write the expression (3.2.16) up to terms of the sixth order of smallness:

$$E = \frac{5}{2}ml^2\left[\dot{\theta}_1^2 + k_{10}^2\left(\theta_1^2 - \frac{\theta_1^4}{12} + \frac{\theta_1^6}{360}\right)\right]. \tag{3.2.31}$$

We calculate $\dot{\theta}_1$ by differentiating the expression (3.2.29), taking into account (3.2.26) and keeping the terms no higher than the fifth order of smallness in a:

$$\dot{\theta}_1^{(\mathrm{II})} = k_{10}\left[-\left(a - \frac{a^3}{16} + \frac{a^5}{1024}\right)\sin\psi + \left(\frac{a^3}{64} - \frac{a^5}{4096}\right)\sin 3\psi - \frac{a^5}{4096}\sin 5\psi\right]. \tag{3.2.32}$$

Substituting the expressions (3.2.29) and (3.2.32) into the formula (3.2.31), we obtain, up to sixth order in a, the following expression:

$$E^{(\mathrm{II})} = E_0\left(1 - \frac{9}{96}a^2 + \frac{17}{4096}a^4\right), \quad E_0 = \frac{3}{2}mgla^2, \tag{3.2.33}$$

which in this approximation also depends only on a and does not depend on ψ.

We note that this problem has an exact solution, and the oscillation frequency k_1 depending on the oscillation amplitude A is determined by the formula [48]:

$$k_1 = \frac{\pi k_{10}}{2K(\kappa)}, \quad \kappa = \sin\frac{A}{2}, \tag{3.2.34}$$

where $K(\kappa)$ is a complete elliptic integral of the first kind with modulus κ.

Discussion of the results. We now study the dependence of the frequency k_1 on the oscillation amplitude A in various approximations. So, within the framework of the linear model, which can be called also the zero approximation, the frequency is equal to k_{10}, and it does not depend on the oscillation amplitude, which is equal to a. In the first approximation, the frequency is (3.2.11), and the amplitude is (3.2.15), and in the second approximation, the frequency is given by (3.2.26), while the amplitude is given by (3.2.30). In both cases, we have a parametric dependence of the frequency on the amplitude through the intermediate parameter a, and each subsequent approximation takes into account the next correction both in the expression for the frequency and in the expression for the amplitude.

The dependence of dimensionless frequency k_1/k_{10} on the oscillation amplitude A (which for clarity is presented in degrees) in two approximations is shown in Fig. 3.1, where the exact dependence is also shown according to (3.2.34). It is easy to see that the approximate asymptotic formulas correlate very well with the exact values, and every next approximation refines the results. The undoubted advantage of the constructed approximate expressions is that they give adequate results not only for sufficiently small amplitudes, but in a very wide range of them. For definiteness, we emphasize that we will not consider oscillations of the system with very large amplitudes, and we will limit the specified range to the values not exceeding $\pi/2$ and shown in Fig. 3.1.

It should also be emphasized that if the expression (3.2.34) is expanded into a Taylor series, then the obtained result will be in full accordance with the asymptotic formulas. Indeed, we have from (3.2.34) the following expansion up to the fourth order of smallness in amplitude A:

$$k_1 = k_{10}\left(1 - \frac{1}{16}A^2 + \frac{1}{3072}A^4\right). \tag{3.2.35}$$

It remains to show that the formula (3.2.26) with the same accuracy, taking into account (3.2.30), will go to (3.2.35). To do this, we obtain an inverse relationship

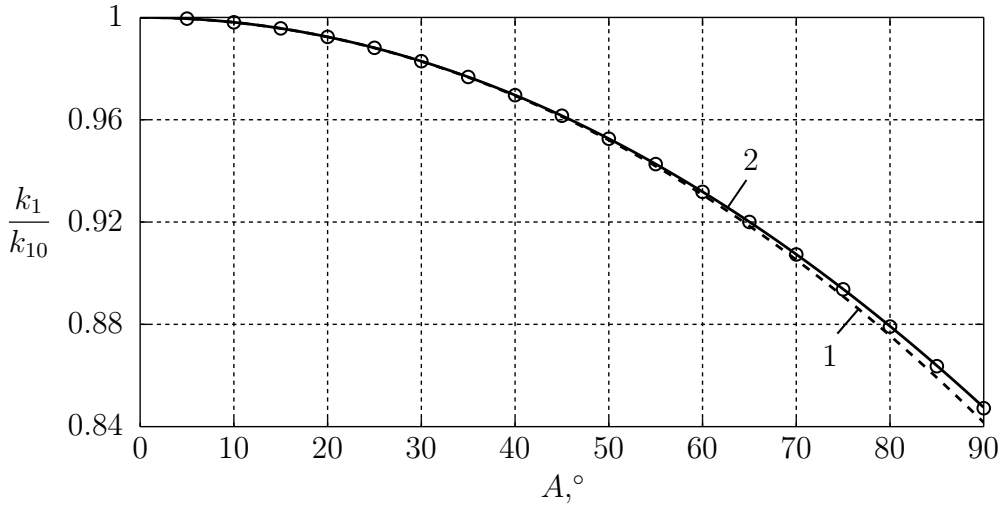

Fig. 3.1. Dependence of dimensionless frequency k_1/k_{10} on amplitude A: 1 – first approximation, 2 – second approximation, ∘ – exact values

with respect to (3.2.30), i.e., we express a in terms of A with the same accuracy. Looking for a in the form $a = A+\mu^{(\mathrm{I})}A^3+\mu^{(\mathrm{II})}A^5$ and substituting this expression into (3.2.30), we equate the coefficients at the same powers of A, whence we find:

$$\mu^{(\mathrm{I})} = \frac{1}{192}, \quad \mu^{(\mathrm{II})} = \frac{17}{61440}, \quad a = A + \frac{1}{192}A^3 + \frac{17}{61440}A^5. \tag{3.2.36}$$

Substituting this expression into (3.2.26) and keeping the terms no higher than the fourth order of smallness in A, we arrive exactly at the formula (3.2.35). It can be seen that for this purpose it was sufficient to obtain the expression (3.2.36) with only one cubic correction, but if necessary, for example, to eliminate a through A in the formula (3.2.29) while preserving the terms not above the fifth order of smallness, then the full expression (3.2.36) would be required.

Let us now turn to a visual graphical illustration of the obtained results. For this purpose, it is appropriate to construct a phase portrait of the system on the phase plane $(\theta_1, \dot\theta_1/k_{10})$, where the division of the generalized velocity by k_{10} is carried out in order to plot dimensionless values on both axes. We will construct phase trajectories using the second approximation formulas (3.2.29) and (3.2.32), treating ψ as an intermediate parameter and compare them with the phase trajectories obtained in the exact solution. It is necessary to carry out this correspondence in such a way that the phase trajectory in the approximate solution corresponds to the phase trajectory in the exact solution, having the same energy level. For further actions, it is convenient to introduce the dimensionless

energy $\varepsilon = E/(mgl)$. Therefore, in the second approximation from the formula (3.2.33) we will have:

$$\varepsilon = \frac{E}{mgl} = \frac{3}{2}a^2\left(1 - \frac{3}{32}a^2 + \frac{17}{4096}a^4\right). \tag{3.2.37}$$

By varying the parameter a, we will also vary the value ε, i.e., we will obtain phase trajectories with different energy levels. At the same time, the phase trajectories in the exact solution for the same values ε can be determined from the expression (3.2.16), resolving it with respect to $\dot{\theta}_1/k_{10}$:

$$\frac{\dot{\theta}_1}{k_{10}} = \pm\sqrt{\frac{2\varepsilon}{3} - 4\sin^2\frac{\theta_1}{2}}. \tag{3.2.38}$$

Note that the phase portrait for the exact solution can also be constructed using this solution, which has the form [48]:

$$\theta_1 = 2\arcsin\left[\kappa\,\mathrm{sn}\left(k_{10}t + \vartheta, \kappa\right)\right], \quad \dot{\theta}_1 = 2\kappa k_{10}\,\mathrm{cn}\left(k_{10}t + \vartheta, \kappa\right), \tag{3.2.39}$$

where sn and cn are Jacobi elliptic functions, $\kappa = \sin A/2 = \sqrt{\varepsilon/6}$, and ϑ is an integration constant. In this case, the time t acts as a parameter. It is easy to see that the formulas (3.2.39) identically satisfy the equation (3.2.38), which once again confirms their validity.

The phase portrait of the system on the plane $(\theta_1, \dot{\theta}_1/k_{10})$ is shown in Fig. 3.2, and for the uniformity of the graphic presentation of the results, it is assumed that the solid lines correspond to the asymptotic formulas of the second approximation, and circles represent exact values. In this case, it should be noted that on each of the phase trajectories, the circles correspond to the values taken at the same time intervals. It can be seen that there is an adequate correspondence between the approximate and exact results, and in the accepted range of amplitudes, their difference does not manifest itself at all. In addition, it can be observed that the form of the phase trajectories is gradually distorted with increasing energy level and becomes more and more different from the circular one, which is characteristic of the linear model, which also emphasizes the nonlinear nature of the problem under consideration.

In addition, we plot the dependencies of the angle θ_1 and the dimensionless angular velocity $\dot{\theta}_1/k_{10}$ in the second approximation on the phase angle ψ on one oscillation period, i.e., when ψ changes from 0 to 2π, which correspond to the

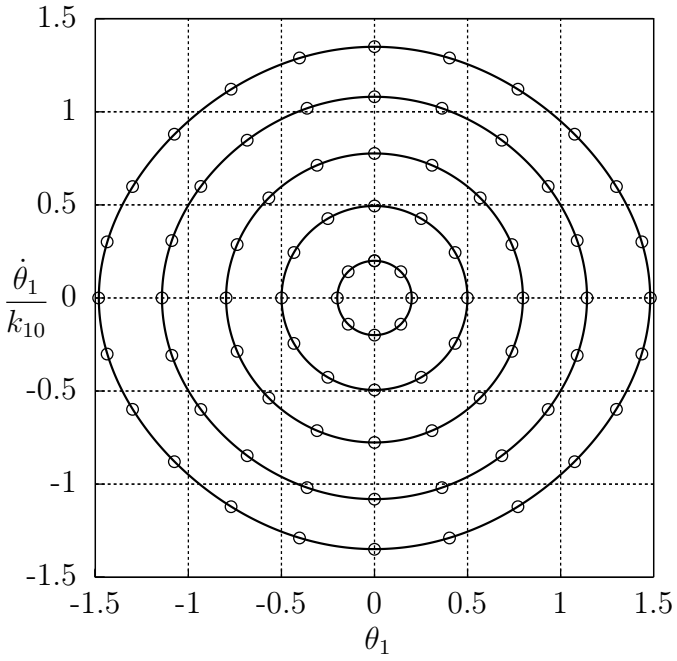

Fig. 3.2. Phase portrait: solid lines – formulas of the second approximation, ∘ – exact values

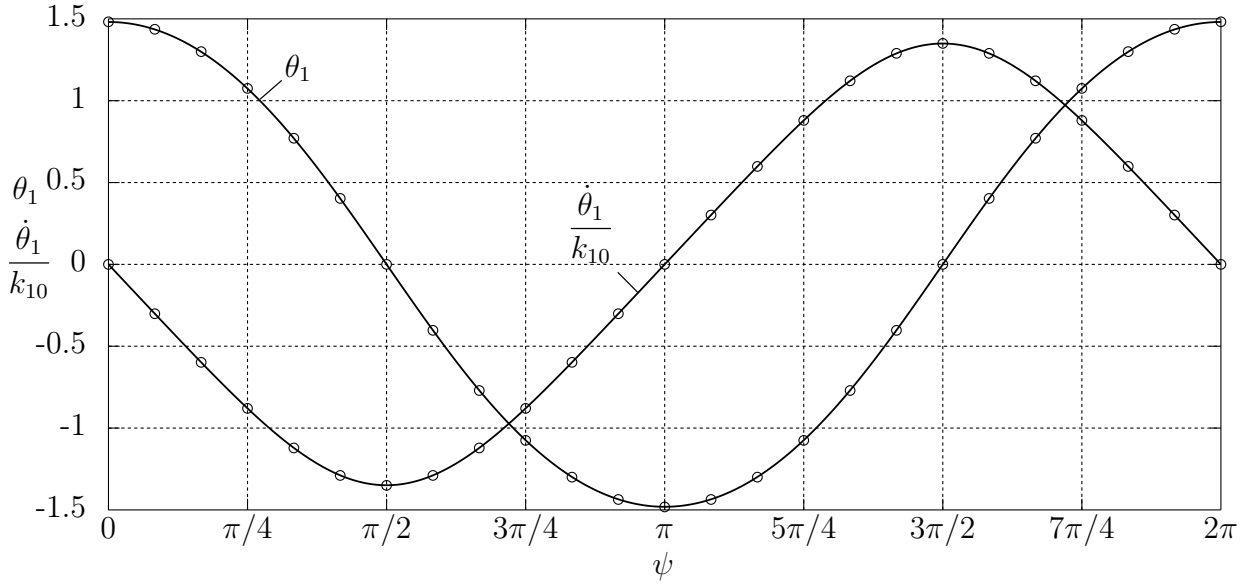

Fig. 3.3. Graphs dependencies of values θ_1 и $\dot\theta_1/k_{10}$ on ψ: solid lines – formulas of the second approximation, ∘ – exact values

phase trajectory with the highest energy level from those shown above in the phase portrait in Fig. 3.2. For a more visual comparison of the behavior of these graphs with similar exact dependencies, it is advisable to introduce the value $\psi = k_1 t$ for the exact solution by analogy, where k_1 is determined by the formula (3.2.34). This scaling leads to the fact that the introduced value ψ in the exact

solution also lies in the range from 0 to 2π. Therefore, the comparison of the results will be carried out not at the same points in time, but when the system reaches a certain part of the oscillation period. This action makes it possible to exclude from consideration the existing mismatch of oscillation frequencies in the approximate and exact solutions and to correlate precisely the character of the oscillatory motion. In this case, we put in the formula (3.2.39) $\vartheta = K(\kappa)$, so that for $t = 0$ we have $\theta_1 = 2\arcsin\kappa = A$ and $\dot{\theta}_1 = 0$. These dependencies are shown in Fig. 3.3, which also shows excellent agreement between approximate and exact results. We note once again that the presented dependencies have a somewhat more complex structure than for harmonic oscillations, which have a purely sinusoidal character and appear at low amplitudes.

It remains to emphasize that numerical integration of the matrix equation (2.2.15) when specifying the appropriate initial conditions for motion according to the first nonlinear oscillation mode with accepted energy levels will give for the angle θ_1 similar results as the exact solution (3.2.39).

3.3. Nonlinear Oscillation Modes of Flat Double Pendulum

We now turn to the problem of constructing approximate asymptotic formulas for the first and second nonlinear oscillation modes of flat double pendulum at $\alpha = 0$. As mentioned earlier in Ch. 2, to study the free motions of this system, it is more convenient to take as generalized coordinates not the joint rotation angles θ_1 and θ_2, but the absolute angles of deviation of the links φ_1 and φ_2 from the vertical, since in this case the motion equations take the most compact form. This circumstance makes it much easier to construct an approximate analytical solution by developing the technique used in the previous section, and it is possible to construct not only the first, but also the second approximation without much difficulty.

We turn to the equation (2.3.8) taking into account (2.3.5) and (2.3.9) and rewrite it in such a way that its left side contains linear terms corresponding to small oscillations, and everything else will be moved to the right side [17, 21]:

$$\mathbf{A}_0\ddot{\boldsymbol{\varphi}} + \mathbf{C}_0\boldsymbol{\varphi} = \widetilde{\mathbf{A}}(\boldsymbol{\varphi})\ddot{\boldsymbol{\varphi}} + \widetilde{\mathbf{B}}(\boldsymbol{\varphi}, \dot{\boldsymbol{\varphi}}) + \widetilde{\mathbf{C}}(\boldsymbol{\varphi}) = \mathbf{Q}(\boldsymbol{\varphi}, \dot{\boldsymbol{\varphi}}, \ddot{\boldsymbol{\varphi}}). \tag{3.3.1}$$

Here the constant matrices $\mathbf{A}_0$ and $\mathbf{C}_0$ have representations (3.3.2), and the following notation is made:

$$\widetilde{\mathbf{A}}(\boldsymbol{\varphi}) = \mathbf{A}_0 - \mathbf{A}(\boldsymbol{\varphi}), \quad \widetilde{\mathbf{B}}(\boldsymbol{\varphi}, \dot{\boldsymbol{\varphi}}) = -\mathbf{B}(\boldsymbol{\varphi}, \dot{\boldsymbol{\varphi}}), \quad \widetilde{\mathbf{C}}(\boldsymbol{\varphi}) = \mathbf{C}_0\boldsymbol{\varphi} - \mathbf{C}(\boldsymbol{\varphi}). \quad (3.3.2)$$

The column $\mathbf{Q}$ in the equation (3.3.1), treated as a column of perturbing forces acting in a linear system, then has the form:

$$\begin{aligned}\mathbf{Q} = ml^2 \sin(\varphi_2 - \varphi_1) \begin{bmatrix} \dot{\varphi}_2^2 \\ -\dot{\varphi}_1^2 \end{bmatrix} + mgl \begin{bmatrix} 2(\varphi_1 - \sin\varphi_1) \\ \varphi_2 - \sin\varphi_2 \end{bmatrix} + \\ + ml^2 (1 - \cos(\varphi_2 - \varphi_1)) \begin{bmatrix} \ddot{\varphi}_2 \\ \ddot{\varphi}_1 \end{bmatrix}.\end{aligned} \quad (3.3.3)$$

Let us expand the trigonometric functions included in the expression (3.3.3) into Taylor series with an accuracy sufficient to construct the first two approximations to the solution. As a result, we get the following representation:

$$\mathbf{Q} = \mathbf{Q}^{(\mathrm{I})} + \mathbf{Q}^{(\mathrm{II})}, \quad (3.3.4)$$

where the column $\mathbf{Q}^{(\mathrm{I})}$ contains terms of the third order of smallness in generalized coordinates, velocities, and accelerations, and $\mathbf{Q}^{(\mathrm{II})}$ – the fifth order:

$$\begin{aligned}\mathbf{Q}^{(\mathrm{I})} &= ml^2(\varphi_2 - \varphi_1) \begin{bmatrix} \dot{\varphi}_2^2 \\ -\dot{\varphi}_1^2 \end{bmatrix} + \frac{mgl}{6} \begin{bmatrix} 2\varphi_1^3 \\ \varphi_2^3 \end{bmatrix} + \frac{ml^2}{2}(\varphi_2 - \varphi_1)^2 \begin{bmatrix} \ddot{\varphi}_2 \\ \ddot{\varphi}_1 \end{bmatrix}, \\ \mathbf{Q}^{(\mathrm{II})} &= -\frac{ml^2}{6}(\varphi_2 - \varphi_1)^3 \begin{bmatrix} \dot{\varphi}_2^2 \\ -\dot{\varphi}_1^2 \end{bmatrix} - \frac{mgl}{120} \begin{bmatrix} 2\varphi_1^5 \\ \varphi_2^5 \end{bmatrix} - \frac{ml^2}{24}(\varphi_2 - \varphi_1)^4 \begin{bmatrix} \ddot{\varphi}_2 \\ \ddot{\varphi}_1 \end{bmatrix}.\end{aligned} \quad (3.3.5)$$

1. Construction of the first approximation. As an initial approximation to the solution of the equation (3.3.1), we take the same expression as for oscillations on one of the modes in the linear system (2.4.17):

$$\boldsymbol{\varphi} = \boldsymbol{\Phi}_{(s)} a \cos\psi, \quad (3.3.6)$$

where $a = \mathrm{const}$ (for brevity, the index "s" of a and ψ is omitted here and below as insignificant), and the oscillation frequency depends on a as follows:

$$\dot{\psi} = k_{s0}(1 + \rho_s^{(\mathrm{I})} a^2) = k_s^{(\mathrm{I})}(a), \quad k_{s0} = \sqrt{2 \pm \sqrt{2}}k. \quad (3.3.7)$$

Here the first correction is introduced, and it will be proportional to a^2, as for a conventional mathematical pendulum. We note that the value a, taking into account (2.4.17), plays the role of the oscillation amplitude of the angle φ_1 in the initial approximation. The coefficient $\rho_s^{(\mathrm{I})}$ in the formula (3.3.7) can be found from the harmonic balance equation for the given mode $\mathbf{\Phi}_{(s)}$ [11, 63]:

$$\int_0^{2\pi} \mathbf{\Phi}_{(s)}^{\mathrm{T}} \left(\mathbf{A}_0\ddot{\boldsymbol{\varphi}} + \mathbf{C}_0\boldsymbol{\varphi} - \mathbf{Q}\right) \cos\psi d\psi = 0. \tag{3.3.8}$$

Based on the expressions (3.3.6) and (3.3.7), we calculate the columns of generalized velocities $\dot{\boldsymbol{\varphi}}$ and accelerations $\ddot{\boldsymbol{\varphi}}$ up to the values of the third order of smallness:

$$\dot{\boldsymbol{\varphi}} = -\mathbf{\Phi}_{(s)} a \sin\psi k_{s0} \left(1 + \rho_s^{(\mathrm{I})} a^2\right), \quad \ddot{\boldsymbol{\varphi}} = -\mathbf{\Phi}_{(s)} a \cos\psi k_{s0}^2 \left(1 + 2\rho_s^{(\mathrm{I})} a^2\right), \tag{3.3.9}$$

as well as perturbing forces with the same accuracy:

$$\mathbf{Q} = \left(\mathbf{U}_s^{(\mathrm{I})} \cos\psi + \mathbf{V}_s^{(\mathrm{I})} \cos 3\psi\right) mgla^3, \tag{3.3.10}$$

where the columns $\mathbf{U}_s^{(\mathrm{I})}$ and $\mathbf{V}_s^{(\mathrm{I})}$ have the following representations:

$$\mathbf{U}_s^{(\mathrm{I})} = \begin{bmatrix} \dfrac{14 \pm 9\sqrt{2}}{4} \\ \dfrac{-22 \mp 17\sqrt{2}}{8} \end{bmatrix}, \quad \mathbf{V}_s^{(\mathrm{I})} = \begin{bmatrix} \dfrac{46 \pm 33\sqrt{2}}{12} \\ \dfrac{-54 \mp 41\sqrt{2}}{24} \end{bmatrix}. \tag{3.3.11}$$

Let us substitute the obtained expressions into the equation of harmonic balance (3.3.8), taking into account that the oscillation modes $\mathbf{\Phi}_{(s)}$ satisfy the equation

$$\left(\mathbf{C}_0 - k_{s0}^2 \mathbf{A}_0\right) \mathbf{\Phi}_{(s)} = 0, \tag{3.3.12}$$

and also using the notation (2.4.27) for the normalization coefficients, we arrive at the following expression for $\rho_s^{(\mathrm{I})}$:

$$\rho_s^{(\mathrm{I})} = -\frac{mgl}{2N_s k_{s0}^2} \mathbf{\Phi}_{(s)}^{\mathrm{T}} \mathbf{U}_s^{(\mathrm{I})} = -\frac{1}{2H_s p_{s0}^2} \mathbf{\Phi}_{(s)}^{\mathrm{T}} \mathbf{U}_s^{(\mathrm{I})} = -\frac{31 \pm 20\sqrt{2}}{32}. \tag{3.3.13}$$

Substituting now (3.3.13) into (3.3.7), we obtain expression for the oscillation frequency in the first approximation:

$$k_s^{(\mathrm{I})}(a) = k_{s0} \left(1 - \frac{31 \pm 20\sqrt{2}}{32} a^2\right). \tag{3.3.14}$$

Thus, when system moves on each of the nonlinear oscillation modes, the frequencies in the first approximation are determined by the following expressions:

$$k_1^{(\mathrm{I})}(a) \approx k_{10}(1 - 0.0849a^2), \quad k_2^{(\mathrm{I})}(a) \approx k_{20}(1 - 1.8526a^2), \tag{3.3.15}$$

whence it can be seen that the second frequency changes more significantly with increasing a than the first frequency.

Now we can obtain a solution up to the third order of smallness. To construct it, we find out separately which forced oscillations $\widetilde{\boldsymbol{\varphi}}$ are excited by the harmonic force $\mathbf{Q} = \mathbf{Q}_0 \cos \omega t$ in the unperturbed (i.e., linear) system, namely, we define a particular solution of the equation:

$$\mathbf{A}_0 \ddot{\boldsymbol{\varphi}} + \mathbf{C}_0 \boldsymbol{\varphi} = \mathbf{Q}_0 \cos \omega t. \tag{3.3.16}$$

To solve this equation, we introduce the modal matrix $\mathbf{U} = [\boldsymbol{\Phi}_{(1)} | \boldsymbol{\Phi}_{(2)}]$, i.e., the matrix of eigenmodes. Next, we pass to the principal coordinates $\boldsymbol{\xi} = [\xi_1, \xi_2]^{\mathrm{T}}$ using the relationship:

$$\boldsymbol{\varphi} = \mathbf{U}\boldsymbol{\xi} = \boldsymbol{\Phi}_{(1)}\xi_1 + \boldsymbol{\Phi}_{(2)}\xi_2. \tag{3.3.17}$$

Substituting this expression into the equation (3.3.16) and multiplying it from the left by $\mathbf{U}^{\mathrm{T}}$, taking into account the orthogonality conditions for the eigenmodes (2.4.26), we arrive at matrix equation:

$$\widetilde{\mathbf{A}}_0 \ddot{\boldsymbol{\xi}} + \widetilde{\mathbf{C}}_0 \boldsymbol{\xi} = \widetilde{\mathbf{Q}}_0 \cos \omega t, \tag{3.3.18}$$

where the following values are introduced:

$$\widetilde{\mathbf{A}}_0 = \mathbf{U}^{\mathrm{T}}\mathbf{A}_0\mathbf{U} = \mathrm{diag}(N_s), \quad \widetilde{\mathbf{C}}_0 = \mathbf{U}^{\mathrm{T}}\mathbf{C}_0\mathbf{U} = \mathrm{diag}(N_s k_{s0}^2), \quad \widetilde{\mathbf{Q}}_0 = \mathbf{U}^{\mathrm{T}}\mathbf{Q}_0. \tag{3.3.19}$$

Since the matrices $\widetilde{\mathbf{A}}_0$ and $\widetilde{\mathbf{C}}_0$ are diagonal, (3.3.18) splits into two independent scalar equations that actually describe the motion of a linear oscillator in the presence of an external harmonic force:

$$\ddot{\xi}_s + k_{s0}^2 \xi_s = \frac{\boldsymbol{\Phi}_{(s)}^{\mathrm{T}}\mathbf{Q}_0}{N_s} \cos \omega t. \tag{3.3.20}$$

The solution of each of these equations, corresponding to the right side, has the form:

$$\xi_s = \frac{\boldsymbol{\Phi}_{(s)}^{\mathrm{T}}\mathbf{Q}_0}{N_s(k_{s0}^2 - \omega^2)} \cos \omega t. \tag{3.3.21}$$

Returning to the original generalized coordinates according to (3.3.17), we finally find:

$$\widetilde{\boldsymbol{\varphi}} = \left[\boldsymbol{\Phi}_{(1)} \frac{\boldsymbol{\Phi}_{(1)}^{\mathrm{T}} \mathbf{Q}_0}{N_1(k_{10}^2 - \omega^2)} + \boldsymbol{\Phi}_{(2)} \frac{\boldsymbol{\Phi}_{(2)}^{\mathrm{T}} \mathbf{Q}_0}{N_2(k_{20}^2 - \omega^2)} \right] \cos \omega t. \tag{3.3.22}$$

Using the resulting expression, it is easy to understand what forced oscillation each of the harmonic components of the expression (3.3.10) excites. We note that when constructing a solution on the first mode, the first harmonic should take into account only the second term in the expression (3.3.22), since this harmonic is already balanced on the first mode. On the contrary, when constructing a solution on the second mode, only the first term should be taken into account [11]. Summing up the solutions corresponding to each harmonic of the expression (3.3.10), we obtain the so-called "regularized oscillation" excited in an unperturbed system by generalized forces $\mathbf{Q}^{(\mathrm{I})}(\boldsymbol{\Phi}_{(s)} a \cos\psi, \ldots)$ in the form:

$$\begin{aligned} \widetilde{\boldsymbol{\varphi}}^{(\mathrm{I})}(a,\psi) = \boldsymbol{\Phi}_{(n)} \frac{\boldsymbol{\Phi}_{(n)}^{\mathrm{T}} \mathbf{U}_s^{(\mathrm{I})} mgla^3}{N_n \left(k_{n0}^2 - k_s^2(a)\right)} \cos\psi + \\ + \left[\boldsymbol{\Phi}_{(1)} \frac{\boldsymbol{\Phi}_{(1)}^{\mathrm{T}} \mathbf{V}_s^{(\mathrm{I})} mgla^3}{N_1 \left(k_{10}^2 - 9k_s^2(a)\right)} + \boldsymbol{\Phi}_{(2)} \frac{\boldsymbol{\Phi}_{(2)}^{\mathrm{T}} \mathbf{V}_s^{(\mathrm{I})} mgla^3}{N_2 \left(k_{20}^2 - 9k_s^2(a)\right)} \right] \cos 3\psi. \end{aligned} \tag{3.3.23}$$

where the additional index n is introduced, and $n = 1$ at $s = 2$ and vice versa $n = 2$ at $s = 1$. It is clear that to keep only the terms of the third order of smallness in this expression, it suffices to substitute the constant value k_{s0} instead of $k_s(a)$. Adding (3.3.23) to the expression (3.3.6), one can obtain a solution up to the third order of smallness in the form:

$$\boldsymbol{\varphi} = \boldsymbol{\Phi}_{(s)} a \cos\psi + \widetilde{\boldsymbol{\varphi}}^{(\mathrm{I})}(a,\psi) = \left(\boldsymbol{\Phi}_{(s)} a + \mathbf{u}_s^{(\mathrm{I})} a^3 \right) \cos\psi + \mathbf{v}_s^{(\mathrm{I})} a^3 \cos 3\psi, \tag{3.3.24}$$

where the columns $\mathbf{u}_s^{(\mathrm{I})}$ and $\mathbf{v}_s^{(\mathrm{I})}$ are:

$$\mathbf{u}_s^{(\mathrm{I})} = \begin{bmatrix} \dfrac{\pm\sqrt{2}+1}{32} \\ \dfrac{2\pm\sqrt{2}}{32} \end{bmatrix}, \quad \mathbf{v}_s^{(\mathrm{I})} = \begin{bmatrix} \dfrac{\mp 552\sqrt{2}-437}{2688} \\ \dfrac{\pm 781\sqrt{2}+576}{2688} \end{bmatrix}. \tag{3.3.25}$$

The expression (3.3.24) together with (3.3.14) describes the motion of flat double pendulum on each of the nonlinear modes in the first approximation. We note

that it is necessary to know both modes of small oscillations $\mathbf{\Phi}_{(1)}$ and $\mathbf{\Phi}_{(2)}$ to construct each of the nonlinear oscillation modes separately.

Let us now calculate the column of generalized velocities corresponding to the expression (3.3.24), taking into account the formula (3.3.14) with the required accuracy:

$$\dot{\boldsymbol{\varphi}} = -k_{s0}\left[\left(\mathbf{\Phi}_{(s)}a + \widetilde{\mathbf{u}}_s^{(\mathrm{I})}a^3\right)\sin\psi + \widetilde{\mathbf{v}}_s^{(\mathrm{I})}a^3\sin 3\psi\right], \tag{3.3.26}$$

where the columns are $\widetilde{\mathbf{u}}_s^{(\mathrm{I})} = \mathbf{u}_s^{(\mathrm{I})} + \rho_s^{(\mathrm{I})}\mathbf{\Phi}_{(s)}$ and $\widetilde{\mathbf{v}}_s^{(\mathrm{I})} = 3\mathbf{v}_s^{(\mathrm{I})}$ look like:

$$\widetilde{\mathbf{u}}_s^{(\mathrm{I})} = \begin{bmatrix} \dfrac{\mp 19\sqrt{2} - 30}{32} \\ \dfrac{21 \pm 16\sqrt{2}}{16} \end{bmatrix}, \quad \widetilde{\mathbf{v}}_s^{(\mathrm{I})} = \begin{bmatrix} \dfrac{\mp 552\sqrt{2} - 437}{896} \\ \dfrac{\pm 781\sqrt{2} + 576}{896} \end{bmatrix}. \tag{3.3.27}$$

Now we can calculate the total mechanical energy of the system according to (2.3.10) up to the fourth order of smallness and make sure that for a given value of a it is a constant value, i.e. does not depend on ψ. Expanding the trigonometric functions included in the formula (2.3.10) into series, we obtain with the required accuracy:

$$E = \frac{1}{2}ml^2\left[2\dot{\varphi}_1^2 + \dot{\varphi}_2^2 + 2\dot{\varphi}_1\dot{\varphi}_2\left(1 - \frac{(\varphi_2 - \varphi_1)^2}{2}\right)\right] + \frac{1}{2}mgl\left(2\varphi_1^2 + \varphi_2^2 - \frac{\varphi_1^4}{6} - \frac{\varphi_2^4}{12}\right). \tag{3.3.28}$$

Substituting here formulas (3.3.24) and (3.3.26), we obtain the desired expression for the total energy up to the fourth order in a in the form:

$$E^{(\mathrm{I})} = E_0\left(1 + \frac{\mp 20\sqrt{2} - 37}{64}a^2\right), \quad E_0 = \frac{1}{2}N_s k_{s0}^2 a^2 = 2mgla^2, \tag{3.3.29}$$

where E_0 is the total energy in the linear model. It is easy to see that the expression (3.3.29) really does not depend on ψ, but depends only on a, which once again confirms the correctness of the performed calculations.

Returning to the formula (3.3.24) and setting $\psi = 0$ in it, we can determine the oscillation amplitudes of links A_{1s} and A_{2s} depending on the parameter a:

$$A_{1s}^{(\mathrm{I})}(a) = a + \frac{\mp 468\sqrt{2} - 353}{2688}a^3, \quad A_{2s}^{(\mathrm{I})}(a) = \mp\sqrt{2}a + \frac{\pm 865\sqrt{2} + 744}{2688}a^3. \tag{3.3.30}$$

It is interesting to estimate how the ratio of oscillation amplitudes of links $\mu_s(a) = A_{2s}/A_{1s}$ changes when system moves on nonlinear mode with a gradual increasing

a. Compose an expression for μ_s using (3.3.30), and then expand it into a series in a, keeping only one correction:

$$\mu_s^{(\mathrm{I})}(a) = \mu_{s0}\left(1 - \frac{16 \mp 3\sqrt{2}}{84}a^2\right). \tag{3.3.31}$$

Here $\mu_{s0} = \mp\sqrt{2}$ is the ratio of oscillation amplitudes in the linear model according to (2.4.16). The expression (3.3.31) already gives a certain representation of the change in the oscillation mode and shows that as a increases in a relatively small range, the ratio of the amplitudes begins to fall when moving both on the first and on the second mode:

$$\mu_1^{(\mathrm{I})}(a) \approx \mu_{10}(1 - 0.2410a^2), \quad \mu_2^{(\mathrm{I})}(a) \approx \mu_{20}(1 - 0.1399a^2). \tag{3.3.32}$$

2. Construction of the second approximation. We now turn to the construction of the second approximation [72]. In this approximation, a fourth-order correction should be introduced into the expression for oscillation frequency:

$$k_s^{(\mathrm{II})}(a) = k_{s0}\left(1 + \rho_s^{(\mathrm{I})}a^2 + \rho_s^{(\mathrm{II})}a^4\right). \tag{3.3.33}$$

Taking into account the orthogonality conditions (2.4.26), we can rewrite the harmonic balance equation (3.3.8) as:

$$\int_0^{2\pi}\left[N_s\left(\frac{d^2x}{dt^2} + k_{s0}^2x\right) - \mathbf{\Phi}_{(s)}^{\mathrm{T}}\mathbf{Q}\right]\cos\psi d\psi = 0, \tag{3.3.34}$$

where $x = a\cos\psi$ is denoted. Let us calculate the expression up to the values of the fifth order of smallness:

$$\frac{d^2x}{dt^2} + k_{s0}^2x = \left[-2\rho_s^{(\mathrm{I})}a^3 - \left(\rho_s^{(\mathrm{I})^2} + 2\rho_s^{(\mathrm{II})}\right)a^5\right]k_{s0}^2\cos\psi, \tag{3.3.35}$$

as well as the column $\mathbf{Q}$ with the same accuracy:

$$\begin{aligned}\mathbf{Q} = \Big[\left(\mathbf{U}_s^{(\mathrm{I})}a^3 + \mathbf{U}_s^{(\mathrm{II})}a^5\right)\cos\psi + \left(\mathbf{V}_s^{(\mathrm{I})}a^3 + \mathbf{V}_s^{(\mathrm{II})}a^5\right)\cos 3\psi + \\ + \mathbf{W}_s^{(\mathrm{II})}a^5\cos 5\psi\Big]mgl,\end{aligned} \tag{3.3.36}$$

where the columns $\mathbf{U}_s^{(\mathrm{II})}$, $\mathbf{V}_s^{(\mathrm{II})}$ and $\mathbf{W}_s^{(\mathrm{II})}$ have the form:

$$\mathbf{U}_s^{(\mathrm{II})} = \begin{bmatrix} \dfrac{\mp 43915\sqrt{2} - 61938}{3584} \\ \dfrac{106634 \pm 76131\sqrt{2}}{7168} \end{bmatrix}, \quad \mathbf{V}_s^{(\mathrm{II})} = \begin{bmatrix} \dfrac{\mp 40077\sqrt{2} - 56722}{1792} \\ \dfrac{74698 \pm 52845\sqrt{2}}{3584} \end{bmatrix},$$
$$\mathbf{W}_s^{(\mathrm{II})} = \begin{bmatrix} \dfrac{\mp 201035\sqrt{2} - 279322}{17920} \\ \dfrac{354770 \pm 252083\sqrt{2}}{35840} \end{bmatrix}, \tag{3.3.37}$$

while the columns $\mathbf{U}_s^{(\mathrm{I})}$ and $\mathbf{V}_s^{(\mathrm{I})}$ retain the same notation (3.3.11). Then from the equation (3.3.34) we obtain for $\rho_s^{(\mathrm{I})}$ the same values (3.3.13) as before, as expected, and also the expression for $\rho_s^{(\mathrm{II})}$:

$$\rho_s^{(\mathrm{II})} = -\frac{\left[\rho_s^{(\mathrm{I})}\right]^2}{2} - \frac{ml^2}{2N_s}\mathbf{\Phi}_{(s)}^{\mathrm{T}}\mathbf{U}_s^{(\mathrm{II})} = \frac{113415 \pm 79872\sqrt{2}}{28672}. \tag{3.3.38}$$

Thus, the oscillation frequency in the second approximation $k_s^{(\mathrm{II})}(a)$ when system moves in nonlinear mode is determined by the expression:

$$k_s^{(\mathrm{II})}(a) = k_{s0}\left(1 - \frac{31 \pm 20\sqrt{2}}{32}a^2 + \frac{113415 \pm 79872\sqrt{2}}{28672}a^4\right), \tag{3.3.39}$$

or in a more visual form:

$$k_1^{(\mathrm{II})}(a) = k_{10}(1 - 0.0849a^2 + 0.01604a^4), \quad k_2^{(\mathrm{II})}(a) = k_{20}(1 - 1.8526a^2 + 7.8952a^4). \tag{3.3.40}$$

We now obtain a solution up to the fifth order of smallness. To do this, we determine which forced oscillation excites $\mathbf{Q}$ from (3.3.36) in the unperturbed system:

$$\widetilde{\boldsymbol{\varphi}}^{(\mathrm{II})}(a,\psi) = \mathbf{\Phi}_{(n)}\frac{\mathbf{\Phi}_{(n)}^{\mathrm{T}}\left(\mathbf{U}_s^{(\mathrm{I})}a^3 + \mathbf{U}_s^{(\mathrm{II})}a^5\right)}{N_n(k_{n0}^2 - k_s^2(a))}mgl\cos\psi +$$
$$+ \left[\mathbf{\Phi}_{(1)}\frac{\mathbf{\Phi}_{(1)}^{\mathrm{T}}\left(\mathbf{V}_s^{(\mathrm{I})}a^3 + \mathbf{V}_s^{(\mathrm{II})}a^5\right)}{N_1(k_{10}^2 - 9k_s^2(a))} + \mathbf{\Phi}_{(2)}\frac{\mathbf{\Phi}_{(2)}^{\mathrm{T}}\left(\mathbf{V}_s^{(\mathrm{I})}a^3 + \mathbf{V}_s^{(\mathrm{II})}a^5\right)}{N_2(k_{20}^2 - 9k_s^2(a))}\right]mgl\cos 3\psi +$$

$$+\left[\boldsymbol{\Phi}_{(1)}\frac{\boldsymbol{\Phi}_{(1)}^{\mathrm{T}}\mathbf{W}_s^{(\mathrm{II})}a^5}{N_1(k_{10}^2-25k_s^2(a))}+\boldsymbol{\Phi}_{(2)}\frac{\boldsymbol{\Phi}_{(2)}^{\mathrm{T}}\mathbf{W}_s^{(\mathrm{II})}a^5}{N_2(k_{20}^2-25k_s^2(a))}\right]mgl\cos 5\psi. \tag{3.3.41}$$

Here, as before, $n=1$ for $s=2$ and vice versa $n=2$ for $s=1$. To keep the terms no higher than the fifth order of smallness in a, it suffices to substitute the expression (3.3.14) in the first three fractions of this formula instead of $k_s(a)$, and replace $k_s(a)$ with the constant value k_{s0} in the remaining two. Adding the expression (3.3.41) to (3.3.6), we obtain with the required accuracy:

$$\begin{aligned}&\boldsymbol{\varphi}=\boldsymbol{\Phi}_{(s)}a\cos\psi+\widetilde{\boldsymbol{\varphi}}^{(\mathrm{II})}(a,\psi)=\\&=\left(\boldsymbol{\Phi}_{(s)}a+\mathbf{u}_s^{(\mathrm{I})}a^3+\mathbf{u}_s^{(\mathrm{II})}a^5\right)\cos\psi+\left(\mathbf{v}_s^{(\mathrm{I})}a^3+\mathbf{v}_s^{(\mathrm{II})}a^5\right)\cos 3\psi+\mathbf{w}_s^{(\mathrm{II})}a^5\cos 5\psi,\end{aligned} \tag{3.3.42}$$

where the columns $\mathbf{u}_s^{(\mathrm{II})}$, $\mathbf{v}_s^{(\mathrm{II})}$ and $\mathbf{w}_s^{(\mathrm{II})}$ have representations:

$$\mathbf{u}_s^{(\mathrm{II})}=\begin{bmatrix}\dfrac{\mp1375\sqrt{2}+233}{28672}\\[2ex]\dfrac{\pm233\sqrt{2}-2750}{28672}\end{bmatrix},\quad \mathbf{v}_s^{(\mathrm{II})}=\begin{bmatrix}\dfrac{812575\pm535236\sqrt{2}}{802816}\\[2ex]\dfrac{-1148584\mp756783\sqrt{2}}{802816}\end{bmatrix},$$
$$\mathbf{w}_s^{(\mathrm{II})}=\begin{bmatrix}\dfrac{\pm2255280\sqrt{2}+2911491}{9748480}\\[2ex]\dfrac{\mp3111099\sqrt{2}-4066960}{9748480}\end{bmatrix}, \tag{3.3.43}$$

and the columns $\mathbf{u}_s^{(\mathrm{I})}$ and $\mathbf{v}_s^{(\mathrm{I})}$ are defined by the former formulas (3.3.25). The expression (3.3.42) together with (3.3.39) describes the motion of flat double pendulum on each of the nonlinear modes in the second approximation. Let us now calculate the column of generalized velocities with the same accuracy:

$$\begin{aligned}\dot{\boldsymbol{\varphi}}=-k_{s0}\Big[&\left(\boldsymbol{\Phi}_{(s)}a+\widetilde{\mathbf{u}}_s^{(\mathrm{I})}a^3+\widetilde{\mathbf{u}}_s^{(\mathrm{II})}a^5\right)\sin\psi+\\&+\left(\widetilde{\mathbf{v}}_s^{(\mathrm{I})}a^3+\widetilde{\mathbf{v}}_s^{(\mathrm{II})}a^5\right)\sin 3\psi+\widetilde{\mathbf{w}}_s^{(\mathrm{II})}a^5\sin 5\psi\Big],\end{aligned} \tag{3.3.44}$$

where the columns $\widetilde{\mathbf{u}}_s^{(\mathrm{I})}$ and $\widetilde{\mathbf{v}}_s^{(\mathrm{I})}$ keep the old representations (3.3.27) and the columns $\widetilde{\mathbf{u}}_s^{(\mathrm{II})}=\mathbf{u}_s^{(\mathrm{II})}+\rho_s^{(\mathrm{I})}\mathbf{u}_s^{(\mathrm{I})}+\rho_s^{(\mathrm{II})}\boldsymbol{\Phi}_{(s)}$, $\widetilde{\mathbf{v}}_s^{(\mathrm{II})}=3\left(\mathbf{v}_s^{(\mathrm{II})}+\rho_s^{(\mathrm{I})}\mathbf{v}_s^{(\mathrm{I})}\right)$ and $\widetilde{\mathbf{w}}_s^{(\mathrm{II})}=$

$5\mathbf{w}_s^{(\mathrm{II})}$ have the following form:

$$\widetilde{\mathbf{u}}_s^{(\mathrm{II})} = \begin{bmatrix} \dfrac{111660 \pm 77069\sqrt{2}}{28672} \\ \dfrac{\mp 57585\sqrt{2} - 82675}{14336} \end{bmatrix}, \quad \widetilde{\mathbf{v}}_s^{(\mathrm{II})} = \begin{bmatrix} \dfrac{3435281 \pm 2329564\sqrt{2}}{802816} \\ \dfrac{\mp 3270817\sqrt{2} - 4820440}{802816} \end{bmatrix},$$
$$\widetilde{\mathbf{w}}_s^{(\mathrm{II})} = \begin{bmatrix} \dfrac{\pm 2255280\sqrt{2} + 2911491}{1949696} \\ \dfrac{\mp 3111099\sqrt{2} - 4066960}{1949696} \end{bmatrix}. \tag{3.3.45}$$

To verify the obtained results, we write down the total mechanical energy of the system up to terms of the sixth order of smallness. Turning again to the formula (2.3.10) and expanding the series of trigonometric functions included in it with the retention of the required number of terms, we obtain the following expression:

$$E = \frac{1}{2}ml^2\left[2\dot{\varphi}_1^2 + \dot{\varphi}_2^2 + 2\dot{\varphi}_1\dot{\varphi}_2\left(1 - \frac{(\varphi_2 - \varphi_1)^2}{2} + \frac{(\varphi_2 - \varphi_1)^4}{24}\right)\right] + \\ + \frac{1}{2}mgl\left(2\varphi_1^2 + \varphi_2^2 - \frac{\varphi_1^4}{6} - \frac{\varphi_2^4}{12} + \frac{\varphi_1^6}{180} + \frac{\varphi_2^6}{360}\right). \tag{3.3.46}$$

Substituting the formulas (3.3.42) and (3.3.44) into it, we finally get:

$$E^{(\mathrm{II})} = E_0\left(1 + \frac{\mp 20\sqrt{2} - 37}{64}a^2 + \frac{2262801 \pm 1577160\sqrt{2}}{802816}a^4\right), \quad E_0 = 2mgla^2. \tag{3.3.47}$$

It can be seen that the total energy does not depend on ψ in this approximation, which is an indicator of the correctness of the constructed solution.

Referring to the formula (3.3.42), we determine the oscillation amplitudes of the pendulum links depending on the parameter a in the second approximation:

$$A_{1s}^{(\mathrm{II})}(a) = a + \frac{\mp 468\sqrt{2} - 353}{2688}a^3 + \frac{22500963 \pm 14502380\sqrt{2}}{17059840}a^5, \\ A_{2s}^{(\mathrm{II})}(a) = \sqrt{2}a + \frac{\pm 865\sqrt{2} + 744}{2688}a^3 + \frac{-33160840 \mp 21387427\sqrt{2}}{17059840}a^5. \tag{3.3.48}$$

Writing down the expression for the ratio of these amplitudes and expanding it

into a series with the retention of two correction terms, we get:

$$\mu_s^{(\mathrm{II})}(a) = \mu_{s0}\left(1 - \frac{16 \mp 3\sqrt{2}}{84}a^2 + \frac{\pm 895665\sqrt{2} - 747064}{9596000}a^4\right), \qquad (3.3.49)$$

or in a more visual form:

$$\mu_1^{(\mathrm{II})}(a) = \mu_{10}(1-0.2410a^2-0.2099a^4), \quad \mu_2^{(\mathrm{II})}(a) = \mu_{20}(1-0.1399a^2+0.0542a^4). \qquad (3.3.50)$$

The formula (3.3.49) refines the expression (3.3.31) obtained earlier in the first approximation and gives a certain representation of the first oscillation mode in a wider range of the parameter a.

We note a regularity that can be traced when we construct formulas in the first and second approximations for system motions on nonlinear oscillation modes: it is clear that all differences between the first and second modes in all expressions are only in the sign in front of the value $\sqrt{2}$.

Discussion of the results. We now turn to the analysis of the obtained results. First, let us analyze the formulas obtained for the first nonlinear oscillation mode. We plot the dependence of the oscillation frequency when the system moves on the first mode in the first (3.3.14) and in the second approximation (3.3.39), divided by the frequency in the linear model (i.e. k_1/k_{10}), on the oscillation amplitude of the first link A_{11} within the same approximations according to (3.3.30) and (3.3.48), respectively. As for orthogonal double pendulum, here in each case we have a parametric dependence of the frequency on this amplitude by means of an intermediate parameter a, and each subsequent approximation takes into account a new correction both in the expression for the frequency and in the expression for the amplitude. However, in contrast to the orthogonal double pendulum, where the study of nonlinear oscillation modes was reduced to the analysis of an ordinary mathematical pendulum, which admits an exact analytical solution, in the case of flat double pendulum such a well-known solution for nonlinear oscillation modes is absent. Therefore, approximate analytical results must be compared with the corresponding numerical results obtained by numerical integration of the matrix equation of motion (2.3.11). To do this, for each specific oscillation amplitude of the first link A_{11}, we should numerically select such an oscillation amplitude of the second link A_{21}, setting them as the initial conditions of motion (the initial angular velocities of the links are assumed to be equal to

zero), so that the motion of the double pendulum will be periodic (more precisely, the closest to periodic) with a frequency near the first oscillation frequency of the linear model k_{10} (so as not to get into the second mode). As a result, one can also determine the oscillation frequency k_1 for each amplitude A_{11}, and we should compare the approximate analytical results with it, and also give the dependence of the dimensionless frequency k_1/k_{10} corresponding to it on A_{11}. All mentioned dependencies are shown in Fig. 3.4. It can be seen that the analytical and numerical results correlate very well, and each subsequent approximation refines the results. Moreover, the oscillation frequency changes in a fairly small range with increasing amplitude. Thus, by analyzing the constructed plots, one can verify that the formulas obtained above give asymptotically correct results.

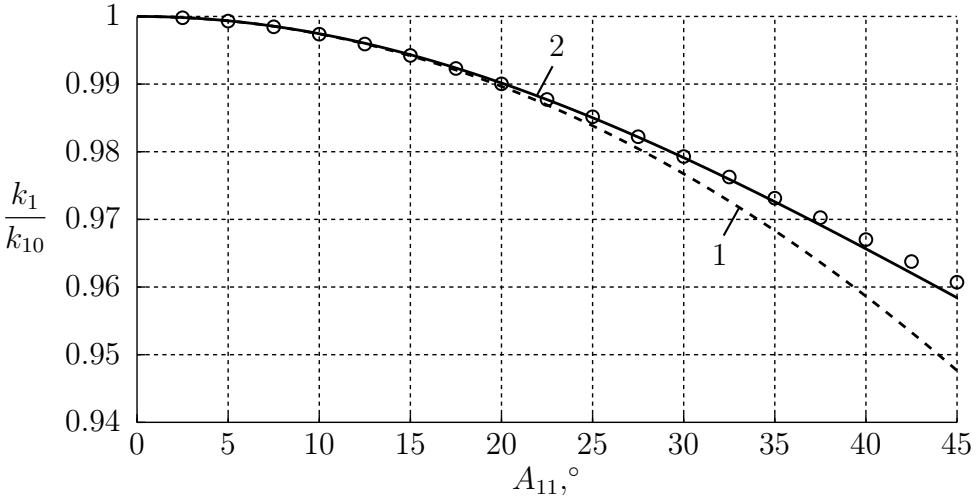

Fig. 3.4. Dependence of the dimensionless frequency k_1/k_{10} on amplitude A_{11}: 1 – first approximation, 2 – second approximation, ∘ – numerical solution

Let us now turn to the expression for the ratio of amplitudes in the first (3.3.31) and second (3.3.49) approximations and plot the dependence of μ_1/μ_{10} on the oscillation amplitude of the first link A_{11} according to (3.3.30) and (3.3.48). In this case, we also compare the results with numerical ones. According to Fig. 3.5, it can be seen that each subsequent approximation refines the results, i.e., the obtained formulas also give asymptotically correct results in this case. It can also be seen that the ratio of the amplitudes decreases with their increase, changing more significantly than the oscillation frequency.

It should be emphasized that for the excitation of oscillations on the first nonlinear mode at sufficiently large amplitudes, it is completely impossible to use

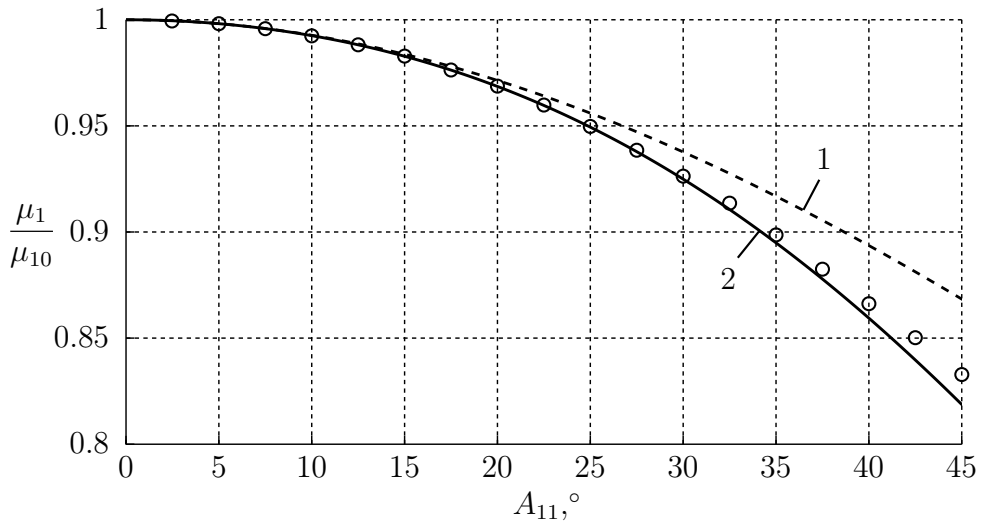

Fig. 3.5. Dependence of value μ_1/μ_{10} on amplitude A_{11}: 1 – first approximation, 2 – second approximation, ∘ – numerical solution

the linear model, since it will already give incorrect results, but it is necessary to use the obtained asymptotic expressions. For example, if it is necessary to excite system oscillations on the first mode with the oscillation amplitude of the first link $A_{11} = 45^\circ$, then from the obtained formulas, by varying the parameter a, it is easy to determine what the oscillation amplitude of the second link A_{21} should be. So, when we use a linear model, it should be $A_{21} = 63.6^\circ$, in the first approximation $A_{21} = 55.8^\circ$, and in the second approximation $A_{21} = 52.6^\circ$. The value obtained by numerical integration will be $A_{21} = 53^\circ$, and, as can be seen, it differs very little from the second approximation, has noticeable differences from the first approximation, and differs quite strongly from the value from linear model.

In order to visually illustrate the process of the drift of the first oscillation mode during the transition from a linear to a nonlinear zone, let us turn to the construction of a phase portrait of the system when it moves on this mode. It is clear that the phase space in the problem under consideration is four-dimensional. Therefore, it is convenient to construct a phase portrait for each generalized coordinate separately, i.e., in the form of projections onto the planes $(\varphi_1, \dot{\varphi}_1/k_{10})$ and $(\varphi_2, \dot{\varphi}_2/k_{10})$, where the division of the generalized velocities by the value k_{10} is carried out from dimension considerations [142]. We will plot a phase portrait using the formulas of the second approximation and compare it with the results obtained using numerical integration. Of course, the accordance between analytical and numerical results here must be made from the condition

of equality of the energy levels corresponding to them. For a numerical solution, it is easiest to set the initial values φ_{10} and φ_{20} of the angles φ_1 and φ_2, leaving the system to itself, as was done above with study of the oscillation frequency and the ratio of oscillation amplitudes. These values must be chosen so that they correspond to a periodic motion on the first mode, and, as mentioned above, that the according numerical phase trajectory corresponds to the same energy level as the phase trajectory from the approximate analytical solution. For convenience, we introduce the dimensionless energy $\varepsilon = E/(mgl)$. On the one hand, for given initial conditions in the numerical solution, it is determined according to (2.3.10):

$$\varepsilon = 3 - 2\cos\varphi_{10} - \cos\varphi_{20}. \tag{3.3.51}$$

On the other hand, the expression for the dimensionless energy in the second approximation according to (3.3.47) will be:

$$\varepsilon = 2a^2\left(1 + \frac{20\sqrt{2}-37}{64}a^2 + \frac{2262801 - 1577160\sqrt{2}}{802816}a^4\right). \tag{3.3.52}$$

By changing the parameter a, we will thereby vary the value of ε, i.e., we will obtain phase trajectories with different energy levels. Figs 3.6 and 3.7 show phase portraits on the planes $(\varphi_1, \dot{\varphi}_1/k_{10})$ and $(\varphi_2, \dot{\varphi}_1/k_{10})$. The solid lines show the phase trajectories corresponding to the asymptotic formulas of the second approximation, and the circles show the values obtained as result of numerical integration and taken at regular time intervals. One can see a very good agreement between the analytical and numerical results, and the process of oscillation mode drift with increase in the dimensionless energy level ε is also clearly observed. Thus, for small ε, the phase trajectories are concentric circles, which correspond to the motion on linear oscillation mode, while as ε increases, the circles gradually begin to be distorted and turn into other, more complex phase trajectories.

In addition, it is also of interest to construct a phase portrait for the interlink angle $\theta_2 = \varphi_2 - \varphi_1$, which can be taken as the second generalized coordinate instead of the absolute angle φ_2, i.e., on the plane $(\theta_2, \dot{\theta}_2/k_{10})$, for the same energy levels. It is shown in Fig. 3.8 and has a very nontrivial form. It demonstrates that as ε increases, the phase trajectories significantly complicate their character and acquire peculiar "loops". In this case, with increase in the energy level, the circles are located on the phase trajectories more and more unevenly. It can also be seen

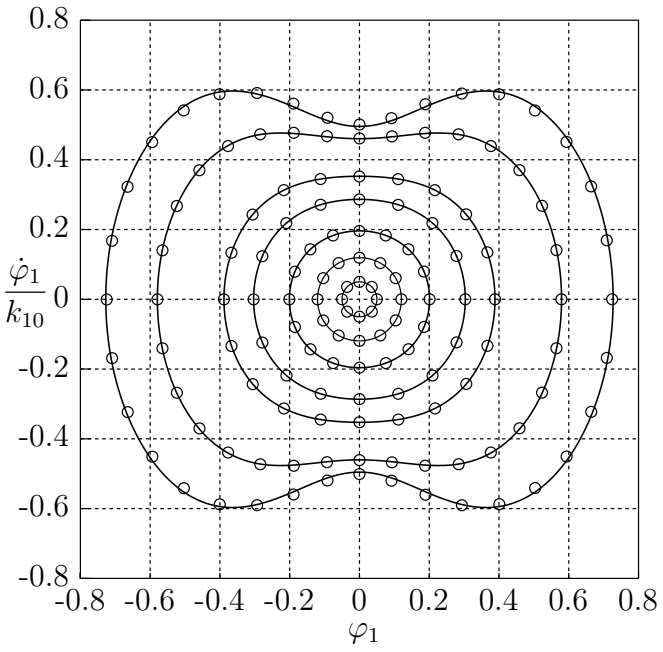

Fig. 3.6. Phase portrait for coordinate φ_1: solid lines – approximate analytical results, ∘ – numerical solution

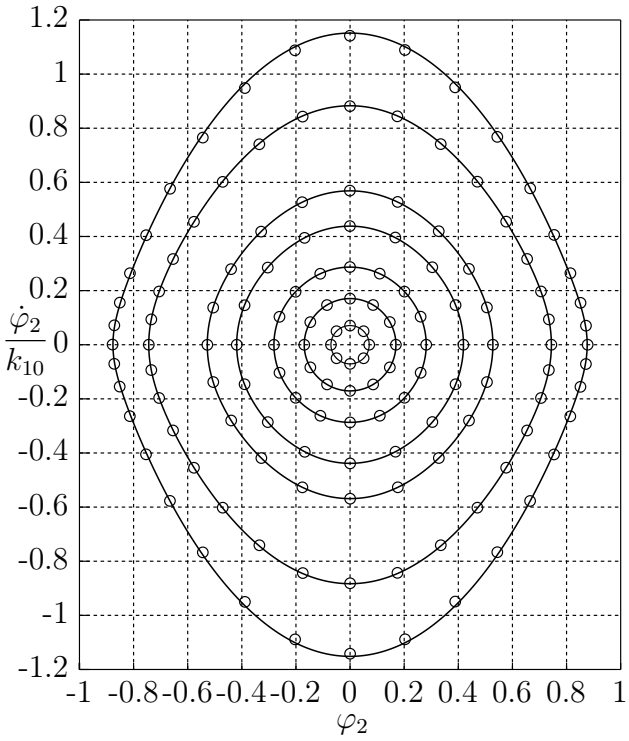

Fig. 3.7. Phase portrait for coordinate φ_2: solid lines – approximate analytical results, ∘ – numerical solution

that as the energy level increases, more tangible differences between the analytical and numerical results begin to appear here than in Figs 3.6 and 3.7. We note that the intersection of phase trajectories with different energy levels in Fig. 3.8 does not at all contradict the proposition that phase trajectories should not intersect each other, since the above Figure shows only projections of phase trajectories onto the plane $(\theta_2, \dot{\theta}_2/k_{10})$, while in reality the phase space is four-dimensional, and no intersections of phase trajectories will be observed in it. In this case, the energy levels corresponding to the constructed trajectories were chosen in such a way that all phase portraits were the most accessible for perception.

For greater clarity, graph dependencies of the absolute angles φ_1 and φ_2 and the interlink angle θ_2 on the phase angle ψ as it changes from 0 to 2π, corresponding to one oscillation period, are presented in Fig. 3.9, and they are in accordance with the phase trajectory with the highest energy level of those plotted in Figs 3.6–3.8. In this case, the value $\psi = k_1 t$ is also introduced for the numerical solution, where k_1 is the frequency obtained in the course of this solution, and the analytical results correspond to the formulas of the second approximation. As before, the analytical dependencies are represented by solid lines, and the

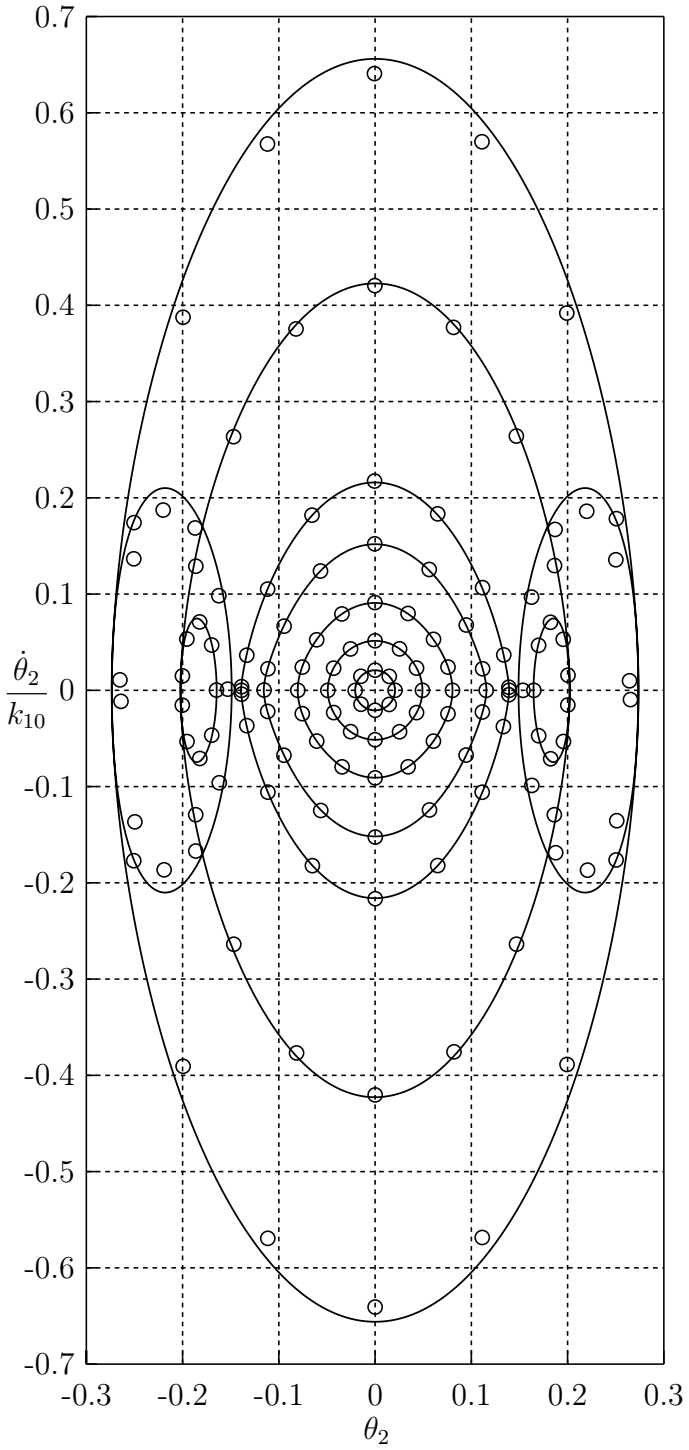

Fig. 3.8. Phase portrait for coordinate θ_2: solid lines – approximate analytical results, ∘ – numerical solution

numerical dependencies are shown by circles. These graphs once again clearly demonstrate the nontrivial character of the movements of flat double pendulum on the first nonlinear mode, and there is also a good agreement between the numerical and analytical results. Similar graphs are presented in Fig. 3.10, but for the corresponding angular velocities. It should be noted that for the given case,

the angle θ_2, as well as the angular velocities $\dot{\varphi}_1/k_{10}$ and $\dot{\theta}_2/k_{10}$ differ significantly from sinusoidal functions and have six extremes on the oscillation period, not two, as is the case of small oscillations. At the same time, the angles φ_1 and φ_2, as well as the angular velocity $\dot{\varphi}_2/k_{10}$, have two extremes on the oscillation period, as in the case of small oscillations, but their form is also significantly different from sinusoidal functions, thereby clearly reflecting the influence of nonlinear factors.

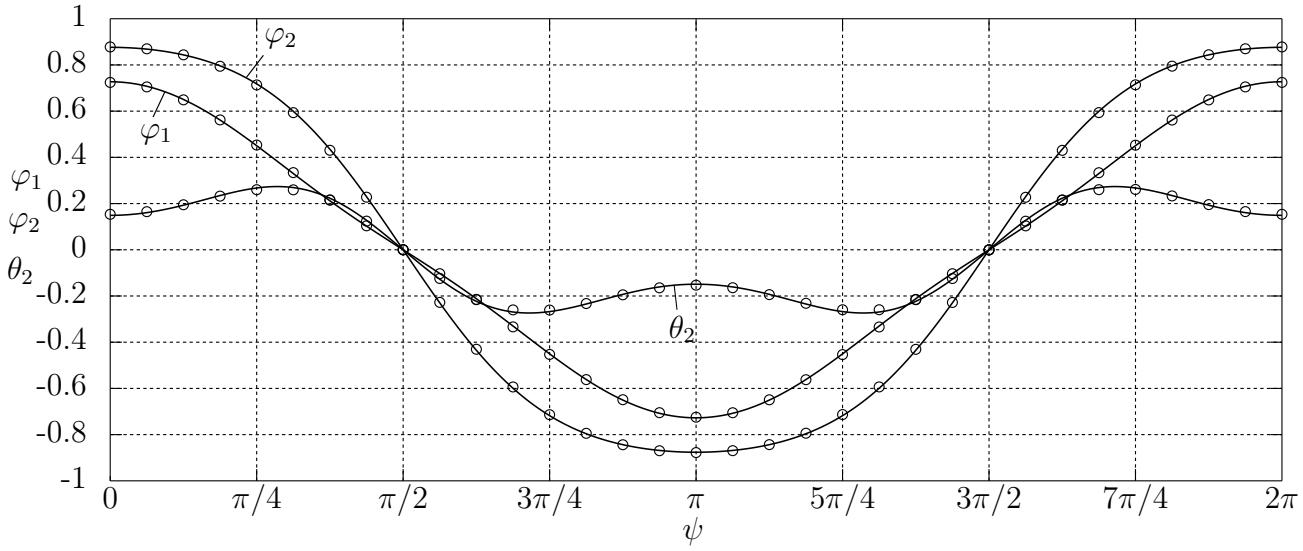

Fig. 3.9. Graph dependencies of φ_1, φ_2 и θ_2 on ψ: solid lines – approximate analytical results, ∘ – numerical solution

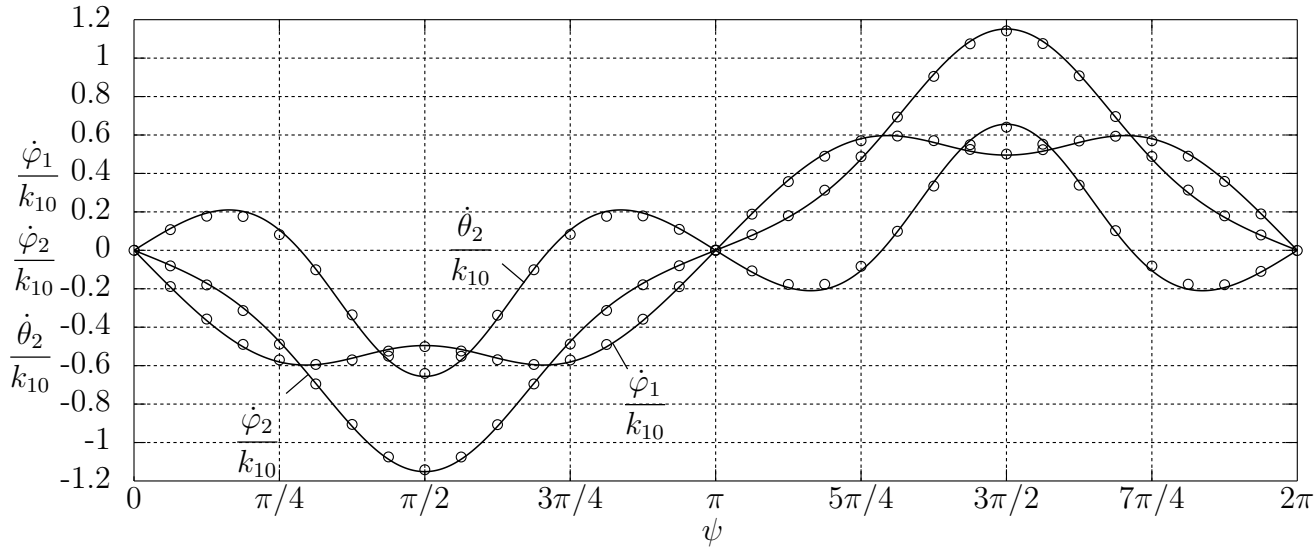

Fig. 3.10. Graph dependencies of $\dot{\varphi}_1/k_{10}$, $\dot{\varphi}_2/k_{10}$ и $\dot{\theta}_2/k_{10}$ on ψ: solid lines – approximate analytical results, ∘ – numerical solution

We can also conclude from these considerations that if the angles φ_1 and θ_2 are taken as generalized coordinates, then the ratio of their values achieved at

$\psi = 0$ and taken as oscillation amplitudes will be an adequate characteristic of the nonlinear oscillation mode only at sufficiently small deviations, since the maximum value of the angle θ_2 with their increase will not be reached at all at $\psi = 0$. In this case, such a ratio will already be meaningless. This circumstance once again emphasizes that in order to describe a nonlinear mode, it is necessary to know the specific dependencies of the generalized coordinates on time (or the phase angle) and the oscillation frequency corresponding to them. These expressions were obtained above, and they made it possible to describe the first nonlinear oscillation mode, i.e., the fundamental tone, which represents the main practical value. It turned out that the limits of applicability of the asymptotic formulas of the second approximation turn out to be quite wide, which ensures their importance in the study of periodic modes of motion of a flat double pendulum. In this case, the limits of applicability of the asymptotic formulas of the second approximation turn out to be quite wide, which ensures their importance in the study of periodic motion modes of flat double pendulum.

Let us now turn to a brief discussion of the results corresponding to the second nonlinear oscillation mode. As before for the first mode, we consider the dependence of the second frequency, divided by the corresponding linear frequency: k_2/k_{20}, on the amplitude of the first link A_{12} using the same formulas that contain the first two approximations. We also plot the dependence μ_2/μ_{20} on the oscillation amplitude of the first link A_{12} in two approximations. In each case, we also apply the results obtained using numerical integration. These dependencies are shown in Figs 3.11 and 3.12 respectively.

It can be seen according to Fig. 3.11 that each next approximation refines the results for the frequency, although it is acceptable in a rather narrow range of amplitudes. In this case, the second oscillation frequency changes strongly even at small amplitudes, in contrast to the first frequency. This also follows from the formulas (3.3.40), where there are very significant numerical coefficients for the second frequency in comparison with the expression for the first frequency. In particular, this also indicates that the area of applicability of the linear theory in studying the system motions on the second oscillation mode is much smaller than on the first mode, and it is limited for both angles to only a few degrees. Formally, this is explained by the fact that when we have oscillations on the first mode, when φ_1 and φ_2 oscillate in phase in the initial approximation, and when

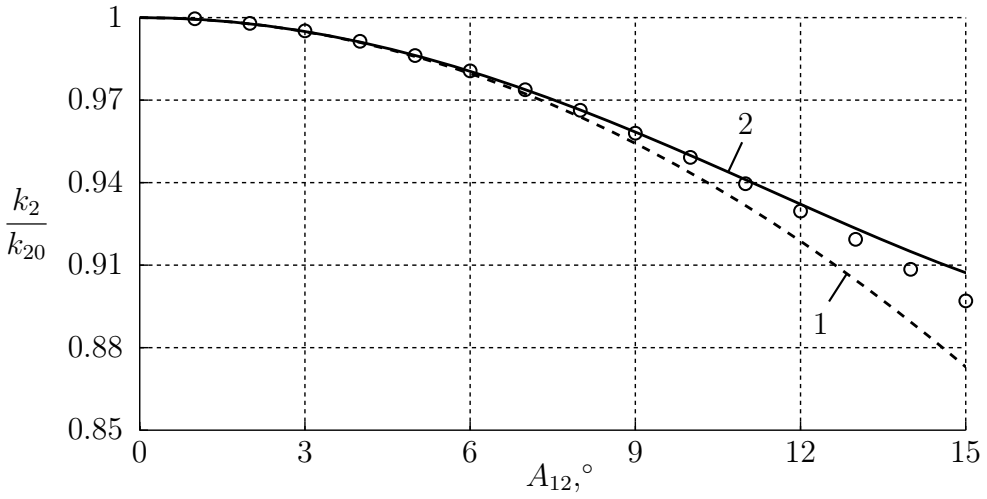

Fig. 3.11. Dependence of dimensionless frequency k_2/k_{20} on amplitude A_{12}:
1 – first approximation, 2 – second approximation, ∘ – numerical solution

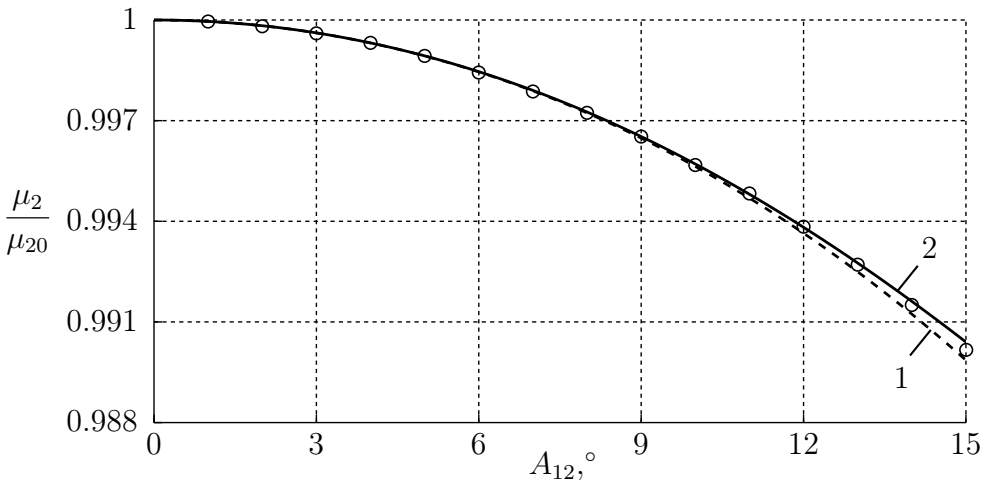

Fig. 3.12. Dependence of value μ_2/μ_{20} on amplitude A_{12}:
1 – first approximation, 2 – second approximation, ∘ – numerical solution

we have oscillations on the second mode, when φ_1 and φ_2 oscillate out of phase, expansion of the nonlinear terms (3.3.5) of the equations under study (3.3.1) into series will adequately describe the behavior of the system in different ranges of oscillation amplitudes. The ratio of amplitudes does not undergo practically any changes in the considered range. However, even in such a narrow range, a reliable asymptotic behavior of the obtained results is clearly demonstrated. Thus, despite the fact that the oscillation frequency strongly depends on the amplitude, i.e., this zone is already nonlinear, the ratio of the amplitudes and the character of the corresponding oscillation mode in the amplitude range under consideration will still be practically indistinguishable from the linear variant.

3.4. Nonlinear Oscillation Modes in General Case of Spatial Double Pendulum

Let us turn to the study of nonlinear oscillation modes in the general case of a spatial double pendulum, using the already proven technique and constructing here only one approximation due to the sufficient cumbersomeness of subsequent calculations [143]. To this purpose, we rewrite the nonlinear matrix motion equation (2.2.12) in the following form:

$$\mathbf{A}_0\ddot{\boldsymbol{\theta}} + \mathbf{C}_0\boldsymbol{\theta} = \widetilde{\mathbf{A}}(\boldsymbol{\theta})\ddot{\boldsymbol{\theta}} + \widetilde{\mathbf{B}}(\boldsymbol{\theta},\dot{\boldsymbol{\theta}}) + \widetilde{\mathbf{C}}(\boldsymbol{\theta}) = \mathbf{Q}(\boldsymbol{\theta},\dot{\boldsymbol{\theta}},\ddot{\boldsymbol{\theta}}), \tag{3.4.1}$$

where the matrices $\mathbf{A}_0$ and $\mathbf{C}_0$ are defined by the formulas (2.4.2), and the notation is made:

$$\widetilde{\mathbf{A}}(\boldsymbol{\theta}) = \mathbf{A}_0 - \mathbf{A}(\boldsymbol{\theta}), \quad \widetilde{\mathbf{B}}(\boldsymbol{\theta},\dot{\boldsymbol{\theta}}) = -\mathbf{B}(\boldsymbol{\theta},\dot{\boldsymbol{\theta}}), \quad \widetilde{\mathbf{C}}(\boldsymbol{\theta}) = \mathbf{C}_0\boldsymbol{\theta} - \mathbf{C}(\boldsymbol{\theta}). \tag{3.4.2}$$

It is enough to keep only the cubic nonlinearity in expression for $\mathbf{Q}$ to construct the first approximation. In turn, this means that the following approximations for matrix $\widetilde{\mathbf{A}}$ and columns $\widetilde{\mathbf{B}}$ and $\widetilde{\mathbf{C}}$ should be used:

$$\begin{gathered}
\widetilde{\mathbf{A}}(\boldsymbol{\theta}) = \frac{1}{2}ml^2\theta_2^2 \begin{bmatrix} 2(1+\sin^2\alpha) & \cos\alpha \\ \cos\alpha & 0 \end{bmatrix}, \\
\widetilde{\mathbf{B}}(\boldsymbol{\theta},\dot{\boldsymbol{\theta}}) = ml^2\theta_2 \begin{bmatrix} \left(2\left(1+\sin^2\alpha\right)\dot{\theta}_1 + \cos\alpha\dot{\theta}_2\right)\dot{\theta}_2 \\ -(1+\sin^2\alpha)\dot{\theta}_1^2 \end{bmatrix}, \\
\widetilde{\mathbf{C}}(\boldsymbol{\theta}) = \frac{1}{6}mgl \begin{bmatrix} 3\theta_1(\theta_1^2+\theta_2^2) + \cos\alpha\theta_2(3\theta_1^2+\theta_2^2) \\ \theta_2(3\theta_1^2+\theta_2^2) + \cos\alpha\theta_1(\theta_1^2+3\theta_2^2) \end{bmatrix},
\end{gathered} \tag{3.4.3}$$

so that the column $\mathbf{Q}$ will contain third-order nonlinear terms at $\boldsymbol{\theta}$, $\dot{\boldsymbol{\theta}}$ and $\ddot{\boldsymbol{\theta}}$. We note that, by virtue of the construction of only the first approximation, its number will be omitted everywhere below. As an initial approximation, we take the following expression:

$$\boldsymbol{\theta} = \boldsymbol{\Theta}_{(s)} a\cos\psi, \tag{3.4.4}$$

where $a = \text{const}$, and the oscillation frequency depends on a as follows:

$$\dot{\psi} = k_{s0}(1+\rho_s a^2) = k_s(a), \tag{3.4.5}$$

and the modes of small oscillations are here taken in the form $\mathbf{\Theta}_{(s)} = [1, \beta_{s0}]^{\mathrm{T}}$ taking into account the expression (2.4.14). Therefore, the value of a according to (3.4.4) will be the amplitude of oscillations of the angle θ_1 in the initial approximation. The correction factor ρ_s in the expression for the frequency k_s will now depend on the angle α, and establishing this dependence is one of the main tasks. As before, it should be determined from the harmonic balance equation for the given oscillation mode $\mathbf{\Theta}_{(s)}$:

$$\int_0^{2\pi} \mathbf{\Theta}_{(s)}^{\mathrm{T}} \Big(\mathbf{A}_0 \ddot{\boldsymbol{\theta}} + \mathbf{C}_0 \boldsymbol{\theta} - \mathbf{Q} \Big) \cos\psi d\psi = 0. \tag{3.4.6}$$

We calculate the column $\ddot{\boldsymbol{\theta}}$ up to terms of the third order of smallness, according to (3.4.4) and taking into account (3.4.5), and also the column of nonlinear terms $\mathbf{Q}$ with the same accuracy:

$$\ddot{\boldsymbol{\theta}} = -\mathbf{\Theta}_{(s)} a \cos\psi k_{s0}^2 (1 + 2\rho_s a^2), \quad \mathbf{Q} = mgl \left(\mathbf{U}_s \cos\psi + \mathbf{V}_s \cos 3\psi \right) a^3, \tag{3.4.7}$$

where the columns $\mathbf{U}_s$ and $\mathbf{V}_s$ have the following representations:

$$\begin{aligned} \mathbf{U}_s = \frac{1}{8} \Bigg\{ \begin{bmatrix} 3 \\ \beta_{s0}^3 \end{bmatrix} + \left(3 - 2p_{s0}^2 (1 + \sin^2\alpha)\right) \beta_{s0} \begin{bmatrix} \beta_{s0} \\ 1 \end{bmatrix} + \\ + \cos\alpha \begin{bmatrix} 3\beta_{s0} \\ 1 \end{bmatrix} + \cos\alpha (1 - p_{s0}^2) \beta_{s0}^2 \begin{bmatrix} \beta_{s0} \\ 3 \end{bmatrix} \Bigg\}, \end{aligned} \tag{3.4.8}$$

$$\begin{aligned} \mathbf{V}_s = \frac{1}{24} \Bigg\{ \begin{bmatrix} 3 \\ \beta_{s0}^3 \end{bmatrix} + 3\beta_{s0} \begin{bmatrix} \beta_{s0} \\ 1 \end{bmatrix} + 6 \left(1 + \sin^2\alpha\right) p_{s0}^2 \beta_{s0} \begin{bmatrix} -3\beta_{s0} \\ 1 \end{bmatrix} + \\ + \cos\alpha \begin{bmatrix} 3\beta_{s0} \\ 1 \end{bmatrix} + \cos\alpha \beta_{s0}^2 \begin{bmatrix} \beta_{s0} \\ 3 \end{bmatrix} - 3\cos\alpha p_{s0}^2 \beta_{s0}^2 \begin{bmatrix} 3\beta_{s0} \\ 1 \end{bmatrix} \Bigg\}. \end{aligned} \tag{3.4.9}$$

Substituting now (3.4.8) and (3.4.9) into (3.4.6) and taking into account that $\left(\mathbf{C}_0 - k_{s0}^2 \mathbf{A}_0\right) \mathbf{\Theta}_{(s)} = 0$, we get after transformations:

$$\rho_s = -\frac{mgl}{2N_s k_{s0}^2} \mathbf{\Theta}_{(s)}^{\mathrm{T}} \mathbf{U}_s = -\frac{1}{2H_s p_{s0}^2} \mathbf{\Theta}_{(s)}^{\mathrm{T}} \mathbf{U}_s, \tag{3.4.10}$$

where the values N_s and H_s are determined by the formulas (2.4.23) and (2.4.24) respectively. It is not difficult to calculate the expression $\mathbf{\Theta}_{(s)}^{\mathrm{T}} \mathbf{U}_s$ in (3.4.10) using

the formula (3.4.8):

$$\boldsymbol{\Theta}_{(s)}^{\mathrm{T}}\mathbf{U}_s = \frac{1}{8}\left[3 + 4\cos\alpha\beta_{s0} + 2\left(3 - 2p_{s0}^2(1+\sin^2\alpha)\right)\beta_{s0}^2 + \right.$$
$$\left. +4\cos\alpha(1-p_{s0}^2)\beta_{s0}^3 + \beta_{s0}^4\right]. \tag{3.4.11}$$

Thus, the dependence (3.4.10), taking into account (2.4.14), (2.4.24) and (3.4.11), determines the dependence of the correction factor ρ_s on the angle α.

It remains to obtain a solution up to the third order of smallness. For this, we find the correction $\widetilde{\boldsymbol{\theta}}(a,\psi)$ due to the value $\mathbf{Q}$ in equation (3.4.1). By analogy with the formula (3.3.23), it is easy to understand what kind of oscillations the force $\mathbf{Q}$ excites in the unperturbed system, up to terms of the third order of smallness:

$$\widetilde{\boldsymbol{\theta}}(a,\psi) = (\mathbf{u}_s\cos\psi + \mathbf{v}_s\cos 3\psi)\,a^3, \tag{3.4.12}$$

where the columns are $\mathbf{u}_s = [u_{1s}, u_{2s}]^{\mathrm{T}}$ and $\mathbf{v}_s = [v_{1s}, v_{2s}]^{\mathrm{T}}$ have the following form:

$$\mathbf{u}_s = \boldsymbol{\Theta}_{(n)}\frac{\boldsymbol{\Theta}_{(n)}^{\mathrm{T}}\mathbf{U}_s}{H_n(p_{n0}^2 - p_{s0}^2)}, \quad \mathbf{v}_s = \boldsymbol{\Theta}_{(1)}\frac{\boldsymbol{\Theta}_{(1)}^{\mathrm{T}}\mathbf{V}_s}{H_1(p_{10}^2 - 9p_{s0}^2)} + \boldsymbol{\Theta}_{(2)}\frac{\boldsymbol{\Theta}_{(2)}^{\mathrm{T}}\mathbf{V}_s}{H_2(p_{20}^2 - 9p_{s0}^2)}, \tag{3.4.13}$$

where $n = 1$ for $s = 2$ and vice versa $n = 2$ for $s = 1$. As before, a "regularized oscillation" is written here, which takes into account that when constructing a solution for a given oscillation mode $\boldsymbol{\Theta}_{(s)}$, it is already balanced due to (3.4.6). Therefore, only the term corresponding to the other oscillation mode is retained in the expression for $\mathbf{u}_s$. It should also be emphasized that the small oscillation frequencies maximally differ at $\alpha = 0$, when $p_{20}/p_{10} = \sqrt{2}+1 \approx 2.4142$, and this ratio tends to the value $p_{20}/p_{10} = \sqrt{5/3} \approx 1.2910$ with increasing α from 0 to $\pi/2$. Consequently, the denominators of fractions in the formula (3.4.13) for $\mathbf{v}_s$ cannot be equal to zero, which ensures the correctness of the constructed solution for the considered double pendulum with noncollinear joints. Summing up the expressions (3.4.12) and (3.4.4), we obtain a solution with the desired accuracy:

$$\boldsymbol{\theta} = \boldsymbol{\Theta}_{(s)}a\cos\psi + \widetilde{\boldsymbol{\theta}}(a,\psi) = \left(\boldsymbol{\Theta}_{(s)}a + \mathbf{u}_s a^3\right)\cos\psi + \mathbf{v}_s a^3\cos 3\psi, \tag{3.4.14}$$

which describes the motion of the system on a nonlinear oscillation mode. Therefore, the expression for the column of generalized velocities $\dot{\boldsymbol{\theta}}$, taking into account (3.4.5), will then look like:

$$\dot{\boldsymbol{\theta}} = -k_{s0}\left[\left(\boldsymbol{\Theta}_{(s)}a + \widetilde{\mathbf{u}}_s a^3\right)\sin\psi + \widetilde{\mathbf{v}}_s a^3\sin 3\psi\right], \tag{3.4.15}$$

where the following notations are made: $\widetilde{\mathbf{u}}_s = \mathbf{u}_s + \rho_s \mathbf{\Theta}_{(s)}$ and $\widetilde{\mathbf{v}}_s = 3\mathbf{v}_s$.

In order to make sure that the constructed solution is correct, we should check the constancy of total mechanical energy with the required accuracy. Considering that the exact expressions for the kinetic and potential energies are respectively (2.2.8) and (2.2.10), we expand the trigonometric functions included in them into Taylor series, as a result of which we get:

$$E = \frac{1}{2}ml^2\left[\left(5-(1+\sin^2\alpha)\theta_2^2\right)\dot{\theta}_1^2 + \cos\alpha(4-\theta_2^2)\dot{\theta}_1\dot{\theta}_2 + \dot{\theta}_2^2\right] + \\ + \frac{1}{2}mgl\left[3\theta_1^2 - \frac{\theta_1^4}{4} + \theta_2^2 - \frac{\theta_2^4}{12} - \frac{\theta_1^2\theta_2^2}{2} + 2\cos\alpha\theta_1\theta_2\left(1-\frac{\theta_1^2}{6}-\frac{\theta_2^2}{6}\right)\right]. \tag{3.4.16}$$

Taking into account the formulas (3.4.14) and (3.4.15), we the obtain an expression for the total energy up to the terms of the fourth order of smallness at a:

$$E = E_{s0}(1+\delta_s a^2), \quad E_{s0} = \frac{1}{2}mglH_s p_{s0}^2 a^2, \tag{3.4.17}$$

which does not depend on ψ. This circumstance can be verified using computational procedures in any computer program, since analytical calculations here turn out to be too cumbersome. We note that E_{s0} in (3.4.17) represents the total mechanical energy in the linear model, and the dependence of the coefficient δ_s on the angle α can also be obtained using computational procedures.

Let us further consider in detail the first nonlinear oscillation mode, which, as mentioned above, represents the main practical value. We plot the dependence of the correction factor ρ_1 on the angle α. It is shown in Fig. 3.13. It is easy to check the results obtained in the special cases $\alpha = 0$ and $\alpha = \pi/2$, which were considered above. At $\alpha = 0$ we have according to (3.4.10) $\rho_1 = -(31-20\sqrt{2})/32 \approx -0.0849$, which agrees with the expression (3.3.13), and at $\alpha = \pi/2$ we get $\rho_1 = -1/16 = -0.0625$, as it should be based on the formula (3.2.10). These values are clearly visible in Fig. 3.13.

Discussion of the results. Let us now discuss the dependencies of the elements of columns $\mathbf{u}_1 = [u_{11}, u_{21}]^{\mathrm{T}}$ and $\mathbf{v}_1 = [v_{11}, v_{21}]^{\mathrm{T}}$, which characterize the correction terms in the formula (3.4.14), on the angle α. They are presented graphically in Figs 3.14 and 3.15 respectively. In case $\alpha = 0$ we find from (3.4.13) values: $u_{11} = (1-\sqrt{2})/32 \approx -0.0129$, $u_{21} = 1/32 = 0.03125$, $v_{11} = (552\sqrt{2} - 437)/2688 \approx 0.1278$ and finally $v_{21} = (1013 - 1333\sqrt{2})/2688 \approx -0.3245$. To

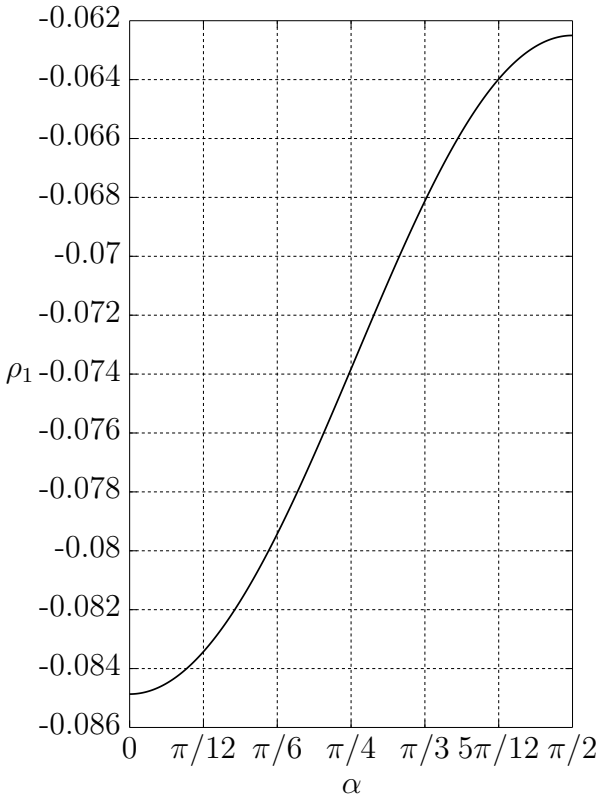

Fig. 3.13. Graph dependence of value ρ_1 on angle α

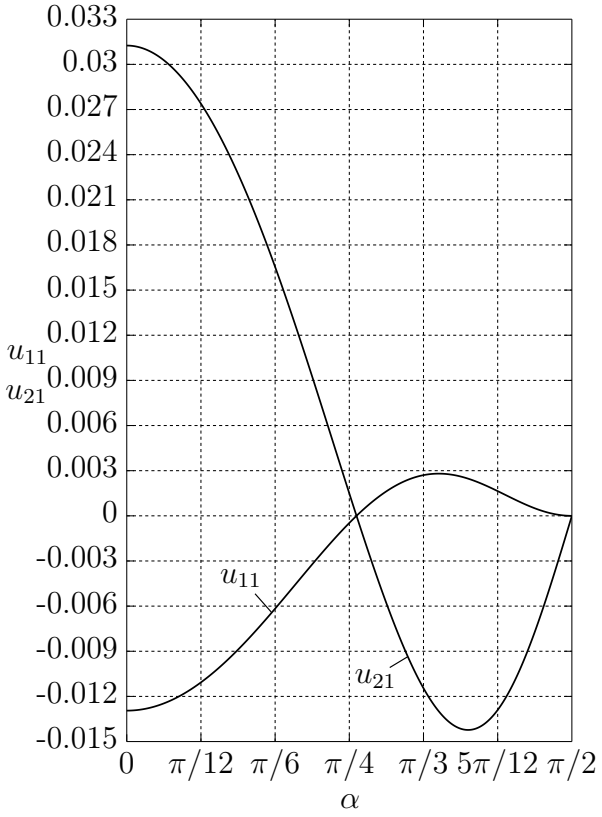

Fig. 3.14. Graph dependencies of values u_{11} and u_{21} on angle α

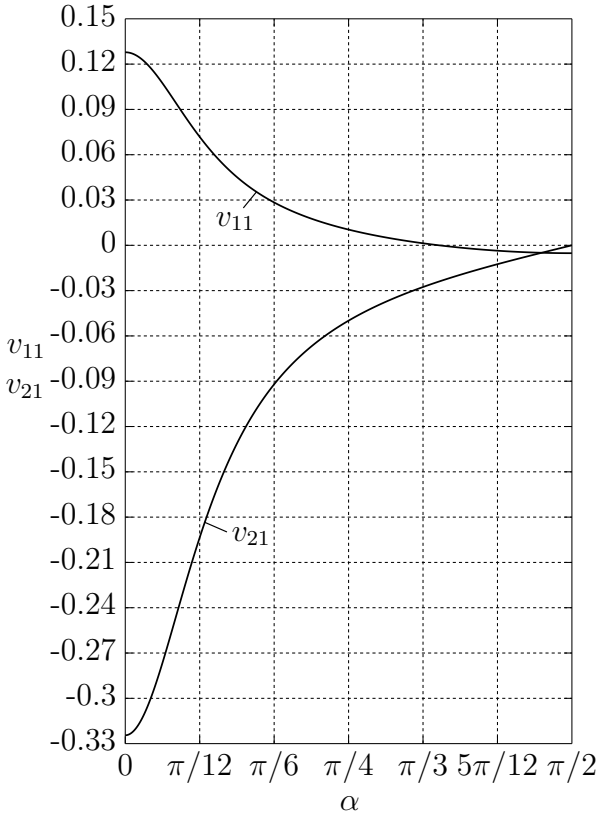

Fig. 3.15. Graph dependencies of values v_{11} and v_{21} on angle α

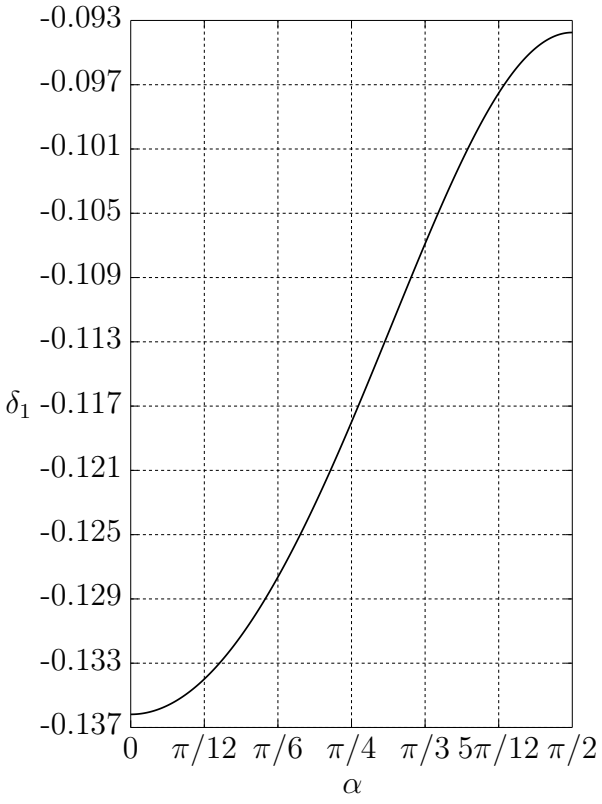

Fig. 3.16. Graph dependence of value δ_1 on angle α

check these results, we should compare them with the values obtained earlier. Recall that when studying the variant $\alpha = 0$, we took as generalized coordinates the absolute deviation angles φ_1 and φ_2 of the pendulum links from the vertical. As mentioned above, these angles are related to the rotation angles in joints by the relations $\varphi_1 = \theta_1$, $\varphi_2 = \theta_1 + \theta_2$, and this should be taken into account when calculating the values u_{11}, u_{21}, v_{11}, v_{21} from the formula (3.4.14) for the case of a flat double pendulum. Referring to the formulas (3.3.24) and (3.3.25), it is easy to check that the indicated values really take at $\alpha = 0$ the same values that were written above. For the case $\alpha = \pi/2$ we find from (3.4.13): $u_{11} = u_{21} = v_{21} = 0$ and $v_{11} = -1/192 \approx -0.005208$, which is in full agreement with the formula (3.2.14). All these values are easily seen in Figs 3.14 and 3.15. We also note that both $u_{11} = 0$ and $u_{21} = 0$ when condition $\mathbf{\Theta}_{(2)}^{\mathrm{T}}\mathbf{U}_1 = 0$ is performed, i.e., at $\alpha = 0.8108$.

The graph dependence of the coefficient δ_1 in the expression for the total energy on the angle α is shown in Fig. 3.16. In the particular cases we have: $\delta_1 = (20\sqrt{2} - 37)/64 \approx -0.1362$ at $\alpha = 0$ и $\delta_1 = -3/32 = -0.09375$ at $\alpha = \pi/2$, and these values are in full agreement with the formulas (3.3.29) and (3.2.19).

Next, we present the phase portrait of the system movement on the first nonlinear oscillation mode, for example, at $\alpha = \pi/6$, considering the motion of the representing point in the projection onto the planes $(\theta_1, \dot{\theta}_1/k_{10})$ and $(\theta_2, \dot{\theta}_2/k_{10})$. We restrict ourselves here to only demonstrating a smooth transition of linear to nonlinear oscillations mode, depicting phase trajectories with not very large energy. It is necessary to use the formulas (3.4.14) and (3.4.15) to construct these trajectories. In addition, we compare qualitatively and quantitatively the obtained solution with the numerical one constructed using numerical integration procedure. To numerically determine the nonlinear mode, as usual, one can set the initial values θ_{10} and θ_{20} of the angles θ_1 and θ_2 without specifying the initial velocities, and these values must be chosen so that they correspond to periodic movement, which frequency should be close to the linear value k_{10}. Finally, the phase trajectories in the analytical and numerical solution must correspond to the same energy level. Reintroducing the dimensionless energy $\varepsilon = E/(mgl)$, we establish that for given initial conditions in the numerical solution it is determined

by the expression:

$$\varepsilon = 3 - (2 + \cos\theta_{20})\cos\theta_{10} + \cos\alpha \sin\theta_{20}\sin\theta_{10}, \tag{3.4.18}$$

which follows from (2.2.10), and at the same time, in the approximate analytical solution according to (3.4.17), it has the form:

$$\varepsilon = \frac{1}{2}H_1 p_{10}^2(1 + \delta_1 a^2) = 1.8924a^2(1 - 0.1276a^2), \tag{3.4.19}$$

where the specific values of the coefficients are also indicated for the case $\alpha = \pi/6$. The phase portraits are shown in Figs 3.17 and 3.18. The solid lines represent the approximate analytical results, and the circles correspond to the results of numerical integration, and they correspond to values which are taken at equal time intervals. It is seen that there is a good agreement between the analytical and numerical results. Moreover, the shape of phase trajectories with energy level increasing is more and more different from the circular one that corresponds to the linear model. This can be seen especially clearly in Fig. 3.18, although the values θ_2 and $\dot{\theta}_2/k_{10}$ are rather small. Nevertheless, the nonlinearity influence is very significant here.

For greater clarity, we finally plot the graphs dependencies of the values of angles θ_1 и θ_2 and dimensionless angular velocities $\dot{\theta}_1/k_{10}$ and $\dot{\theta}_2/k_{10}$, where $k_{10}/k = p_{10} = 0.7672$ at $\alpha = \pi/6$, on phase angle ψ when it changes from 0 to 2π, which correspond to the trajectory with the highest energy level from the above. To pass from time t to a similar value in the numerical solution using the formula $\psi = k_1 t$, it is necessary to know the frequency of nonlinear oscillations in this solution: $k_1/k = 0.7415$. We notice that for approximate analytical solution according to (3.4.5), this value turns to $k_1/k = 0.7405$, i.e. it does not differ practically from the numerical one. The indicated dependencies are shown in Fig. 3.19, and they clearly describe the motion process of the system on the first nonlinear oscillation mode, demonstrating also adequate agreement between analytical and numerical results. It can be seen that the given dependencies have more complex nature than when the system moves on a linear oscillation mode.

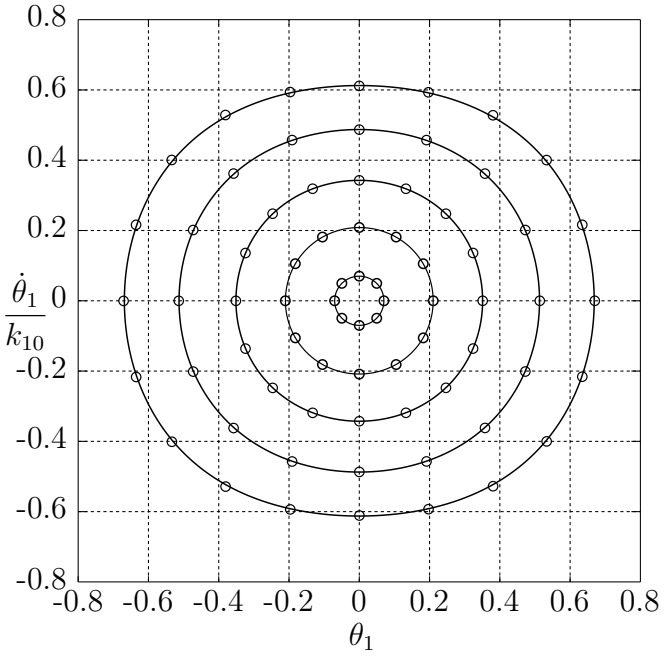

Fig. 3.17. Phase portrait for coordinate θ_1: solid lines – approximate analytical results, ∘ – numerical solution

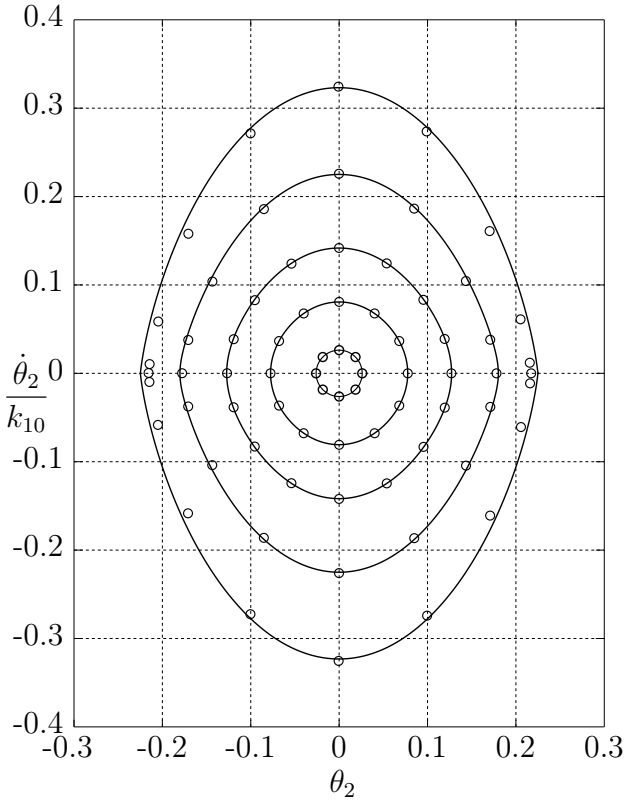

Fig. 3.18. Phase portrait for coordinate θ_2: solid lines – approximate analytical results, ∘ – numerical solution

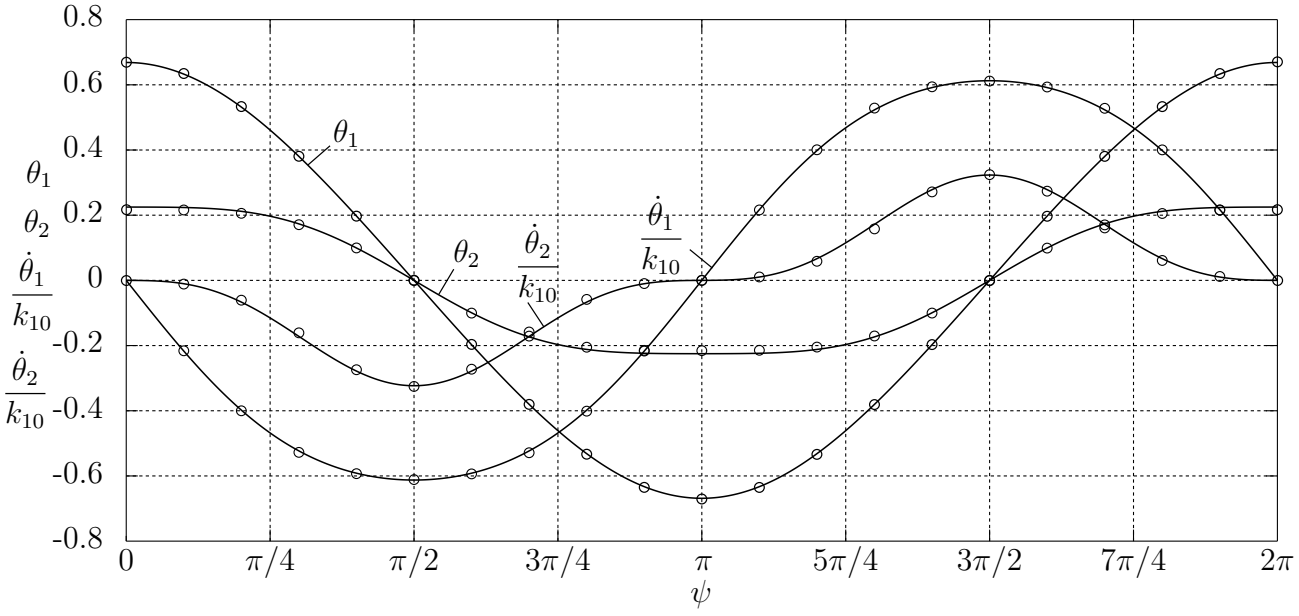

Fig. 3.19. Graph dependencies of θ_1, θ_2, $\dot\theta_1/k_{10}$ и $\dot\theta_2/k_{10}$ on ψ: solid lines – approximate analytical results, ∘ – numerical solution

3.5. Conclusions on Third Chapter

The approximate analytical solutions constructed in this chapter for oscillation frequencies and modes of double pendulum with noncollinear joints make it possible to consider from a unified standpoint a smooth transition from its linear model to a nonlinear one and vice versa. For the general case, the solution was obtained only in the first approximation, while for particular variants of the orthogonal and flat double pendulum, it was possible to construct a solution in two approximations. These approximations demonstrate that the motion of the system on the oscillation mode is periodic and is the sum of several harmonic components when nonlinear effects are taken into account. In this case, the first approximation is described by rather compact expressions and gives a qualitatively correct picture of the change in the key parameters of the nonlinear mode, while the second approximation, being more cumbersome in its structure, makes it possible to obtain more accurate results in quantitative terms. The undoubted advantage of all the above expressions is their convenient formula representation and adequate correspondence to the results of numerical integration, as well as a clear graphical interpretation of the oscillation frequencies, the ratio of oscillation amplitudes, phase portraits, generalized coordinates and dimensionless generalized velocities in one oscillation period.

The obtained results may be necessary in the development and design of various devices of modern robotics, first of all, spatial manipulators, which can oscillate with sufficiently large amplitudes. In addition, the significant value of these results lies in the fact that they are important for further research, and first of all, for the problems of adequate control of the working movements of such manipulators. This is due to the fact that in this case it is necessary to provide for transient overclocking modes from their small oscillations on any mode to large ones, where the role of nonlinear terms in the overall picture of behavior sharply increases, so that it is necessary for this purpose to have a detailed representation of the qualitative and quantitative character of these movements.

4. Collinear Control of Oscillation Modes of Spatial Double Pendulum

4.1. Principles of Formation of Rational Control Actions

Oscillation control of pendulum structures is one of the main directions of modern control theory, and a large number of publications are devoted to this issue. Herewith, controlled processes in pendulum systems with several degrees of freedom are of particular interest. This is due to the fact that in this case, in order to achieve certain purposes, it is necessary to pay closer attention to the formation of control actions than in the study of systems with one degree of freedom. In particular, a significant number of works are devoted to the control of the movements of a double pendulum and its modifications [3, 88, 94, 120].

It is clear that one of the most important tasks is to propose an approach to the formation of a fairly simple control law that allows such pendulum system to swing on each of its oscillation modes separately with their gradual transition to a nonlinear zone. This path should be considered rational, since during its implementation, all the energy supplied to the system will be directed to the development of only one oscillation mode, without exciting other modes. In this case, it is important also to ensure the gradual transition of the system to the required functioning mode which corresponds to a predetermined energy level and represents a regular periodic motion with sufficient large amplitude. As mentioned above, these motions are the most valuable of all possible movement modes of

nonlinear systems, because they are advisable for practical use in the operation of manipulators and other robotic devices. In this regard, the main purpose of this chapter is to construct and study a control with the indicated properties.

As noted, the oscillation frequencies of nonlinear systems begin to drift with an increase in the oscillation amplitudes, while the oscillation modes also gradually begin to change. Therefore, the traditional methods of swinging of the system, that is, the organization of resonant oscillations, associated with harmonic excitation in the form of a given program in time with prescribed frequency from the outside and widely used in linear systems, are unsuitable here. This is due to the fact that in this case the main condition for the occurrence of the resonant process will be violated – the action of an external force in time with natural oscillations of the system. This means that in order to organize truly resonant effects in nonlinear systems, it is necessary to create control actions in accordance with the state of the system, i.e. when the excitation frequency is not externally prescribed, but fed to the excitation drive as a feedback signal [65]. Such a controlled resonant mode is well known for systems with one degree of freedom, and its research begins from fundamental work [4], where the concept of "autoresonance" was introduced for it. This controlled mode ensures that the frequency and phase of the feedback signal will exactly correspond to the current frequency and phase of the system oscillations, due to which all the energy entering the system will be transferred to it. However, term "autoresonance" remained practically unnoticed for many years, and the interest in this concept gradually increased only in the last several decades [5, 32]. For example, the works [109, 110] are devoted to the feedback resonance. The main difficulty in the practical implementation of such resonance is the need to use a feedback loop in order to form the required drive control law.

It is known that the formation of a control law using feedback can be carried out in many different ways for systems with one degree of freedom, when there will be a monotonic increase in the total energy of the system [108]. The organization of such an overclocking mode turns out to be more difficult for multidimensional nonlinear systems. Feedback resonance in similar systems is studied in some works, for example, in [102]. In this situation, the difficulty arises due to such mechanical systems have several degrees of freedom, i.e., several frequencies and modes. As mentioned above, it is necessary for swinging of the system in this case not only to increase the energy of the system, but also to be able to swing the system on

one of its free oscillation modes separately. Otherwise, the energy supplied to the system will go to excite all modes at once, which will lead to a sharp decrease of the resonant properties of control and the quality of the motion processes. This means that the required control should not violate the linear oscillation modes of the system and allow a gradual transition of each oscillation mode to a corresponding nonlinear one, swinging the system from small amplitudes up to the sufficiently large ones. We note that the preservation of the topological structure of the nonlinear oscillations mode becomes extremely important for the running movement modes of living organisms with amplitudes of limb swaying, reaching up to sufficiently large values. Therefore, the required control will play an extremely important role in the problems of biomechanics and robotics, where the transition from stepping to running amplitudes is possible only in the autoresonance mode, and both when walking and running, the movement remains single-frequency, although its frequency is gradually changing, and there is also a smooth change in the oscillation mode. Consequently, the control actions constructed in this way will be of great practical importance and will be able to find application in the running of androids, where the creation of a nonlinear resonant mode plays a primary role [81], so their formation and analysis seems to be the actual task.

4.2. Formation of Control Actions According to the Principle of Collinear Control

Let us turn to the study of controlled motions of spatial double pendulum. We will assume that sensors are installed in both of its joints that can read information about state variables, i.e., the values θ_1, $\dot{\theta}_1$, θ_2, $\dot{\theta}_2$, corresponding to the current system configuration. The control moments acting in the pendulum joints are formed according to the feedback principle on the basis of these values. We write the nonlinear matrix equation of the controlled motion of the system by adding the column of control actions $\mathbf{Q}$ to the right side of the equation (2.2.11):

$$\frac{d}{dt}\frac{\partial T}{\partial \dot{\boldsymbol{\theta}}} - \frac{\partial T}{\partial \boldsymbol{\theta}} = -\frac{\partial \Pi}{\partial \boldsymbol{\theta}} + \mathbf{Q}. \tag{4.2.1}$$

To find out how the feedback control law should be formed, we first establish the energy relation by multiplying the equation (4.2.1) by the string $\dot{\boldsymbol{\theta}}^{\mathrm{T}}$ on the left.

The resulting equality can be transformed, taking into account that according to (2.2.8) and (2.2.10) we have $T = T(\boldsymbol{\theta}, \dot{\boldsymbol{\theta}})$, $\Pi = \Pi(\boldsymbol{\theta})$, and in addition

$$\frac{d}{dt}\left(\dot{\boldsymbol{\theta}}^{\mathrm{T}}\frac{\partial T}{\partial \dot{\boldsymbol{\theta}}}\right) = \dot{\boldsymbol{\theta}}^{\mathrm{T}}\frac{d}{dt}\frac{\partial T}{\partial \dot{\boldsymbol{\theta}}} + \ddot{\boldsymbol{\theta}}^{\mathrm{T}}\frac{\partial T}{\partial \dot{\boldsymbol{\theta}}}, \quad \frac{dT}{dt} = \dot{\boldsymbol{\theta}}^{\mathrm{T}}\frac{\partial T}{\partial \boldsymbol{\theta}} + \ddot{\boldsymbol{\theta}}^{\mathrm{T}}\frac{\partial T}{\partial \dot{\boldsymbol{\theta}}}, \quad \frac{d\Pi}{dt} = \dot{\boldsymbol{\theta}}^{\mathrm{T}}\frac{\partial \Pi}{\partial \boldsymbol{\theta}}. \tag{4.2.2}$$

As a result, we get the following relation:

$$\frac{d}{dt}\left(\dot{\boldsymbol{\theta}}^{\mathrm{T}}\frac{\partial T}{\partial \dot{\boldsymbol{\theta}}} - T + \Pi\right) = \dot{\boldsymbol{\theta}}^{\mathrm{T}}\mathbf{Q}. \tag{4.2.3}$$

Since T is the quadratic form of generalized velocities, then

$$\dot{\boldsymbol{\theta}}^{\mathrm{T}}\frac{\partial T}{\partial \dot{\boldsymbol{\theta}}} = \dot{\boldsymbol{\theta}}^{\mathrm{T}}\mathbf{A}(\boldsymbol{\theta})\dot{\boldsymbol{\theta}} = 2T, \tag{4.2.4}$$

and after that we finally arrive from (4.2.3) at a simple energy relation:

$$\dot{E} = \dot{\boldsymbol{\theta}}^{\mathrm{T}}\mathbf{Q}, \tag{4.2.5}$$

where $E = T + \Pi$ is the total mechanical energy of the system. This implies the obvious conclusion that in order to increase in energy, it is necessary to choose the column of control actions $\mathbf{Q}$ in order to fulfill the condition

$$\dot{\boldsymbol{\theta}}^{\mathrm{T}}\mathbf{Q} \geq 0. \tag{4.2.6}$$

It seemed that the simplest way here is to choose the column of control actions in proportion to the column of angular velocities, i.e., in the form

$$\mathbf{Q} = \gamma\dot{\boldsymbol{\theta}}, \tag{4.2.7}$$

where γ is the gain factor, which is a constant value in its simplest form. It is clear that in this case the energy relation (4.2.6) will take the form:

$$\dot{E} = \gamma\dot{\boldsymbol{\theta}}^{\mathrm{T}}\dot{\boldsymbol{\theta}} = \gamma\|\dot{\boldsymbol{\theta}}\|^2 \geq 0, \tag{4.2.8}$$

where $\|\dot{\boldsymbol{\theta}}\| = \sqrt{\dot{\theta}_1^2 + \dot{\theta}_2^2}$ is the norm of the column $\dot{\boldsymbol{\theta}}$, and this relation will be satisfied for any positive value γ. It is easy to understand that with such formation of the control law, it will imitate the dissipative forces of viscous friction in the pendulum joints, taken with opposite signs. Based on the analysis of the dissipative model of the spatial double pendulum under consideration, carried out

in Ch. 2, we can conclude that in this case, within the framework of the linear model, at values γ that ensure the oscillatory character of the motion, the second mode will grow much faster than the first one. This means that if the initial conditions of motion are set not exactly corresponding to the first mode, then the second mode will also be excited, which will disrupt the smooth growth of the first mode and eventually begin to dominate. We note that such behavior will also be characteristic of other mechanical systems if, instead of dissipative forces of viscous friction, analogous control actions are organized in articulated joints. Indeed, usually in oscillatory systems with many degrees of freedom, the presence of friction in articulated joints leads to the rapid disappearance of higher oscillation modes [11], so that in the case of a controlled process organized in the indicated way, we will have the opposite effect. Moreover, as was also mentioned in Ch. 2, in the problem under consideration, dissipative forces do not violate the natural oscillation modes of the system, however, in the general case, these forces can significantly distort them. At the same time, it is highly desirable to form a control that can be recommended for use in a wide class of mechanical systems. These circumstances do not allow us to recommend the control law (4.2.7) for practical use, and therefore the question of construction a control that would not violate the modes of conservative oscillations and would allow swinging each of them equally becomes more serious than it seemed at first sight.

To form a control that has the required resonant properties that would allow to transfer all the supplied energy to the excitation of only one oscillation mode for an arbitrary oscillatory mechanical system, let us turn to physical considerations. They suggest that it is expedient to apply control actions in "unison" with the inertia forces that arise when the system is overclocked, while not changing their general character. Such a controlled motion mode is called *collinear control* [76]. In a multidimensional mechanical system, the collinearity condition means that the column of control actions $\mathbf{Q}$ is proportional to the column of generalized impulses of the system $\mathbf{K} = \partial T/\partial\dot{\boldsymbol{\theta}}$:

$$\mathbf{Q} = \gamma\frac{\partial T}{\partial\dot{\boldsymbol{\theta}}}, \tag{4.2.9}$$

where γ is the gain factor, which is a constant value in the simplest case. It can be seen from the control structure (4.2.9) that it is kinetic, i.e. it takes into account the own dynamic properties of the system [51]. Initially, this idea

was applied to the problem of overclocking a free rigid body to a certain level of angular velocity by means of an external torque (for example, using gas-jet engines mounted on the carrier body), constructed on the principle of collinear control. Considering that for a rigid body the generalized impulse is directly the vector of the kinetic moment, then the torque here is formed in proportion to the kinetic moment [51]. This mode turned out to be extremely useful, and, moreover, optimal in terms of such criteria as consumption of working substance or speed. Therefore, it was subsequently used to control the movement of various manipulators, where it also demonstrated its effectiveness [76]. All this prompted the use this method for autoresonant excitation in multidimensional oscillatory systems that are functioning in various force fields. The expression (4.2.5), taking into account (4.2.9), is reduced to the following form:

$$\dot{E} = \gamma \dot{\boldsymbol{\theta}}^{\mathrm{T}} \frac{\partial T}{\partial \dot{\boldsymbol{\theta}}} = 2\gamma T, \tag{4.2.10}$$

and since the kinetic energy is a positive-definite quadratic form of generalized velocities, then for $\gamma > 0$ there is a system overclock, and for $\gamma < 0$ there is its braking, as expected from physical considerations. We note that in the case $\gamma = \text{const} > 0$, collinear control can also be interpreted as dissipative actions taken with the opposite sign, for which the dissipative function is defined by the expression $R = \gamma T$. It is clear that in this analogy we are already talking about external viscous friction acting on the loads of the pendulum, and in our problem the dissipative coefficients will be equal to $b = \gamma m$. It should be noted one more important feature of the control (4.2.9) – like the Lagrange equations of the second kind, it will have the same formula for any choice of generalized coordinates. Therefore, for example, to study the controlled motion of a flat double double, we can take $\boldsymbol{\varphi}$ as a column of generalized coordinates, so that the equations have the simplest form, and then the column of control actions will be $\mathbf{Q} = \gamma\, \partial T/\partial \dot{\boldsymbol{\varphi}}$, where the kinetic energy T must be expressed in terms of $\boldsymbol{\varphi}$ and $\dot{\boldsymbol{\varphi}}$ as (2.3.4) [41, 72, 73]. It should keep in mind that with such a choice, the column $\mathbf{Q}$ will no longer be a column of control moments in the joints, but will simply be a column of generalized forces corresponding to the chosen generalized coordinates. However, the resulting equations will describe the same controlled process.

The motion equations of spatial double pendulum in the presence of collinear control can be obtained by adding a column (4.2.9) to the right side (2.2.11). As

a result, we arrive at the following matrix equation for the controlled motion of the system:

$$\mathbf{A}(\boldsymbol{\theta})(\ddot{\boldsymbol{\theta}} - \gamma\dot{\boldsymbol{\theta}}) + \mathbf{B}(\boldsymbol{\theta}, \dot{\boldsymbol{\theta}}) + \mathbf{C}(\boldsymbol{\theta}) = 0, \tag{4.2.11}$$

which is the main subject of further research. It is necessary to show that this control satisfies all the requirements which were presented above, and we move on to this.

4.3. Analysis of Linear and Nonlinear Controlled Models at Constant Gain

Before directly studying the nonlinear equation (4.2.11), let us consider in detail the corresponding linear model, assuming $\gamma = \text{const}$. Linearizing this equation, we obtain the following matrix equation:

$$\mathbf{A}_0(\ddot{\boldsymbol{\theta}} - \gamma\dot{\boldsymbol{\theta}}) + \mathbf{C}_0\boldsymbol{\theta} = 0. \tag{4.3.1}$$

Looking for its solution in the form (2.5.4), we arrive at a linear matrix equation with respect to the unknown column $\boldsymbol{\Theta}$:

$$\left[(\lambda^2 - \gamma\lambda)\mathbf{A}_0 + \mathbf{C}_0\right]\boldsymbol{\Theta} = 0, \tag{4.3.2}$$

for which the condition for the existence of a nontrivial solution has the form:

$$\det\left[(\lambda^2 - \gamma\lambda)\mathbf{A}_0 + \mathbf{C}_0\right] = 0. \tag{4.3.3}$$

Comparing (4.3.3) with (2.4.6), it can be established that the solutions of the characteristic equation (4.3.3) satisfy the following equations:

$$\lambda^2 - 2\delta\lambda + k_{s0}^2 = 0, \quad \delta = \frac{\gamma}{2}, \quad s = 1, 2. \tag{4.3.4}$$

This also implies the most important conclusion that the oscillation modes of the controlled system within the framework of the linear model remain the same as in the original conservative system, i.e., they are not distorted by control actions. This confirms what was said earlier about the worth of collinear control. Solving the equations (4.3.4), we find the roots of the characteristic equation (4.3.3) for the problem under consideration:

$$\lambda_{1,2} = \delta \pm ik_1, \quad \lambda_{3,4} = \delta \pm ik_2, \tag{4.3.5}$$

where the notation is introduced:

$$k_s = \sqrt{k_{s0}^2 - \delta^2}, \tag{4.3.6}$$

and the values k_s depending on δ can be both real and imaginary. In the case when these values are real, they represent the oscillation frequencies of spatial double pendulum considering collinear control, otherwise, there will already be an aperiodic motion according to the mode $\boldsymbol{\Theta}_{(s)}$. As in the case of dissipative forces, we write expressions for dimensionless oscillation frequencies $p_s = k_s/k$:

$$p_s = \sqrt{p_{s0}^2 - \sigma^2}, \tag{4.3.7}$$

where $\sigma = \delta/k$ is a dimensionless control coefficient, where $\sigma > 0$ corresponds to system overclocking and $\sigma < 0$ to its braking. It can be seen from (4.3.7) that the values p_1 and p_2 are real if the following conditions are satisfied, respectively:

$$p_s \in R \Rightarrow |\sigma| < \sigma_{s0} = p_{s0}. \tag{4.3.8}$$

It follows from this that $\sigma_{10} < \sigma_{20}$, therefore, as $|\sigma|$ increases, the first frequency will first turn to zero, remaining always less than the second according to (4.3.7). Graphs dependencies of values p_1 and p_2 on $|\sigma|$ are shown in Fig. 4.1.

Thus, the solution of the equation (4.3.1) can be written as:

$$\boldsymbol{\theta} = e^{\delta t}\left[\boldsymbol{\Theta}_{(1)}\left(A_1 e^{ik_1 t} + B_1 e^{-ik_1 t}\right) + \boldsymbol{\Theta}_{(2)}\left(A_2 e^{ik_2 t} + B_2 e^{-ik_2 t}\right)\right], \tag{4.3.9}$$

where A_s and B_s, $s = 1, 2$ are complex integration constants, and, as in the case of a dissipative system considered earlier, it follows from the reality of $\boldsymbol{\theta}$ that $B_s = \overline{A}_s$. These constants are defined similarly to (2.5.28) and have the form:

$$\begin{aligned} A_s &= \frac{(-\delta + ik_s)\boldsymbol{\Theta}_{(s)}^{\mathrm{T}}\mathbf{A}_0\boldsymbol{\theta}_0 + \boldsymbol{\Theta}_{(s)}^{\mathrm{T}}\mathbf{A}_0\dot{\boldsymbol{\theta}}_0}{2ik_s N_s}, \\ B_s &= \frac{(\delta + ik_s)\boldsymbol{\Theta}_{(s)}^{\mathrm{T}}\mathbf{A}_0\boldsymbol{\theta}_0 - \boldsymbol{\Theta}_{(s)}^{\mathrm{T}}\mathbf{A}_0\dot{\boldsymbol{\theta}}_0}{2ik_s N_s}. \end{aligned} \tag{4.3.10}$$

All conclusions regarding the linear model of collinear control are of a general character and remain valid for an arbitrary oscillatory mechanical system, which initial linearized equation is described by equation in the form (2.4.1) [73].

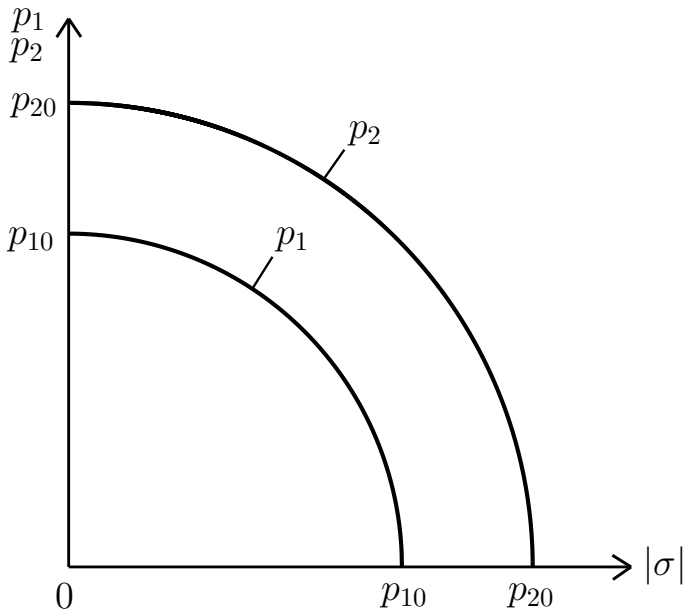

Fig. 4.1. Oscillation frequencies of spatial double pendulum with collinear control

Thus, collinear control at $\delta > 0$ in the linear model does not violate oscillation modes of the original conservative system, but only enhances their amplitudes. Therefore, it is possible with its help to separately swing spatial double pendulum both on the first and on the second oscillation mode, setting the appropriate initial conditions. The most important for applications is the case $\delta \ll k_{10}$, when the system is overclocked at a not too fast pace, and the oscillation frequencies practically do not differ from the conservative variant. This situation is of main practical interest, when small control actions can swing the system to sufficiently large amplitudes. In this case, all roots of the characteristic equation are complex conjugate and have the same real part δ. This means that the oscillation amplitudes of each modes will exponentially increase absolutely in the same way, and therefore, even if the initial conditions are not set strictly according to one of the oscillation modes, the other mode that appears in the solution will not be able to dominate the main mode and will not introduce any noticeable contribution to overclocking process. This fact should also be attributed to the advantages of collinear control.

However, it is clear that with increasing deviations, the presence of nonlinear factors in the equation (4.2.11) will gradually affect, and the linear theory will no longer give acceptable results. In this case, there will be a smooth transition from the linear zone to the nonlinear one according to the selected oscillation mode. It should be emphasized that this process already depends entirely on the features of the system and the character of its nonlinearity.

To illustrate the controlled processes during the transition from the linear to the nonlinear zone, let us adapt the equation (4.2.11) for numerical integration, resolving it with respect to the column of generalized accelerations:

$$\ddot{\boldsymbol{\theta}} = \gamma\dot{\boldsymbol{\theta}} - \mathbf{A}^{-1}(\boldsymbol{\theta})\left[\mathbf{B}(\boldsymbol{\theta},\dot{\boldsymbol{\theta}}) + \mathbf{C}(\boldsymbol{\theta})\right]. \tag{4.3.11}$$

It is natural to assume that if we set small initial conditions corresponding to linear oscillation mode, then it will be possible over time to observe how the frequency drifts and the oscillation mode evolves with increasing oscillation amplitudes. For example, for simplicity, we can assume that at $t = 0$ the initial conditions are given in the form: $\boldsymbol{\theta}_0 = a_0\boldsymbol{\Theta}_{(s)}$, $\dot{\boldsymbol{\theta}}_0 = 0$, where a_0 is small enough. We note that under the chosen control law, there will be an unlimited increase in the total mechanical energy of the system. However, as a rule, the final goal of such control is to bring the system to a certain desired energy level E_*, when the oscillation amplitudes are not yet too large, the oscillations are still regular and close to periodic, and they are also suitable for use in practical purposes. It is easy to understand that to ensure this condition, the control should be turned off when the predetermined and not so high energy level E_* is reached, and as a result a transition to the required conservative motion mode will occur.

Let us consider the processes of overclocking of spatial double pendulum on the first and second oscillation modes, starting from small deviations, and compare the final conservative modes with the motion on nonlinear oscillation modes, which were obtained and analyzed in Ch. 3.

1. Orthogonal double pendulum ($\alpha = \pi/2$). As before in the study of nonlinear oscillation modes in the conservative version, let us first turn to the study of orthogonal double pendulum. It is easy to see that in this case the matrix equation of motion (4.2.11), taking into account the representations (2.3.12) and (2.3.13), allows two particular modes of motion:

$$\ddot{\theta}_1 + k_{10}^2 \sin\theta_1 = \gamma\dot{\theta}_1, \quad \theta_2 \equiv 0, \quad k_{10} = \sqrt{\frac{3}{5}}k, \tag{4.3.12}$$

$$\ddot{\theta}_2 + k_{20}^2 \sin\theta_2 = \gamma\dot{\theta}_2, \quad \theta_1 \equiv 0, \quad k_{20} = k, \tag{4.3.13}$$

and they correspond to the process of controlled motion of ordinary mathematical pendulum in the presence of a control proportional to the angular velocity, which represents viscous friction, taken with the opposite sign [71]. It can be seen that

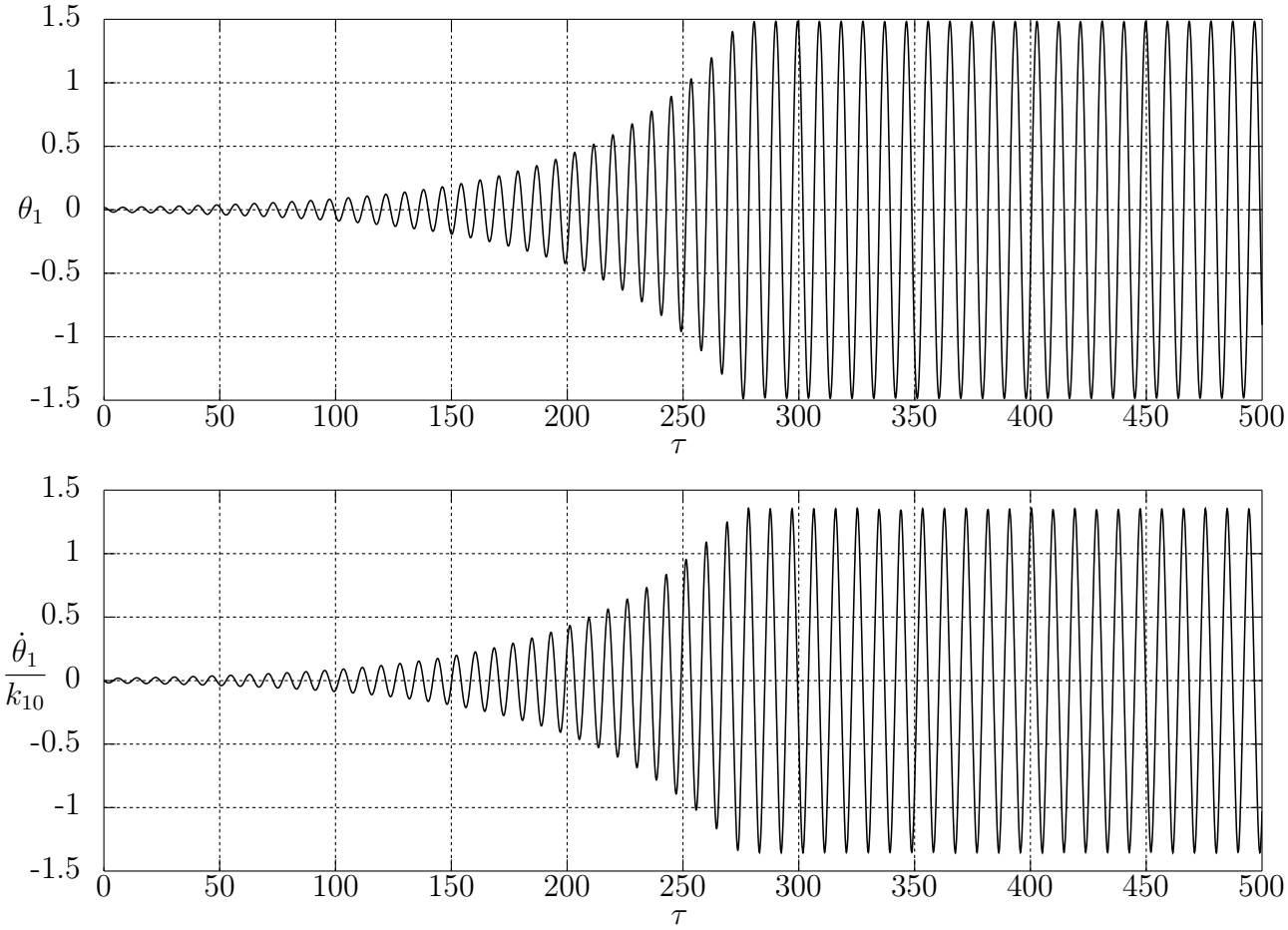

Fig. 4.2. Overclocking of orthogonal double pendulum ($\alpha = \pi/2$)

in these modes one generalized coordinate can oscillatory increase, while the second generalized coordinate is identically equal to zero, and they correspond to overclocking on the first or second oscillation modes of orthogonal double pendulum. Turning, for example, to the equation (4.3.12), we integrate it using numerical methods, setting small initial conditions. In this case, we will assume that the control is turned off when the energy reaches the value corresponding to that phase trajectory on the phase portrait in Fig. 3.2, which has the highest energy level among all the trajectories presented on it. The behavior of the angle θ_1 and the dimensionless angular velocity $\dot{\theta}_1/k_{10}$, which characterize the controlled process, is shown in Fig. 4.2, and the abscissa axis here and on subsequent graphs plots the dimensionless time $\tau = kt$. These graphs clearly illustrate the overclocking of orthogonal double pendulum on the first oscillation mode up to significant amplitudes, having a fairly distinctly character. We note that the same dependencies can also be obtained by numerically integrating the matrix equation (4.3.11) with the appropriate initial conditions, which is easy to verify directly.

2. Flat double pendulum ($\alpha = 0$). Let us now turn to the case of flat double pendulum [72,73]. We turn to the matrix equation (4.3.11) and perform its numerical integration, first setting small initial conditions on the first oscillation mode. In this case, we will assume that the desired energy level corresponds to that phase trajectory in the phase portraits in Figs 3.6–3.8, which has the highest energy level among all the trajectories shown on them. It can be expected that the final conservative mode will be in accordance with the dependencies shown in Figs 3.9 and 3.10. The picture obtained as a result of the numerical

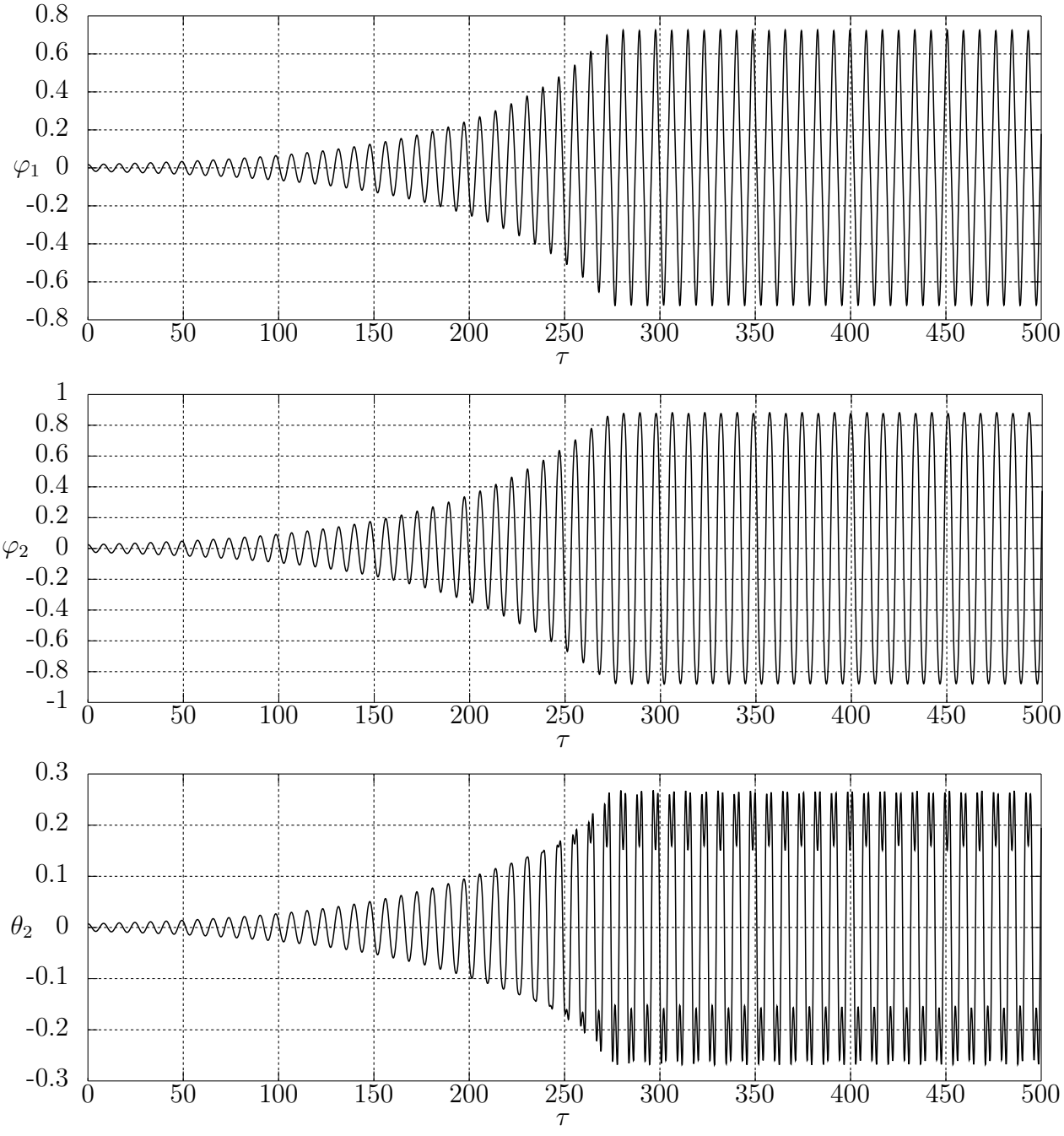

Fig. 4.3. Overclocking of flat double pendulum ($\alpha = 0$) on first oscillation mode: angles φ_1, φ_2 and θ_2

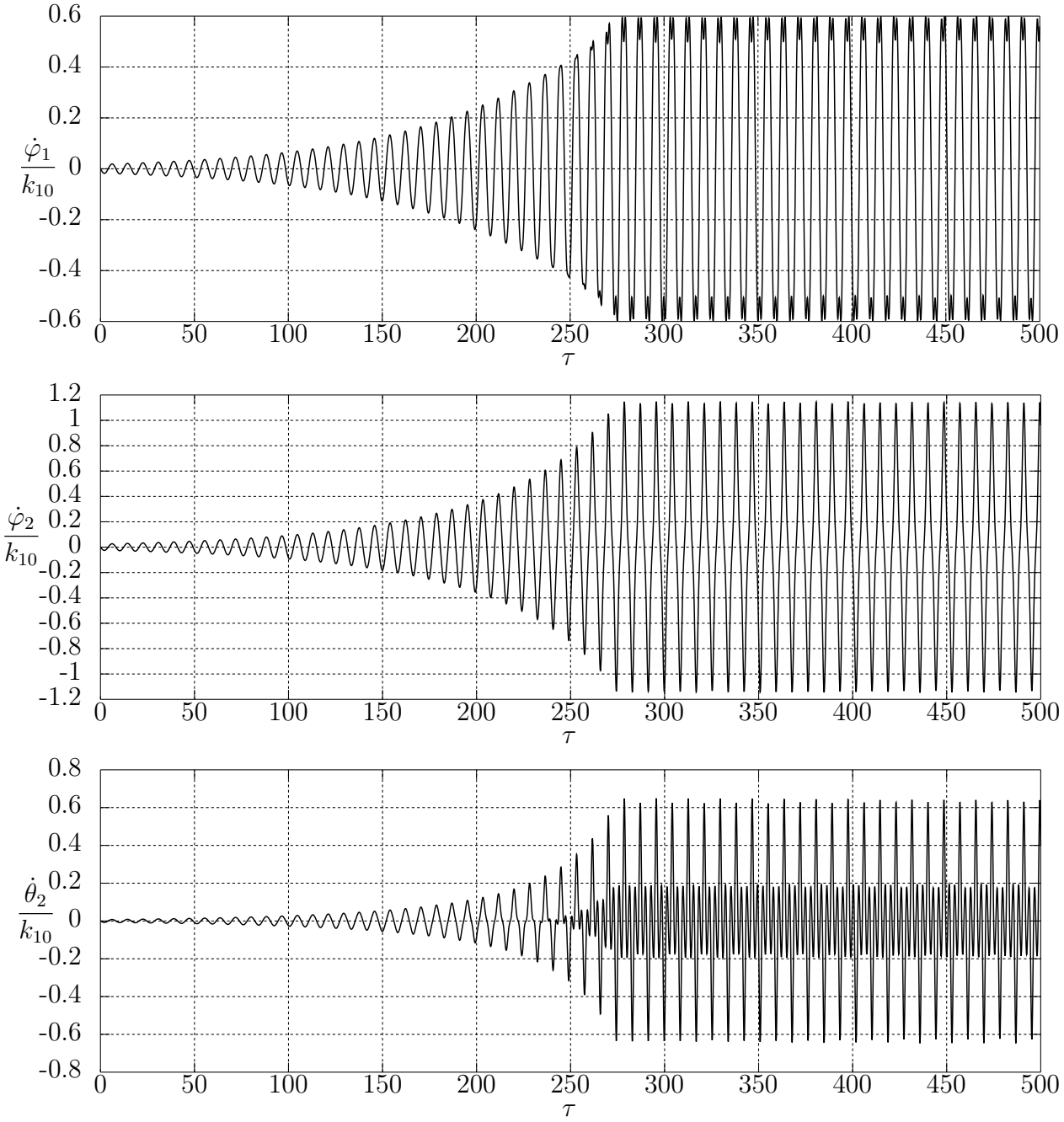

Fig. 4.4. Overclocking of flat double pendulum ($\alpha = 0$) on first oscillation mode: dimensionless angular velocities $\dot{\varphi}_1/k_{10}$, $\dot{\varphi}_2/k_{10}$ and $\dot{\theta}_2/k_{10}$

study is shown in Figs 4.3 and 4.4, where the dependence graphs of the angles $\varphi_1 = \theta_1$, $\varphi_2 = \theta_1 + \theta_2$ and θ_2 and the dimensionless angular velocities $\dot{\varphi}_1/k_{10}$, $\dot{\varphi}_2/k_{10}$ and $\dot{\theta}_2/k_{10}$ on dimensionless time τ are presented respectively. It can be seen that the overclocking process smoothly transforms the linear mode into a nonlinear one and brings the oscillations to the desired energy level, and the final mode corresponds to almost periodic motion. However, there are some distortions that are most clearly seen in the plots of values θ_2, $\dot{\varphi}_1/k_{10}$ and $\dot{\theta}_2/k_{10}$ on τ, and they are associated with the presence of more than two extremes on these

dependencies on one oscillation period, which was discussed in detail in Ch. 3. It is easy to understand that the mentioned distortions occur as a result of a rather intensive increase in amplitudes at a constant and even very small gain γ and a sharp turning off the control when desired energy level is reached. It affects the quality of the controlled process and does not allow to obtain a completely "pure" nonlinear oscillation mode at such a high achieved energy level and with such a complex geometry of the nonlinear oscillation mode at large amplitudes. Further,

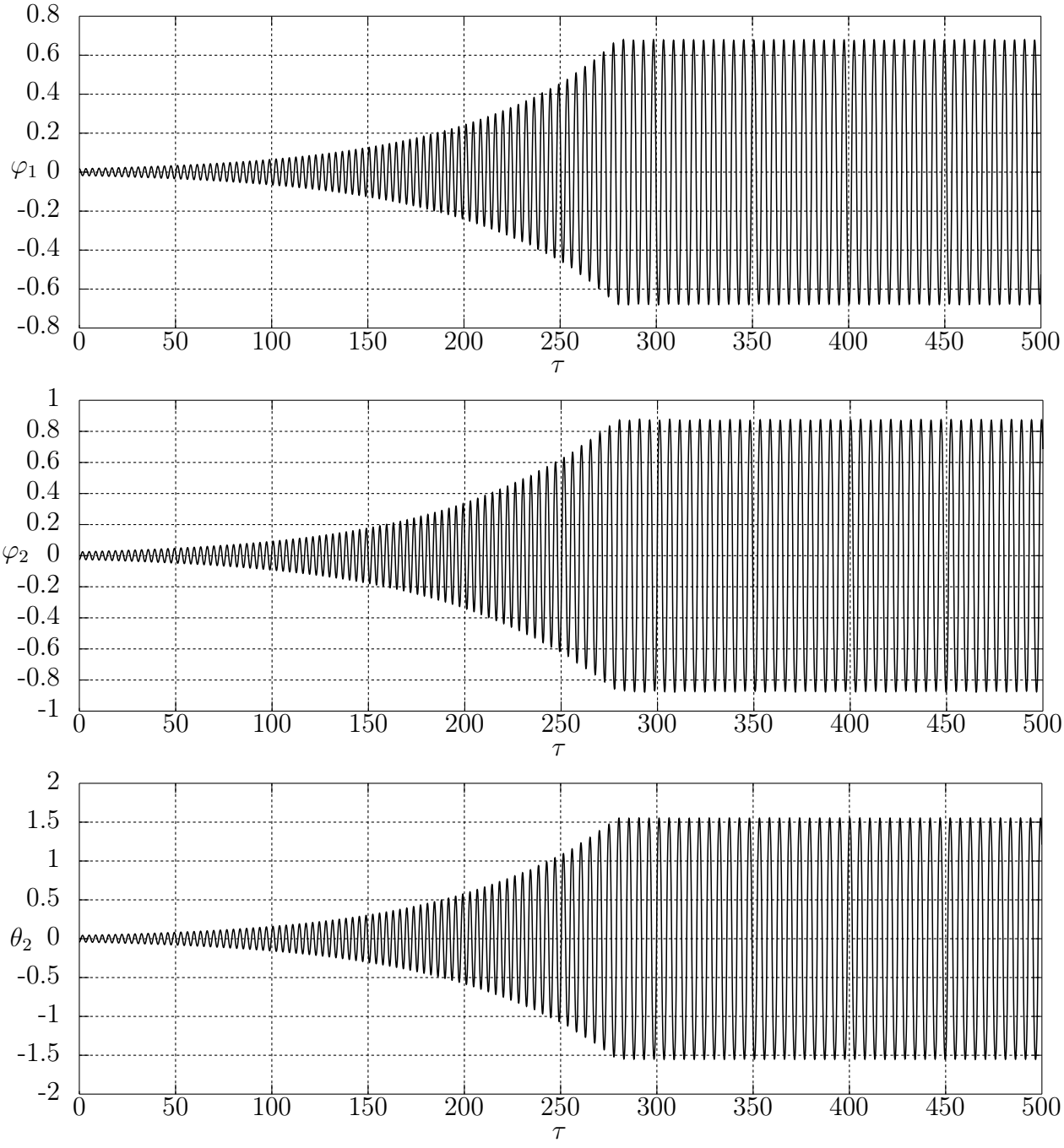

Fig. 4.5. Overclocking of flat double pendulum ($\alpha = 0$) on second oscillation mode: angles φ_1, φ_2 and θ_2

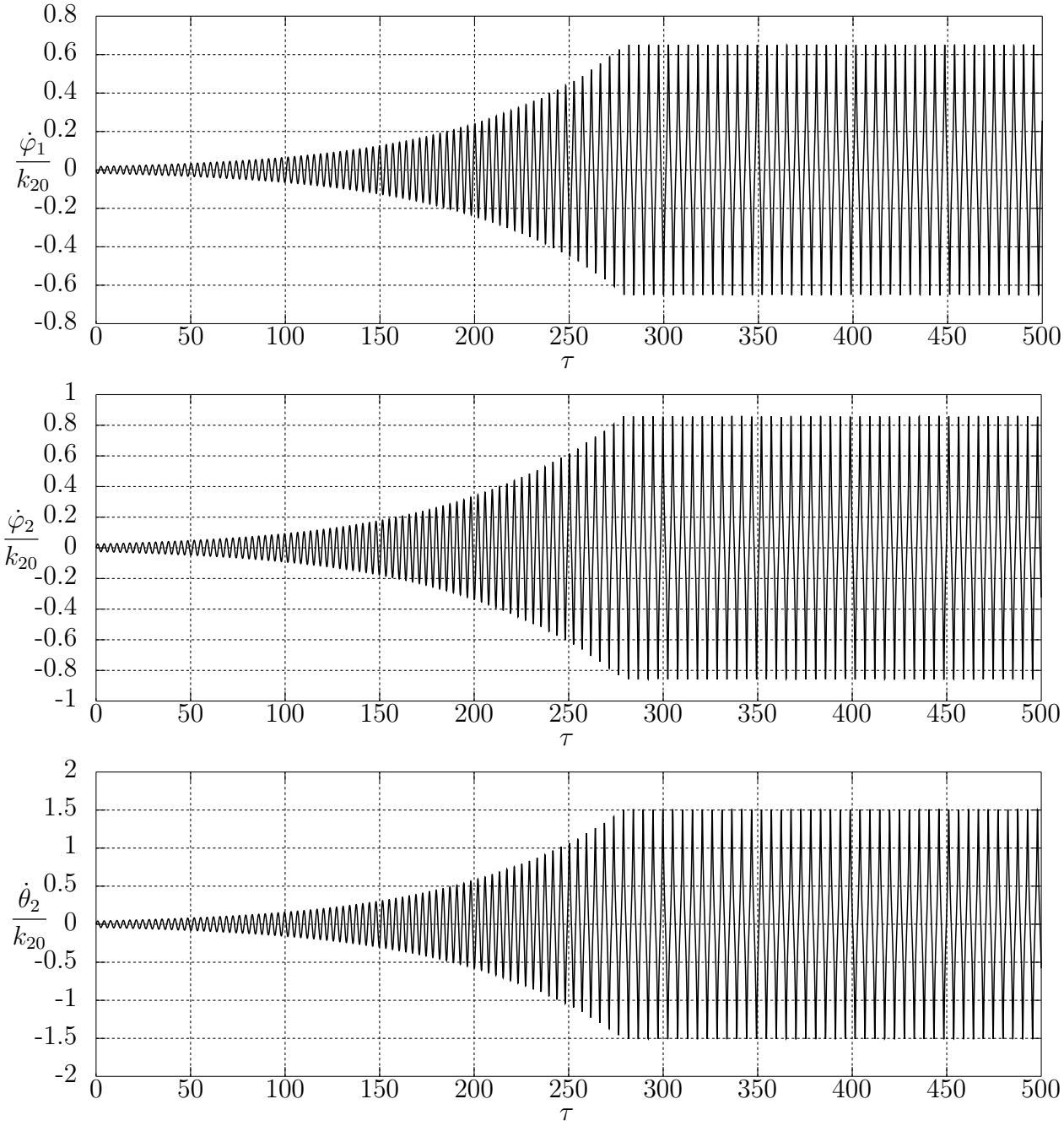

Fig. 4.6. Overclocking of flat double pendulum ($\alpha = 0$) on second oscillation mode: dimensionless angular velocities $\dot{\varphi}_1/k_{20}$, $\dot{\varphi}_2/k_{20}$ and $\dot{\theta}_2/k_{20}$

a modification of the collinear control law with adjustable gain γ depending on the energy level will be considered, which allows to obtain much smoother overclocking processes without visible distortions of the final nonlinear mode.

For completeness, let us also illustrate the overclocking of flat double pendulum on the second oscillation mode. The corresponding picture is shown in Figs 4.5 and 4.6, where the dependencies of the angles φ_1, φ_2 and θ_2, as well as the dimensionless angular velocities $\dot{\varphi}_1/k_{20}$, $\dot{\varphi}_2/k_{20}$ and $\dot{\theta}_2/k_{20}$ on the dimensionless time τ are plotted. It is easy to see that when the system is overclocked on

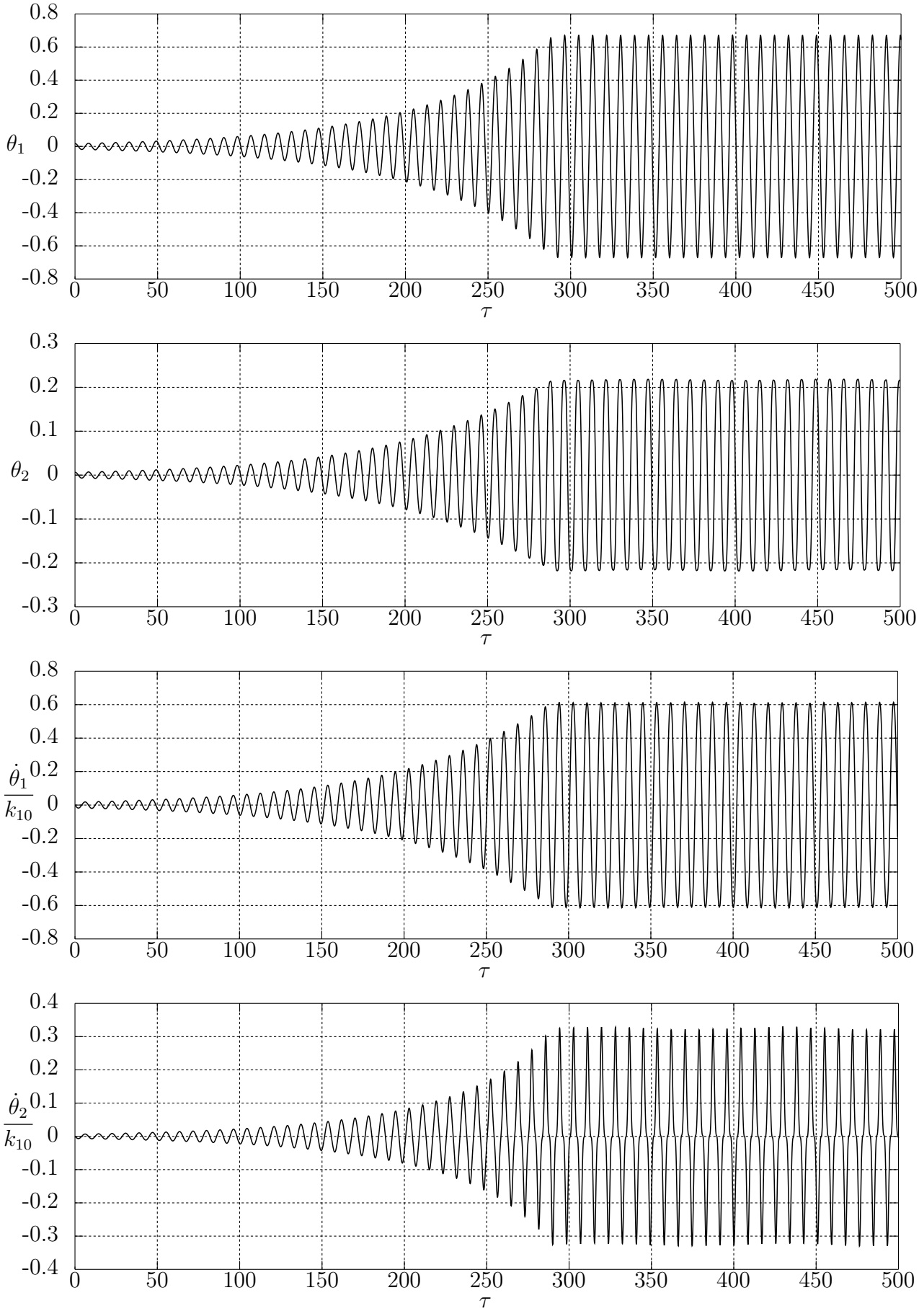

Fig. 4.7. Overclocking of spatial double pendulum ($\alpha = \pi/6$)

the second mode, the effects mentioned above are already absent, associated with the presence of more than two extremes at any generalized coordinates or dimensionless generalized velocities on one period. Therefore, a conservative mode can be observed at the output, which practically does not differ from the periodic one and without any noticeable distortion. This circumstance allows us not to discuss the second oscillation mode further in this chapter, paying all attention to the first mode, which is of primary importance in practice and has a sufficient number of nontrivial features.

Thus, overclocking of flat double pendulum on each of the oscillation modes with the help of collinear control allows, with increasing deviations of the pendulum links, to gradually transfer the linear mode of oscillation to a nonlinear one, and turning off the control in both cases, even at a sufficiently high energy level, transfers the system to a nonlinear conservative mode, which turns out to be quite close to periodic and is characterized by very significant oscillation amplitudes.

3. Spatial double pendulum. Finally, we consider the process of controlled motion on the first oscillation mode for the general variant of a spatial double pendulum. Let us accept for definiteness, as before in Ch. 3, $\alpha = \pi/6$. We will assume that the desired energy level corresponds to that phase trajectory on the phase portraits in Figs 3.17–3.18, which has the highest energy level among all the trajectories shown on them. Therefore, we can suppose that the final conservative mode will be in agreement with the dependencies shown in Fig. 3.19. By numerically integrating the matrix equation (4.3.11), we arrive at the graphs in Fig. 4.7, which show the angles θ_1 and θ_2, as well as the dimensionless angular velocities $\dot{\theta}_1/k_{10}$ and $\dot{\theta}_2/k_{10}$ depending on dimensionless time τ. These graphs also clearly demonstrate the drift of the oscillation mode during a gradual transition from a linear zone to a nonlinear one by means of collinear control and the output of oscillations to a nonlinear conservative mode, which once again emphasizes the expediency of forming control actions in this way.

4.4. Collinear Control with Variable Gain

As mentioned above, collinear control with constant gain γ, even at fairly small values of it, leads to a very intensive energy increasing in time, which stops abruptly when the desired value E_* is reached. So that, the question arises, how is

it necessary to set the gain in order to achieve a smooth transition of the system to the steady motion with the desired energy level E_* [140]? It is clear that it is necessary to gradually lower the gain γ as the energy approaches this value, that is, to set this gain in the form of a function depending on the state variables $\gamma = \gamma(\boldsymbol{\theta}, \dot{\boldsymbol{\theta}})$. It is easy to understand that this dependence can be formed in the various ways. The most preferable option seems to be similar to that described in [108]:

$$\gamma(\boldsymbol{\theta}, \dot{\boldsymbol{\theta}}) = \gamma_0 \frac{E_* - E(\boldsymbol{\theta}, \dot{\boldsymbol{\theta}})}{mgl}, \tag{4.4.1}$$

where the factor mgl is introduced in the denominator for dimensional reasons, so that constant value γ_0 has the same dimension as γ.

It can be seen that γ gradually decreases to zero as the energy approaches the value E_*, so in this situation the transition to the steady oscillatory mode will be smooth. Assuming that the function (4.4.1) changes rather slowly, we can assume that this change will have practically no effect on the main property of collinear control – the preservation of the oscillation modes of the original conservative model. Let us note again that this circumstance is decisive, since the main task of the control action means the development of one or another oscillation mode of the system. In the case under consideration, the controlled motion equation retains the form (4.2.11), where now γ is determined by the expression (4.4.1), and the total energy $E(\boldsymbol{\theta}, \dot{\boldsymbol{\theta}})$ – by the relation (2.2.14).

1. Orthogonal double pendulum ($\alpha = \pi/2$). Consider first the overclocking of orthogonal pendulum on the first oscillation mode, specifying the gain in the form (4.4.1). It is clear that in this situation, the gain factor, taking into account the formula (3.2.16), will be determined by the expression:

$$\gamma(\theta_1, \dot{\theta}_1) = \gamma_0 \left[\varepsilon_* - \frac{3}{2} \left(\frac{\dot{\theta}_1^2}{k_{10}^2} + 2(1 - \cos\theta_1) \right) \right], \tag{4.4.2}$$

where $\varepsilon_* = E_*/(mgl)$ is the dimensionless energy level corresponding to the desired energy E_*. The equation of controlled motion for the generalized coordinate θ_1 will be similar to (4.3.12) [66]:

$$\ddot{\theta}_1 + k_{10}^2 \sin\theta_1 = \gamma(\theta_1, \dot{\theta}_1)\dot{\theta}_1. \tag{4.4.3}$$

By numerically integrating this equation with small initial conditions, one can obtain the controlled motion process of orthogonal double pendulum corresponding

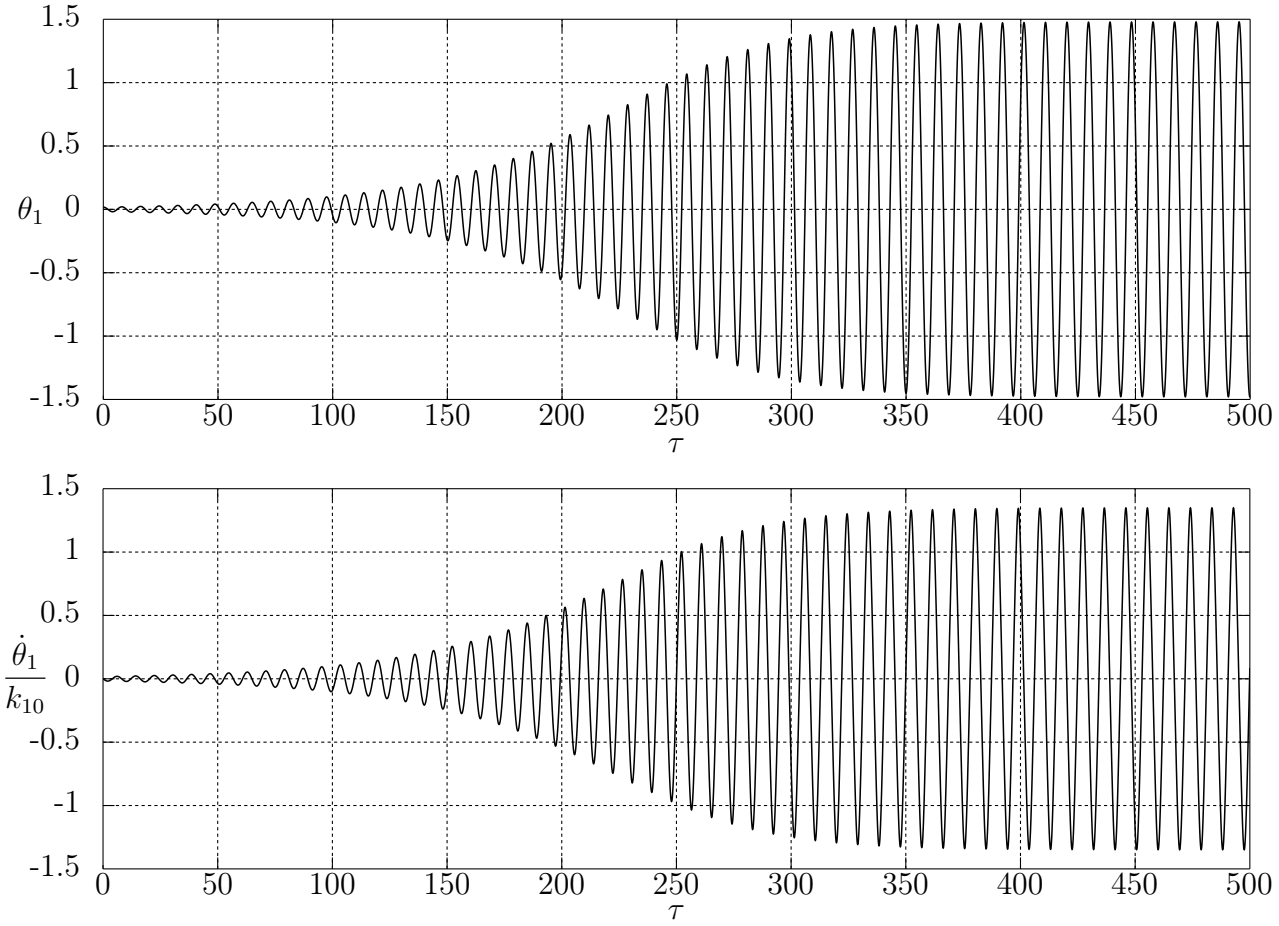

Fig. 4.8. Overclocking of orthogonal double pendulum ($\alpha = \pi/2$)

to its overclocking on the first mode, and it is shown in Fig. 4.8, where we can clearly see the smooth output of the movement to the steady oscillatory motion with a sufficiently large amplitude. We note that these graphs can also be obtained by numerically integrating the complete matrix equation of motion with appropriate initial conditions.

Let us consider separately the case when the desired energy level is not very large, i.e. when the deviations are not significant. The important feature of this variant is that it is possible to construct an approximate analytical solution for it. Introducing into consideration the oscillation amplitude A of the final oscillatory mode and taking into account that we have $E_* = 3mgl(1 - \cos A)$ according to (3.2.16), we rewrite the equation (4.4.3) in the form:

$$\ddot{\theta}_1 + k_{10}^2 \sin\theta_1 = \frac{3}{2}\gamma_0 \left[2(\cos\theta_1 - \cos A) - \frac{\dot{\theta}_1^2}{k_{10}^2}\right] \dot{\theta}_1, \tag{4.4.4}$$

which is absolutely exact. Considering further the generalized coordinate θ_1 and the amplitude $A = \text{const}$ as values of the same order of smallness, we simplify the

equation (4.4.4) by replacing $\sin\theta_1$ on its left side by θ_1, and on the right side, replacing $\cos\theta_1$ and $\cos A$ with $1-\theta_1^2/2$ and $1-A^2/2$ respectively. We note that in this approximation we will have $E_* = 3mglA^2/2$, so $\varepsilon_* = 3A^2/2$, and we will need further this expression. As a result of these actions, the equation (4.4.4) will be reduced to the form [66]:

$$\ddot{\theta}_1 + k_{10}^2\theta_1 = Q(\theta_1, \dot{\theta}_1), \tag{4.4.5}$$

where the value Q, characterizing the control actions, is determined by the expression:

$$Q(\theta_1, \dot{\theta}_1) = \frac{3}{2}\gamma_0\left(A^2 - \theta_1^2 - \frac{\dot{\theta}_1^2}{k_{10}^2}\right)\dot{\theta}_1. \tag{4.4.6}$$

Under our assumption that the nonlinear term $Q(\theta_1, \dot{\theta}_1)$ is small, we will look for a solution to the equation (4.4.5) in the form:

$$\theta = a\cos\psi, \tag{4.4.7}$$

where $a = a(t)$ is a slowly changing time function characterizing the oscillation amplitude, and $\psi = k_{10}t + \psi_0$ (where $\psi_0 = \text{const}$) is the full phase of oscillations, expression for which will not differ from the linear model, since the conservative nonlinearity in the equation (4.4.5) was not taken into account. The dependence of value a on t should be found from the following harmonic balance equation [11]:

$$\int_0^{2\pi}\left(\ddot{\theta}_1 + k_{10}^2\theta_1 - Q\right)\sin\psi d\psi = 0. \tag{4.4.8}$$

Assuming that $\dot{a} = F(a)$, where the function $F(a)$, as it is easy to understand, has the third order of smallness in a and A, considered as values of the first order of smallness, we calculate $\dot{\theta}_1$ and $\ddot{\theta}_1$ according to (4.4.7) with the required accuracy:

$$\dot{\theta}_1 = F(a)\cos\psi - a\sin\psi k_{10}, \quad \ddot{\theta}_1 = -2F(a)\sin\psi k_{10} - a\cos\psi k_{10}^2. \tag{4.4.9}$$

Next, we determine the value Q by the formula (4.4.6) up to the third order of smallness:

$$Q = -\frac{3}{2}\gamma_0(A^2 - a^2)a\sin\psi k_{10}. \tag{4.4.10}$$

Substituting now the formulas (4.4.7), (4.4.9) and (4.4.10) into the harmonic balance equation (4.4.8), we obtain after transformations:

$$F(a) = -\frac{1}{2k_{10}\pi}\int_0^{2\pi} Q\sin\psi d\psi = \frac{3}{4}\gamma_0 a(A^2 - a^2). \tag{4.4.11}$$

Thus, we arrive at the following equation for determining $a(t)$:

$$\dot{a} = \kappa a(A^2 - a^2), \quad \kappa = \frac{3}{4}\gamma_0, \tag{4.4.12}$$

which, obviously, is equation with separable variables and is reduced to the form:

$$\int \frac{da}{a(A-a)(A+a)} = \kappa \int dt. \tag{4.4.13}$$

The integral on the left side of the equation (4.4.13) can be calculated by expanding the fraction in the integrand into simple fractions:

$$\int \frac{da}{a(A-a)(A+a)} = \frac{1}{2A^2}\int \left(\frac{2}{a} + \frac{1}{A-a} - \frac{1}{A+a}\right) = \frac{1}{2A^2}\ln\frac{a^2}{A^2-a^2}. \tag{4.4.14}$$

As a result, the equation (4.4.13) will look like:

$$\frac{1}{2A^2}\ln\frac{a^2}{A^2-a^2} = \kappa t + C, \tag{4.4.15}$$

where $C = \text{const}$ is an integration constant. Let us assume that at the initial time $t = 0$ there will be $\theta_1 = a_0$, $\dot{\theta}_1 = 0$, where a_0 is a small value. Referring to the formulas (4.4.7) and (4.4.9) and taking into account that $F(a)$ is small in comparison with a, we can approximately obtain that $\psi_0 = 0$, $a = a_0$, and also express the constant C:

$$C = \frac{1}{2A^2}\ln\frac{a_0^2}{A^2-a_0^2}. \tag{4.4.16}$$

Finally, we resolve the equation (4.4.15) taking into account that (4.4.16) with

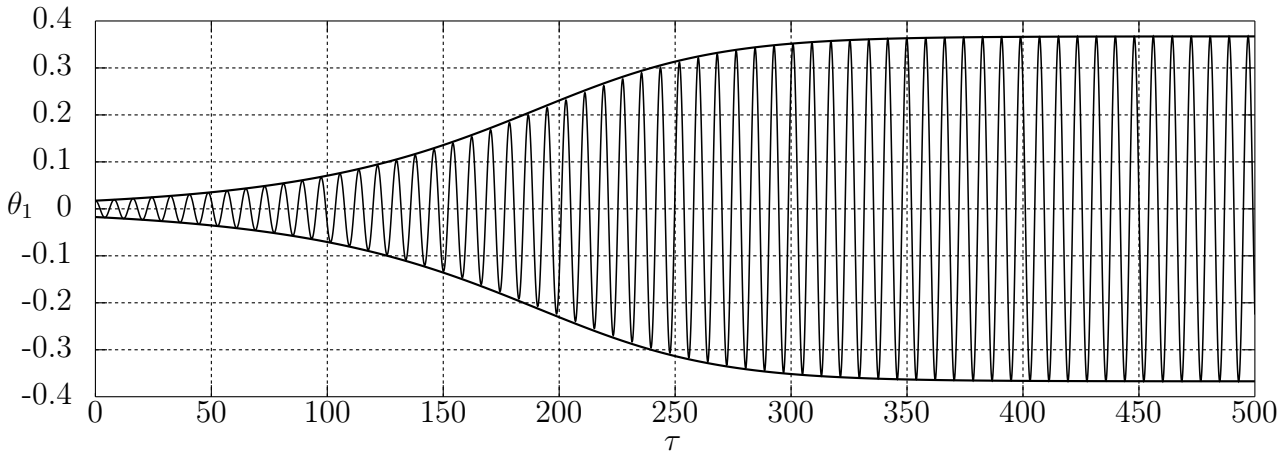

Fig. 4.9. Overclocking of orthogonal double pendulum ($\alpha = \pi/2$) in case of small deviations

respect to a and remembering that $\kappa = 3\gamma_0/4$ and $\varepsilon_* = 3A^2/2$, and as a result, we find the desired dependency:

$$a(t) = \frac{a_0 A e^{\kappa A^2 t}}{\sqrt{A^2 + a_0^2\,(e^{2\kappa A^2 t} - 1)}} = \frac{a_0 A e^{\gamma_0 \varepsilon_* t/2}}{\sqrt{A^2 + a_0^2\,(e^{\gamma_0 \varepsilon_* t} - 1)}}. \qquad (4.4.17)$$

This shows that for $t \to \infty$ we indeed have $a \to A$, i.e., $E \to E_*$, as it should be. The process of controlled motion for small deviations, obtained by numerical integration and demonstrating the change in the angle θ with increasing dimensionless time τ, is shown in Fig. 4.9, where the envelope lines characterize the oscillation amplitude of the angle θ_1, and they are plotted according to (4.4.17). It can be seen that these lines are in complete agreement with the results of numerical integration, which confirms the correctness of the analytical solution.

2. Flat double pendulum ($\alpha = 0$). Turning to the case of flat double pendulum, we plot based on the numerical integration the graph dependencies of the main values characterizing the controlled overclocking of the system on the first mode – generalized coordinates (Fig. 4.10) and generalized velocities (Fig. 4.11) – on the dimensionless time τ. Analyzing them, one can observe a pronounced drift of the oscillation modes as a gradual transition from a linear zone to a nonlinear one with output to a steady movement for all the indicated values, which has a periodic character.

It should be noted that due to the variability of the gain, the process of the system reaching the final mode in this situation has a smooth character, therefore, here it was possible to obtain the most "pure" nonlinear oscillation modes without any visible distortions that could be observed in Figs 4.3 and 4.4, where the overclocking was carried out at constant gain and abruptly stopped when the desired energy level was reached [67]. This circumstance confirms the expediency of varying the gain, subjecting it to the condition (4.4.1).

3. Spatial double pendulum. Now we consider the controlled motion of spatial double pendulum on the first mode for $\alpha = \pi/6$. The graphic dependencies obtained by means of numerical integration for this case are shown in Fig. 4.12. It is again easy to see upon a detailed examination of the presented graphs that there is a gradual transition of the oscillation mode from a linear to a nonlinear variant with the preservation of single-frequency motion and reaching the final conservative mode corresponding to the desired energy level.

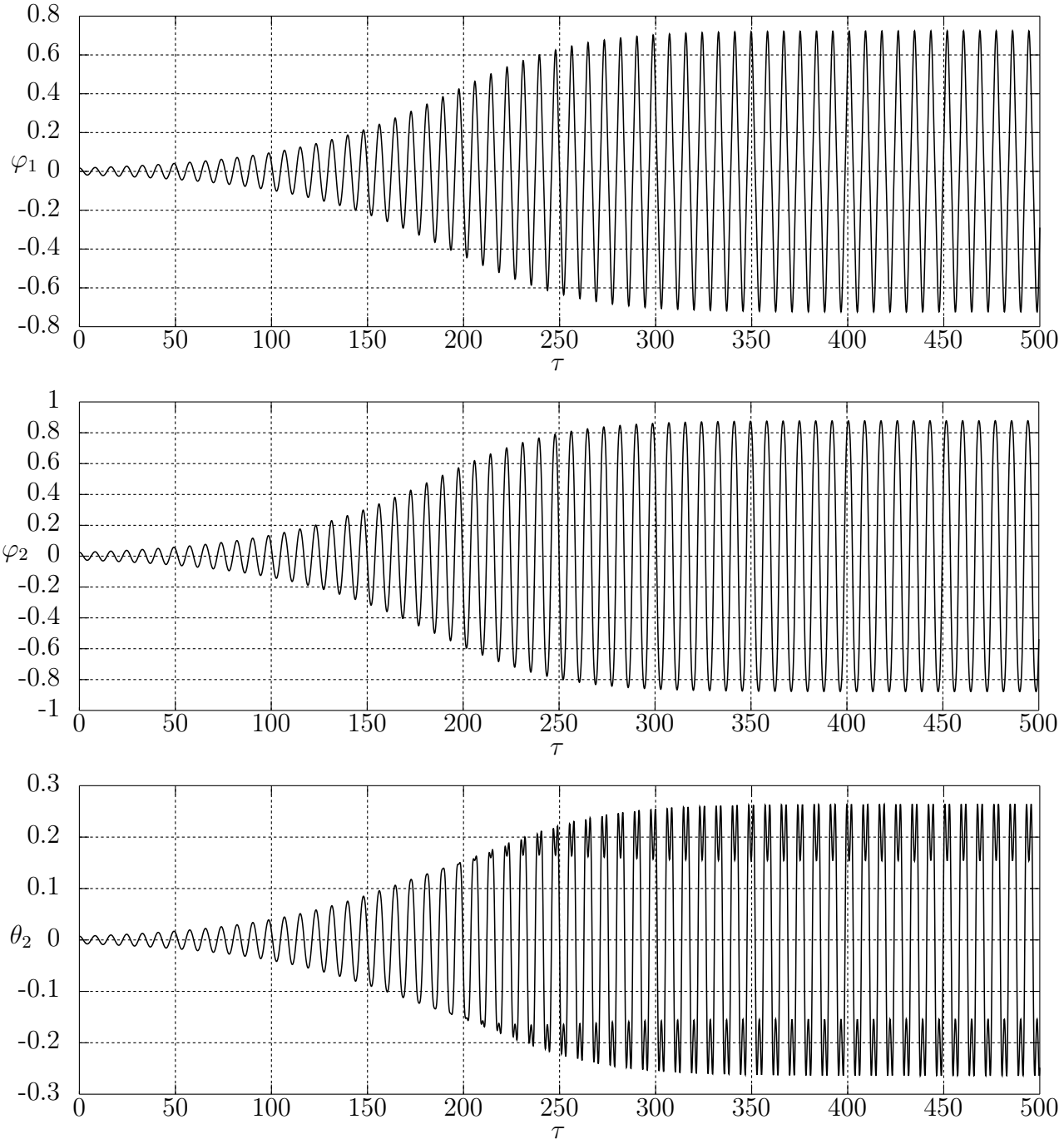

Fig. 4.10. Overclocking of flat double pendulum ($\alpha = 0$): angles φ_1, φ_2 and θ_2

It should be noted that the desired energy levels of the final mode for the dependencies shown in Figs 4.8, 4.10–4.11, 4.12, were taken exactly the same as in Figs 4.2, 4.3–4.4, 4.7, and specific numerical values of the gain γ (if it is constant) and γ_0 (if it is variability) in each case were chosen in such a way as to demonstrate the processes of controlled motion on the same interval of dimensionless time, and it was done solely for uniformity and is not of fundamental character.

It remains to find out what the approximate analytical solution of the equation (4.2.11) will look like when we choose the gain according to the formula (4.4.1)

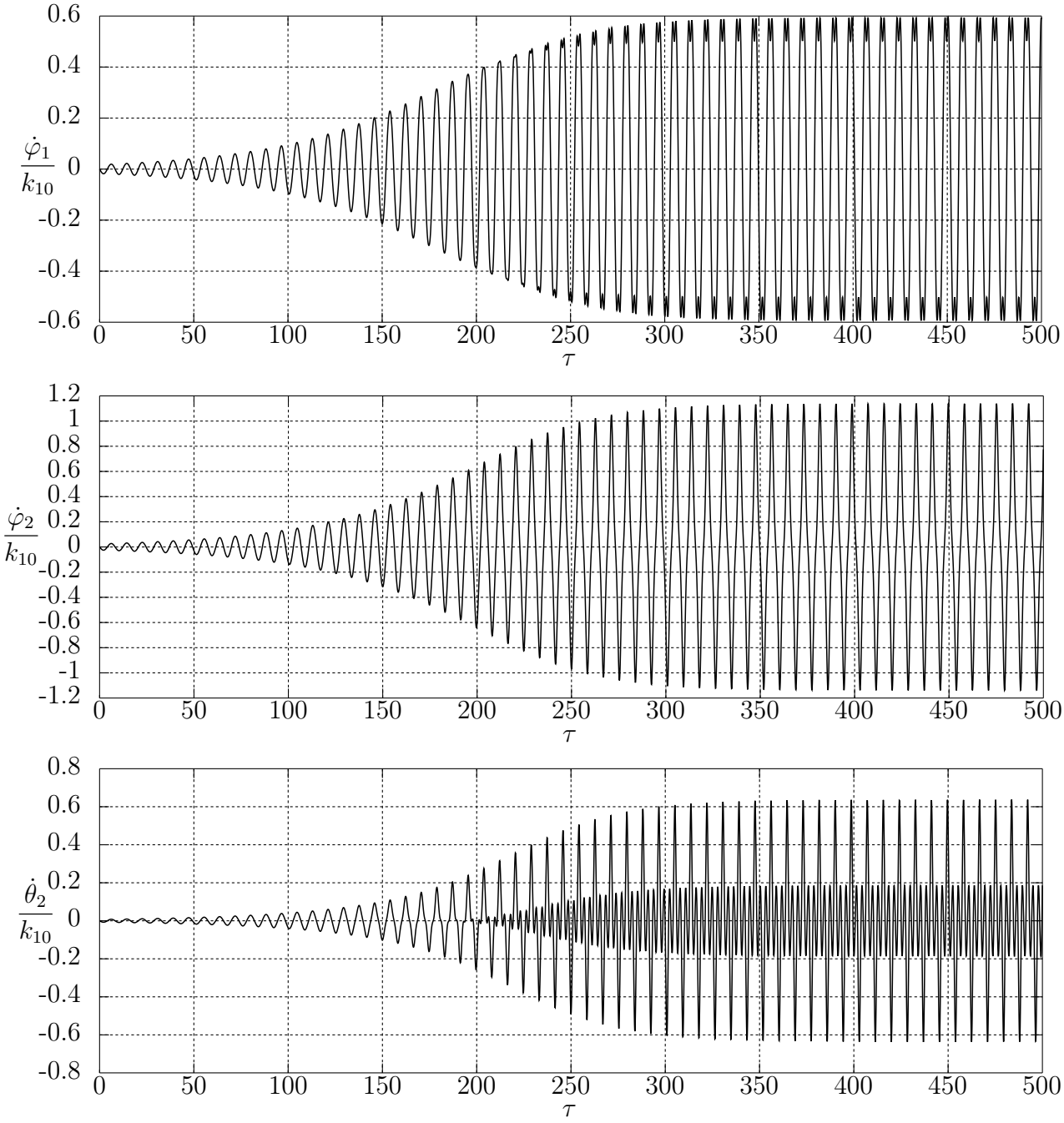

Fig. 4.11. Overclocking of flat double pendulum ($\alpha = 0$): dimensionless angular velocities $\dot\varphi_1/k_{10}$, $\dot\varphi_2/k_{10}$ and $\dot\theta_2/k_{10}$

and the system is overclocked on one of the oscillation modes for the case of sufficiently small deviations. To this purpose, we write the expression of the total mechanical energy in a quadratic approximation according to (2.4.3):

$$E = \frac{1}{2}\dot{\boldsymbol{\theta}}^{\mathrm{T}}\mathbf{A}_0\dot{\boldsymbol{\theta}} + \frac{1}{2}\boldsymbol{\theta}^{\mathrm{T}}\mathbf{C}_0\boldsymbol{\theta}. \tag{4.4.18}$$

We will assume that it is required to bring the system to the harmonic oscillations on one of the oscillation modes $\boldsymbol{\Theta}_{(s)}$ of the linear model with the corresponding

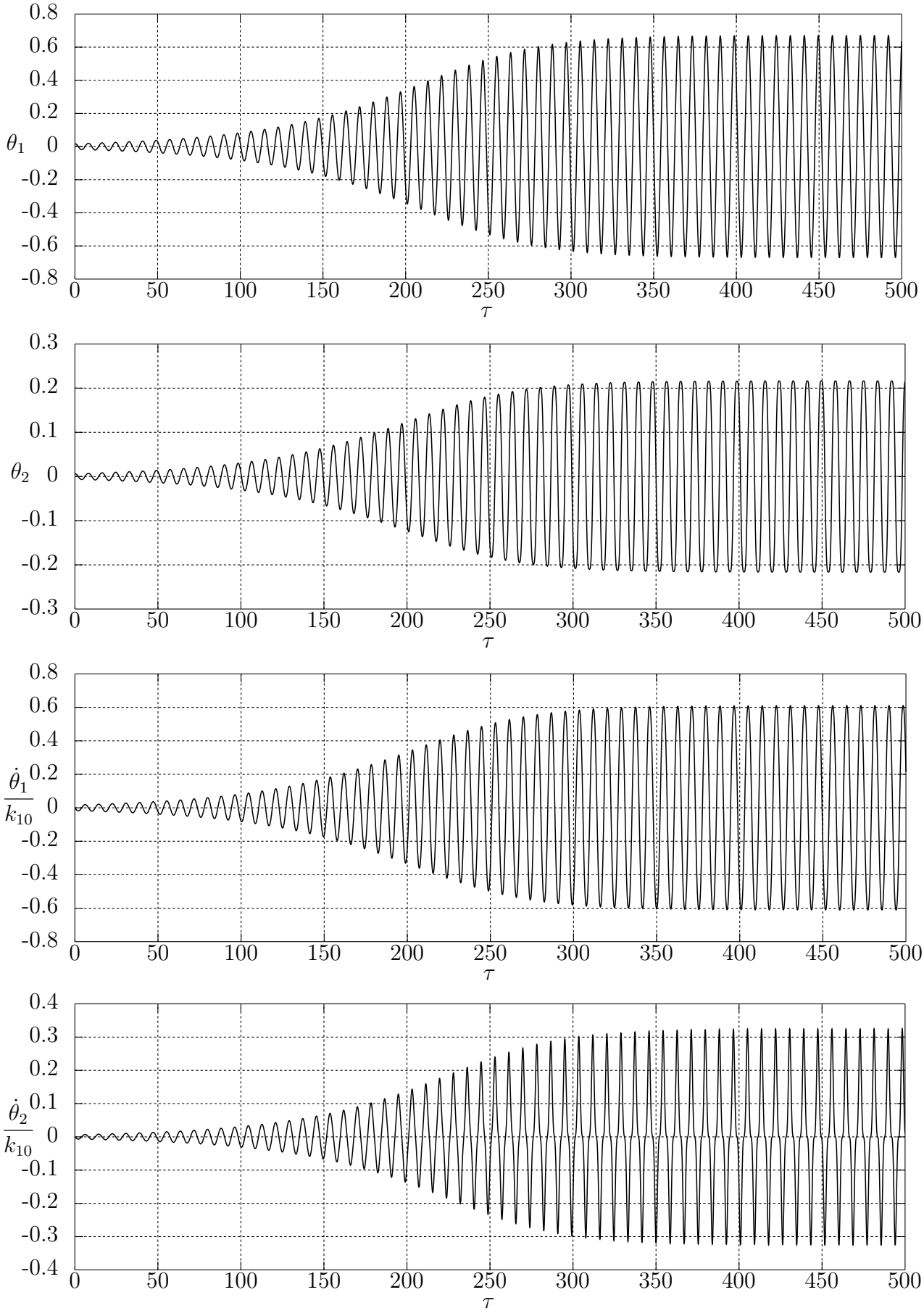

Fig. 4.12. Overclocking of spatial double pendulum ($\alpha = \pi/6$)

oscillation frequency k_{s0}:

$$\boldsymbol{\theta} = \boldsymbol{\Theta}_{(s)} A \cos\psi, \tag{4.4.19}$$

where A is some constant parameter that has the meaning of amplitude and is also sufficiently the small one, and $\psi = k_{s0}t + \psi_{s0}$, where the specific value of ψ_{s0} does not play here no significant role, and in it will be determined the future by the initial conditions of motion. We calculate the desired energy level corresponding to the mode (4.4.19) using the formula (4.4.18):

$$E_* = \frac{1}{2}A^2\left[\boldsymbol{\Theta}_{(s)}^{\mathrm{T}}\mathbf{A}_0\boldsymbol{\Theta}_{(s)}k_{s0}^2\sin^2\psi + \boldsymbol{\Theta}_{(s)}^{\mathrm{T}}\mathbf{C}_0\boldsymbol{\Theta}_{(s)}\cos^2\psi\right] = \frac{1}{2}N_s k_{s0}^2 A^2, \tag{4.4.20}$$

where conditions (2.4.22) are used. Since $H_s = N_s/(ml^2)$ and $p_{s0} = k_{s0}/k$, it follows that $\varepsilon_* = E_*/(mgl) = H_s p_{s0}^2 A^2/2$. It is clear that for small deviations the equation (4.2.11) can be simplified by reducing it to the form:

$$\mathbf{A}_0\ddot{\boldsymbol{\theta}} + \mathbf{C}_0\boldsymbol{\theta} = \mathbf{Q}(\boldsymbol{\theta}, \dot{\boldsymbol{\theta}}), \tag{4.4.21}$$

where the column of control actions here is determined by the expression:

$$\mathbf{Q}(\boldsymbol{\theta}, \dot{\boldsymbol{\theta}}) = \frac{\gamma_0}{2mgl}\left(N_s k_{s0}^2 A^2 - \dot{\boldsymbol{\theta}}^{\mathrm{T}}\mathbf{A}_0\dot{\boldsymbol{\theta}} - \boldsymbol{\theta}^{\mathrm{T}}\mathbf{C}_0\boldsymbol{\theta}\right)\mathbf{A}_0\dot{\boldsymbol{\theta}}. \tag{4.4.22}$$

As in the construction of approximate solution for the case of orthogonal double pendulum, we excluded here the own nonlinearity of the system, which affects only the oscillation frequency in the first approximation, and we have left only third-order nonlinear terms that arise due to control actions and directly affect the increase in oscillation amplitudes. We will seek solution of equation (4.4.21) in the form:

$$\boldsymbol{\theta} = \boldsymbol{\Theta}_{(s)} a \cos\psi, \tag{4.4.23}$$

where $a = a(t)$ is some unknown time function, which is to be determined, and $\psi = k_{s0}t + \psi_{s0}$. The dependence of a on t will be found from the following harmonic balance equation for the given mode $\boldsymbol{\Theta}_{(s)}$ [11]:

$$\int_0^{2\pi} \boldsymbol{\Theta}_{(s)}^{\mathrm{T}}\left(\mathbf{A}_0\ddot{\boldsymbol{\theta}} + \mathbf{C}_0\boldsymbol{\theta} - \mathbf{Q}\right)\sin\psi d\psi = 0. \tag{4.4.24}$$

Assuming that $\dot{a} = F(a)$, where the function $F(a)$ has the third order of smallness, we calculate the columns $\dot{\boldsymbol{\theta}}$ and $\ddot{\boldsymbol{\theta}}$ according to (4.4.23) with required accuracy:

$$\dot{\boldsymbol{\theta}} = \boldsymbol{\Theta}_{(s)}\left[F(a)\cos\psi - a\sin\psi k_{s0}\right], \quad \ddot{\boldsymbol{\theta}} = \boldsymbol{\Theta}_{(s)}\left[-2F(a)\sin\psi k_{s0} - a\cos\psi k_{s0}^2\right]. \tag{4.4.25}$$

In addition, we calculate the column of control actions (4.4.22) also up to the third order of smallness:

$$\mathbf{Q} = -\frac{\gamma_0 N_s k_{s0}^2}{2mgl}(A^2 - a^2)a \sin\psi k_{s0}\mathbf{A}_0\mathbf{\Theta}_{(s)}. \tag{4.4.26}$$

Substituting now formulas (4.4.23), (4.4.25) and (4.4.26) into the harmonic balance equation (4.4.24), we obtain after some transformations:

$$F(a) = -\frac{1}{2N_s k_{s0}\pi}\int\limits_0^{2\pi} \mathbf{\Theta}_{(s)}^{\mathrm{T}}\mathbf{Q}\sin\psi d\psi = \frac{\gamma_0 N_s k_{s0}^2}{4mgl}a(A^2 - a^2), \tag{4.4.27}$$

so the equation for determining the function $a(t)$ will take the form:

$$\dot{a} = \kappa_s a(A^2 - a^2), \quad \kappa_s = \frac{\gamma_0 H_s p_{s0}^2}{4}. \tag{4.4.28}$$

It is easy to see that the equation (4.4.28) is completely similar to the previously obtained equation (4.4.12) for the case of orthogonal double pendulum. Setting the initial conditions in the original form, namely $\boldsymbol{\theta}_0 = a_0\mathbf{\Theta}_{(s)}$, $\dot{\boldsymbol{\theta}}_0 = 0$, referring to the formulas (4.4.23) and (4.4.25), and, in addition, taking into account that $F(a)$ is small in comparison with a, we can approximately obtain that $\psi_{s0} = 0$, and $a = a_0$ at $t = 0$. Therefore, the equation (4.4.28) will have a solution that is completely similar in structure to the expression (4.4.17), where it is also taken into account that $\kappa_s = \gamma_0 H_s p_{s0}^2/4$, and $\varepsilon_* = H_s p_{s0}^2 A^2/2$ [140]:

$$a(t) = \frac{a_0 A e^{\kappa_s A^2 t}}{\sqrt{A^2 + a_0^2\left(e^{2\kappa_s A^2 t} - 1\right)}} = \frac{a_0 A e^{\gamma_0\varepsilon_* t/2}}{\sqrt{A^2 + a_0^2\left(e^{\gamma_0\varepsilon_* t} - 1\right)}}. \tag{4.4.29}$$

It is again easy to see from here that for $a \to A$ we have $t \to \infty$, i.e. $E \to E_*$.

Graphs of the controlled movement of the system on the first mode are shown in Fig. 4.13 for the case $\alpha = \pi/6$ for sufficiently small angles θ_1 and θ_2. . The envelope lines are also shown here, and they characterize the oscillation amplitudes of these angles and are constructed according to the formulas obtained above. It can be seen that these lines are in complete agreement with the results of numerical integration. Thus, the obtained analytical results make it possible to evaluate the character of the increase in the oscillation amplitudes within the framework of the considered simplified model. We emphasize once again that despite the approximations carried out and the absence of a drift of frequency and oscillation mode in this model, it still remains nonlinear due to the control actions.

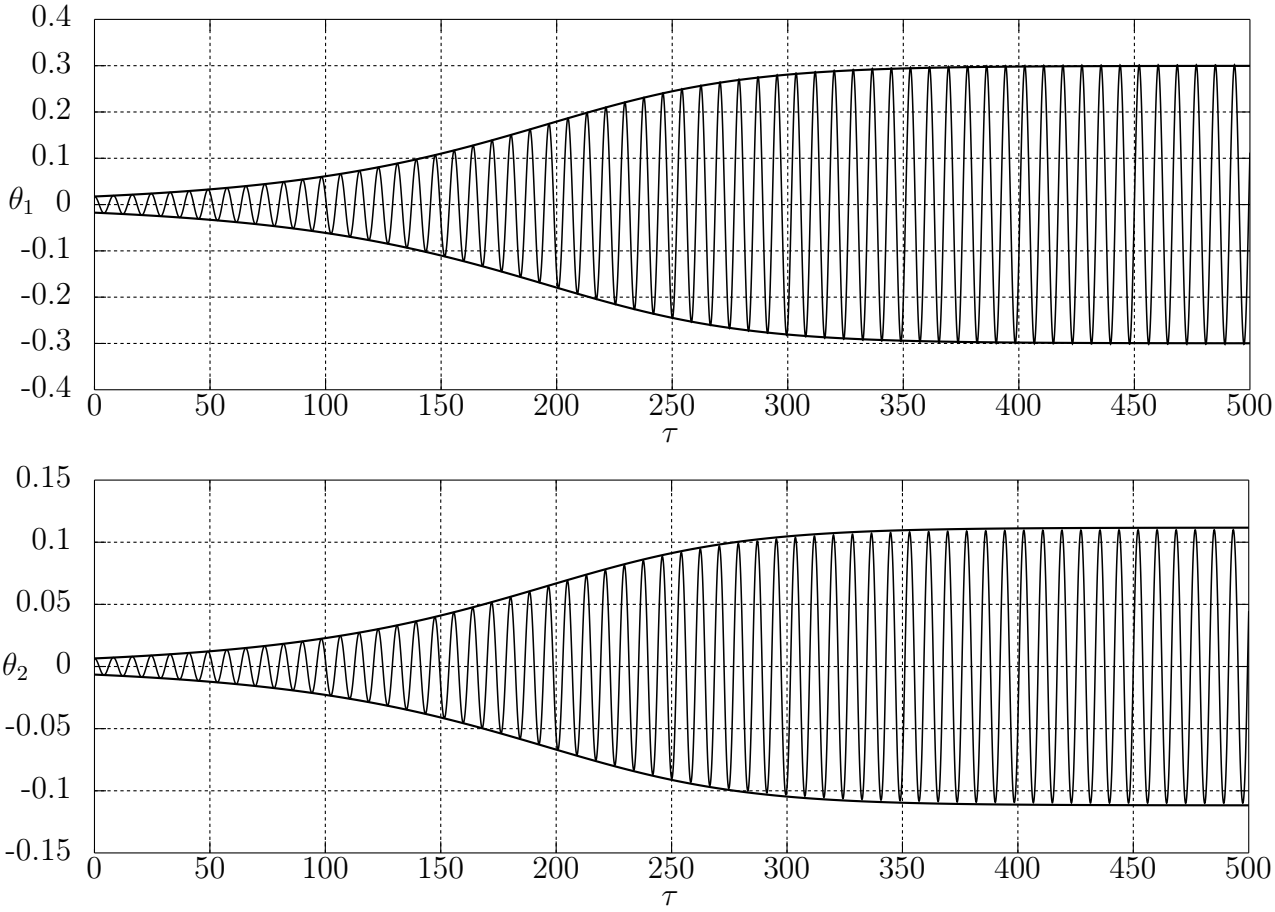

Fig. 4.13. Overclocking of spatial double pendulum ($\alpha = \pi/6$) in case of small deviations

Analyzing the obtained results, we can conclude that the presented modification of the collinear control law, which has variable gain, as well as the collinear control with constant gain, allows to transfer all the energy supplied to the system to the growth of oscillations only on one oscillation mode. This means, that it is possible to excite resonant oscillations on a given oscillation mode with the help of such control, i.e., swing the system on this mode with its gradual transition from a linear to a nonlinear variant, and a smooth transition to a steady oscillatory motion with a given energy level will be carried out over time. As a result, it is possible to observe the system movement on a nonlinear oscillation mode which is characterized by periodicity and is very different from the corresponding linear oscillation mode, which has a harmonic, i.e., purely sinusoidal character.

4.5. Collinear Control in Presence of Dissipative Forces

In conclusion of the conversation about the controlled motions of the system, we consider the situation when control moments act in the joints of a spatial double pendulum, constructed on the principle of collinear control with a constant gain γ, and viscous friction is also taken into account with the dissipative coefficient b [41]. It is clear that the motion equations of such a system, written in matrix form, will look like:

$$\frac{d}{dt}\frac{\partial T}{\partial \dot{\boldsymbol{\theta}}} - \frac{\partial T}{\partial \boldsymbol{\theta}} = -\frac{\partial \Pi}{\partial \boldsymbol{\theta}} - \frac{\partial R}{\partial \dot{\boldsymbol{\theta}}} + \gamma \frac{\partial T}{\partial \dot{\boldsymbol{\theta}}}. \tag{4.5.1}$$

Bearing in mind the further study of the linear model of the process under consideration, let us substitute into (4.5.1) the quadratic approximations of the kinetic and potential energies (2.4.3), as well as the dissipative function (2.5.1). As a result, we obtain the following linear matrix equation:

$$\mathbf{A}_0\ddot{\boldsymbol{\theta}} + (\mathbf{B}_0 - \gamma\mathbf{A}_0)\dot{\boldsymbol{\theta}} + \mathbf{C}_0\boldsymbol{\theta} = 0. \tag{4.5.2}$$

Multiplying the motion equation (4.5.2) by $\dot{\boldsymbol{\theta}}^{\mathrm{T}}$ on the left, it is easy to obtain the following energy relation:

$$\begin{aligned} \dot{E} = 2(\gamma T - R) = 2ml^2\left[(5\delta - n)\dot{\theta}_1^2 + 4\delta\cos\alpha\dot{\theta}_1\dot{\theta}_2 + (\delta - n)\dot{\theta}_2^2\right] = \\ = N(\dot{\boldsymbol{\theta}}) = \frac{1}{2}\dot{\boldsymbol{\theta}}^{\mathrm{T}}\mathbf{D}_0\dot{\boldsymbol{\theta}}, \end{aligned} \tag{4.5.3}$$

where it is taken into account that $2n = b/(ml^2)$, $2\delta = \gamma$. It can be seen that the total power of the dissipative and control forces $N(\dot{\boldsymbol{\theta}})$ is the quadratic form of the column of generalized velocities with the matrix

$$\mathbf{D}_0 = 2ml^2\begin{bmatrix} 5\delta - n & 2\delta\cos\alpha \\ 2\delta\cos\alpha & \delta - n \end{bmatrix}. \tag{4.5.4}$$

First, let us determine the conditions on the parameters δ and n when the total energy of the system will always be an increasing or, conversely, decreasing function. It follows from the formula (4.5.3) that for this the power N must always take positive or negative values for any values of the generalized velocities $\dot{\theta}_1$ and

$\dot{\theta}_2$. Therefore, the matrix $\mathbf{D}_0$ must be sign-definite positive or negative, as dictated by Sylvester's conditions [23]. Thus, for this matrix to be positive definite, it is required that

$$5\delta > n, \quad (5\delta - n)(\delta - n) - 4\delta^2 \cos^2\alpha > 0. \tag{4.5.5}$$

Solving this system of inequalities, we obtain

$$\delta > \frac{3 + 2\sqrt{2 - \sin^2\alpha}}{1 + 4\sin^2\alpha} n = n_2, \quad \sigma > \eta_2 \nu, \tag{4.5.6}$$

where the relation (2.5.11) is taken into account, and the resulting condition is presented in dimensionless form, where $\sigma = \delta/k$, $\nu = n/k$, and also $\eta_s = n_s/n$, and these values are determined by the formula (2.5.14). For the matrix $\mathbf{D}_0$ to be negative definite, the inequalities must be satisfied

$$5\delta < n, \quad (5\delta - n)(\delta - n) - 4\delta^2 \cos^2\alpha > 0, \tag{4.5.7}$$

which, in turn, give

$$\delta < \frac{3 - 2\sqrt{2 - \sin^2\alpha}}{1 + 4\sin^2\alpha} n = n_1, \quad \sigma < \eta_1 \nu, \tag{4.5.8}$$

where all the same relations are used. These considerations also lead to the conclusion that under the condition

$$\eta_1 \nu < \sigma < \eta_2 \nu \tag{4.5.9}$$

the power N will be an sign-changing function of the generalized velocities $\dot{\theta}_1$ and $\dot{\theta}_2$, so that some intermediate modes will correspond to this double inequality.

Let us now consider in detail the entire spectrum of possible modes of motion of the system. To construct these modes and give them an adequate interpretation and classification, we construct an exact analytical solution of the equation (4.5.2). Seeking this solution in the form (2.5.4), we arrive at a matrix algebraic equation:

$$\left[\mathbf{A}_0\lambda^2 + (\mathbf{B}_0 - \gamma\mathbf{A}_0)\lambda + \mathbf{C}_0\right]\boldsymbol{\Theta} = 0, \tag{4.5.10}$$

which has a non-trivial solution under the condition

$$\det\left[\mathbf{A}_0\lambda^2 + (\mathbf{B}_0 - \gamma\mathbf{A}_0)\lambda + \mathbf{C}_0\right] = 0. \tag{4.5.11}$$

Considering the relation (2.5.7) between the matrices $\mathbf{A}_0$, $\mathbf{B}_0$ and $\mathbf{C}_0$, we get:

$$\det\left[\mathbf{A}_0\left(\lambda^2 - (2n + \gamma)\lambda\right) + \mathbf{C}_0\left(1 + \frac{4n}{k^2}\lambda\right)\right] = 0. \tag{4.5.12}$$

Comparing this equation with (2.4.6), to which the frequencies of conservative oscillations k_{s0} correspond, it follows that the values λ are found from the following equations:

$$\lambda^2 - (2n+\gamma)\lambda = -k_{s0}^2\left(1+\frac{4n}{k^2}\lambda\right), \quad s=1,2, \tag{4.5.13}$$

and the oscillation modes remain the same as in the original conservative system. Transforming the equations (4.5.13), we get:

$$\lambda^2 + 2(n_s-\delta)\lambda + k_{s0}^2 = 0, \tag{4.5.14}$$

where the old designations for n_s are kept according to (2.5.11). Solutions of equations (4.5.14) obviously have the form:

$$\lambda_{1,2} = \delta - n_1 \pm ik_1, \quad \lambda_{3,4} = \delta - n_2 \pm ik_2, \tag{4.5.15}$$

where the notation is introduced:

$$k_s = \sqrt{k_{s0}^2 - (\delta - n_s)^2}. \tag{4.5.16}$$

We note that the solution of equation (4.5.2) can be written as:

$$\boldsymbol{\theta} = e^{\delta t}\left[\boldsymbol{\Theta}_{(1)}e^{-n_1 t}\left(A_1 e^{ik_1 t} + B_1 e^{-ik_1 t}\right) + \boldsymbol{\Theta}_{(2)}e^{-n_2 t}\left(A_2 e^{ik_2 t} + B_2 e^{-ik_2 t}\right)\right], \tag{4.5.17}$$

where the complex integration constants A_s and B_s, $s=1,2$ are again determined by analogy with (2.5.28), and they have the form:

$$\begin{aligned} A_s &= \frac{(n_s - \delta + ik_s)\boldsymbol{\Theta}_{(s)}^{\mathrm{T}}\mathbf{A}_0\boldsymbol{\theta}_0 + \boldsymbol{\Theta}_{(s)}^{\mathrm{T}}\mathbf{A}_0\dot{\boldsymbol{\theta}}_0}{2ik_sN_s}, \\ B_s &= \frac{(-n_s + \delta + ik_s)\boldsymbol{\Theta}_{(s)}^{\mathrm{T}}\mathbf{A}_0\boldsymbol{\theta}_0 - \boldsymbol{\Theta}_{(s)}^{\mathrm{T}}\mathbf{A}_0\dot{\boldsymbol{\theta}}_0}{2ik_sN_s}. \end{aligned} \tag{4.5.18}$$

Introducing now for convenience the dimensionless eigenvalues $\kappa = \lambda/k$, we can write them according to (4.5.15) and using the dimensionless parameters ν and σ in the final form:

$$\kappa_{1,2} = \sigma - \eta_1\nu \pm i\sqrt{p_{10}^2 - (\sigma - \eta_1\nu)^2}, \quad \kappa_{3,4} = \sigma - \eta_2\nu \pm i\sqrt{p_{20}^2 - (\sigma - \eta_2\nu)^2}. \tag{4.5.19}$$

It can be seen that, depending on the relation between ν and σ, the values κ can be either real (positive or negative) or complex (having a positive or negative

real part). All these cases predetermine the fundamentally different qualitative character of the emerging motion modes of the system. In order to introduce the character of these modes and estimate their total number, we construct a family of boundary lines on the plane $\nu\sigma$, on which the character of motion on each of the modes $\mathbf{\Theta}_{(s)}$ changes from damped to overclocking and from oscillatory to aperiodic. It is clear from the expressions (4.5.19) that these boundary lines are the following six straight lines:

$$\sigma = \eta_1\nu, \quad \sigma = \eta_2\nu,$$
$$\sigma = \eta_1\nu \pm p_{10} = p_{10}\left(\pm 1 + \frac{\nu}{\nu_{10}}\right), \quad \sigma = \eta_2\nu \pm p_{20} = p_{20}\left(\pm 1 + \frac{\nu}{\nu_{20}}\right). \tag{4.5.20}$$

The real parts of the roots $\kappa_{1,2}$ and $\kappa_{3,4}$, respectively, turn to zero on the first two of the straight lines, and the imaginary parts are zero on the remaining two pairs. Straight lines (4.5.20) are shown in Fig. 4.14. Taking into account that $\nu > 0$, and σ can be both positive and negative, we can conclude that these lines divide the half-plane $\nu > 0$ into 11 regions with different motion character of spatial double pendulum.

Let's give a detailed classification of these regions:
1 – aperiodic overclocking of both modes $\mathbf{\Theta}_{(1)}$ and $\mathbf{\Theta}_{(2)}$;
2 – aperiodic overclocking of mode $\mathbf{\Theta}_{(1)}$, oscillatory overclocking of mode $\mathbf{\Theta}_{(2)}$;
3 – oscillatory overclocking of both modes $\mathbf{\Theta}_{(1)}$ and $\mathbf{\Theta}_{(2)}$;
4 – oscillatory overclocking of mode $\mathbf{\Theta}_{(1)}$, oscillatory damping of mode $\mathbf{\Theta}_{(2)}$;
5 – aperiodic overclocking of mode $\mathbf{\Theta}_{(1)}$, oscillatory damping of mode $\mathbf{\Theta}_{(2)}$;
6 – oscillatory overclocking of mode $\mathbf{\Theta}_{(1)}$, aperiodic damping of mode $\mathbf{\Theta}_{(2)}$;
7 – aperiodic overclocking of mode $\mathbf{\Theta}_{(1)}$, aperiodic damping of mode $\mathbf{\Theta}_{(2)}$;
8 – oscillatory damping of both modes $\mathbf{\Theta}_{(1)}$ and $\mathbf{\Theta}_{(2)}$;
9 – oscillatory damping of mode $\mathbf{\Theta}_{(1)}$, aperiodic damping of mode $\mathbf{\Theta}_{(2)}$;
10 – aperiodic damping of mode $\mathbf{\Theta}_{(1)}$, oscillatory damping of mode $\mathbf{\Theta}_{(2)}$;
11 – aperiodic damping of both modes $\mathbf{\Theta}_{(1)}$ and $\mathbf{\Theta}_{(2)}$.
It can be seen that at $\gamma = 0$ and at $\nu = 0$, conclusions follow from this diagram, which are in full agreement with the previously obtained results.

Returning now to the results obtained above, we can see that the condition (4.5.6) occurs in regions 1, 2 and 3, where both modes sway, and the condition

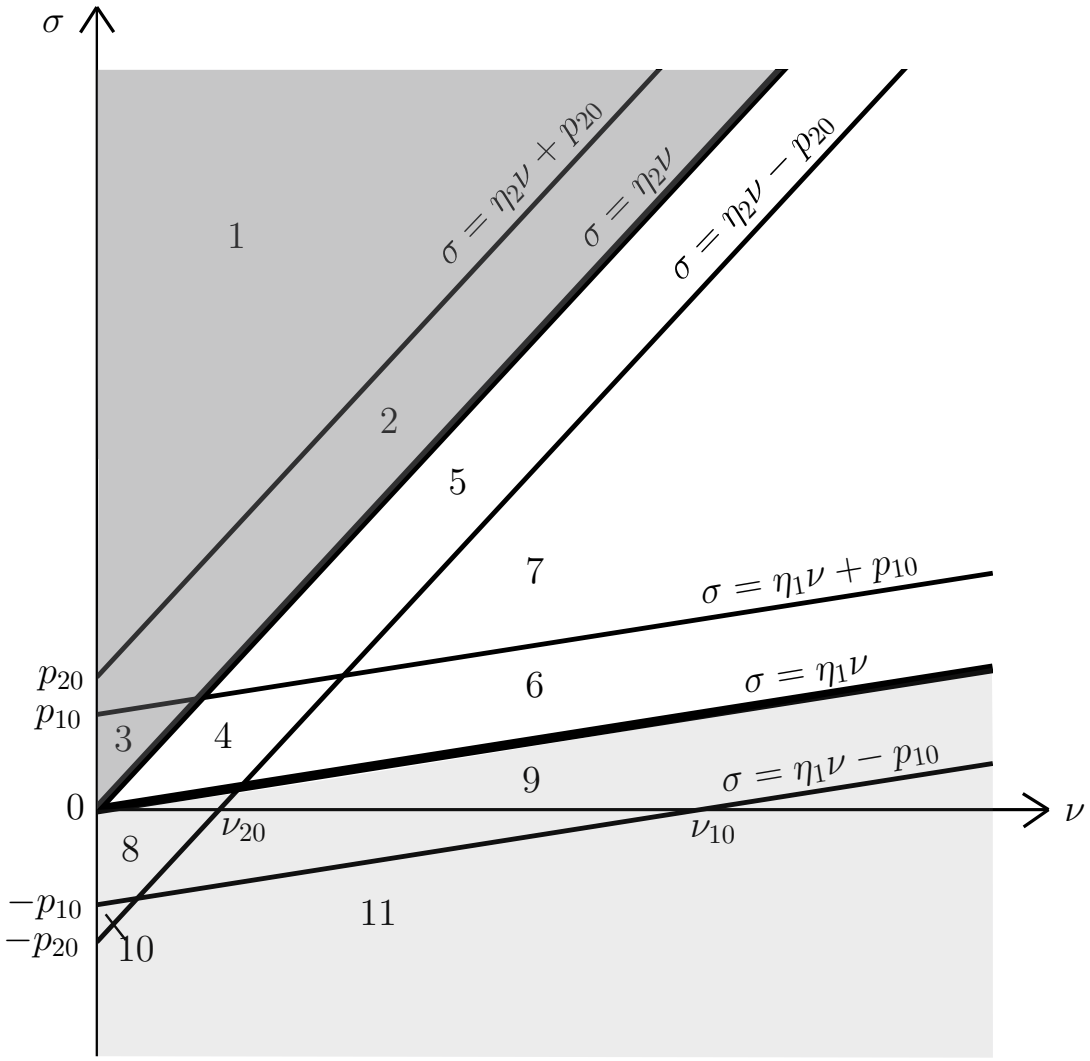

Fig. 4.14. Diagram of system motion modes

(4.5.8) is satisfied in regions 8, 9, 10 and 11 when both modes are extinguished, as one would expect. For clarity, these groups of regions are highlighted in the mode diagram with dark and light backgrounds, respectively. In regions 4, 5, 6, and 7, intermediate modes are realized, when the first mode is swinging, and the second mode is extinguished, and the condition (4.5.9) corresponds to them. Regions 4 and 6 may be of particular practical interest, since if the parameters ν and σ are chosen in these regions, the second mode will be damped (oscillatory or aperiodically, respectively), and as a result, only one swinging first mode can be observed over time. We also note that if we choose the parameters ν and σ on the boundary $\sigma = \eta_1\nu$, then it will be possible to observe undamped oscillations only on the first mode over time.

Thus, the cooperative consideration of both control and dissipative actions significantly complicates the picture of possible motion modes of spatial double

pendulum and makes it possible to choose the most suitable of them for specific practical purposes.

4.6. Conclusions on Fourth Chapter

In this chapter, it was demonstrated that with the help of collinear control it is possible to overclock spatial double pendulum on each of its modes of oscillation separately up to sufficiently large amplitudes. This remarkable feature of such a control means the existence of autoresonant oscillation mode, when all the energy supplied to the system is completely spent on its overclocking on one oscillation mode, providing a single-frequency growth of these oscillations. At the same time, the oscillation mode gradually drifts with the frequency during the transition from the linear zone to the nonlinear one, however, with the complication of its qualitative character, it retains regular structure and it is characterized by periodicity. In addition to collinear control with a constant gain, when the steady motion is reached by simply turning it off, an effective modification of the original control law is also proposed, which consists in using a variable gain and allows a smooth transition to the mode of periodic oscillations with the desired energy level. Finally, the cooperative influence of dissipative and control actions on the dynamic behavior of the system within the framework of a linear model was studied, and as a result a diagram of possible motion modes was presented, which have their own distinctive features and can find certain practical applications.

We note once again that, based on the above advantages of the proposed method of forming control actions, it is advisable to use it not only to control the motion of a spatial double pendulum, but also of any other mechanical system. This conclusion is especially true for systems from the field of modern robotics and biodynamics, since the described controlled modes are widespread in the animal world, where all running, swimming and flying animals perform their locomotions in resonant motion on one of the oscillation modes. This emphasizes the importance of using these principles to control the movement of modern androids and many other devices encountered in various applied problems.

5. Optimization of Oscillation Damping Modes of Spatial Double Pendulum

5.1. Problem Statement of Optimization of Passive and Active Oscillation Damping and Optimization Criteria Formation

In the previous chapters, the spatial double pendulum motions were considered under the action of dissipative forces of viscous friction and control actions built on the principle of collinear control, which make it possible to suppress oscillations of the system. The first type of damping is usually called passive, while the second is called active. In this case, the question naturally arises of finding the best parameters for each of the mentioned types of damping separately and under their combined action [69,70]. It is clear that in order for oscillations to be damped most efficiently, an optimization criterion should be proposed, on the basis of which the parameters of each type of damping would be selected [9, 31, 35, 40, 127, 131]. It is of interest to use different criteria and compare the results obtained according to these criteria.

In the existing literature, as an optimization criterion for systems with several degrees of freedom, the criterion based on maximizing the degree of system stability is most often taken [53, 54]. As is known, the *degree of stability* of a linear dynamical system is the distance Δ from the imaginary axis of the plane of the roots of the characteristic equation to the root closest to it, under the condition

that all these roots lie to the left of the imaginary axis [12, 62, 76] (Fig. 5.1):

$$\Delta = \min_i |\mathrm{Re}\,\lambda_i| = \max\,. \tag{5.1.1}$$

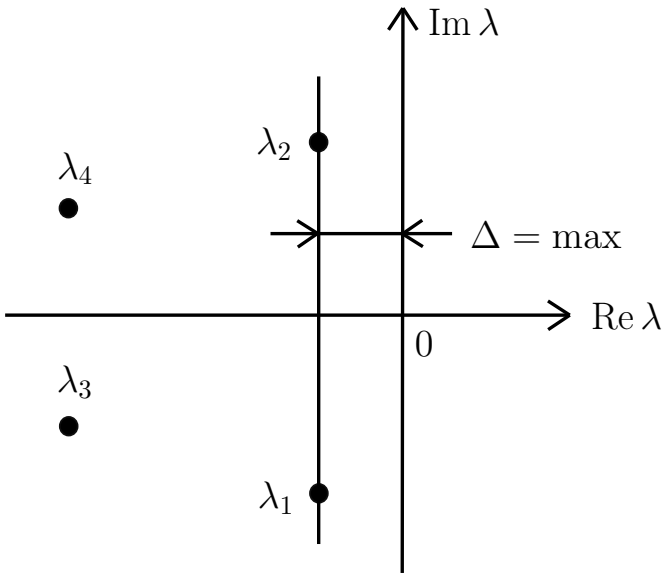

Fig. 5.1. Degree of stability

This optimization criterion is maximin, and its important advantages include the fact that it does not depend on the initial conditions of the system motion. However, it can be constructed only for a linear system, since in a nonlinear system the concept of the degree of stability is meaningless, which is a disadvantage of this criterion. Besides, this criterion is not directly related to the energy parameters of the system, characterizing only the degree of attenuation of component of the solution that decreases the slowest. Therefore, this criterion should be considered purely mathematical rather than physical. Nevertheless, the criterion based on the degree of stability is widely used in various practical problems, due to its relative simplicity of calculation.

However, it is more natural from a physical point of view in the problems of mechanics to choose the parameters of active or passive damping of oscillations from the consideration of the best dissipation of the total mechanical energy in time. Based on this, we can take as an optimization criterion the value of the integral [20, 29, 76]:

$$F = \int_0^\infty E(t)dt = \min, \tag{5.1.2}$$

where $E = T + \Pi$ is the total mechanical energy of the system. Integral criteria of this kind are also often used in automatic control theory [6,27,79]. It is important to emphasize that the criterion (5.1.2) has the following geometric meaning – the value F is the area under the energy curve $E(t)$ on an infinite time interval, and the optimization problem then reduces to determining such damping parameters, when this area is minimal (Fig. 5.2).

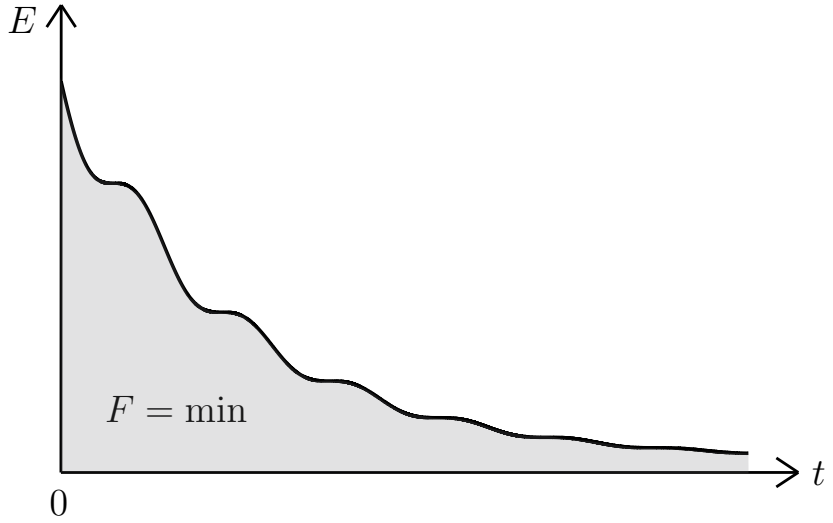

Fig. 5.2. The geometric meaning of the energy-time criterion

We also note that the criterion (5.1.2) is energy-time, since it harmoniously combines in its structure both energy and time characteristics of the process of damping free oscillations. Moreover, in contrast to the degree of stability, this criterion can be used for both linear and nonlinear systems, which significantly expands the scope of its applicability. However, using the energy-time criterion, we have a significant difficulty in determining the optimal parameters, due to the fact that in the general case these parameters will significantly depend on the initial conditions of motion, which is typical of any integral criterion. This is the main disadvantage of the criterion under discussion, which the criterion based on the degree of stability was deprived of. Nevertheless, since the initial conditions are by no means always precisely defined, it is advisable to act according to the *principle of guaranteed success*, i.e., to determine the best damping mode parameters for the worst set of initial conditions (the one for which the criterion value is the largest at the specified damping parameters). In this case, we arrive at a minimax procedure.

As a rule, when solving problems of optimizing the parameters of mechanical

systems with several degrees of freedom, it is necessary to resort exclusively to numerical methods of analysis, since the construction of exact analytical solutions turns out to be laborious or even impossible. This circumstance significantly reduces the value of such a solution in qualitative terms. However, in the present example of spatial double pendulum with dissipative and control factors, it is possible to construct an analytical solution and use numerical methods only to determine the roots of algebraic equations, which is a very important point for the most visual and accessible interpretation of the results.

5.2. Optimization of Viscous Oscillation Damping

Let us first raise the question of finding the coefficient of viscous friction b (or the value n corresponding to it) in the joints from the optimization condition for the damping process of small oscillations of spatial double pendulum [42].

1. Degree of stability. Let us discuss in more detail the trajectories of the roots (2.5.12) of the characteristic equation in the dimensionless form $\kappa = \lambda/k$ on the root hodograph with increasing coefficient $\nu = n/k$ from 0 to ∞. At $\nu = 0$ all four roots obviously lie on the imaginary axis of the hodograph plane. As ν increases in the range $0 < \nu < \nu_{20}$, these roots move along semicircles lying to the left of the imaginary axis:

$$(\operatorname{Re}\kappa_{1,2})^2 + (\operatorname{Im}\kappa_{1,2})^2 = p_{10}^2, \quad (\operatorname{Re}\kappa_{3,4})^2 + (\operatorname{Im}\kappa_{3,4})^2 = p_{20}^2. \tag{5.2.1}$$

In this case, the roots $\kappa_{3,4}$ move along the larger semicircle (5.2.1) and approach each other until, at $\nu = \nu_{20}$, they merge into one multiple real root, and after that they are already move in different directions along the real axis. The roots $\kappa_{1,2}$ also move along their semicircle in the range $\nu_{20} < \nu < \nu_{10}$ until at $\nu = \nu_{10}$ they merge into one multiple root. After that, they, like the pair of roots $\kappa_{3,4}$, begin to diverge in different directions along the real axis. Thus, at $\nu \to \infty$ in each pair one root tends to -0 and the other tends to $-\infty$. The root hodograph of this process is shown in Fig. 5.3.

Let us show that there exists a value ν_* in the range $\nu_{20} < \nu_* < \nu_{10}$ when the roots $\kappa_{3,4}$ have already diverged from their merge point to different sides along the real axis, while the roots $\kappa_{1,2}$ are still on their semicircle, i.e. are complex conjugate, and the real part of the roots $\kappa_{1,2}$ coincides with the smaller in modulus

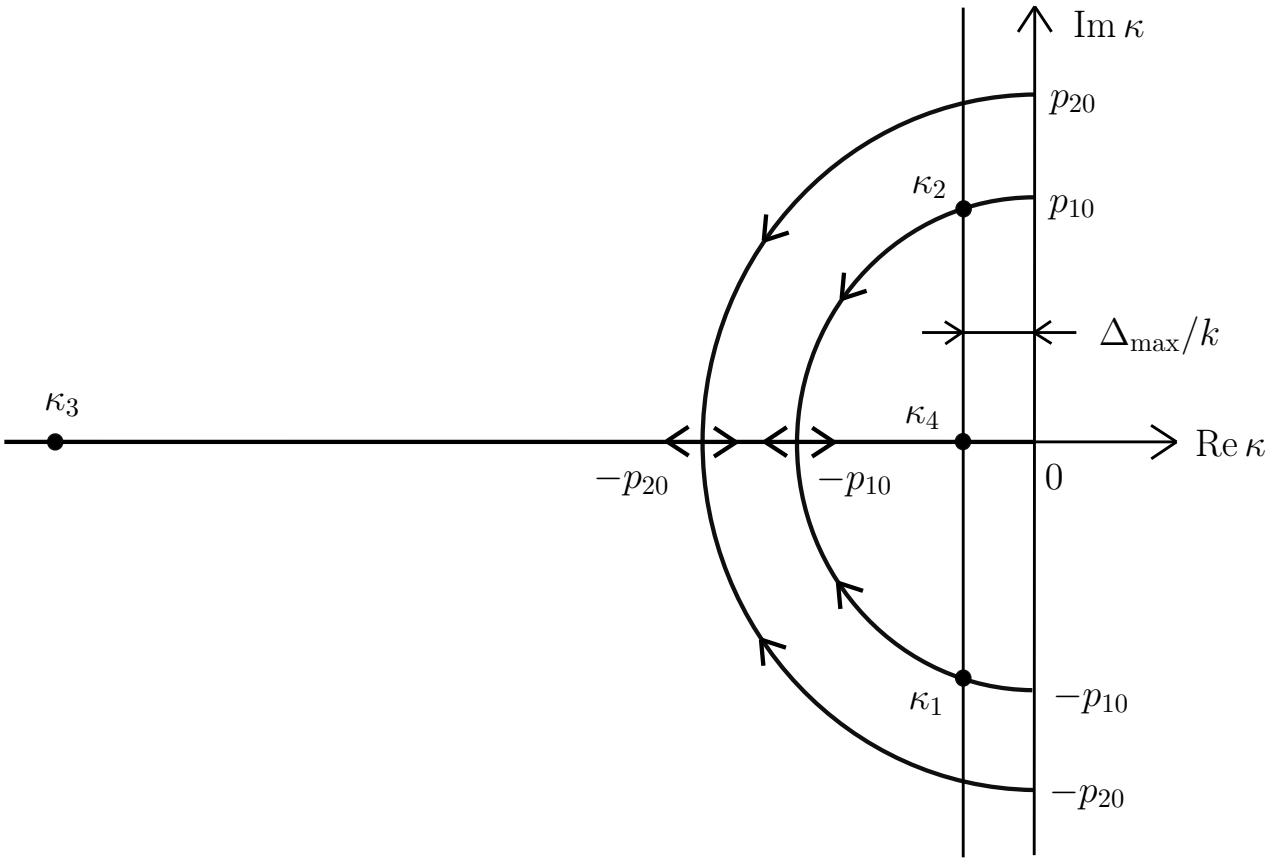

Fig. 5.3. The root hodograph

of the real roots κ_4. In this case, three roots will be located on the root hodograph on the same vertical, and the fourth one will be much to the left of them. Indeed, by equating the real parts of these roots, which are $-n_1$ and $-n_2 + \sqrt{n_2^2 - k_{20}^2}$, and passing to dimensionless notation, we obtain the equation:

$$-\eta_1\nu = -\eta_2\nu + \sqrt{\eta_2^2\nu^2 - p_{20}^2}. \tag{5.2.2}$$

Resolving it relative to ν, we find the desired value ν_*:

$$\nu_* = \frac{p_{20}}{\sqrt{\eta_1(2\eta_2 - \eta_1)}}. \tag{5.2.3}$$

Fig. 5.4 shows the location of ν_* relative to the values ν_{20} and ν_{10} depending on the angle α, and it clearly demonstrates its location in the range $\nu_{20} < \nu_* < \nu_{10}$.

Thus, it is possible to qualitatively represent the behavior of the dependence graphs of the modules of the real parts of all four roots of the characteristic equation in a dimensionless version (Fig. 5.5). Here, the solid lines mark the sections corresponding to the root closest to the imaginary axis, which determines the dimensionless degree of stability Δ/k. To be convincing, we additionally show

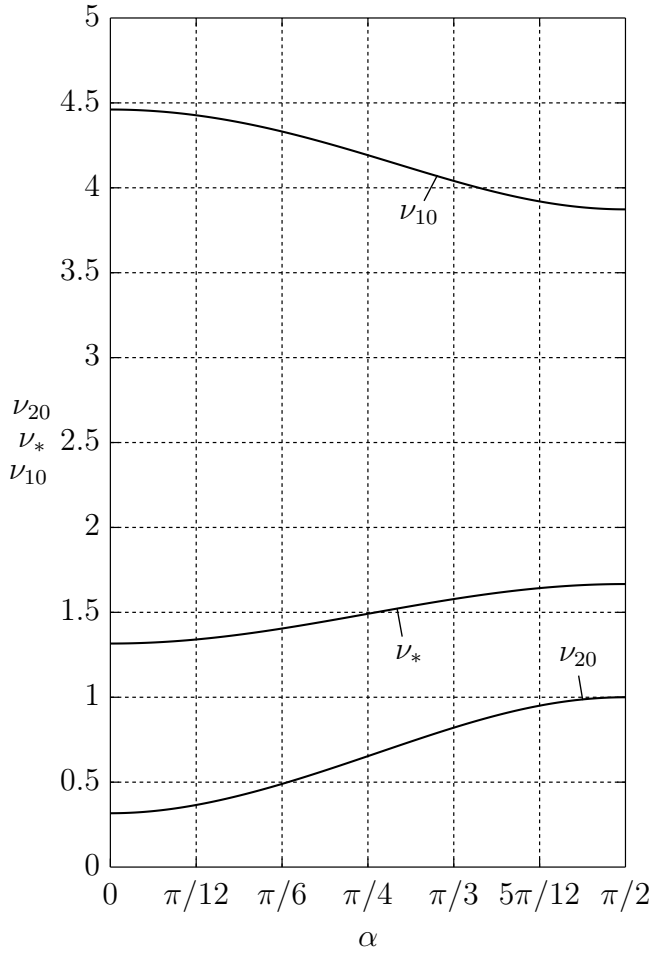

Fig. 5.4. Graph dependencies of values ν_{20}, ν_* and ν_{10} on angle α

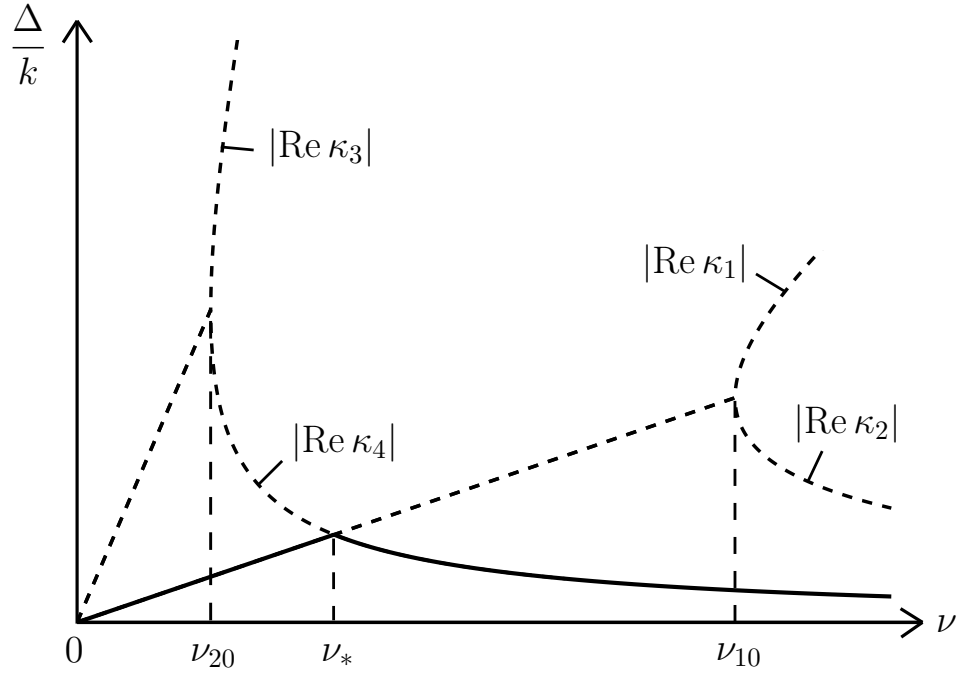

Fig. 5.5. Graph dependence of dimensionless degree of stability Δ/k on ν

that the curve $|\operatorname{Re}\kappa_2| = \eta_1\nu - \sqrt{\eta_1^2\nu^2 - p_{10}^2}$ at $\nu > \nu_{10}$ lies above the curve $|\operatorname{Re}\kappa_4| = \eta_2\nu - \sqrt{\eta_2^2\nu^2 - p_{20}^2}$. Indeed, the following chain of relations holds:

$$|\operatorname{Re}\kappa_2| = \frac{p_{10}^2/\eta_1}{\nu + \sqrt{\nu^2 - \nu_{10}^2}} > \frac{p_{20}^2/\eta_2}{\nu + \sqrt{\nu^2 - \nu_{20}^2}} = |\operatorname{Re}\kappa_4|, \tag{5.2.4}$$

where it is taken into account that $\nu_{10} > \nu_{20}$ according to (2.5.17), and also

$$\frac{p_{10}^2}{\eta_1} = \frac{1}{2 - 1/p_{10}^2} > \frac{1}{2 - 1/p_{20}^2} = \frac{p_{20}^2}{\eta_2} \tag{5.2.5}$$

due to the relations (2.5.14) and the fact that $p_{10} < p_{20}$. According to Fig. 5.5, it is easy to see that it is the value ν_* that provides the maximum degree of stability, and this extremum is acute. The maximum value of the degree of stability, taking into account the non-dimensionality, will be:

$$\frac{\Delta_{\max}}{k} = \eta_1\nu_* = p_{20}\sqrt{\frac{\eta_1}{2\eta_2 - \eta_1}}. \tag{5.2.6}$$

We can determine from the formulas (5.2.3) and (5.2.6) the values ν_* and $\Delta_{\max}/k$ in particular cases. Thus, at $\alpha = 0$ we find

$$\nu_* = \sqrt{\frac{13\sqrt{2} + 18}{21}} \approx 1.3163, \quad \frac{\Delta_{\max}}{k} = \sqrt{\frac{5\sqrt{2} - 6}{21}} \approx 0.2268, \tag{5.2.7}$$

and at $\alpha = \pi/2$ we have

$$\nu_* = \frac{5}{3} \approx 1.6667, \quad \frac{\Delta_{\max}}{k} = \frac{1}{3} \approx 0.3333. \tag{5.2.8}$$

Finally, according to Fig. 5.5 it can be seen that for $0 < \nu \le \nu_*$ the dimensionless degree of stability is determined by the real part of the complex conjugate roots $\kappa_{1,2}$, while for $\nu > \nu_*$ is the smallest of the real roots of κ_4, so that

$$\frac{\Delta}{k} = \begin{cases} \eta_1\nu, & 0 < \nu \le \nu_* \\ \eta_2\nu - \sqrt{\eta_2^2\nu^2 - p_{20}^2}, & \nu > \nu_* \end{cases}. \tag{5.2.9}$$

Of course, both at $\nu \to 0$ and $\nu \to \infty$ the degree of stability tends to zero.

2. Energy-time criterion. To solve the problem by the second criterion, we will use the solution in complex form (2.5.26). Its convenience lies in the fact that the integral (5.1.2) will then be calculated most simply. Substituting formulas

(2.5.26) and (2.5.27) into the expressions (2.4.3) for the kinetic and potential energies, as well as using the formulas (2.4.21) and (2.4.22), we calculate the total mechanical energy:

$$E = \frac{1}{2}\left[N_1 e^{-n_1 t} f_1(t) + N_2 e^{-n_2 t} f_2(t)\right], \tag{5.2.10}$$

where the functions $f_s(t)$ have the following form:

$$\begin{aligned} f_s(t) = A_s^2 e^{2ik_s t}\left[(n_s + ik_s)^2 + k_{s0}^2\right] + \\ + B_s^2 e^{-2ik_s t}\left[(-n_s + ik_s)^2 + k_{s0}^2\right] + 4A_s B_s k_{s0}^2, \quad s = 1, 2. \end{aligned} \tag{5.2.11}$$

Let us now substitute the expression (5.2.10), taking into account (5.2.11), into the integral (5.1.2), and also taking into account that

$$\int_0^\infty e^{-2(n_s \pm ik_s)t} dt = \frac{1}{2(n_s \pm ik_s)}, \quad \int_0^\infty e^{-2n_s t} dt = \frac{1}{2n_s}, \quad s = 1, 2. \tag{5.2.12}$$

Then we get the following expression for F:

$$F = \frac{1}{2}\left[N_1 \frac{(A_1 + B_1)^2 n_1^2 + 2A_1 B_1 k_1^2}{n_1} + N_2 \frac{(A_2 + B_2)^2 n_2^2 + 2A_2 B_2 k_2^2}{n_2}\right]. \tag{5.2.13}$$

We note that the complex integration constants A_s and B_s in this expression have representations (2.5.28). In addition, we emphasize that the expression (5.2.13) has no singularities when multiple roots of the characteristic equation appear, i.e., at $k_s \to 0$. Indeed, it is easy to see that both the values $A_s + B_s$ and $A_s B_s k_s^2$ turn out to be finite in this case according to (2.5.28). Thus, the resulting expression (5.2.13) is valid for any values of the dimensionless dissipative coefficient ν.

Let us now turn to determining the optimal value ν for the worst set of initial conditions. To this puprose, we represent the initial conditions $\boldsymbol{\theta}_0$ and $\dot{\boldsymbol{\theta}}_0$ as the sum of two modes $\boldsymbol{\Theta}_{(1)}$ and $\boldsymbol{\Theta}_{(2)}$ with some coefficients P_s and R_s:

$$\boldsymbol{\theta}_0 = P_1 \boldsymbol{\Theta}_{(1)} + P_2 \boldsymbol{\Theta}_{(2)}, \quad \dot{\boldsymbol{\theta}}_0 = R_1 \boldsymbol{\Theta}_{(1)} + R_2 \boldsymbol{\Theta}_{(2)}, \tag{5.2.14}$$

and these coefficients are uniquely determined by the given $\boldsymbol{\theta}_0$ and $\dot{\boldsymbol{\theta}}_0$ [10]. However, they are not very convenient for further analysis. Therefore, instead of pairs of coefficients (P_s, R_s), it is advisable to introduce two other pairs (r_s, μ_s) using the formulas:

$$P_s = \frac{r_s}{\sqrt{N_s k_{s0}^2}} \cos\mu_s, \quad R_s = \frac{r_s}{\sqrt{N_s}} \sin\mu_s. \tag{5.2.15}$$

It is clear that the transition from first coefficients to another actually represents the transition from Cartesian to polar coordinates with some scale factors. In this case, $\mu_s \in [0, 2\pi)$, and $r_s \in [0, \infty)$. It is convenient to set the pair (r_1, r_2) also by polar coordinates:

$$r_1 = \rho \cos\vartheta, \quad r_2 = \rho \sin\vartheta, \tag{5.2.16}$$

where $\rho \in [0, \infty)$, and $\vartheta \in [0, \pi/2]$. Convenience of replacement of initial condition columns $\boldsymbol{\theta}_0$ and $\dot{\boldsymbol{\theta}}_0$ by parameters ρ, ϑ, μ_1 and μ_2 is that the initial energy of the system is then expressed most simply:

$$E_0 = \frac{1}{2}\dot{\boldsymbol{\theta}}_0^{\mathrm{T}}\mathbf{A}_0\dot{\boldsymbol{\theta}}_0 + \frac{1}{2}\boldsymbol{\theta}_0^{\mathrm{T}}\mathbf{C}_0\boldsymbol{\theta}_0 = \frac{1}{2}\rho^2. \tag{5.2.17}$$

This implies an important conclusion that the parameter ρ characterizes the initial energy level of the system, while the parameters ϑ, μ_1, and μ_2 do not affect it in any way.

Substituting now (2.5.28), (5.2.14), (5.2.15), (5.2.16) into (5.2.13) and taking into account (5.2.17), we arrive at the expression for $F(\nu, \mu_1, \mu_2, \vartheta)$:

$$\begin{aligned} F = \frac{E_0}{2}\Bigg[\frac{\cos^2\vartheta}{k_{10}}\left(\frac{1}{\nu_1} + \nu_1 + \nu_1\cos 2\mu_1 + \sin 2\mu_1\right) + \\ + \frac{\sin^2\vartheta}{k_{20}}\left(\frac{1}{\nu_2} + \nu_2 + \nu_2\cos 2\mu_2 + \sin 2\mu_2\right)\Bigg], \end{aligned} \tag{5.2.18}$$

where, for convenience, two more dimensionless dissipative coefficients ν_1 and ν_2 are also introduced, which are related to ν by the following formulas:

$$\nu_1 = \frac{n_1}{k_{10}} = \frac{\eta_1}{p_{10}}\nu, \quad \nu_2 = \frac{n_2}{k_{20}} = \frac{\eta_2}{p_{20}}\nu. \tag{5.2.19}$$

Turning to the expression (5.2.18) for the integral optimization criterion, we now proceed directly to finding the optimal value ν for the worst set of initial conditions. Here we have the minimax problem of finding the extremum points of the function $F(\nu, \mu_1, \mu_2, \vartheta)$, i.e. about finding $\min\limits_{\nu} \max\limits_{\mu_1,\mu_2,\vartheta} F(\nu, \mu_1, \mu_2, \vartheta)$. It can be seen that in this case the value of the initial energy E_0 does not play a role, but only the relation between the columns of initial conditions $\boldsymbol{\theta}_0$ and $\dot{\boldsymbol{\theta}}_0$ has the meaning, which is determined is determined by μ_1, μ_2, ϑ. Discarding further the insignificant factor $E_0/(2k)$ in the expression for F, we denote the resulting

dimensionless expression by f:

$$f = \frac{\cos^2\vartheta}{p_{10}}\left[\frac{1}{\nu_1} + \nu_1 + \sqrt{1+\nu_1^2}\sin\left(2\mu_1+\psi_1\right)\right] + \\ + \frac{\sin^2\vartheta}{p_{20}}\left[\frac{1}{\nu_2} + \nu_2 + \sqrt{1+\nu_2^2}\sin\left(2\mu_2+\psi_2\right)\right], \quad \operatorname{tg}\psi_s = \nu_s, \quad s = 1,2. \tag{5.2.20}$$

It is easy to see from (5.2.20) that f reaches its maximum values in μ_1 and μ_2 equal to

$$f_{\substack{\max\\ \mu_1,\mu_2}} = \frac{\cos^2\vartheta}{p_{10}}\left(\frac{1}{\nu_1} + \nu_1 + \sqrt{1+\nu_1^2}\right) + \frac{\sin^2\vartheta}{p_{20}}\left(\frac{1}{\nu_2} + \nu_2 + \sqrt{1+\nu_2^2}\right) \tag{5.2.21}$$

at points when $\sin\left(2\mu_1+\psi_1\right) = 1$, $\sin\left(2\mu_2+\psi_2\right) = 1$. Next, we need to maximize the expression (5.2.21) in ϑ. It is clear that this expression reaches its extreme values either at $\vartheta = 0$ (when the initial conditions are given on the first mode) or at $\vartheta = \pi/2$ (when the initial conditions are given on the second mode). Let us determine at which of these points the function $f_{\substack{\max\\ \mu_1,\mu_2}}$ reaches its maximum value in ϑ. To do this, we write out the values of this function at extreme points:

$$\begin{aligned} \vartheta = 0: \quad & f_{\substack{\max\\ \mu_1,\mu_2}} = \frac{1}{p_{10}}\left(\frac{1}{\nu_1} + \nu_1 + \sqrt{1+\nu_1^2}\right), \\ \vartheta = \frac{\pi}{2}: \quad & f_{\substack{\max\\ \mu_1,\mu_2}} = \frac{1}{p_{20}}\left(\frac{1}{\nu_2} + \nu_2 + \sqrt{1+\nu_2^2}\right). \end{aligned} \tag{5.2.22}$$

If ν_1 and ν_2 are expressed in terms of ν using the relations (5.2.19), then each of these expressions can be obtained as a function of ν and α. In order to compare the values (5.2.22) with each other, let us write down their simplified representations. Thus, for $\nu \to 0$ we have

$$f_{\substack{\max\\ \mu_1,\mu_2}}(\vartheta = 0) \approx \frac{1}{\eta_1\nu} + \frac{1}{p_{10}}, \quad f_{\substack{\max\\ \mu_1,\mu_2}}\left(\vartheta = \frac{\pi}{2}\right) \approx \frac{1}{\eta_2\nu} + \frac{1}{p_{20}}, \tag{5.2.23}$$

while for $\nu \to \infty$ it will be

$$f_{\substack{\max\\ \mu_1,\mu_2}}(\vartheta = 0) \approx 2\left(2 - \frac{1}{p_{10}^2}\right)\nu, \quad f_{\substack{\max\\ \mu_1,\mu_2}}\left(\vartheta = \frac{\pi}{2}\right) \approx 2\left(2 - \frac{1}{p_{20}^2}\right)\nu, \tag{5.2.24}$$

where the formulas (2.5.14) are taken into account. Since $p_{10} < p_{20}$, $\eta_1 < \eta_2$, we can conclude from this that at $\nu \to 0$ there will be $f_{\substack{\max\\ \mu_1,\mu_2}}(\vartheta = 0) > f_{\substack{\max\\ \mu_1,\mu_2}}(\vartheta = \pi/2)$,

while at $\nu \to \infty$ we already have $f_{\max\limits_{\mu_1,\mu_2}}(\vartheta = 0) < f_{\max\limits_{\mu_1,\mu_2}}(\vartheta = \pi/2)$. This means that the equation $f_{\max\limits_{\mu_1,\mu_2}}(\vartheta = 0) = f_{\max\limits_{\mu_1,\mu_2}}(\vartheta = \pi/2)$ has for any value α on the interval $0 < \nu < \infty$ at least one real root, which can be determined using numerical procedures. A numerical study shows that such a root ν_* is unique for any α.

Из этих рассуждений следует, что максимальное значение функции $f_{\max\limits_{\mu_1,\mu_2}}$ по ϑ зависит от величины коэффициента ν следующим образом:

$$f_{\max\limits_{\mu_1,\mu_2,\vartheta}} = \begin{cases} \dfrac{1}{p_{10}}\left(\dfrac{1}{\nu_1} + \nu_1 + \sqrt{1+\nu_1^2}\right), & 0 < \nu \le \nu_* \\ \dfrac{1}{p_{20}}\left(\dfrac{1}{\nu_2} + \nu_2 + \sqrt{1+\nu_2^2}\right), & \nu > \nu_* \end{cases}. \tag{5.2.25}$$

It remains to find the minimum value of the function (5.2.25) in ν. To do this, we first determine the extremum points of each of the functions (5.2.22) on the interval $0 < \nu < \infty$. Since $f_{\max\limits_{\mu_1,\mu_2}}$ at $\vartheta = 0$ is a function of the variable ν_1, then to find its extremum point, it suffices to calculate its derivative by this variable and equate the resulting expression to zero. As a result, after a series of transformations, we will have:

$$\nu_1^4 + \nu_1^2 - 1 = 0, \quad \nu_1 = \sqrt{\frac{\sqrt{5}-1}{2}}, \quad \nu_{*1} = \frac{p_{10}}{\eta_1}\nu_1 = \frac{p_{10}}{\eta_1}\sqrt{\frac{\sqrt{5}-1}{2}}. \tag{5.2.26}$$

Similarly, we determine the extremum point of the function $f_{\max\limits_{\mu_1,\mu_2}}$ at $\vartheta = \pi/2$:

$$\nu_2^4 + \nu_2^2 - 1 = 0, \quad \nu_2 = \sqrt{\frac{\sqrt{5}-1}{2}}, \quad \nu_{*2} = \frac{p_{20}}{\eta_2}\nu_2 = \frac{p_{20}}{\eta_2}\sqrt{\frac{\sqrt{5}-1}{2}}. \tag{5.2.27}$$

Let us plot the dependencies of ν_*, ν_{*1} and ν_{*2} on the angle α on one graph (Fig. 5.6). It is easy to see that for any value α we will have $\nu_{*2} < \nu_* < \nu_{*1}$. This means that the value ν_{*1} does not fall within the interval $0 < \nu \le \nu_*$ and the value ν_{*2} does not fall within the interval $\nu > \nu_*$. Therefore, the graph of the function (5.2.25) over the entire interval $0 < \nu < \infty$ can be schematically represented as follows (Fig. 5.7). In this case, the necessary segments of the functions are highlighted by solid lines, and the extraneous ones are dotted. It is clear from this that the minimum of the function $f_{\max\limits_{\mu_1,\mu_2,\vartheta}}$ is reached exactly at $\nu = \nu_*$, and this extremum is sharp, as it was when considering the optimization criterion based on the degree of stability. We note that at the point $\nu = \nu_*$ both values in (5.2.22)

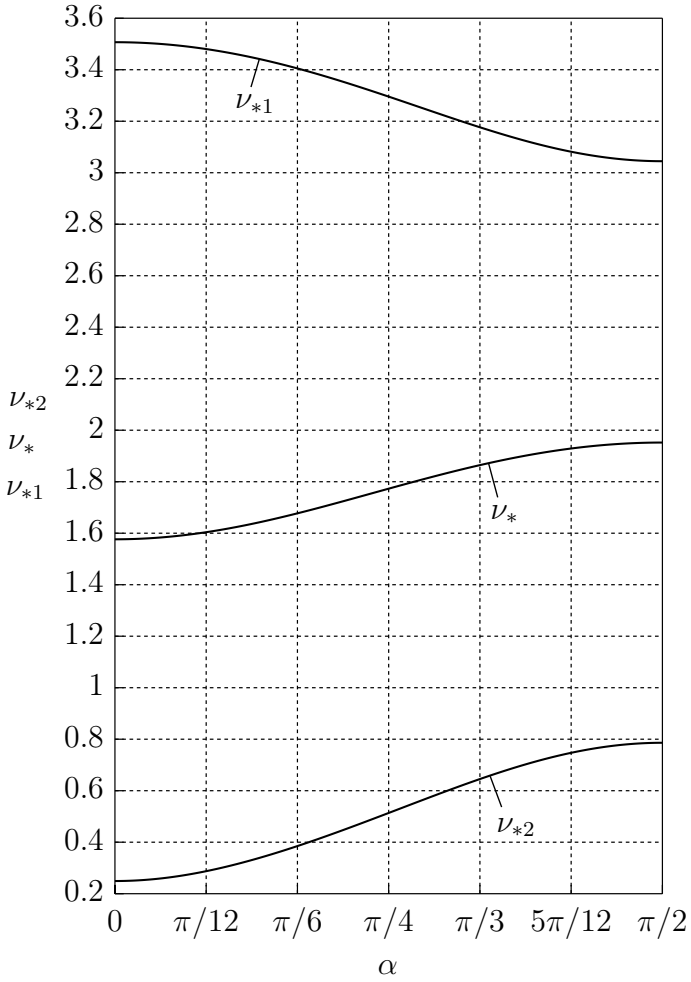

Fig. 5.6. Graph dependencies of values ν_{*2}, ν_* и ν_{*1} on angle α

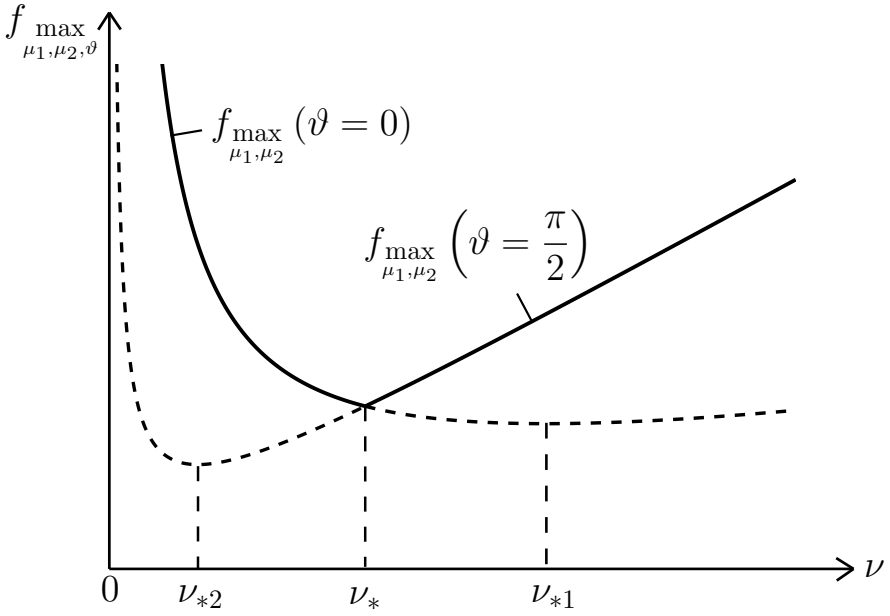

Fig. 5.7. Graph dependence of $f_{\max\limits_{\mu_1,\mu_2,\vartheta}}$ on ν

are equal, so if we return to the formula (5.2.21), we can see that for a given value ν it will not depend on ϑ, since the equal factor can be taken out of the bracket, and $\cos^2\vartheta+\sin^2\vartheta=1$. The left branch of the graph shown in Fig. 5.7 corresponds to the value $\vartheta=\pi/2$, and the right branch corresponds to the value $\vartheta=0$. At the found optimal point $\nu=\nu_*$, the value ϑ does not play any role – it can be any value, and the value of the criterion (5.2.21) will not change.

Finally, we write down the specific values ν_* and the corresponding values of criterion $f_{\max\limits_{\mu_1,\mu_2,\vartheta}}$ in particular cases. Thus, at $\alpha=0$ we find

$$\nu_*=1.5764, \quad f_{\max\limits_{\mu_1,\mu_2,\vartheta}}=5.5458, \tag{5.2.28}$$

and at $\alpha=\pi/2$ we have

$$\nu_*=1.9521, \quad f_{\max\limits_{\mu_1,\mu_2,\vartheta}}=4.6577. \tag{5.2.29}$$

5.3. Optimization of Collinear Oscillation Damping

Let us now assume that the oscillations of spatial double pendulum are damped by means of collinear braking, i.e., it is active. Based on the same optimization criteria as for the case of passive oscillation suppression, let us determine the optimal values of the parameter $\gamma<0$ (or the corresponding value $\delta=\gamma/2$).

1. Degree of stability. As before, we first consider a criterion based on the degree of stability and discuss the behavior of the dimensionless roots of the characteristic equation $\kappa=\lambda/k$, referring to the formulas (4.3.5). It is easy to understand that the root hodograph here will have the same form as in Fig. 5.3, however, the movement of the roots when changing the coefficient $\sigma=\delta/k$ now occurs differently on it. So, at $\sigma=0$ all four roots lie on the imaginary axis. When σ decreases in the range $-p_{10}<\sigma<0$, the roots move along semicircles (5.2.1), while being on the same vertical. At $\sigma=-p_{10}$, the roots $\kappa_{1,2}$ merge into one multiple real root, and as σ decreases further, they diverge along the real axis in different directions from the merging point. The pair of roots $\kappa_{3,4}$ in the range $-p_{20}<\sigma<-p_{10}$ continues to move along their semicircle, until at $\sigma=-p_{20}$ they merge into a multiple root, after which, for $\sigma<-p_{20}$, they also diverge along the real axis.

Considering what has been said, it is possible to plot the graph dependencies of the modules of the real parts of all four roots of the characteristic equation in a dimensionless variant (Fig. 5.8). As before, the solid lines here highlight sections corresponding to the root closest to the imaginary axis, which determines the dimensionless degree of stability Δ/k. We emphasize additionally that, in contrast to the case of viscous damping considered above, here for $\sigma < -p_{20}$ the curve $|\operatorname{Re}\kappa_2| = -\sigma - \sqrt{\sigma^2 - p_{10}^2}$ lies below the curve $|\operatorname{Re}\kappa_4| = -\sigma - \sqrt{\sigma^2 - p_{20}^2}$, and this is obvious because $p_{10} < p_{20}$. It is clear that in the problem under study the maximum degree of stability is reached at the point when the roots $\kappa_{1,2}$ merge, i.e., under the condition that they are multiplicity. Thus, we obtain the optimal value

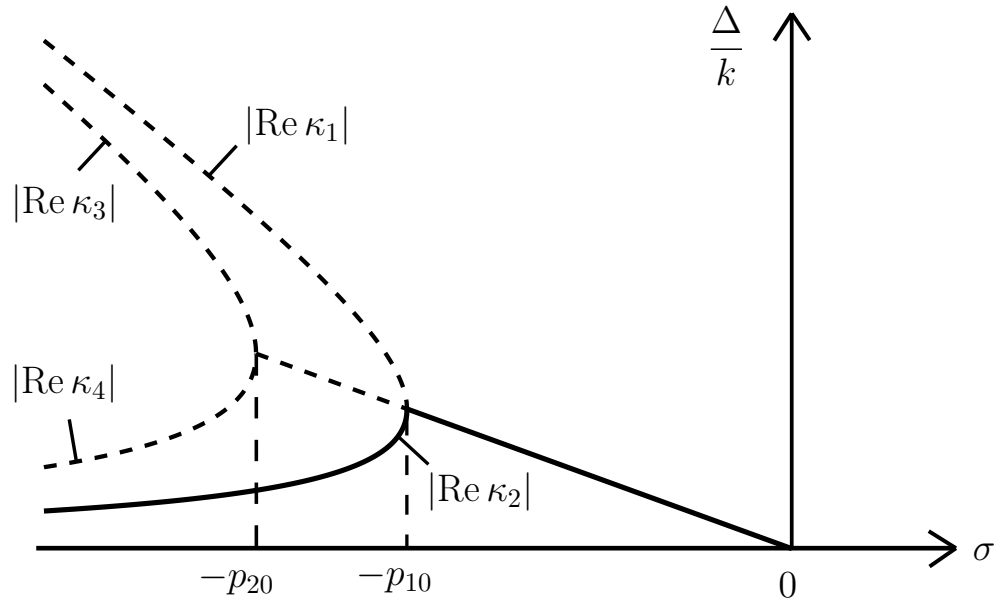

Fig. 5.8. Graph dependence of the dimensionless degree of stability Δ/k on σ

σ_* and the maximum degree of stability corresponding to it in the dimensionless version:

$$\sigma_* = -p_{10}, \quad \frac{\Delta_{\max}}{k} = p_{10}. \tag{5.3.1}$$

Therefore, the dependence of σ_* on the angle α completely repeats the dependence of the first frequency on this angle, shown in Fig. 2.6, and therefore the value of σ_* is practically independent of the angle α. It is clear that for $-p_{10} \le \sigma < 0$ the dimensionless degree of stability is determined by the real part of the complex conjugate roots $\kappa_{1,2}$, and after this point, by the smaller modulus of these roots

κ_2 which are already real:

$$\frac{\Delta}{k} = \begin{cases} -\sigma, & -p_{10} \le \sigma < 0 \\ -\sigma - \sqrt{\sigma^2 - p_{10}^2}, & \sigma < -p_{10} \end{cases} . \tag{5.3.2}$$

However, two important things should be kept in mind here. First, as mentioned above, in the case of a multiple root, one of the functions in the fundamental system of solutions has the form $te^{-k_{10}t}$. This function grows at small times, although it decays at $t \to \infty$, and, nevertheless, it is hardly advisable to have such a component of the solution if we are talking about optimal oscillation damping [76]. Secondly, the left part of the graph shown in Fig. 5.8 has a vertical tangent at the point $\sigma = -p_{10}$. This means that even the slightest error in the value σ in the smaller direction can lead to a sharp drop in the degree of stability. It follows from this that if we are guided by a criterion based on the degree of stability, then it is best to choose in practice the value σ_* slightly larger than the value $-p_{10}$ so that it is located on the linear section of the graph. In this case, both of these disadvantages will be eliminated: there will be no multiple roots, and an error in the value σ will lead to exactly the same error in the value Δ/k.

2. Energy-time criterion. Turning now to the integral criterion (5.1.2) without stopping again on transformations, we arrive at the following expression for this criterion after completely analogous actions:

$$F = \frac{E_0}{2}\left[\frac{\cos^2\vartheta}{k_{10}}\left(\frac{1}{\sigma_1} + \sigma_1 + \sigma_1\cos 2\mu_1 + \sin 2\mu_1\right) + \right. \\ \left. + \frac{\sin^2\vartheta}{k_{20}}\left(\frac{1}{\sigma_2} + \sigma_2 + \sigma_2\cos 2\mu_2 + \sin 2\mu_2\right)\right], \tag{5.3.3}$$

where the dimensionless coefficients σ_1 and σ_2 are also introduced, which are related to σ by the formulas:

$$\sigma_1 = -\frac{\delta}{k_{10}} = -\frac{\sigma}{p_{10}}, \quad \sigma_2 = -\frac{\delta}{k_{20}} = -\frac{\sigma}{p_{20}}. \tag{5.3.4}$$

It can be seen that the expression (5.3.3) coincides with (5.2.18) up to notation, but the dependence of the coefficients σ_1 and σ_2 on σ according to the expression (5.3.4) is fundamentally different from how ν_1 and ν_2 previously depended on ν in (5.2.19). Therefore, it makes sense to proceed further in more detail.

Discarding in (5.3.3) the insignificant constant factor $E_0/(2k)$ and finding the maximum value of the resulting expression in μ_1 and μ_2

$$f_{\max\limits_{\mu_1,\mu_2}} = \frac{\cos^2\vartheta}{p_{10}}\left(\frac{1}{\sigma_1}+\sigma_1+\sqrt{1+\sigma_1^2}\right)+\frac{\sin^2\vartheta}{p_{20}}\left(\frac{1}{\sigma_2}+\sigma_2+\sqrt{1+\sigma_2^2}\right), \quad (5.3.5)$$

we see that, as before, it reaches an extremum in ϑ at the points $\vartheta = 0$ and $\vartheta = \pi/2$. Comparing the values of the function $f_{\max\limits_{\mu_1,\mu_2}}$ at these points

$$\begin{aligned} \vartheta = 0: &\quad f_{\max\limits_{\mu_1,\mu_2}} = \frac{1}{p_{10}}\left(\frac{1}{\sigma_1}+\sigma_1+\sqrt{1+\sigma_1^2}\right), \\ \vartheta = \frac{\pi}{2}: &\quad f_{\max\limits_{\mu_1,\mu_2}} = \frac{1}{p_{20}}\left(\frac{1}{\sigma_2}+\sigma_2+\sqrt{1+\sigma_2^2}\right), \end{aligned} \quad (5.3.6)$$

and taking into account the expressions (5.3.4), it is easy to establish that

$$\begin{aligned} f_{\max\limits_{\mu_1,\mu_2}}(\vartheta = 0) &= -\frac{1}{\sigma}-\frac{\sigma}{p_{10}^2}+\frac{1}{p_{10}}\sqrt{1+\frac{\sigma^2}{p_{10}^2}}, \\ f_{\max\limits_{\mu_1,\mu_2}}\left(\vartheta = \frac{\pi}{2}\right) &= -\frac{1}{\sigma}-\frac{\sigma}{p_{20}^2}+\frac{1}{p_{20}}\sqrt{1+\frac{\sigma^2}{p_{20}^2}}. \end{aligned} \quad (5.3.7)$$

It is easy to see from here that the maximum value of the function $f_{\max\limits_{\mu_1,\mu_2}}$ in ϑ is reached at $\vartheta = 0$ for any value σ, since $p_{20} > p_{10}$. It remains to minimize the expression

$$f_{\max\limits_{\mu_1,\mu_2,\vartheta}} = \frac{1}{p_{10}}\left(\frac{1}{\sigma_1}+\sigma_1+\sqrt{1+\sigma_1^2}\right) \quad (5.3.8)$$

in σ (or, more simply, in σ_1). Differentiating (5.3.8) by σ_1 and equating the derivative to zero, we get:

$$\sigma_1^4+\sigma_1^2-1=0, \quad \sigma_1 = \sqrt{\frac{\sqrt{5}-1}{2}} = -\frac{\sigma_*}{p_{10}}. \quad (5.3.9)$$

Thus, the optimal value σ is determined by the expression:

$$\sigma_* = -\sqrt{\frac{\sqrt{5}-1}{2}}p_{10} \approx -0.7862p_{10}. \quad (5.3.10)$$

The resulting optimal value is closely related to the famous *"golden section"*, which often occurs when solving a wide variety of optimization problems. In particular, a similar result takes place in the problem of the damping optimization

of a single-link manipulator, i.e., a system with one degree of freedom (when the collinear control action is actually identical to viscous friction), where the same optimization criterion was used [76]. In addition, the presented method for finding the optimal collinear damping parameter can be generalized to the case of a mechanical system with an arbitrary finite number of degrees of freedom [68]. Finally, we also calculate the value of the criterion $f_{\max\limits_{\mu_1,\mu_2,\vartheta}}$ at the found point, which we will need later:

$$f_{\max\limits_{\mu_1,\mu_2,\vartheta}} = \frac{\sqrt{11+5\sqrt{5}}}{p_{10}\sqrt{2}} \approx \frac{3.3302}{p_{10}}. \tag{5.3.11}$$

5.4. Comparison of Optimal Parameters of Passive and Active Oscillation Damping

Let us proceed to a comparison of the obtained results for passive and active damping of oscillations of spatial double pendulum. First, we plot the dependencies of the values ν_* and σ_* on the angle α, obtained by studying both optimization criteria. Herewith, to avoid confusion, we supplement the designations of these values with indices showing their belonging to a certain criterion: (1) – criterion based on the degree of stability, (2) – energy-time criterion. These dependencies are shown in Figs 5.9 and 5.10 respectively.

It can be seen that for both cases of damping there are differences in the optimal values obtained in the study of various optimization criteria, but their scatter is not too significant. Therefore, it is possible to estimate in what range it is most advantageous to choose the parameters ν and σ in order to ensure the extreme properties of the considered criteria. Wherein, it is easy to understand that in the case of optimal passive damping, according to both criteria, the motion of the system is *oscillatory-aperiodic*, i.e., $\nu_{20} < \nu_* < \nu_{10}$ for any angle α: roots $\kappa_{1,2}$ are complex conjugate, and roots $\kappa_{3,4}$ are real. This means that the first mode is damped rather slowly and retains an oscillatory character, while the second form is strongly damped, and instead of oscillations on it, aperiodic damping takes place. In the case of optimal active damping according to both criteria, the character of the damping of the modes is *oscillatory* (of course, provided that the optimal value according to the criterion based on the degree of stability is taken

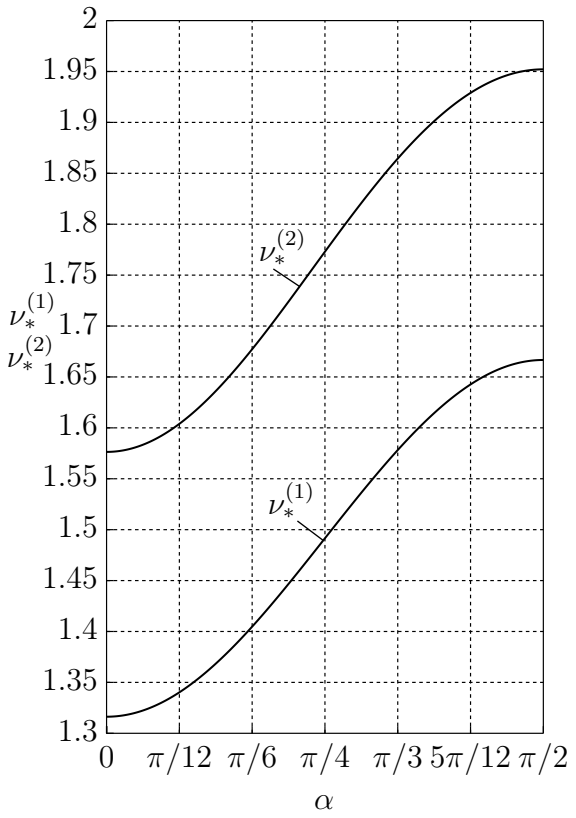

Fig. 5.9. Graph dependencies of values $\nu_*^{(1)}$ and $\nu_*^{(2)}$ on angle α

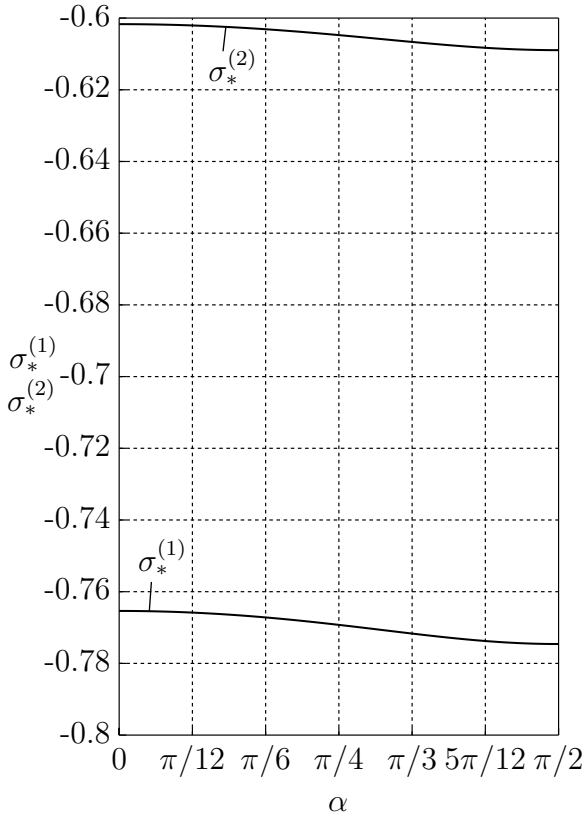

Fig. 5.10. Graph dependencies of values $\sigma_*^{(1)}$ and $\sigma_*^{(2)}$ on angle α

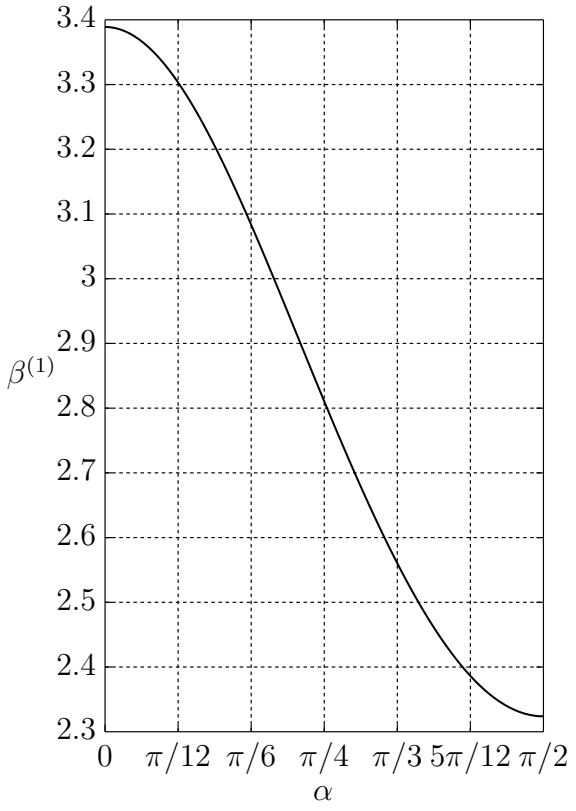

Fig. 5.11. Graph dependence of value $\beta^{(1)}$ on angle α

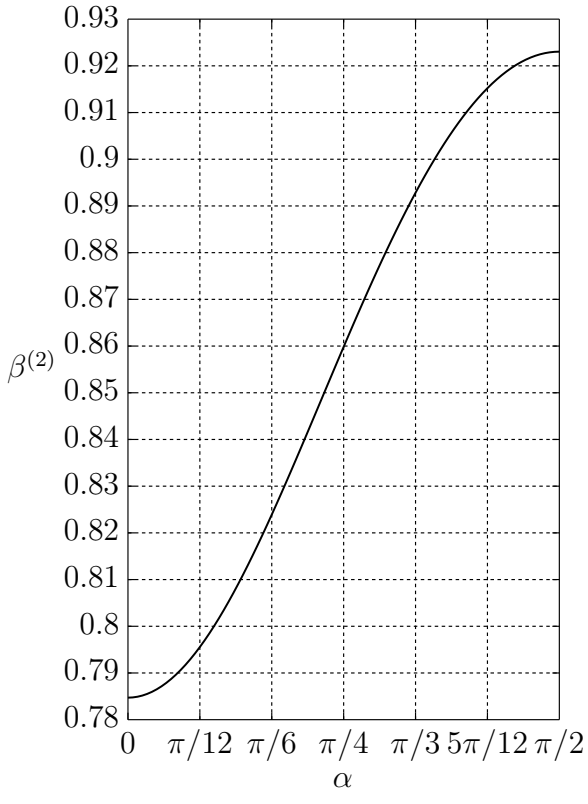

Fig. 5.12. Graph dependence of value $\beta^{(2)}$ on angle α

in practice slightly to the right of the maximum point).

To assess the advantages of the active method of oscillation damping over the passive one, we plot the dependence of the ratio $\beta^{(1)}$ of the degree of stability at the optimal value $\sigma = \sigma_*^{(1)}$ in the case of active damping to the degree of stability at the optimal value $\nu = \nu_*^{(1)}$ in the case of passive damping on the angle α. In addition, referring to the integral criterion, we consider its values at the optimal points $\sigma = \sigma_*^{(2)}$ and $\nu = \nu_*^{(2)}$, which give the best result in the worst case for active and passive damping respectively, and also plot their ratio $\beta^{(2)}$. These graphs are shown in Figs 5.11 and 5.12 respectively. It can be seen that $\beta^{(1)} > 1$ and $\beta^{(2)} < 1$, as expected. In this case, active damping makes it possible to significantly increase the maximum degree of stability in comparison with the passive damping variant, while the gain in the value of the energy-time indicator is not so tangible.

5.5. Optimization of Collinear Oscillation Damping in Presence of Viscous Damping

In conclusion, we consider the situation when the system already has some given damping in both joints with a dimensionless dissipative coefficient ν. Let us find out how the parameters of the active collinear action should be chosen in order to improve the damping processes of the movements of a double pendulum. It is clear that in this case the roots of the characteristic equation in the dimensionless version will be determined by the formulas (4.5.19). As before, we analyze both criteria and determine the dependence of the optimal value σ_* according to these criteria on ν.

1. Degree of stability. It is easy to see that for ν not exceeding some value ν_{**}, it will still be possible to merge the roots $\kappa_{1,2}$, as this was also true at $\nu = 0$, and the roots $\kappa_{3,4}$ will then be to the left of these roots. Then the maximum dimensionless degree of stability will be equal to $\Delta_*/k = p_{10}$, and the value σ_* corresponding to it will be determined by the condition:

$$\sigma - \eta_1\nu = -p_{10}, \quad \sigma_{*1}(\nu) = -p_{10} + \eta_1\nu, \tag{5.5.1}$$

and everything said earlier in Sect. 5.3 about multiple roots also applies to it. However, if ν exceeds the value ν_{**}, then this situation will no longer be possible, since the root κ_4, when σ decreases, will lie on the same vertical with the roots $\kappa_{1,2}$ before they merge into one multiple root. This situation is similar to the case that took place in Sect. 5.2. The real part of these three roots will determine the maximum degree of stability. Therefore, in this case, the value σ_* is determined from the equation:

$$\sigma - \eta_1\nu = \sigma - \eta_2\nu + \sqrt{(\sigma - \eta_2\nu)^2 - p_{20}^2}, \tag{5.5.2}$$

and resolving it with respect to σ, we find the required value:

$$\sigma_{*2}(\nu) = \eta_2\nu - \sqrt{(\eta_2 - \eta_1)^2\,\nu^2 + p_{20}^2}. \tag{5.5.3}$$

Equating the expressions (5.5.1) and (5.5.3), after solving the resulting equation, we find the boundary value ν_{**}:

$$\nu_{**} = \frac{p_{20}^2 - p_{10}^2}{2p_{10}(\eta_2 - \eta_1)}. \tag{5.5.4}$$

It is easy to understand that at $\nu = \nu_{**}$ the maximum degree of stability will correspond to the case when the three roots are the same. Combining now the expressions (5.5.1) and (5.5.3), we get that the optimal value σ_* is given by the following formula:

$$\sigma_*(\nu) = \begin{cases} -p_{10} + \eta_1\nu, & 0 < \nu \le \nu_{**} \\ \eta_2\nu - \sqrt{(\eta_2 - \eta_1)^2\,\nu^2 + p_{20}^2}, & \nu > \nu_{**} \end{cases}. \tag{5.5.5}$$

It can be seen that this expression vanishes at $\nu = \nu_*$, determined from (5.2.3), i.e., when the viscous damping coefficient is taken according to the optimal variant. As expected, it will be impossible in this situation to improve the degree of stability by introducing collinear control. It is important to emphasize here that at $\nu > \nu_*$ the value of σ_* becomes positive, and this indicates that in this case the collinear control should be overclocked. However, the combined effect of damping and collinear control has the effect of oscillation suppressing, since it is easy to see that in this case from (5.5.5) it follows that $\sigma_* < \eta_1\nu$, and according to the diagram presented in Fig. 4.14, this zone that is responsible for damping the

system movements. Moreover, σ_* as $\nu \to \infty$ tends from below to the oblique asymptote $\sigma_* = \eta_1 \nu$. We note that we can write the approximate character of the dependence (5.5.5) for large values ν:

$$\begin{aligned} \sigma_*(\nu) = \eta_2 \nu - (\eta_2 - \eta_1)\,\nu \sqrt{1 + \frac{p_{20}^2}{(\eta_2 - \eta_1)^2\,\nu^2}} \approx \\ \approx \eta_1 \nu - \frac{p_{20}^2}{2(\eta_2 - \eta_1)\nu} + \frac{p_{20}^4}{8(\eta_2 - \eta_1)^3 \nu^3}. \end{aligned} \tag{5.5.6}$$

At last, we obtain an expression for the dimensionless degree of stability corresponding to the optimal choice of the value σ_* according to (5.5.5), depending on the value ν. It is clear that for any ν from the range $0 < \nu \le \nu_{**}$, by proper selection of σ, one can ensure the maximum possible value of the dimensionless degree of stability, equal to p_{10}, when the roots $\kappa_{1,2}$ are multiples. If $\nu > \nu_{**}$, then the maximum degree of stability in the dimensionless version will correspond to the coincidence of the real parts of the three roots, which in absolute value according to (5.5.2) and (5.5.3) are $\eta_1 \nu - \sigma_{*2} = -(\eta_2 - \eta_1)\nu + \sqrt{(\eta_2 - \eta_1)^2 \nu^2 + p_{20}^2}$. Naturally, this value will decrease as ν increases. Combining the obtained expressions, we will have:

$$\frac{\Delta_*}{k} = \begin{cases} p_{10}, & 0 < \nu \le \nu_{**} \\ -(\eta_2 - \eta_1)\nu + \sqrt{(\eta_2 - \eta_1)^2 \nu^2 + p_{20}^2}, & \nu > \nu_{**} \end{cases}. \tag{5.5.7}$$

The graph dependence of Δ_*/k on ν when choosing the optimal value σ_* is shown in Fig. 5.13.

2. Energy-time criterion. Turning to the study of the integral criterion for the problem under consideration, it is easy to understand that the expression for it, by analogy with (5.2.18) and (5.3.3), will have the following form:

$$\begin{aligned} F = \frac{E_0}{2} \left[\frac{\cos^2 \vartheta}{k_{10}} \left(\frac{1}{\nu_1 + \sigma_1} + \nu_1 + \sigma_1 + (\nu_1 + \sigma_1) \cos 2\mu_1 + \sin 2\mu_1 \right) + \right. \\ \left. + \frac{\sin^2 \vartheta}{k_{20}} \left(\frac{1}{\nu_2 + \sigma_2} + \nu_2 + \sigma_2 + (\nu_2 + \sigma_2) \cos 2\mu_2 + \sin 2\mu_2 \right) \right], \end{aligned} \tag{5.5.8}$$

where the old designations (5.2.19) for ν_s and (5.3.4) for σ_s are retained. Again discarding the constant factor $E_0/(2k)$, we immediately write down the maximum

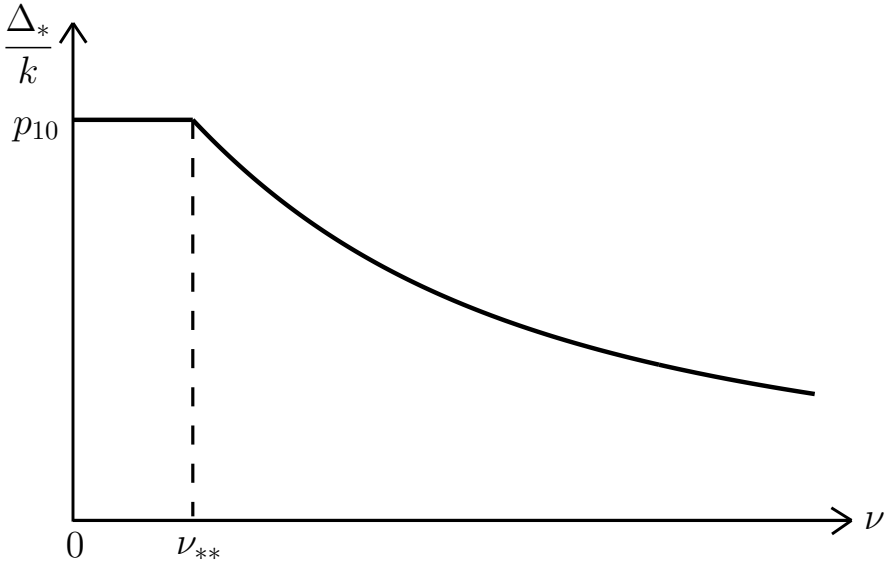

Fig. 5.13. Dimensionless degree of stability depending on ν when choosing the optimal value σ_*

value of the resulting expression in μ_1 and μ_2:

$$f_{\max\limits_{\mu_1,\mu_2}} = \frac{\cos^2\vartheta}{p_{10}}\left(\frac{1}{\nu_1+\sigma_1}+\nu_1+\sigma_1+\sqrt{1+(\nu_1+\sigma_1)^2}\right)+ \\ +\frac{\sin^2\vartheta}{p_{20}}\left(\frac{1}{\nu_2+\sigma_2}+\nu_2+\sigma_2+\sqrt{1+(\nu_2+\sigma_2)^2}\right). \tag{5.5.9}$$

As before, the next step is to understand which of the expressions is greater:

$$\vartheta=0: \quad f_{\max\limits_{\mu_1,\mu_2}} = \frac{1}{p_{10}}\left(\frac{1}{\nu_1+\sigma_1}+\nu_1+\sigma_1+\sqrt{1+(\nu_1+\sigma_1)^2}\right), \\ \vartheta=\frac{\pi}{2}: \quad f_{\max\limits_{\mu_1,\mu_2}} = \frac{1}{p_{20}}\left(\frac{1}{\nu_2+\sigma_2}+\nu_2+\sigma_2+\sqrt{1+(\nu_2+\sigma_2)^2}\right). \tag{5.5.10}$$

It was established above that at $\nu=0$ we have $f_{\max\limits_{\mu_1,\mu_2}}(\vartheta=0) > f_{\max\limits_{\mu_1,\mu_2}}(\vartheta=\pi/2)$ for any value of σ. To find out the behavior of these functions at $\nu\neq 0$, we write their approximate expressions at $\sigma\to-\infty$:

$$f_{\max\limits_{\mu_1,\mu_2}}(\vartheta=0)\approx 2\left[2\nu-(\nu+\sigma)\frac{1}{p_{10}^2}\right], \quad f_{\max\limits_{\mu_1,\mu_2}}\left(\vartheta=\frac{\pi}{2}\right)\approx 2\left[2\nu-(\nu+\sigma)\frac{1}{p_{20}^2}\right], \tag{5.5.11}$$

and for the first of them, also when σ approaches another boundary $\sigma=\eta_1\nu$, which is the boundary of the motion damping zone in the regime diagram in Fig. 5.13:

$$f_{\max\limits_{\mu_1,\mu_2}}(\vartheta=0)\approx\frac{1}{\eta_1\nu-\sigma}+\frac{1}{p_{10}}, \tag{5.5.12}$$

while $f_{\underset{\mu_1,\mu_2}{\max}}(\vartheta = \pi/2)$ tends to a finite limit as $\sigma \to \eta_1\nu$. It is easy to see that for both cases $\sigma \to -\infty$ and $\sigma \to \eta_1\nu$ we have $f_{\underset{\mu_1,\mu_2}{\max}}(\vartheta = 0) > f_{\underset{\mu_1,\mu_2}{\max}}(\vartheta = \pi/2)$. It is clear that as ν increases from 0 to some boundary value ν_{**}, the graphs of these functions will still have no common points, so that $f_{\underset{\mu_1,\mu_2}{\max}}(\vartheta = 0)$ will be the largest of the specified two values. Its minimization, as it is easy to understand, leads to the following value σ_* in the investigated range:

$$\sigma - \eta_1\nu = -\sqrt{\frac{\sqrt{5}-1}{2}}p_{10}, \quad \sigma_{*1}(\nu) = -\sqrt{\frac{\sqrt{5}-1}{2}}p_{10} + \eta_1\nu. \tag{5.5.13}$$

As ν increases, at some point the two curves $f_{\underset{\mu_1,\mu_2}{\max}}(\vartheta = 0)$ and $f_{\underset{\mu_1,\mu_2}{\max}}(\vartheta = \pi/2)$ will touch. However, the boundary situation corresponding to the value ν_{**} is not the case of tangency, but the case of intersection of these curves at the extremum point of the curve $f_{\underset{\mu_1,\mu_2}{\max}}(\vartheta = 0)$, because it has been still the minimum point of the function $f_{\underset{\mu_1,\mu_2,\vartheta}{\max}}$. To determine this point, it is enough to solve the equation $f_{\underset{\mu_1,\mu_2}{\max}}(\vartheta = 0) = f_{\underset{\mu_1,\mu_2}{\max}}(\vartheta = \pi/2)$ taking into account representations (5.5.10) and substituting the expression (5.5.13) into it. Numerical investigation allows to find the dependence $\nu_{**}(\alpha)$. Turning to the analysis of the case $\nu > \nu_{**}$, we note first that the function $f_{\underset{\mu_1,\mu_2}{\max}}(\vartheta = \pi/2)$ in the range $\sigma < \eta_1\nu$ will be decreasing, since its extremum point

$$\sigma = -\sqrt{\frac{\sqrt{5}-1}{2}}p_{20} + \eta_2\nu \tag{5.5.14}$$

will not fall into the interval of interest to us, being greater than the value $\eta_1\nu$. Indeed, using numerical methods for solving algebraic equations, it can be established that if this point is located on the boundary $\sigma = \eta_1\nu$, which is realized at

$$\nu = \sqrt{\frac{\sqrt{5}-1}{2}}\frac{p_{20}}{\eta_2 - \eta_1}, \tag{5.5.15}$$

then the equation $f_{\underset{\mu_1,\mu_2}{\max}}(\vartheta = 0) = f_{\underset{\mu_1,\mu_2}{\max}}(\vartheta = \pi/2)$ will not have solutions for any values α, i.e., the curves $f_{\underset{\mu_1,\mu_2}{\max}}(\vartheta = 0)$ and $f_{\underset{\mu_1,\mu_2}{\max}}(\vartheta = \pi/2)$ will not overlap yet. Then in the range $\nu > \nu_{**}$, due to the decrease of the function $f_{\underset{\mu_1,\mu_2}{\max}}(\vartheta = \pi/2)$ on the interval under study, these curves will have two intersection points, and the minimum of the function $f_{\underset{\mu_1,\mu_2,\vartheta}{\max}}$ is the intersection point σ_{*2}, which lies closer to the right boundary of the interval. This situation is shown in Fig. 5.14, where dependence $f_{\underset{\mu_1,\mu_2,\vartheta}{\max}}$ is marked by a solid line, and the extraneous sections are marked by a dotted line.

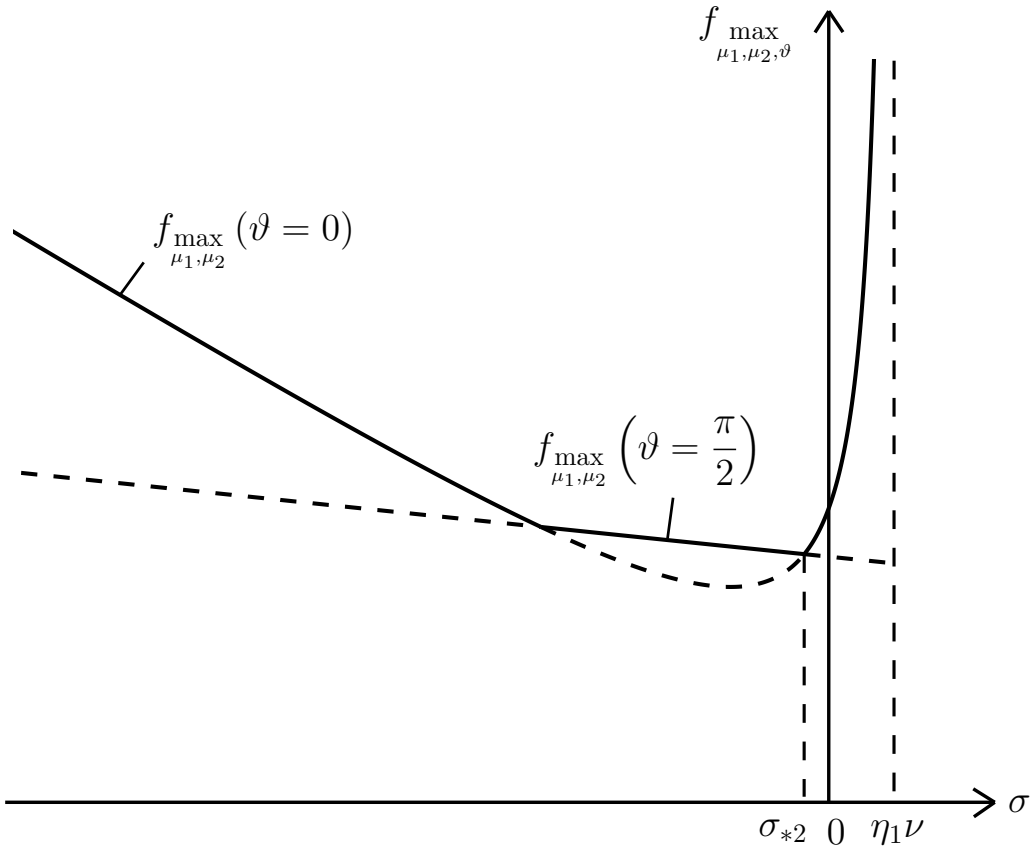

Fig. 5.14. Graph dependence of $f_{\max\limits_{\mu_1,\mu_2,\vartheta}}$ on σ at given value $\nu > \nu_{**}$

It is easy to understand that with increase in ν at $\nu = \nu_*$ this point will be $\sigma_{*2} = 0$, since when ν is chosen according to the optimal variant based on the energy-time criterion it will be impossible to improve this indicator. Indeed, if we look at the equation $f_{\max\limits_{\mu_1,\mu_2}}(\vartheta = 0) = f_{\max\limits_{\mu_1,\mu_2}}(\vartheta = \pi/2)$ taking into account the representations (5.5.10), it is easy to see that it is satisfied precisely at $\nu = \nu_*$ and $\sigma = 0$, since the value ν_* was obtained earlier from exactly the same equation, in which σ was missing, so that the expressions (5.5.10) in this situation completely turn into (5.2.22). With a subsequent increase in ν, we already have $\sigma_{*2} > 0$, and $\sigma_{*2} \to \eta_1\nu$ at $\nu \to \infty$. To determine an approximate expression for the point σ_{*2} for large values of ν, we return to the equation $f_{\max\limits_{\mu_1,\mu_2}}(\vartheta = 0) = f_{\max\limits_{\mu_1,\mu_2}}(\vartheta = \pi/2)$ from which it is found, and set

$$\sigma_{*2} = \eta_1\nu + \frac{A}{\nu} + \frac{B}{\nu^2}, \tag{5.5.16}$$

where A and B are undefined coefficients. Substituting the expression (5.5.16) into the equation $f_{\max\limits_{\mu_1,\mu_2}}(\vartheta = 0) = f_{\max\limits_{\mu_1,\mu_2}}(\vartheta = \pi/2)$, we retain in its left and right sides only the main terms at $\nu \to \infty$ corresponding to their oblique asymptotes.

Then we get that

$$-\frac{1}{A}\nu+\frac{B}{A^2}+\frac{1}{p_{10}}=\frac{2(\eta_2-\eta_1)}{p_{20}^2}\nu. \tag{5.5.17}$$

Equating the coefficients in this expression at the same powers ν, we find the values A and B:

$$A=-\frac{p_{20}^2}{2(\eta_2-\eta_1)},\quad B=-\frac{A^2}{p_{10}}=-\frac{p_{20}^4}{4(\eta_2-\eta_1)^2p_{10}}. \tag{5.5.18}$$

Therefore, the approximate character of the dependence of value σ_{*2} on ν according to (5.5.16) will take the form:

$$\sigma_{*2}(\nu)\approx\eta_1\nu-\frac{p_{20}^2}{2(\eta_2-\eta_1)\nu}-\frac{p_{20}^4}{4(\eta_2-\eta_1)^2p_{10}\nu^2}. \tag{5.5.19}$$

Comparing the formulas (5.5.6) and (5.5.19), we can make an important conclusion that the curve corresponding to the maximum degree of stability at large ν is located higher than the curve corresponding to the minimum of the integral criterion, and in the limit at $\nu\to\infty$ they have the same oblique asymptote $\sigma_*=\eta_1\nu$. In this case, not only the first terms corresponding to the oblique asymptote coincide in these approximate expressions, but also the second terms, which are inversely proportional to ν. Therefore, we can conclude that in a wide range of sufficiently large values ν, both optimization criteria will lead to almost identical results.

Thus, the optimal value σ_* is determined by the expression:

$$\sigma_*(\nu)=\begin{cases}-\sqrt{\dfrac{\sqrt{5}-1}{2}}p_{10}+\eta_1\nu, & 0<\nu\le\nu_{**}\\ \sigma_{*2}, & \nu>\nu_{**}\end{cases}. \tag{5.5.20}$$

It remains only to obtain an expression for $f_{\max\limits_{\mu_1,\mu_2,\vartheta}}$ depending on ν when choosing the optimal value of σ_* according to (5.5.20). In the range $0<\nu\le\nu_{**}$ this value will be equal to $f_{\max\limits_{\mu_1,\mu_2}}(\vartheta=0)$ calculated taking into account (5.5.13), which leads to the expression (5.3.11). Of course, this can also be understood from elementary considerations, since a change in ν only leads to a parallel horizontally shift of the dependence of the function $f_{\max\limits_{\mu_1,\mu_2}}(\vartheta=0)$ on σ according to (5.5.10), which does not affect its extreme value. Thus, we can ensure by proper selection of σ the minimum possible value of $f_{\max\limits_{\mu_1,\mu_2,\vartheta}}$ equal to (5.3.11) in the specified range ν. For

the case $\nu > \nu_{**}$ the desired value $f_{\max\limits_{\mu_1,\mu_2,\vartheta}}$ should be calculated at $\sigma = \sigma_{*2}$, and it will be already greater than (5.3.11). As a result, we find the desired dependence

$$f_{\max\limits_{\mu_1,\mu_2,\vartheta}*} = \begin{cases} \dfrac{\sqrt{11+5\sqrt{5}}}{p_{10}\sqrt{2}}, & 0 < \nu \le \nu_{**} \\ f_{\max\limits_{\mu_1,\mu_2,\vartheta}}(\sigma_{*2}), & \nu > \nu_{**} \end{cases}, \tag{5.5.21}$$

which is shown in Fig. 5.15.

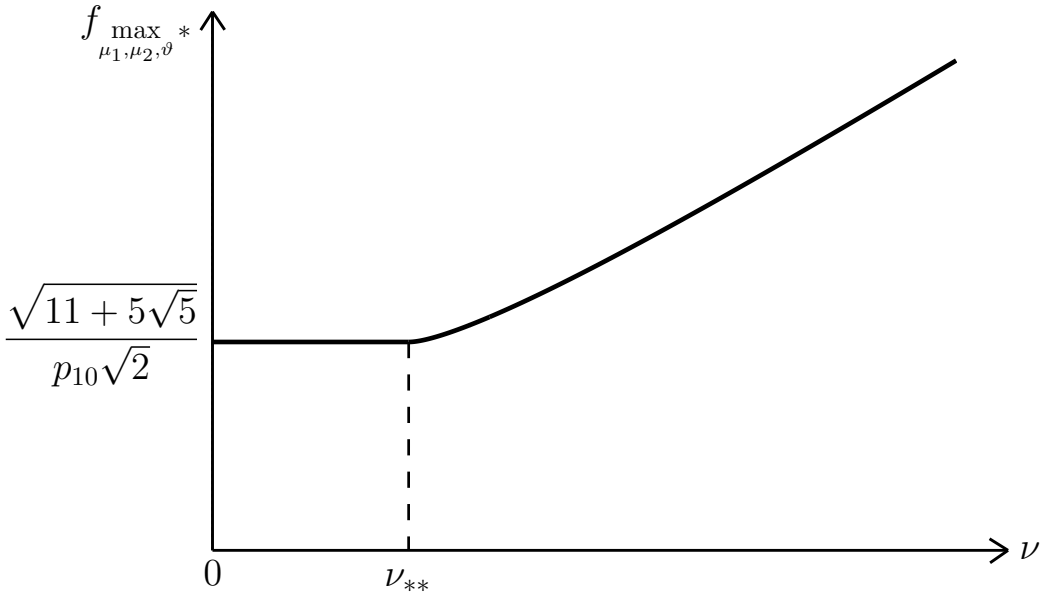

Fig. 5.15. Graph dependence $f_{\max\limits_{\mu_1,\mu_2,\vartheta}*}$ on ν when choosing the optimal value σ_*

Turning now to the evaluation of the obtained results, let us discuss the dependencies σ_* on ν obtained by the formulas (5.5.6) and (5.5.20) and corresponding to two different optimization criteria. To do this, we first turn to the characteristic values ν_* and ν_{**}, obtained in the study of each criterion, and plot these dependencies on the angle α (Fig. 5.16). As before, these values are here provided with indexes indicating their belonging to a certain criterion: (1) – criterion based on the degree of stability, (2) – energy-time criterion.

It can be seen that the values $\nu_*^{(1)}$, $\nu_*^{(2)}$, $\nu_{**}^{(1)}$ and $\nu_{**}^{(2)}$ in ascending order for any value of the angle α always turns out to be the same, so the graph dependencies of the values $\sigma_*^{(1)}$ and $\sigma_*^{(2)}$ on ν will have the form shown in Fig. 5.17. The given curves have quantitative differences, although they are qualitatively very similar. It is interesting to note that there is a point ν_{12} where both criteria give the same result. Since this point lies in the range $\nu_{**}^{(1)} < \nu_{12} < \nu_{**}^{(2)}$, the following equation

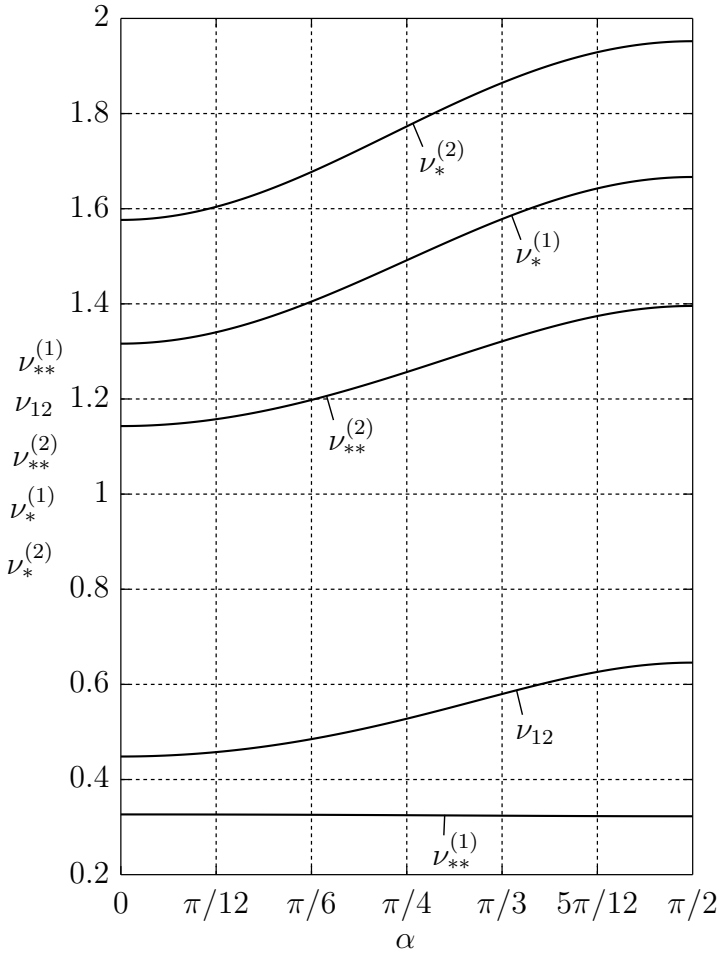

Fig. 5.16. Graph dependencies of values $\nu_{**}^{(1)}$, ν_{12}, $\nu_{**}^{(2)}$, $\nu_{*}^{(1)}$ and $\nu_{*}^{(2)}$ on angle α

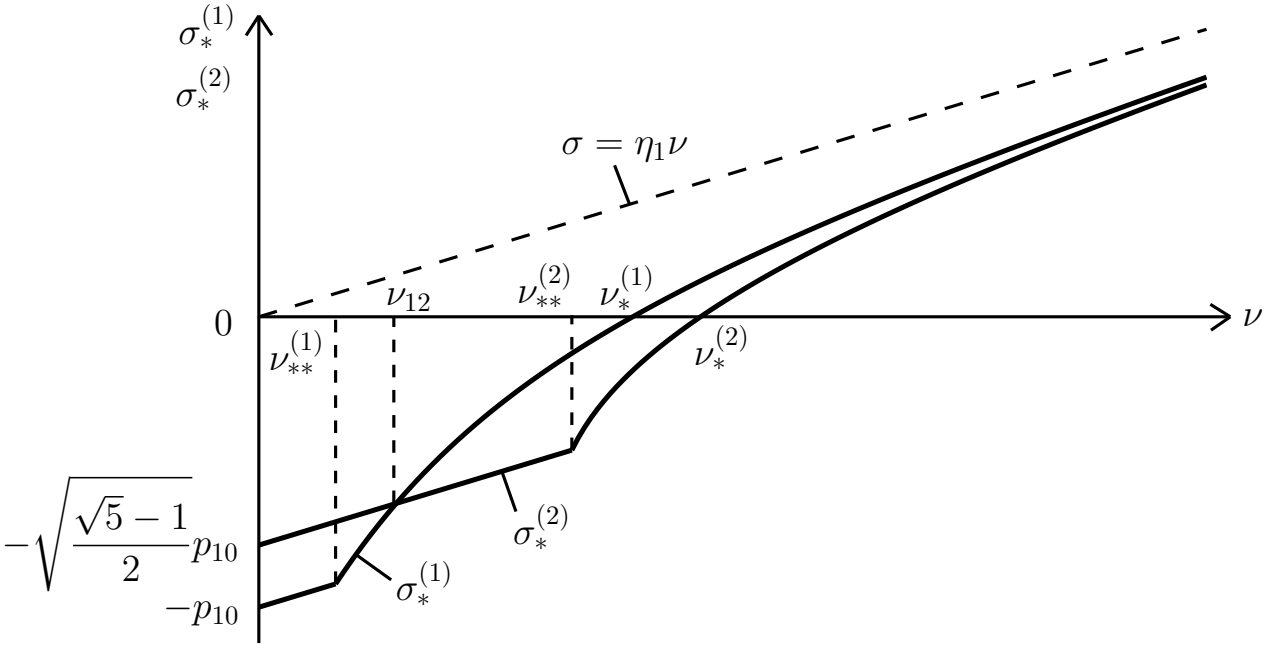

Fig. 5.17. Graph dependencies of values $\sigma_*^{(1)}$ и $\sigma_*^{(2)}$ on ν

should be written to determine it:

$$\eta_2\nu - \sqrt{(\eta_2-\eta_1)^2\nu^2 + p_{20}^2} = -\sqrt{\frac{\sqrt{5}-1}{2}}p_{10} + \eta_1\nu. \tag{5.5.22}$$

Resolving it with respect to ν, we get:

$$\nu_{12} = \frac{1}{2\sqrt{2}p_{10}}\left(\sqrt{\sqrt{5}+1}p_{20}^2 - \sqrt{\sqrt{5}-1}p_{10}^2\right). \tag{5.5.23}$$

The dependence of value ν_{12} on the angle α is also shown in Fig. 5.16. Thus, for any α the following chain of inequalities holds:$\nu_{**}^{(1)} < \nu_{12} < \nu_{**}^{(2)} < \nu_{*}^{(1)} < \nu_{*}^{(2)}$.

In conclusion, it is of interest to evaluate how much the quality indicators improved when collinear control was introduced into the system with the best-tuned parameters. First, we plot the ratio $\beta^{(1)}$ of the dimensionless degree of stability Δ_*/k according to (5.5.7) to the dimensionless degree of stability Δ/k at $\sigma = 0$, i.e. according to (5.2.9), on the parameter ν. It is clear that at $\nu = 0$ this ratio is equal to $+\infty$, and at $\nu = \nu_*^{(1)}$ it reaches a minimum equal to 1 when the collinear control for any parameters cannot improve the degree of stability. Finally, to establish the behavior of this relation at $\nu \to \infty$, we write approximate representations of the functions under study (5.5.7) and (5.2.9):

$$\frac{\Delta_*}{k} \approx \frac{p_{20}^2}{2(\eta_2-\eta_1)\nu}, \quad \frac{\Delta}{k} \approx \frac{p_{20}^2}{2\eta_2\nu}. \tag{5.5.24}$$

This implies that limit of the function $\beta^{(1)}$ as $\nu \to \infty$ is equal to $\eta_2/(\eta_2-\eta_1) > 1$. We note that this value will be the greater, the larger the ratio η_1/η_2, i.e., the closer the angle α to $\pi/2$. This dependence is shown in Fig. 5.18.

In addition, we plot the dependence of the ratio $\beta^{(2)}$ of the value of the function $f_{\max\limits_{\mu_1,\mu_2,\vartheta}*}$ according to (5.5.21) in the presence of the best-tuned control to the value of the function $f_{\max\limits_{\mu_1,\mu_2,\vartheta}}$ in the absence of control, i.e. according to (5.2.25), on the parameter ν. It is clear that at $\nu = 0$ this ratio is equal to zero, and at $\nu = \nu_*^{(2)}$ it reaches a maximum equal to 1, when collinear control cannot improve the value of criterion. Finally, to establish the behavior of this relation at $\nu \to \infty$, we write simplified representations of the functions (5.5.21) taking into account the approximate expression (5.5.19) and (5.2.25):

$$f_{\max\limits_{\mu_1,\mu_2,\vartheta}*} \approx \frac{2(\eta_2-\eta_1)\nu}{p_{20}^2}, \quad f_{\max\limits_{\mu_1,\mu_2,\vartheta}} \approx \frac{2\eta_2\nu}{p_{20}^2}. \tag{5.5.25}$$

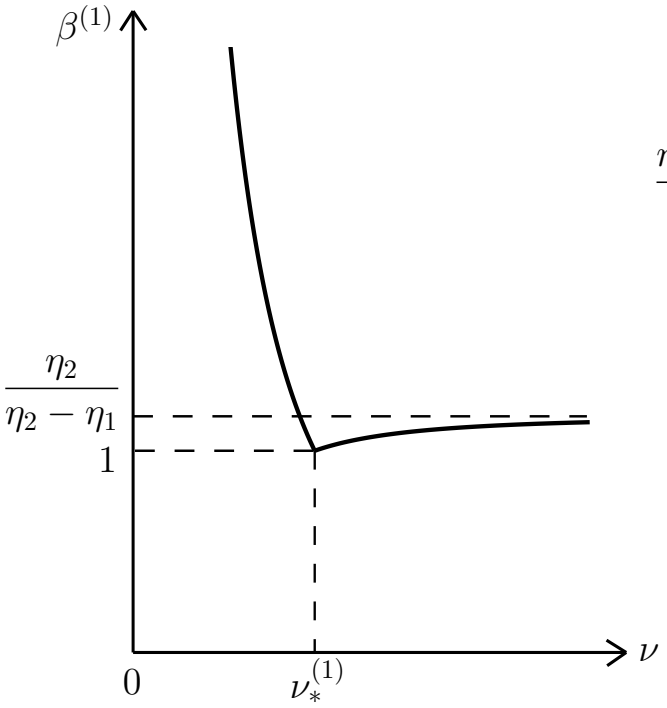

Fig. 5.18. Graph dependence of value $\beta^{(1)}$ on ν

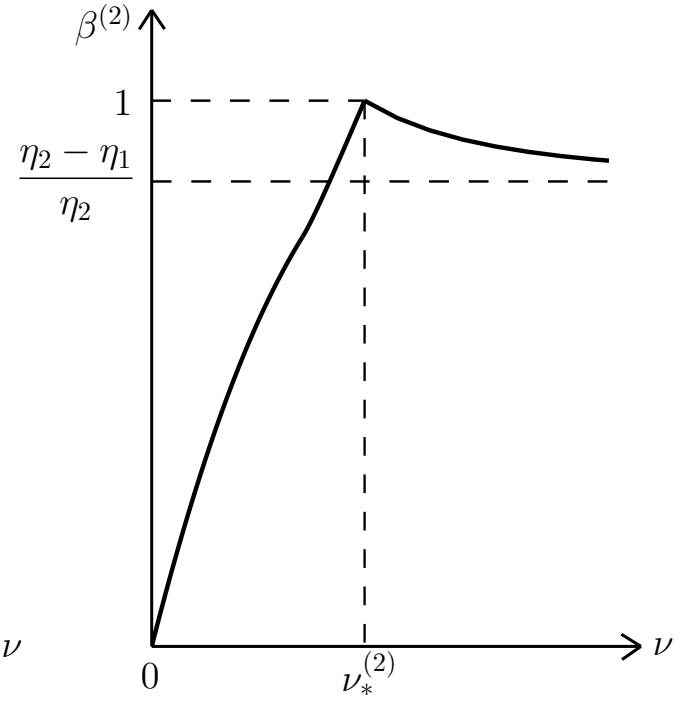

Fig. 5.19. Graph dependence of value $\beta^{(2)}$ on ν

This implies that limit of the function $\beta^{(2)}$ as $\nu \to \infty$ is equal to $(\eta_2 - \eta_1)/\eta_2 < 1$. Of course, this value is the smaller, the larger the ratio η_1/η_2, i.e., the closer α is to $\pi/2$. The mentioned dependence is shown in Fig. 5.19.

5.6. Conclusions on Fifth Chapter

In this chapter, questions of optimal oscillation damping of spatial double pendulum were studied. In this case, the possibility of both passive damping (viscous damping) and active damping (collinear control), as well as their joint accounting, was considered. Two optimization criteria were adopted that characterize the efficiency of the attenuation processes of system movements: maximization of the degree of stability and minimization of the energy-time indicator. The main advantages and disadvantages of these criteria were discussed. In the course of the exact solution of the problem within the framework of the linear model, the optimal parameters of each of the damping options were determined as a function of the angle between the joint axes of spatial double pendulum according to both optimization criteria and the results were compared. In addition, visual graphical estimates are given, demonstrating the advantage of active damping.In

conclusion, the problem of cooperative passive and active damping was considered and the optimal values of active damping parameters were obtained for given passive damping parameters, and dependencies illustrating the efficiency of using such parameters were presented. These results clearly demonstrate the expediency of adding appropriate control actions to a dissipative system to ensure the most pronounced processes of attenuation of its motions. The nontrivial structure of the constructed solutions should be emphasized. The obtained conclusions may be of serious practical interest in the study of the dynamic behavior of real two-link manipulators.

Conclusion

Turning to the final section of the dissertation, we present its main results and draw conclusions, demonstrating once again the close connection between the sections of this work with each other.

The object of the study was a double mathematical pendulum with identical parameters of its links and weights, whose joint axes were assumed not to be collinear to each other. Therefore, the double pendulum became spatial, which significantly affected the complexity of studying its dynamic behavior compared to a simpler version of a flat double pendulum. The main geometric and kinematic relations were obtained, on the basis of which the nonlinear motion equations of the system under consideration were derived, and particular variants of a flat and orthogonal double pendulum were discussed. As a result of a detailed analysis of the linear model, the frequencies and modes of small oscillations were found, and graphical illustrations of their dependencies on the angle between the joint axes were also given. It is shown that viscous friction in articulated joints with identical dissipative coefficients does not violate the modes of free oscillations of the original conservative model and damps the system motions exactly by these modes without distorting their character. In addition, during the study of the dissipative model, the key values describing the attenuation process of the system motions were analyzed and illustrated graphically.

Much attention was paid to the construction of nonlinear oscillation modes both for particular variants of the flat and orthogonal double pendulum, and for the general case of a spatial double pendulum. On the basis of the expressions obtained for the linear model and using asymptotic methods of nonlinear mechanics, approximate analytical solutions were obtained for the system motion on nonlinear oscillation modes in the first approximation for the general case, and for particular variants, due to their simpler character, these formulas were obtained

in second approximation. It was shown that the found expressions are in good agreement with the results of numerical integration of the motion equations. The results of this study were clearly presented in the form of graphs explaining the character of the system motion on nonlinear oscillation mode, namely, graphs dependencies of oscillation frequencies on amplitudes, phase portraits for each generalized coordinate separately, as well as graphs of changes in generalized coordinates and velocities in one oscillation period. All these illustrations show how significantly nonlinear oscillation modes differ from their corresponding linear version, which must be taken into account in the analysis of large oscillations of the system.

A very extensive section of the work is the analysis of controlled motions of a spatial double pendulum. The control moments in the articulated joints were formed with the help of feedback on the principle of collinear control, which takes into account the dynamic features of the system and acts in unison with the generalized inertia forces. With the help of a reasonable combination of analytical and numerical studies, it was shown that such a control at a constant gain makes it possible to direct all the energy supplied to the system only to the evolution of the selected oscillation mode. This means that it is possible to overclock the system for each of its natural modes separately from small and up to sufficiently large amplitudes with preservation the single-frequency character of the motion and a gradual drift of the frequency and mode of the oscillations from the linear version to the nonlinear one. Thus, a clear demonstration of the phenomenon of autoresonance in a system with two degrees of freedom was obtained. Herewith, to bring the system to the mode of nonlinear conservative oscillations close to periodic and corresponding to the desired sufficiently high energy level, it is necessary to turn off the control at the moment when the system reaches this energy. It was noted that the obtained modes in this way are in accordance with the nonlinear oscillation modes constructed earlier. In addition to the collinear control with a constant gain, its useful modification was considered, and it has a variable gain that gradually decreases as the total energy of the system increases and approaches the desired value, the achievement of which is the purpose of the control. This allows to realize more flexible control of the system movement, avoiding abrupt shutdown of control actions and thus ensuring the best quality and smoothness of control processes. Moreover, approximate analytical

expressions for this modification were also obtained, which also agree with the results of numerical integration. Finally, a cooperative account of dissipative and control actions was made, leading to the possibility of implementing a number of motion modes that have their own features and are illustrated using a diagram of modes on the plane of dimensionless dissipative and control parameters.

The last chapter of the work was devoted to determining the optimal parameters of the passive and active damping options for a spatial double pendulum, which are viscous friction and collinear control with a constant gain respectively, whose properties were established in the previous sections. Both the criterion based on the degree of stability and the integral energy-time criterion were taken as optimization criteria characterizing the efficiency of the attenuation processes of system motions, and their advantages and disadvantages were discussed. In the course of solving the optimization problem in the framework of a linear model, the optimal parameters of each of the damping options were first determined by both criteria separately, and then the joint accounting of two damping options was considered and the optimal values of the control coefficient were found for a given value of the dissipative parameter. All the obtained results are displayed graphically and it is shown that the use of different criteria leads to qualitatively similar results, which, however, have some quantitative differences. In addition, the expediency assessment of the additional consideration of appropriately tuned control actions in the dissipative system in order to ensure the most pronounced attenuation processes was made.

Summarizing all the results of this dissertation, we can conclude that the aim stated at its beginning is **achieved**.

References

[1] *Agareva O. Yu.* Relative equilibria of a double spherical pendulum and their stability. Dep. v VINITI 4.12.1996. N3493-B96. (In Russian).

[2] *Akbirov R. R., Malikov A. I.* Control of a double inverted pendulum on a cart. Vestnik KGTU im. A. N. Tupoleva. 2018. No. 74(2). Pp. 168–177. (In Russian)

[3] *Andreev A. S., Peregudova O. A.* On control for double-link manipulator with elastic joints. Russian Journal of Nonlinear Dynamics. 2015. No. 11(2). Pp. 267–277. (In Russian)

[4] *Andronov A. A, Vitt A. A., Khaikin S. E.* The Theory of Oscillations. 2nd ed. Moscow, Nauka, 1981. 918 p. (In Russian)

[5] *Astashev V. K.* On new directions of using the resonance phenomenon in machines. Vestnik nauchno-tekhnicheskogo razvitiya. 2011. No. 8 (48). Pp. 10–15. (In Russian)

[6] *Afanasyev V. N., Kolmanovskiy V. B., Nosov V. R.* Mathematical theory of design of control systems. Moscow, Vysshaya shkola, 2003. 614 p. (In Russian)

[7] *Babakov I. M.* Theory of oscillations. Moscow, Nauka, 1968. 559 p. (In Russian)

[8] *Bezglasnyi S. P., Zharenkov S. V.* Construction of the programmed motion of double pendulum of variable length with fixed point of suspension. Izvestia of Samara Scientific Center of the Russian Academy of Sciences. 2012. Vol. 14. No. 6. Pp. 33–37. (In Russian)

[9] *Besekersky V. A., Popov E. P.* Theory of automatic control systems. 2nd ed. Moscow, Nauka, 1972. 768 p. (In Russian)

[10] *Biderman V. L.* The theory of mechanical oscillations. Moscow, Vyshaya shkola, 1980. 480 p. (In Russian)

[11] *Bogoliubov N. N., Mitropolsky Y. A.* Asymptotic methods in the theory of nonlinear oscillations. Moscow, GIFML, 1958. 406 p.

[12] *Bolotnik N. N.* Optimization of amortization systems. Moscow, Nauka, 1983. 257 p. (In Russian)

[13] *Bulanchuk P. O.* Controlling the motion of a double pendulum by vibration the suspension point. Vestnik Nizhegorodskogo universiteta im. N. I. Lobachevskogo. 2011. No. 4 (5). Pp. 2041–2042. (In Russian)

[14] *Butenin N. V, Lunts Ya. L., Merkin D. R.* Theoretical Mechanics Course. Part 2. Dynamics. Moscow, Nauka, 1979. 543 p. (In Russian)

[15] *Vetchinkin V. P., Chentsov N. G.* A flat pendulum with two degrees of freedom and the determination of the center of gravity height and the moment of inertia of a rigid body using it. Trudy TSAGI. 1923. No. 3. (In Russian)

[16] Vibrations in technology. Directory. Vol. 1. Oscillations of linear systems. Ed. by V. V. Bolotin. Moscow, Mashinostroenie, 1978. 352 p. (In Russian)

[17] Vibrations in technology. Directory. Vol. 2. Oscillations of nonlinear systems. Ed. by I. I. Blekhman. Moscow, Mashinostroenie, 1979. 351 p. (In Russian)

[18] *Vilnit L. N.* Differential equations of mechanical systems motion with dry friction. Novosibirsk, Novosibirsk State Technical University, 2004. 30 p. (In Russian)

[19] *Vishenkova E. A., Kholostova O. V.* To dynamics of a double pendulum with a horizontally vibrating point of suspension. Vestnik Udmurtskogo Universiteta. Matematika. Mekhanika. Komp'yuternye Nauki. 2012. No. 2. Pp. 114–129. (In Russian)

[20] *Voronov A. A.* Fundamentals of the theory of automatic control. Automatic control of continuous linear systems. Moscow, Energiya, 1980. 312 p. (In Russian)

[21] *Ganiev R. F., Kovalchuk P. S.* Dynamics of systems of rigid and elastic bodies. Moscow, Mashinostroenie, 1980. 208 p. (In Russian)

[22] *Gantmakher F. R.* Lectures on analytical mechanics. Moscow, Nauka, 1966. 300 p. (In Russian)

[23] *Gantmakher F. R.* Theory of matrices. Moscow, Nauka, 1968. 576 p. (In Russian)

[24] *Gernet M. M.* Theoretical mechanics course. 3rd ed. Moscow, Vysshaya shkola. 1973. 464 p. (In Russian)

[25] *Gernet M. M., Ratobylskiy V. F.* Defining moments of inertia. Moscow, Mashinostroyeniyem 1969. 250 p. (In Russian)

[26] *Geronimus Ya. L.* Theoretical mechanics. Moscow, Nauka, 1973. 512 p. (In Russian)

[27] *Glushkov V. M., Amosov N. M., Artemenko I. A.* Encyclopedia of Cybernetics. Vol. 1. Kiev, Main edition of the Ukrainian Soviet encyclopedia, 1974. 608 p. (In Russian)

[28] *Golubeva O. V.* Theoretical mechanics. Moscow, Vysshaya shkola, 1968. 487 p. (In Russian).

[29] *Dakev N. V.* Optimization of dissipative properties of articulated manipulators of industrial robots: dissertation for the degree of candidate of technical sciences. Leningrad, 1986. 131 p. (In Russian).

[30] *Danilov O. E.* The use of an educational computer model of a double mathematical pendulum in teaching physics. Molodoy uchenyy. 2016. No. 8. Pp. 38–43. (In Russian).

[31] *Degilevich E. A., Smirnov A. S.* Optimization of oscillations damping of a linear oscillator by time criterion. The Ninth Polyakhov's Reading.

Proceedings of the International Scientific Conference on Mechanics. March 9-12, 2021, St. Petersburg. 2021. Pp. 92–94. (In Russian)

[32] Machine dynamics and control. Directory. Ed. by G. V. Kreinin. Moscow, Mashinostroenie, 1988. 240 p. (In Russian)

[33] *Erdakova N. N., Ivanov A. P.* Mathematical modeling of the impact of a double pendulum on an obstacle. Trudy MFTI. 2013. Vol. 5. No. 2. Pp. 134–141. (In Russian)

[34] *Zhongolovich I. D., Lisyutin A. Ya., Roze N. V.* Theoretical mechanics. Part 2. Mechanics of the material system and solid body. Leningrad, Moscow, GTTI, 1933. 428 p. (In Russian)

[35] *Zaitsev A. P.* Fundamentals of the automatic control theory. Tomsk, TPU, 2000. 152 p. (In Russian)

[36] *Zegzhda S. A., Shatrov E. A., Yushkov M. P.* Suppression of oscillations of a trolley with a double pendulum by means of control of its acceleration. Vestnik of St. Petersburg University. Ser. 1. 2016. Vol. 3(61). No. 4. Pp. 683–688. (In Russian)

[37] *Klimenko A. A, Mikhlin Yu. V.* Normal oscillations modes in a nonlinear system containing a pendulum vibration damper. Problems of mechanical engineering. 2014. Vol. 17. No. 3. Pp. 38–44. (In Russian)

[38] *Kocheva M. D.* On oscillations of a double pendulum. Differentsial'nye Uravneniya. 1965. Vol. 1, No. 3. Pp. 374–386. (In Russian)

[39] *Kocheva M. D.* On the circular motions of a double pendulum. Differentsial'nye Uravneniya. 1965. Vol. 1. No. 2. Pp. 187–195. (In Russian)

[40] *Kumakshev S. A.* Active Damping of Vibrations of Load-bearing Structures by Moving the Internal Mass. Stability and Oscillations of Nonlinear Control Systems (Pyatnitskiy's Conference). Proceedings of the XV International Conference. Moscow, June 3–5, 2020. 2020. Pp. 250–252. (In Russian)

[41] *Leontev V. A., Smirnov A. S., Smolnikov B. A.* Collinear control of dissipative double pendulum. Robotics and Technical Cybernetics. 2019. Vol. 7. No. 1. Pp. 65–70. (In Russian)

[42] *Leontev V. A., Smirnov A. S., Smolnikov B. A.* Optimal damping of two-link manipulator oscillations. Robotics and Technical Cybernetics. 2018. No. 2 (19). Pp. 52–59. (In Russian)

[43] *Loytsyansky L. G., Lurie A. I.* Theoretical mechanics, Vol. 3. Dynamics of a non-free system and the theory of oscillations. Leningrad, Moscow, ONTI GTTI, 1934. 626 p. (In Russian)

[44] *Lupina T. A.* Evaluation of the sustainability of the vertical equilibrium of the inverted double pendulum with visco-elastic elements. Vodniy transport. 2012. No. 3(15). Pp. 67–73. (In Russian)

[45] *Lurie A. I.* Analytical Mechanics. Moscow, GIFML, 1961. 824 p. (In Russian)

[46] *Manevich L. I., Mikhlin Yu. V., Pilipchuk V. N.* The method of normal vibrations for essentially nonlinear systems. Moscow, Nauka, 1989. 216 p. (In Russian)

[47] *Markeev A. P.* A motion of connected pendulums. Russian Journal of Nonlinear Dynamics. 2013. Vol. 9. No. 1. Pp. 27–38. (In Russian)

[48] *Markeev A. P.* Theoretical Mechanics. Moscow, Izhevsk: Regular and Chaotic Dynamics, 2007. 591 p. (In Russian)

[49] *Matrosov V. M., Rumyantsev V. V., Karapetyan A. V.* Nonlinear Mechanics. Moscow, Fizmatlit, 2001. 432 p. (In Russian)

[50] *Merkin D. R., Bauer S. M., Smirnov A. L., Smolnikov B. A.* The theory of stability in examples and problems. Moscow, Izhevsk, Regular and Chaotic Dynamics, 2007. 208 p. (In Russian)

[51] *Merkin D. R., Smolnikov B. A.* Applied problems of rigid body dynamics. St. Petersburg, SPbSU publ., 2003. 534 p. (In Russian)

[52] *Moauro V., Negrini P.* Chaotic trajectories of a double mathematical pendulum. Journal of Applied Mathematics and Mechanics. Vol. 62. No. 5. Pp. 892–895. (In Russian)

[53] *Muravyov A. S., Smirnov A. S.* Optimization of damping of oscillations of a pendulum with an elastic-movable suspension point. The Ninth Polyakhov's Reading. Proceedings of the International Scientific Conference on Mechanics. March 9-12, 2021, St. Petersburg. 2021. Pp. 115–117. (In Russian)

[54] *Nagaev R. F., Stepanov A. V.* On optimization of the damping coefficient of free oscillations of a two-mass system. Bulletin of the Academy of Sciences of the USSR. Mechanics of Rigid Body. 1979. No. 4. Pp. 24–28. (In Russian)

[55] *Neymark Yu. I.* Mathematical modeling as science and art. Nizhniy Novgorod: izd-vo Nizhegorodskogo un-ta. 2010. 420 p. (In Russian)

[56] *Petrov A. G.* Nonlinear free and forced oscillations of pendulum systems at resonances. XII All-Russian Congress on Fundamental Problems of Theoretical and Applied Mechanics. Collection of works. In 4 volumes. Vol. 1. General and applied mechanics. 2019. Pp. 29–31. (In Russian)

[57] *Pobedonostsev Yu. A.* Experimental determination of the aircraft moments of inertia. Trudy Vsesoyuznoy konferentsii po aerodinamike. Izd. TSAGI., 1931. (In Russian)

[58] *Pobedonostsev Yu. A.* Experimental determination of the aircraft moments of inertia. Trudy TSAGI, 1935. No. 1. (In Russian)

[59] *Polyakhov N. D., Galiullin R. I.* Control of double inverted pendulums. Izvestiya SPbGETU LETI. 2015. No. 6. Pp. 65–70. (In Russian)

[60] *Poretsky A. S.* Methods of stabilization of a single and multi-link inverted pendulum. Physics and Progress: Abstracts of the youth scientific conference. St. Petersburg. 2006. Pp. 230–235. (In Russian)

[61] Strength, stability, vibrations. Vol. 3. Ed. by Birger I. A. and Panovko Ya. G. Moscow, Mashinostroenie, 1968. 567 p. (In Russian)

[62] *Skubov D. Yu.* Fundamentals of the nonlinear oscillations theory. St. Petersburg, Moscow, Krasnodar, Lan, 2013. 311 p. (In Russian)

[63] *Smirnov A. S., Degilevich E. A.* Oscillations of chain systems. St. Petersburg, Potytech-Press, 2021. 246 p. (In Russian)

[64] *Smirnov A. S., Smolnikov B. A.* Double pendulum research history. History of Science and Engineering. 2020. No. 12. Pp. 3–12. (In Russian)

[65] *Smirnov A. S., Smolnikov B. A.* The history of mechanical resonance – from initial studies to autoresonance. Chebyshevskii sbornik. 2022. Vol. 23. No. 1. Pp. 269–292. (In Russian)

[66] *Smirnov A. S., Smolnikov B. A.* Collinear control of single-link manipulator motion with variable gain. Youth and Science: actual problems of fundamental and applied research. Materials of the IV All-Russian scientific conference of students, postgraduates and young scientists. Komsomolsk-on-Amur. April 2021, 12-16. Vol. 2. Pp. 70–73. (In Russian)

[67] *Smirnov A. S., Smolnikov B. A.* Nonlinear autoresonance in problems of controlling oscillations of multidimensional mechanical systems. XIII All-Russian Congress on Theoretical and Applied Mechanics: collection of works in 4 volumes. August 21-25, 2023, St. Petersburg, Russia. Vol. 1. General and applied mechanics. 2023. Pp. 214–216. (In Russian)

[68] *Smirnov A. S., Smolnikov B. A.* Optimal damping of free oscillations in linear mechanical systems. Mashinostroenie i inzhenernoe obrazovanie. 2017. No. 3 (52). Pp. 8–15. (In Russian)

[69] *Smirnov A. S., Smolnikov B. A.* Optimization of oscillation damping modes of spatial double pendulum. I. Formulation of the problem. Vestnik of St. Petersburg University. Mathematics. Mechanics. Astronomy. 2022. Vol. 9 (67). Iss. 2. Pp. 357–365. (In Russian) [Engl. transl.: *Smirnov A. S., Smolnikov B. A.* Optimization of Oscillation Damping Modes of a Spatial Double Pendulum: 1. Formulation of the Problem. Vestnik St. Petersburg University, Mathematics. 2022. Vol. 55. No. 2. Pp. 243–248.]

[70] *Smirnov A. S., Smolnikov B. A.* Optimization of oscillation damping modes of spatial double pendulum. II. Solving the problem and analyzing the results. Vestnik of St. Petersburg University. Mathematics. Mechanics. Astronomy. 2023. Vol. 10 (68). Iss. 1. Pp. 121–138. (In Russian) [Engl. transl.: *Smirnov A. S., Smolnikov B. A.* Optimization of Oscillation Damping Modes of a Spatial Double Pendulum: 2. Solution of the Problem and Analysis of the Results. Vestnik St. Petersburg University, Mathematics. 2023. Vol. 56. No. 1. Pp. 93–106.]

[71] *Smirnov A. S., Smolnikov B. A.* Controlling the sway process of the swing. Week of Science SPbPU. Materials of the scientific forum with international participation. Institute of Applied Mathematics and Mechanics. 2016. Pp. 106–109. (In Russian)

[72] *Smirnov A. S., Smolnikov B. A.* Resonance oscillations control in the nonlinear mechanical systems. Transactions of seminar "Computer methods in continuum mechanics" 2016-2017. St. Petersburg University publishing house. 2018. Pp. 23–39. (In Russian).

[73] *Smirnov A. S., Smolnikov B. A.* Resonance oscillations control of the non-linear mechanical systems based on the principles of biodynamics. Mashinostroenie i inzhenernoe obrazovanie. 2017. No. 4 (53). Pp. 11–19. (In Russian)

[74] *Smolnikov B. A.* Prospects of biomechanical principles application in robotics. Robotics and Technical Cybernetics. 2017. No. 1(14). Pp. 61–68. (In Russian)

[75] *Smolnikov B. A.* Mechanics problems in advances robotics. Robotics and Technical Cybernetics. 2016. No. 1(10). Pp. 3–6. (In Russian)

[76] *Smolnikov B. A.* The problems of mechanics and robotoptimization. Moscow, Nauka, 1991. 232 p. (In Russian)

[77] *Smolnikov B. A., Smirnov A. S.* About the problem of biomorphic robot motion control. Robotics and Technical Cybernetics. 2015. No. 1(6). Pp. 17–20. (In Russian)

[78] *Strelkov S. P.* Introduction to the oscillation theory. Moscow, Nauka, 1964. 440 p. (In Russian)

[79] Technical cybernetics. Theory of automatic control. Book 1. Ed. by Solodovnikov V. V. Moscow, Mashinostroenie, 1967. 770 p. (In Russian)

[80] Control of Mechatronic Vibrational Units. Ed. by Blekhman I. I. and Fradkov A. L. St. Petersburg, Nauka, 2001. 278 p. (In Russian)

[81] *Usvitsky I.* Mechanics convenient to Mechanisms. Znanie – sila. No 6. (In Russian)

[82] *Filipkovskiy S. V.* Nonlinear normal modes properties of a rotor system. Visnik SevNTU. Mekhanika, energetika, ekologiya. 2010. No. 110. Pp. 26–31. (In Russian)

[83] *Formalskii A. M.* Motion control of unstable objects. Moscow, Fizmatlit, 2014. 232 p. (In Russian)

[84] *Kholostova O. V.* Problems of solid body dynamics with vibrating suspension. Moscow, Izhevsk, Institute of Computer Sciences. 2016. 308 p. (In Russian)

[85] *Chernousko F. L., Ananievskiy I. M., Reshmin S. A.* Control Methods of nonlinear mechanical systems. Moscow, Fismalit, 2006. 328 p. (In Russian)

[86] *Yablonskiy A. A., Noreyko S. S.* Oscillation theory course. Moscow, Vysshaya shkola. 1975. 248 p. (In Russian)

[87] *Yakovlev V. I.* Background of analytical mechanics. Izhevsk: Regular and Chaotic Dynamics, 2001. 328 p. (In Russian)

[88] *Awrejcewicz J., Wasilewski G., Kudra G., Reshmin S. A.* An experiment with swinging up a double pendulum using feedback control. Journal of Computer and Systems Sciences International. 2012. 51(2). Pp. 176–182.

[89] *Badoniya P., George J.* Two Link Planar Robot Manipulator Mechanism Analysis with MATLAB. International Journal for Research in Applied

Science & Engineering Technology (IJRASET). 2018. Vol. 6. Iss. VII. Pp. 778–788.

[90] *Bendersky S., Sandler B.* Investigation of a spatial double pendulum: an engineering approach. Discrete Dynamics in Nature and Society. 2006. Pp. 1–22.

[91] *Bernoulli D. Bernoulli D.* Commentatio physico-mechanica specialior de motibus reciprocis compositis. Multifariis nondum exploratis, qui in pendulis bimembribus facilius observari possint in confirmationem principii sui de coexistentia vibrationum simpliciorum. Novi commentarii Academiae Scientiarum Imperialis Petropolitanae. 1774. Vol. 19. Pp. 260–284.

[92] *Bernoulli D.* Theoremata de oscillationibus corporum filo flexili connexorum et catenae verticaliter suspensae. Novi commentarii Academiae Scientiarum Imperialis Petropolitanae. Vol. 6, 1738. Pp. 108–122.

[93] *Biglari H., Jami A. R.* The double pendulum numerical analysis with Lagrangian and the Hamiltonian equations of motions. International Conference on Mechanical and Aerospace Engineering. 2016. Pp. 1–12.

[94] *Bogdanov A.* Optimal Control of a Double Inverted Pendulum on a Cart. Technical Report CSE-04-006. 2004.

[95] *Bouasse H.* Pendule, Spiral, Diapason. Vol. II. Paris: Librairi Delagrave, 1920. 518 p.

[96] *Brown E. W.* Elements of theory of resonance. Cambridge: at the University press, 1932. 60 p.

[97] *Bulanchuk P. O., Petrov A. G.* Suspension point vibration parameters for a given equilibrium of a double mathematical pendulum. Mechanics of Solids. 2013. 48(4). Pp. 380–387.

[98] *Chunawala T., Ghandchi-Tehrani M., Yan J.* An optimum design of a double pendulum in autoparametric resonance for energy harvesting

applications. The 22nd Vibroengineering Conference. 2016. Vol. 8. Pp. 163–168.

[99] *Clairaut A.-C.* Solution de quelques problèmes de dynamique. Mémoires de l'Académie des sciences. 1736. Pp. 1–22.

[100] *Cross R.* A double pendulum swing experiment: In search of a better bat. American Journal of Physics. 2005. 73(4). Pp. 330–339.

[101] *Dudkowski D., Wojewoda J, Czołczyński K., Kapitaniak T.* Is it really chaos? The complexity of transient dynamics of double pendula. Nonlinear Dynamics. 2020. Vol. 102. Pp. 759–770.

[102] *Efimov D., Fradkov A., Iwasaki T.* Exciting multi-DOF systems by feedback resonance. Automatica. 2013. 49(6). Pp. 1782–1789.

[103] *Elbori A., Abdalsmd L.* Simulation of Double Pendulum. Quest Journals. Journal of Software Engineering and Simulation. 2017. Vol. 3. Iss. 7. Pp. 1–13.

[104] *Espíndola R., Del Valle G., Hernández G., Pineda I., Muciño D., Díaz P., Guijosa S.* The Double Pendulum of Variable Mass: Numerical Study for different cases. IX International Congress of Physics Engineering. IOP Conference Series: Journal of Physics. 2019. Vol. 1221. 012049.

[105] *Eulero L.* De oscillationibus fili flexilis quotcunque ponduscul is onusti. Commentarii academiae scientiarum Petropolitanae. 1741. Vol. 8. Pp. 30–47.

[106] *Fontaine des Bertins A.* Une courbe etant donnee, trouver celle qui seroit decrite par le sommet d'un angle. Mèmoires de l'Acadèmie des sciences. 1734. Pp. 527–530.

[107] *Formalskii A. M.* On stabilization of an inverted double pendulum with one control torque. Journal of Computer and Systems Sciences International. 2006. 45(3). Pp. 337–344.

[108] *Fradkov A. L.* Cybernetical physics. From Control of Chaos to Quantum Control. Springer-Verlag, Berlin, Heidelberg: 2007. 242 p.

[109] *Fradkov A. L.* Exploring nonlinearity by feedback. Physica D. 1999. 128(2–4). Pp. 159–168.

[110] *Fradkov A. L.* Investigation of physical systems by feedback. Automation and Remote Control. 1999. 60(3). Pp. 471–483.

[111] *Gerres J. M., Jacobs R. M., Kasun S. F., Bacon M. E., Nagolu C. M., Owens E. L., Siehl K. F., Thomsen M., Troyer J. S.* Large Amplitude Oscillations of a Double Pendulum. American Physical Society. 2008. Spring Meeting of the Ohio-Region Section of APS, March 28-29, 2008. P1.004.

[112] *Gracey W.* The Experimental Determination of the Moments of Inertia of Airplanes by a Simplified Compound-Pendulum Method. NAGA. 1948. TN № 1629. 29 p.

[113] *Ivanov A. V.* Study of the double mathematical pendulum – III Melnikov's method applied to the system in the limit of small ratio of pendulums masses. Regular and chaotic dynamics. 2000. Vol. 5. № 3. Pp. 329–343.

[114] *Jadlovská S., Sarnovský J.* Classical Double Inverted Pendulum – a Complex Overview of a System. IEEE 10th International Symposium on Applied Machine Intelligence and Informatics (SAMI). 2012. Pp. 103–108.

[115] *Karman von T., Biot M. A.* Mathematical Methods in Engineering. McGraw, Hill Publishing Co., 1940. 505 p.

[116] *Kholostova O. V.* On the motions of a double pendulum with vibrating suspension point. Mechanics of Solids. 2009. 44(2). Pp. 184–197.

[117] *Klotter K.* Technische Schwingungslehre. Bd. 2. Springer-Verlag, 1960. 484 s.

[118] *Kovacic I., Zukovic M., Radomirovic D.* Normal modes of a double pendulum at low energy levels. Nonlinear Dynamics. 2020. Vol. 99. Pp. 1893–1908.

[119] *Lamb H.* Dynamics. Cambridge: The University press, 1914. 344 p.

[120] *Lavrovskii E. K., Formalskii A. M.* The optimal control synthesis of the swinging and damping of a double pendulum. Journal of Applied Mathematics and Mechanics. 2001. 65(2). Pp. 219–227.

[121] *Levi-Civita T., Amaldi A.* Lezioni di meccanica razionale. Volume secondo. Dinamica dei sistemi con un numero di gradi di libertà. Parte seconda. Bologna: N. Zanichelli, 1927. 684 p.

[122] *Levien R. B., Tan S. M.* Double pendulum: an experiment in chaos. American journal of physics. 1993. Vol. 61. № 11. Pp. 1038–1044.

[123] *Lin J., Kajitani M., Masuda T.* Control of double pendulum. Nippon Kikai Gakkai Ronbunshu, C Hen. Transactions of the Japan Society of Mechanical Engineers. 1990. Part C. 56(522). Pp. 431–434.

[124] *Ludwicki M., Awrejcewicz J., Kudra G.* Spatial double physical pendulum with axial excitation: computer simulation and experimental set-up. International Journal of Dynamics and Control. 2015. Vol. 3. Pp. 1–8.

[125] *Luo A. C. J., Guo C.* A Period-1 Motion to Chaos in a Periodically Forced, Damped, Double-Pendulum. Journal of Vibration Testing and System Dynamics. 2019. 3(3). Pp. 259–280.

[126] *MacMillan W. D.* Dynamics of rigid bodies. New York: Dover publications, inc, 1936. 478 p.

[127] *Magnus K.* Schwingungen. Eine Einführung in die theoretische Behandlung von Schwingungsproblemen. Stuttgart, Teubner, 1961. 251 s.

[128] *Maiti S., Roy J., Mallik A. K., Bhattacharjee J.* Nonlinear dynamics of a rotating double pendulum. Physics Letters. 2015. 380(3). Pp. 408–412.

[129] *Mendonça G. L. T., Paiva A., Savi M. A.* Numerical investigation of the nonlinear behavior of a double pendulum. 23rd ABCM International Congress of Mechanical Engineering, December 6-11, 2015, Rio de Janeiro, Brazil. 2015. Pp. 1–8.

[130] *Mikhlin Y. V.* Normal vibrations of a general class of conservative oscillators. Nonlinear Dynamics. 1996. 11(1). Pp. 1–15.

[131] *Mirer S. A., Prilepskiy I. V.* Optimum parameters of a gravitational satellite-stabilizer system. Cosmic Research. 2010. No. 48(2). Pp. 194–204.

[132] *Moon F. C.* Chaotic Vibrations. An Introduction for Applied Scientists and Engineers. New York, Chichester, Brisbane, Toronto, Singapore, A Wiley-Interscience Publication, 1987. 309 p.

[133] *Rafat M., Wheatland M., Bedding T.* Dynamics of a double pendulum with distributed mass. American Journal of Physics. 2009. 77(3). Pp. 216–223.

[134] *Reshmin S. A.* Decomposition method in the problem of controlling an inverted double pendulum with the use of one control moment. Journal of Computer and Systems Sciences International. 2005. 44(6). Pp. 861–877.

[135] *Rosenberg R. M.* The normal modes of nonlinear n-degrees-of-freedom systems. Journal of Applied Mechanics. 1962. Vol. 30. Pp. 7–14.

[136] *Sawant K. R., Shrikanth V.* Energy dissipation and behavioral regimes in an autonomous double pendulum subjected to viscous and dry friction damping. European Journal of Physics. 2021. 42(5). 055008.

[137] *Shaw S. W., Pierre C.* Normal modes for nonlinear vibratory systems. Journal of Sound and Vibration. 1993. 164(1). Pp. 85–124.

[138] *Shinbrot T., Grebogi C., Wisdom J., Yorke J.* Chaos in a Double Pendulum. American Journal of Physics. 1992. 60(6). Pp. 491–499.

[139] *Skeldon A. C., Mullin T.* Mode interaction in a double pendulum. Physics Letter. 1992. Vol. 166. Pp. 224–229.

[140] *Smirnov A. S., Smolnikov B. A.* Collinear control of oscillation modes of spatial double pendulum with variable gain. Cybernetics and physics. 2021. Vol. 10. Iss. 2. Pp. 90–96.

[141] *Smirnov A. S., Smolnikov B. A.* Dissipative Model of Double Mathematical Pendulum with Noncollinear Joints. Advances in Mechanical Engineering. Selected Contributions from the Conference "Modern Engineering: Science and Education". Saint Petersburg, Russia, June 2021. 2022. Pp. 38–47.

[142] *Smirnov A. S., Smolnikov B. A.* Nonlinear oscillation modes of double pendulum. IOP Conference Series: Materials Science and Engineering.

IOP Conference Series: Materials Science and Engineering. International Conference of Young Scientists and Students "Topical Problems of Mechanical Engineering" (ToPME 2020) 2nd–4th December 2020, Moscow, Russia. 2021. Vol. 1129, 012042.

[143] *Smirnov A. S., Smolnikov B. A.* Nonlinear oscillation modes of spatial double pendulum. Journal of Physics: Conference Series. The International Scientific Conference on Mechanics "The Ninth Polyakhov's Reading" (ISCM) 9-12 March 2021, Saint Petersburg, Russian Federation. 2021. Vol. 1959, 012046.

[144] *Smirnov A. S., Smolnikov B. A.* Oscillations of Double Mathematical Pendulum with Noncollinear Joints. Advances in Mechanical Engineering. Selected Contributions from the Conference "Modern Engineering: Science and Education". Saint Petersburg, Russia, June 2020. 2021. Pp. 185–193.

[145] *Stachowiak T., Okada T.* A numerical analysis of chaos in the double pendulum. Chaos, Solitons and Fractals. 2006. 29(2). Pp. 417–422.

[146] *Stachowiak T., Szumiński W.* Non-integrability of restricted double pendula. Physics Letters A. 2015. Vol. 379. Iss. 47–48. Pp. 3017–3024.

[147] *Timoshenko S. P.* Vibration Problems in Engineering. New York: Van Nostrand, 1928. 351 p.

[148] *Vakakis A., Manevitch L., Mikhlin Yu., Pilipchuk V., Zevin A.* Normal Modes and Localization in Nonlinear Systems. New-York: Wiley, 1996. 552 p.

[149] *Vakakis A. F., Rand R.* Normal modes and global dynamics of a two-degree-of-freedom non-linear system. I. Low energies. International Journal of Non-Linear Mechanics. 1992. 27(5). Pp. 861–874.

[150] *Vakakis A. F., Rand R.* Normal modes and global dynamics of a two-degree-of-freedom non-linear system. II. High energies. International Journal of Non-Linear Mechanics. 1992. 27(5). Pp. 875–888.

[151] *Veltmann W.* Über die Bewegung einer Glocke. Polytechnisches Journal. 1876. Vol. 220. S. 481–495.

[152] *Viba J., Eiduks M., Irbe M.* Double pendulum vibration motion in fluid flow. Proceedings of 14th International Scientific Conference on Engineering for Rural Development. 2015. Pp. 434–439.

[153] *Wang F., Bajaj A., Kamiya K.* Nonlinear normal modes and their bifurcations for an inertially coupled nonlinear conservative system. Nonlinear Dynamics. 2005. 42(3). Pp. 233–265.

[154] *Xinjilefu, Hayward V., Michalska H.* Stabilization of the Spatial Double Inverted Pendulum Using Stochastic Programming Seen as a Model of Standing Postural Control. 9th IEEE-RAS International Conference on Humanoid Robots. 2009. Pp. 367–372.

[155] *Young A., Cao C., Hovakimyan N., Lavretsky E.* Control of a Nonaffine Double-Pendulum System via Dynamic Inversion and Time-Scale Separation. Proceedings of the 2006 American Control Conference Minneapolis, Minnesota, USA, June 14-16, 2006. Pp. 1820–1825.

[156] *Zhou Z., Whiteman C.* Motions of a double pendulum. Nonlinear Analysis, Theory, Methods & Applications. 1996. 26(7). Pp. 1177–1191.